

2016

Iridium porphyrin synthesis, reactivity and catalysis, and the nanogold-catalyzed synthesis of lactams

Taiwo Olawale Dairo
Iowa State University

Follow this and additional works at: <https://lib.dr.iastate.edu/etd>

 Part of the [Inorganic Chemistry Commons](#)

Recommended Citation

Dairo, Taiwo Olawale, "Iridium porphyrin synthesis, reactivity and catalysis, and the nanogold-catalyzed synthesis of lactams" (2016).
Graduate Theses and Dissertations. 15146.
<https://lib.dr.iastate.edu/etd/15146>

This Dissertation is brought to you for free and open access by the Iowa State University Capstones, Theses and Dissertations at Iowa State University Digital Repository. It has been accepted for inclusion in Graduate Theses and Dissertations by an authorized administrator of Iowa State University Digital Repository. For more information, please contact digirep@iastate.edu.

Iridium porphyrin synthesis, reactivity and catalysis, and the nanogold-catalyzed synthesis of lactams

by

Taiwo Olawale Dairo

A dissertation submitted to the graduate faculty
in partial fulfillment of the requirements for the degree of

DOCTOR OF PHILOSOPHY

Major: Inorganic Chemistry

Program of Study Committee:
L. Keith Woo, Major Professor
Javier Vela
Levi M. Stanley
Aaron D. Sadow
Arthur Winter

Iowa State University

Ames, Iowa

2016

Copyright © Taiwo Olawale Dairo, 2016. All rights reserved.

TABLE OF CONTENTS

	Page
ACKNOWLEDGEMENTS.....	iv
ABSTRACT.....	v
CHAPTER 1. INTRODUCTION.....	1
Synthesis and Catalytic Activities of Iridium Porphyrins.....	5
Gold-Catalyzed Amine Oxidation	9
Summary and Outlook	10
Dissertation Organization	11
References	12
CHAPTER 2. ADDITION OF AMINES TO A CARBONYL LIGAND: SYNTHESES, CHARACTERIZATION, AND REACTIVITIES OF IRIDIUM(III) PORPHYRIN CARBAMOYL COMPLEXES.....	17
Abstract.....	17
Introduction.....	18
Results and Discussion	21
Conclusions	37
Experimental Section.....	38
References.....	60
Supporting Information.....	64
CHAPTER 3. SCOPE AND MECHANISM OF IRIDIUM PORPHYRIN- CATALYZED S-H INSERTION REACTIONS.....	101
Abstract.....	101
Introduction.....	102
Results and Discussion	103
Conclusions	117
Experimental Section.....	117
References.....	121
Supporting Information.....	124
CHAPTER 4. AEROBIC OXIDATION OF CYCLIC AMINES TO LACTAMS CATALYZED BY CERIA-SUPPORTED NANOGOLD.....	137
Abstract.....	137
Introduction.....	138

Results and Discussion	141
Conclusions	158
Experimental Section	159
References	169
Supporting Information	173
CHAPTER 5. PRELIMINARY RESULTS OF THE NANOGOLD- CATALYZED SYNTHESIS OF N,N'-DISUBSTITUTED UREAS FROM THE REACTIONS OF AMINES WITH CARBON MONOXIDE AND OXYGEN	183
Abstract	183
Introduction	183
Results and Discussion	185
Conclusions	188
Experimental Section	189
References	190
Supporting Information	194
CHAPTER 6. CONCLUSIONS	196

ACKNOWLEDGEMENTS

My gratitude goes to Professor L. Keith Woo, who agreed to supervise my doctoral work. The stellar mentorship I received under him has undoubtedly prepared me for a career in research, and I will always appreciate the opportunity that I was given.

I'm also grateful to the members of my POS Committee (Professors Javier Vela, Levi M. Stanley, Aaron D. Sadow, and Arthur Winter) for their devotion and support over the past few years. In the same vein, I owe a debt of gratitude to Distinguished Professor Emeritus Robert "Bob" J. Angelici for his genuine interest in my professional development. I'm particularly grateful for his soothing words, pieces of advice, and the numerous long candid conversations we often had.

I'd also like to thank my biggest fans: Mojeed and Mojisola Dairo (dear father and mother), Kehinde Dairo (dearly beloved twin brother), and Ayodeji Dairo (dear elder brother). I enjoyed (and still enjoy) unalloyed moral and spiritual support from these beautiful people, and am very much blessed to call them family. My other siblings are appreciated as well, so are my cousins that are resident in the United States (the Aremus in particular).

Lastly, my sojourn in the city of Ames would have been lonely if not for the good company of my fellow Nigerians (Yomi and Christy Abatan, Inya and Ezy Nlenanya, Seyi Olatujoye, Benaiah Anabaraonye, Richie Oyeleke, Chinwe Ozoh, Bisoye Odubanjo, Dotun Akintayo) as well as other friends and colleagues from other parts of the world (Gina, Regina, Fadzai, Sinele, Jagadeesh, B.J., Nick, Casmir, Sherman, Shelbee, the Castleberrys, the Graveses). I am indeed glad to have met you all.

ABSTRACT

The work presented in this report focuses on the synthesis and characterization of new iridium(III) porphyrin complexes, the iridium porphyrin-catalyzed insertion of diazo esters into the S-H bond of thiols (S-H insertion), and the efficient nanogold-catalyzed oxidation of amines into lactams, in the presence of atmospheric oxygen. Preliminary results of the nanogold-catalyzed synthesis of N,N'-disubstituted ureas from the room temperature reaction between primary amines, carbon monoxide and oxygen, are presented as well.

Upon treatment of (carbonyl)chloro(*meso*-tetra-*p*-tolylporphyrinato)iridium(III), (TTP)Ir(CO)Cl, with excess primary amines (amine = RNH₂ = benzylamine, n-butylamine, isopropylamine, and tert-butylamine), at 23 °C, in the presence of Na₂CO₃, *trans*-amine-coordinated iridium carbamoyl complexes, (TTP)Ir(NH₂R)[C(O)NHR], were isolated in yields up to 94%. The lability of the amine ligands was established by variable-temperature NMR studies, ligand replacement reactions, and equilibrium binding studies. Consequently, hexacoordinate complexes of the type (TTP)Ir(L)[C(O)NHR] were synthesized, where L included quinuclidine, 1-methylimidazole, triethylphosphite, and dimethylphosphine. A series of ligand binding studies showed that both electronic and steric factors influenced ligand binding to the metal center. Furthermore, the nature of the *trans* ligand determined the reactivity of the carbamoyl ligand with the electrophile HBF₄. On the other hand, the carbamoyl ligand reacted with CH₃I in a similar fashion, whether the *trans* ligand contained a nitrogen or phosphorus donor.

This work also reports that the pentacoordinated Ir(TTP)CH₃ efficiently catalyzed the insertion of the carbene moieties from methyl diazoacetate (MDA), ethyl diazoacetate

(EDA), methyl phenyldiazoacetate (MPDA) and methyl (*p*-tolyl)diazoacetate (MTDA) into the S-H bond of different aromatic and aliphatic thiols. Product yields ranged from 70 – 97%. UV-visible titration showed that electron-rich thiols bind more strongly to iridium than their electron-poor counterparts. Substrate competition and trapping experiments also suggested that the insertion reactions proceed via an ylide intermediate. Furthermore, kinetic experiments showed that the observed reaction rates were a consequence of the competitive binding of thiol to the metal center of the catalyst and the nucleophilic attack of the thiol on the metal carbene intermediate.

The oxidation of cyclic amines into lactams was efficiently catalyzed by CeO₂-supported gold nanoparticles (Au/CeO₂) in the presence of 1 atmosphere of O₂. The complete conversion of pyrrolidine was achieved in 6.5 hours at 160 °C, affording a 97% yield of the lactam product 2-pyrrolidone (γ -butyrolactam), while 2-piperidone (δ -valerolactam) was synthesized from piperidine (83% yield) in of 2.5 hours. Caprolactam, the precursor to nylon-6, was obtained from hexamethyleneimine in 37% yield in 3 hours. The intermediacy of 5-(pyrrolidin-1-yl)-3,4-dihydro-2*H*-pyrrole (amidine-5) and 4-amino-1-(pyrrolidin-1-yl)butan-1-one) in the oxidation of pyrrolidine was established by their independent syntheses and catalytic conversions into 2-pyrrolidone. In addition, Au/CeO₂ efficiently catalyzed the oxidation of N-methyl cyclic tertiary amines to the corresponding lactams at 80 °C and 100 °C.

Finally, CeO₂-supported gold nanoparticles (Au/CeO₂) was found to catalyze the synthesis of N,N'-disubstituted ureas from the reactions of primary amines with 1 atmosphere each of CO and O₂. These reactions were found to proceed at 23 °C. The isolated

yield of N,N'-di-*n*-butylurea was 75%, while N,N'-dicyclohexylurea and N,N'-diisopropylurea were isolated in 40% yield and 37% yield, respectively.

CHAPTER 1. INTRODUCTION

Over the past few decades, transition metal complexes have been employed as catalysts in several chemical transformations. Thus, the efficiency of transition metals in various catalytic transformations necessitates the synthesis of novel transition metal complexes. During the 1950s, a mixture of TiCl_4 and AlEt_3 (now known as the Ziegler-Natta catalyst) was shown to catalyze the polymerization of alkenes.^{1,2} Today, variants of the catalyst incorporate cobalt and magnesium.³ Years after the discovery that tris(triphenylphosphine)rhodium(I)chloride [$\text{RhCl}(\text{PPh}_3)_3$] was capable of catalyzing the hydrogenation of olefins under ambient conditions of temperature and pressure,⁴ dicobalt octacarbonyl [$\text{Co}_2(\text{CO})_8$] was also found to catalyze the hydroformylation of alkenes into aldehydes in the presence of carbon monoxide and hydrogen.^{5,6} Other prominent carbon-carbon bond-forming reactions that are catalyzed by transition metal complexes include metathesis and coupling reactions. Following the seminal work by Chauvin in seeking to understand the mechanism behind olefin metathesis,⁷ several transition metal complexes have been developed to efficiently catalyze this class of chemical transformation. Notable among these catalysts were first reported in the 1980s^{8,9} and 1990s^{10,11}. Years later, modified versions of these molybdenum-based^{12,13} and ruthenium-based catalysts¹⁴⁻¹⁸ are now commercially available (Figure 1). Furthermore, the Heck,^{19,20} Sonogashira,²¹ Negishi,^{22,23} and Suzuki-Miyaura²⁴ coupling reactions, which are now widely-used methods of C-C bond formation,²⁵ are all catalyzed by palladium-based complexes.

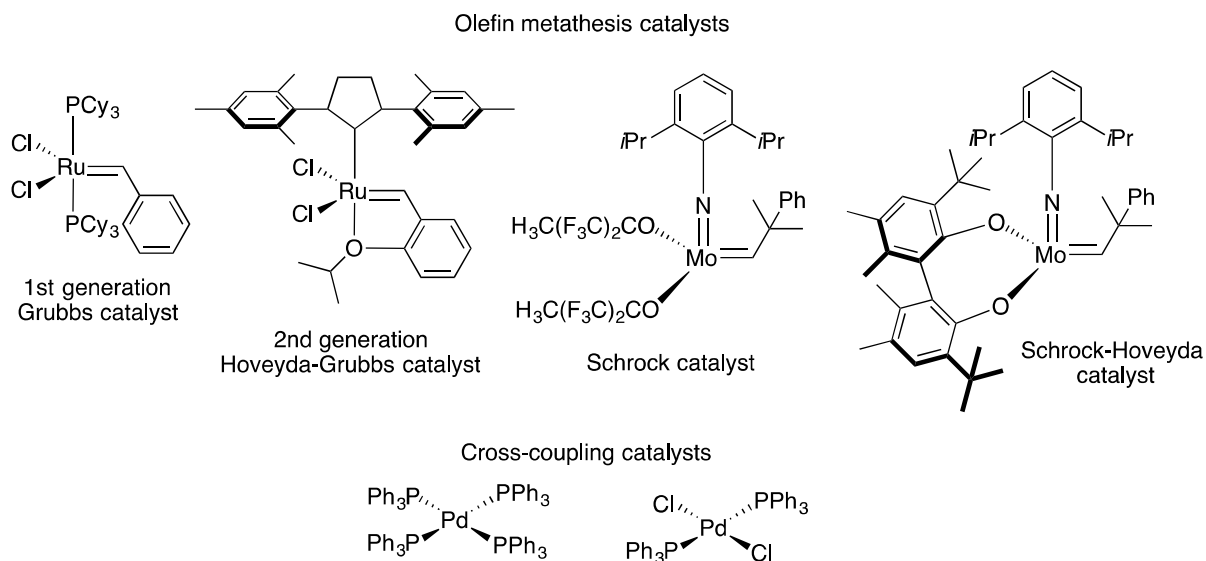
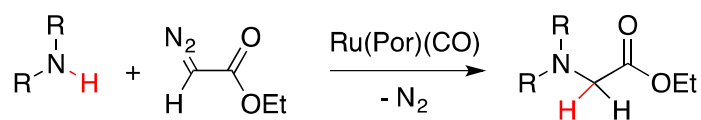


Figure 1. Some commercially available catalysts for olefin metathesis and cross-coupling reactions

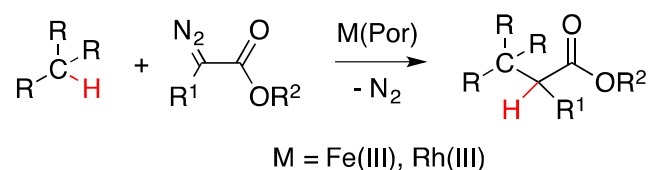
By virtue of the porphyrin macrocycle, metalloporphyrins are robust and tunable, and are known to be highly active catalysts for the selective synthesis of several industrially and biologically relevant organic molecules via atom and group transfer reaction.²⁶ An atom-economical route to new organic molecules involves carbene transfer reactions, with the use of diazo compounds as carbene precursors. In such reactions, non-toxic nitrogen gas (N_2) is the only by-product.²⁷ Interestingly, several porphyrin complexes of rhodium, cobalt, osmium, ruthenium, and iron have been employed as catalysts for such chemical transformations (Scheme 1).²⁶

Another versatile route to the synthesis of industrially important organic fragments is the oxidation of amines.^{28,29} For example, Hoh and co-workers,²⁸ in 1963, reported the synthesis of *N,N*-dimethyldodecylamine *N*-oxide (**1**) from the oxidation reaction between *N,N*-dimethyldodecylamine and hydrogen peroxide (H_2O_2) (eq. 1) For many decades, **1** has found use as a surfactant in the manufacture of soaps and detergents.^{30,31}

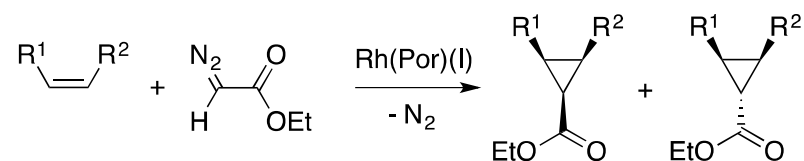
1.) N-H INSERTION



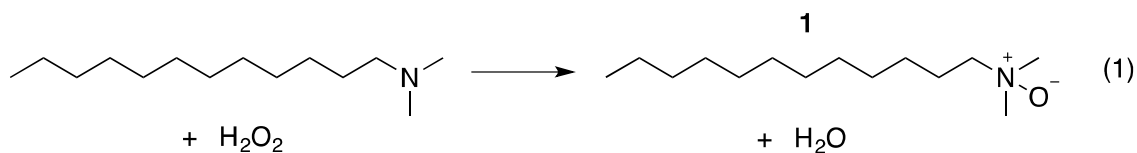
2.) C-H INSERTION



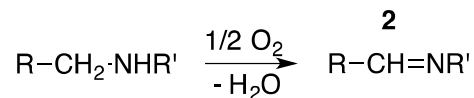
3.) CYCLOPROPANATION



Scheme 1. Examples of carbene transfer reactions that have been catalyzed by metalloporphyrins.



Imines (**2**; Scheme 2) also make up an important class of nitrogen-containing organic compounds, and they can be synthesized from the oxidation of amines.³² Several cases in w-



Scheme 2. Oxidation of amines into imines.

-hich imines were generated from the oxidative dehydrogenation (ODH) of amines in the presence of copper catalysts have been reported in the literature.³³⁻³⁶ Such a report was made

in 1995 by Shimizu and co-workers,³³ wherein copper(II)chloride (CuCl_2) was found to catalyze the oxidation of tetrahydroisoquinolines and tetrahydroquinoline into the corresponding imines **3** and **4**, respectively (Figure 2). Indole (**5**) was also synthesized at 80 °C from the reaction between indoline and atmospheric oxygen, in the presence of copper(I) chloride (CuCl).³⁴ Furthermore, CuCl catalyzed the air oxidation of different substituted benzylamines into the corresponding N-benzylidene benzylamine (**6**) at 100 °C.³⁵

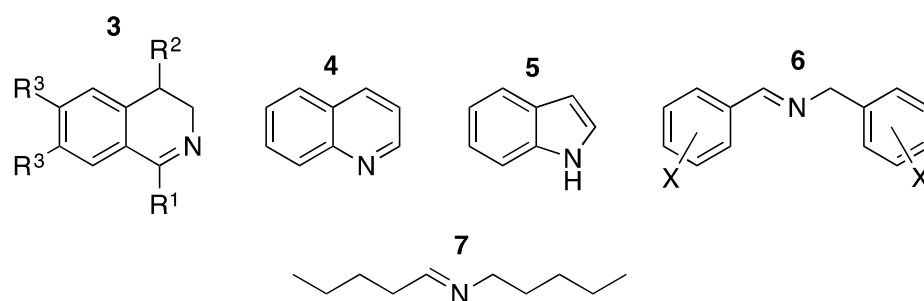


Figure 2. Examples of imines that have been generated from the copper-catalyzed oxidation of primary and secondary amines.

In a groundbreaking 1987 report, nanogold supported on metal oxides was shown to have catalyzed the oxidation of CO into CO_2 at -77 °C.³⁷ In 2006, Angelici reported the bulk-gold catalyzed formation of carbodiimides from the reaction of amines with isocyanides and O_2 ,³⁸ as well as the bulk gold-catalyzed synthesis of $\text{N,N}'$ -substituted ureas from amines, carbon monoxide and molecular oxygen.³⁹ Furthermore, the synthetic and catalytic literature of iridium porphyrin is relatively sparse, despite the catalytic roles of metalloporphyrins in chemical transformations. In view of the aforementioned, the work that is reported in this thesis was undertaken to demonstrate the rich stoichiometric and

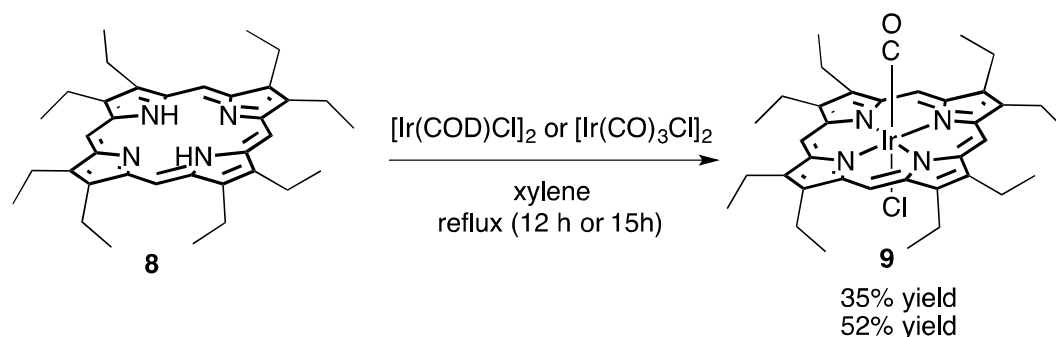
catalytic reactivity of iridium porphyrins, and also explore the catalytic activity of nanogold in the synthesis of industrially relevant compounds from the aerobic oxidation of amines.

Following the general introduction above is a brief literature review of iridium porphyrin complexes, and gold-catalyzed amine oxidation reactions.

Synthesis and Catalytic Activities of Iridium Porphyrins

In 1967, Sadasivan and Fleischer reported the first synthesis of an iridium(III) porphyrin complex.⁴⁰ In that work, a solution of $[\text{Ir}(\text{CO})_3\text{Cl}]$ in ethylene glycol monomethyl ether was refluxed with hematoporphyrin diethyl ester in the presence of sodium carbonate or sodium acetate. After purification by column chromatography, the iridium porphyrin product was assigned as $[\text{Ir}(\text{CO})(\text{por})][\text{X}]$. The axial ligand X was assumed to be acetate or chloride, and the existence of a CO ligand in this new complex was established by its intense IR band at around 2060 cm^{-1} .⁴⁰ The same authors reported, in 1968, a new method for synthesizing iridium(III) porphyrins.⁴¹ This method involved the use of in situ generated iridium(I) cyclooctene complexes. After treatment with sodium carbonate, the iridium(I) intermediates were then refluxed with acetic acid solutions of free base porphyrins. Each iridium porphyrin complex that was produced from these reactions contained one carbonyl and one cyclooctene ligand in each of the two axial positions.⁴¹ Ten years later, Ogoshi⁴² and co-workers reported that when octaethylporphyrin, OEP (**8**; Scheme 3), was refluxed with $[\text{Ir}(\text{CO})_3\text{Cl}]_2$ or $[\text{Ir}(\text{COD})\text{Cl}]_2$ in xylene, the major iridium porphyrin product was $(\text{OEP})\text{Ir}(\text{CO})\text{Cl}$ (**9**) (Scheme 3). In the same report, some other compounds that were synthesized include $(\text{OEP})\text{Ir}(\text{CH}_2\text{CH}_2\text{R})$ ($\text{R} = \text{CN}, \text{CO}_2\text{Et}$), $(\text{OEP})\text{Ir}(\text{R}')$ ($\text{R}' = \text{CH}_3, \text{C}_2\text{H}_5, n-$

C₆H₁₃), (OEP)Ir(H), and (OEP)Ir(I). Subsequently, Sugimoto and co-workers⁴³ described the synthesis of several iridium(III) porphyrin complexes from (OEP)Ir(CO)Cl (**9**). The syn-



Scheme 3. Synthesis of (carbonyl)chloro(octaethylporphyrinato)iridium(III).

-thesized compounds were (OEP)Ir(CO)X (X = BF₄, CN, Br), (OEP)Ir(CH₃)L (L = CO, 1-MeIm, py, NH₃), and [(OEP)Ir(CH₃)CN]⁻. The synthesis of (OEP)Ir(*n*-C₃H₇) and (OEP)Ir(*n*-C₃H₇)L (L = CO, NEt₃, 1-MeIm, py, Me₂SO, PPh₃) have been reported as well.⁴⁴ The relative binding constants for the L ligands were determined by UV-visible studies, and the structures of (OEP)Ir(C₃H₇)Me₂SO and (OEP)Ir(C₃H₇)PPh₃ were confirmed by x-ray diffraction studies. Furthermore, the same authors reported the synthesis and characterization of [(OEP)Ir(Cl)]₂dppe [dppe = 1,2-bis(diphenylphosphino)ethane] from (OEP)Ir(C₃H₇).⁴⁵ It is noteworthy that phosphorescent iridium complexes of the octaethylporphyrin ligand have been reported as well.⁴⁶ It has also been found that treatment of (TTP)Ir(CO)Cl or (TTP)Ir(CH₃) (TTP = *meso*-tetra-*p*-tolylporphyrin dianion) with aryl aldehydes (ArCHO; Ar = C₆H₅, 4-OCH₃-C₆H₄, 4-CH₃-C₆H₄, 4-^tBu-C₆H₄, 4-F-C₆H₄, 4-Cl-C₆H₄, 4-CF₃-C₆H₄) and C₂H₅CHO resulted in the formation of (TTP)Ir(COAr) and (TTP)Ir(COC₂H₅), respectively.⁴⁷ In addition, compounds of the type (TTP)Ir(CH₂Ar) (Ar = C₆H₅, 4-CH₃-C₆H₄, 4-F-C₆H₄) have been isolated from base-promoted C-H activation

reactions between (TTP)Ir(CO)Cl and toluenes,⁴⁸ while the synthesis of (TTP)Ir(C₂H₄OH), (TTP)Ir(py)(CH₂CH₂Phth), (TTP)Ir(THF)(Phth), and (TTP)Ir(py)(Phth) (Phth = phthalimide anion) have been reported as well.⁴⁹ Other known iridium porphyrin complexes feature N-heterocyclic carbene (NHC), diaminocarbene, as well as mono- and bis(isocyanide) ligands (10 – 13, Figure 3).⁵⁰

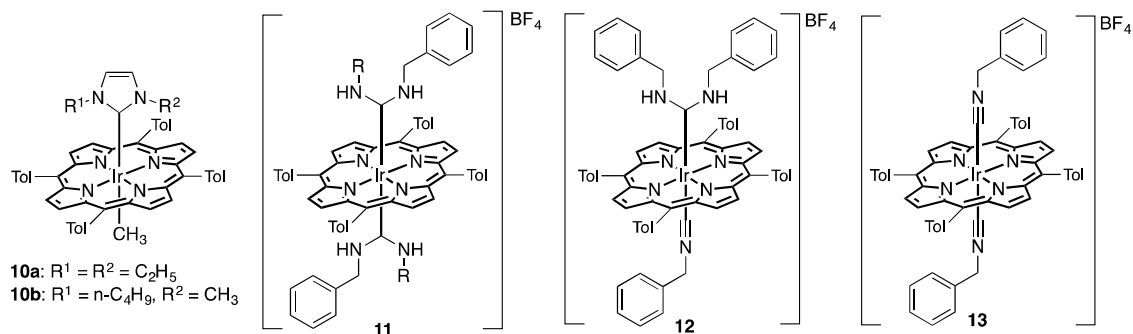


Figure 3. Iridium(III) porphyrin complexes containing NHC, diaminocarbene, mono- and bis(isocyanide) groups as axial ligands.

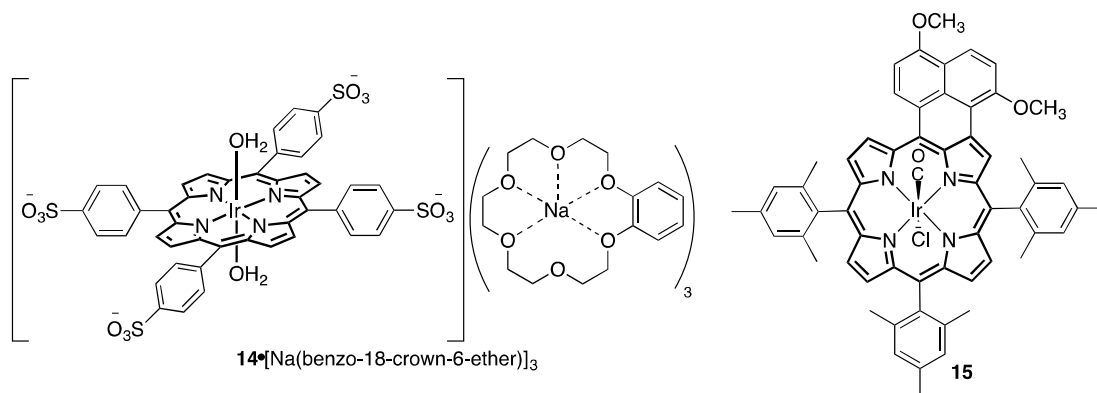


Figure 4. Water-soluble iridium(III) diaqua porphyrin (14) and an iridium(III) complex of a π – extended porphyrin (15).

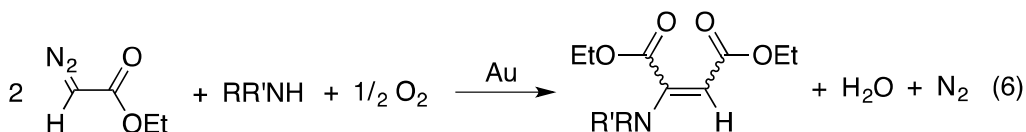
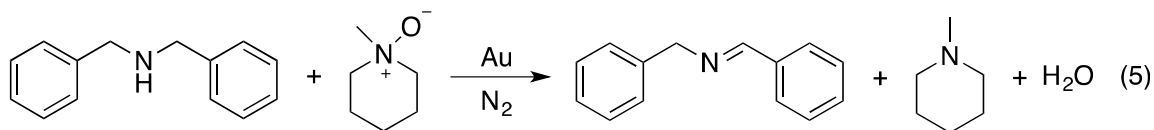
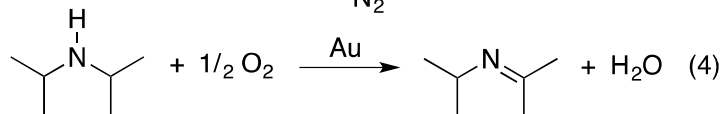
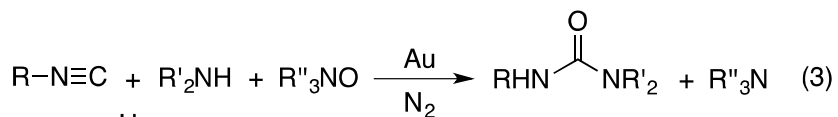
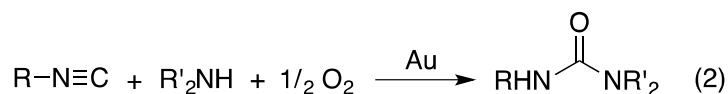
While Ogo *et al.* have reported the synthesis of a water-soluble diaqua iridium(III) porphyrin (14),⁵¹ there's also been a report of an iridium complex of a π – extended

porphyrin (**15**) by Kadish and co-workers.⁵² The catalytic activities of iridium porphyrin complexes have been demonstrated as well. van Baar and co-workers demonstrated the electrocatalytic (at potentials between 0 and 0.25 V) oxidation of CO into CO₂ in the presence of a carbon-supported iridium(III) porphyrin complex in an aqueous medium.⁵³ The oxidation was proposed to proceed via a nucleophilic attack of a water molecule on a molecule of CO which is adsorbed on the surface of the iridium metal. Furthermore, the electrocatalytic reduction of O₂ into H₂O, in the presence of iridium porphyrin catalysts, has been reported independently by Collman⁵⁴ and Anson.⁵⁵ In the latter case, improved catalyst performance was achieved when the surfactant didodecyldimethylammonium bromide (DDAB) was used in combination with the iridium catalyst.⁵⁵ Also, a U.S. patent was granted for an invention describing olefin epoxidation in the presence of air or pure oxygen, catalyzed by an iridium porphyrin complex, as well as other metalloporphyrins, at ambient temperature and pressure.⁵⁶ The use of iridium porphyrins as catalysts for carbene transfer has also been encouraging. Woo has demonstrated that Ir(TTP)CH₃ is an active catalyst for cyclopropanation,⁵⁷ N-H insertion,⁵⁸ and C-H insertion⁵⁹ reactions, with diazo compounds as carbene sources. Catalytic turnovers up to 4.8×10^5 were achieved for the cyclopropanation reaction of styrene, with ethyl diazoacetate. In that work, the catalytic activities of Ir(TTP)CO(X) (X = Cl, Br, I, SCN) and Ir(TTP)Cl(NMe₃) were also demonstrated.⁵⁷ In the case of N-H insertion reactions catalyzed by Ir(TTP)CH₃, the substrate scope included primary aromatic and aliphatic amines, secondary amines, ethyl and methyl diazoacetate, as well as the bulky methyl phenyl diazoacetate.⁵⁸ However, a narrow substrate scope was observed for the Ir(TTP)CH₃-catalyzed C-H insertion system.⁵⁹ Subsequently, Rodríguez-García et al reported the iridium porphyrin-catalyzed

intramolecular C-H insertion reactions of diazo compounds. The catalytic activities of OEP[Ir(CO)₃]₂, TPP[Ir(CO)₃]₂, Ir(OEP)CO(Cl), and Ir(TTP)CO(Cl) were demonstrated in that study.⁶⁰ A chiral iridium(III) porphyrin complex has also been shown to catalyze the enantioselective intramolecular C-H insertion reactions of diazo substrates.⁶¹

Gold-Catalyzed Amine Oxidation

Angelici and co-workers were the first to demonstrate the catalytic activity of bulk gold powder. They reported the bulk gold-catalyzed synthesis of carbodiimides from reactions of



isocyanides with primary amines and O₂,³⁸ as well as the bulk gold-catalyzed reactions of amines with CO and O₂ to give substituted ureas.³⁹ Subsequent bulk gold-catalyzed amine oxidation reactions include the formation of ureas from the reactions between secondary amines, isocyanides, and gaseous oxygen (eq. 2).⁶² The urea yields ranged from 19 – 51%, within 24 h of reaction at 60 °C, and the reaction rates were only slightly dependent on

oxygen concentration. Imines (from bulky secondary amine substrates) (eq. 4) and amidines (from cyclic secondary amines) have also been obtained in yields of 15 – 46% (at 60 °C in a reaction time of 40 h) and 75 – 93% yields (at 100 °C in a reaction time of 24 h) from the bulk gold-catalyzed aerobic oxidation reactions of amines.⁶³ In addition, enamines have been obtained in yields up to 94% when primary and secondary amines were heated with ethyl diazoacetate (EDA) in the presence of 1.00 g of bulk gold powder in acetonitrile solvent (eq. 6) In that study, neither N-H insertion products nor dimerization products of EDA were obtained.⁶⁴ In place of oxygen gas, amine N-oxides have been shown to be capable of oxidizing amine substrates in the presence of bulk gold catalyst (eq. 3 and 5).^{65,66} In all cases, the gold-to-amine substrate ratio ranged from 8.5:1 to 317:1. However, nanogold has been shown to catalyze the oxidation of many substrates such as CO,⁶⁷⁻⁷¹ cyclohexane,⁷² cyclohexene,⁷³ aldehydes,⁷⁴ alcohols,^{75,76} and glucose,⁷⁷ including primary and secondary amines,⁷⁸⁻⁸⁰ and the catalyst loading in the nanogold-catalyzed reactions were much lower than the bulk gold-catalyzed systems.

Summary and Outlook

The foregoing introduction and literature review re-emphasize the importance of transition metals in the transformations of organic chemical substrates. In particular, iridium porphyrins and metal oxide-supported nanogold represent a class of transition metal catalysts, which show promise. Thus, we were driven to further explore the stoichiometric and catalytic reactions of iridium porphyrin complexes, and also apply the well-established catalytic activity of supported nanogold in the synthesis of organic molecules. Reported herein, is the synthesis and reactivity of novel iridium porphyrin carbamoyl complexes, the

iridium porphyrin-catalyzed insertion of carbene moieties into the S-H bonds of thiols, and the efficient synthesis of industrially relevant secondary and tertiary lactams from ceria-supported-nanogold-catalyzed oxidation of cyclic amines. Preliminary results of the nanogold-catalyzed synthesis of synthesis of N,N'-disubstituted ureas from the reactions of amines with carbon monoxide and oxygen are reported as well.

Dissertation Organization

This dissertation contains a total of six (6) chapters. Chapter 1 contains a general introduction as well as a literature review of iridium porphyrin complexes, and gold-catalyzed amine oxidation reactions. Chapter 2 is a modified version of a published paper, while chapter 3 is modified from a manuscript that is being prepared for submission to a peer-reviewed journal. Chapter 4 is modified from a manuscript that has been submitted for publication, while chapter 5 represents preliminary results from a new project. The final chapter describes the general conclusions that can be drawn from the contents of this dissertation.

All of the experimental work in chapter 2 was done by Taiwo O. Dairo, apart from x-ray data collection and analysis which were done by the crystallographer, Dr. Arkady Ellern. Furthermore, Taiwo O. Dairo carried out all of the work reported in chapters 3 and 5. About 90% of the work reported in chapter 4 was performed by Taiwo O. Dairo, while Nicholas C. Nelson carried out catalyst characterization.

References

- (1) Ziegler, K.; Holzkamp, E.; Martin, H.; Breil, H. *Angew. Chem.* **1955**, *67*, 541-547.
- (2) Natta, G. *J. Polym. Sci.* **1955**, *16*, 143-154.
- (3) Hoff, R., Mathers, R.T., Eds.; In *Handbook of Transition Metal Polymerization Catalysts*; John Wiley & Sons, Inc.: Hoboken, NJ, USA, 2010.
- (4) Osborn, J.A.; Jardine, F.H.; Young, J.F.; Wilkinson, G. *J. Chem. Soc. A* **1966**, 1711-1732.
- (5) Halpern, J. *Pure Appl. Chem.* **1986**, *58*, 575-584.
- (6) Tyler, D. R. *Prog. Inorg. Chem.* **1988**, *36*, 125-194.
- (7) Hérisson, J.-L.; Chauvin, Y. *Makromol. Chem.* **1971**, *141*, 161-176.
- (8) Wengrovius, J.H.; Schrock, R.R.; Churchill, M.R.; Missert, J.R.; Youngs, W.J. *J. Am. Chem. Soc.* **1980**, *102*, 4515-4516.
- (9) Churchill, M.R.; Rheingold, A.L.; Youngs, W.J.; Schrock, R.R.; Wengrovius, J.H. *J. Organomet. Chem.* **1981**, *204*, C17-C20.
- (10) Nguyen, S.B.T.; Johnson, L.K.; Grubbs, R.H.; Ziller, J.W. *J. Am. Chem. Soc.* **1992**, *114*, 3974-3975.
- (11) Wu, Z.; Benedicto, A.D.; Grubbs, R.H. *Macromolecules* **1993**, *26*, 4975-4977.
- (12) Oskam, J.H.; Fox, H.H.; Yap, K.B.; McConville, D.H.; O'Dell, R.; Lichtenstein, B.J.; Schrock, R.R. *J. Organomet. Chem.* **1993**, *459*, 185-198.
- (13) Alexander, J.B.; Schrock, R.R.; Davis, W.M.; Hultsch, K.C.; Hoveyda, A.H.; Houser, J.H. *Organometallics* **2000**, *19*, 3700-3715.
- (14) Schwab, P.; France, M. B.; Ziller, J. W.; Grubbs, R. H. *Angew. Chem. Int. Ed. Engl.* **1995**, *34*, 2039-2041.
- (15) Schwab, P.; Grubbs, R. H.; Ziller, J. W. *J. Am. Chem. Soc.* **1996**, *118*, 100-110.
- (16) Kingsbury, J. S.; Harrity, J. P. A.; Bonitatebus, P. J., Jr.; Hoveyda, A. H. *J. Am. Chem. Soc.* **1999**, *121*, 791-799.
- (17) Garber, S. B.; Kingsbury, J. S.; Gray, B. L.; Hoveyda, A. H. *J. Am. Chem. Soc.* **2000**, *122*, 8168-8179.

- (18) Gessler, S.; Randl, S.; Blechert, S. *Tetrahedron Lett.* **2000**, *41*, 9973-9976.
- (19) Heck, R.F.; Nolley, J.P., Jr. *J. Org. Chem.* **1972**, *37*, 2320-2322.
- (20) Dieck, H.A.; Heck, R.F. *J. Am. Chem. Soc.* **1974**, *96*, 1133-1136.
- (21) Sonogashira, K.; Tohda, Y.; Hagihara, N. *Tetrahedron Lett.* **1975**, *16*, 4467-4470.
- (22) Negishi, E.; King, A.O.; Okukado, N. *J. Org. Chem.* **1977**, *42*, 1821-1823.
- (23) King, A.O.; Okukado, N.; Negishi, E. *J. Chem. Soc. Chem. Commun.* **1977**, 683-684.
- (24) Miyaura, N.; Suzuki, A. *J. Chem. Soc. Chem. Commun.* **1979**, 866-867.
- (25) Johansson Seechurn, C.C.C.; Kitching, M.O.; Colacot, T.J.; Snieckus, V. *Angew. Chem. Int. Ed.* **2012**, *51*, 5062-5085.
- (26) Anding, B.J.; Woo, L.K. In *Handbook of Porphyrin Science*; Kadish, K.M.; Guillard, R.; Smith, K., Eds.; World Scientific Publishing Company: Hackensack, NJ, 2012; Vol. 21, p 145.
- (27) Doyle, M.P.; McKervey, M.A.; Ye, T. *Modern Catalytic Methods for Organic Synthesis with Diazo Compounds: From Cyclopropanes to Ylides*. Wiley-Interscience: New York, 1998.
- (28) Hoh, G.L.K.; Barlow, D.O.; Chadwick, A.F.; Lake, D.B.; Sheeran, S.R. *J. Am. Oil Chem. Soc.* **1963**, *40*, 268-271.
- (29) Rawalay, S.S.; Shechter, H. *J. Org. Chem.* **1967**, *32*, 3129-3131.
- (30) Smith, K.R.; Borland, J.E.; Corona, R.J.; Sauer, J.D. *J. Am. Oil Chem. Soc.* **1991**, *68*, 619-622.
- (31) Arif, S.; Friedli, F.E. In *Detergency of Specialty Surfactants*; Friedli, F.E., Ed.; Marcel Dekker, Inc: New York, Basel, 2001; Vol. 98, p 107-108.
- (32) Schümperli, M.T.; Hammond, C.; Hermans, I. *ACS Catal.* **2012**, *2*, 1108-1117.
- (33) Shimizu, M.; Orita, H.; Hayakawa, T.; Suzuki, K.; Takehira, K. *Heterocycles* **1995**, *41*, 773-779.
- (34) Maeda, Y.; Nishimura, T.; Uemura, S. *Bull. Chem. Soc. Jpn.* **2003**, *76*, 2399-2403.
- (35) Patil, R.D.; Adimurthy, S. *Adv. Synth. Catal.* **2011**, *353*, 1695-1700.

- (36) Patil, R.D.; Adimurthy, S. *RSC Adv.* **2012**, *2*, 5119-5122.
- (37) Haruta, M.; Kobayashi, T.; Sano, H.; Yamada, N. *Chem. Lett.* **1987**, *2*, 405–408.
- (38) Lazar, M.; Angelici, R. J. *J. Am. Chem. Soc.* **2006**, *128*, 10613–10620.
- (39) Zhu, B.; Angelici, R. J. *J. Am. Chem. Soc.* **2006**, *128*, 14460–14461.
- (40) Fleischer, E.B.; Sadasivan, N. *Chem. Commun.* **1967**, 159b -160.
- (41) Sadasivan, N.; Fleischer, E.B. *J. Inorg. Nucl. Chem.* **1968**, *30*, 591- 601.
- (42) Ogoshi, H.; Setsune, J.-I.; Yoshida, Z.-I. *J. Organomet. Chem.* **1978**, *159*, 317 - 328.
- (43) Sugimoto, H.; Ueda, N.; Mori, M. *J. Chem. Soc., Dalton Trans.* **1982**, 1611-1616.
- (44) Kadish, K.M.; Cornillon, J.-L.; Mitaine, P.; Deng, Y.J.; Korp, J.D. *Inorg. Chem.* **1989**, *28*, 2534-2542.
- (45) Kadish, K.M.; Deng, Y.J.; Korp, J.D. *Inorg. Chem.* **1990**, *29*, 1036-1042.
- (46) Koren, K.; Borisov, S.M.; Saf, R.; Klimant, I. *Eur. J. Inorg. Chem.* **2011**, 1531–1534.
- (47) Song, Xu.; Chan, K.S. *Organometallics* **2007**, *26*, 965-970.
- (48) Cheung, C.W.; Chan, K.S. *Organometallics* **2008**, *27*, 3043-3055.
- (49) Tsang, J.Y.K.; Chan, K.S. *Can. J. Chem.* **2011**, *89*, 1506-1511.
- (50) Anding, B.J.; Ellern, A.; Woo, L.K. *Organometallics* **2014**, *33*, 2219–2229.
- (51) Kanemitsu, H.; Harada, R.; Ogo, S. *Chem. Commun.* **2010**, *46*, 3083-3085.
- (52) Fang, Y.; Koszelewski, D.; Kadish, K.M.; Gryko, D.T. *Chem. Commun.* **2014**, *50*, 8864-8867.
- (53) van Baar, J.F.; van Veen, J.A.R.; de Wit, N. *Electrochim. Acta* **1982**, *27*, 57-59.
- (54) Collman, J.P.; Chng, L.L.; Tyvoll, D.A. *Inorg. Chem.* **1995**, *34*, 1311-1324.
- (55) Shi, C.; Mak, K.W.; Chan, K.S.; Anson, F.C. *J. Electroanal. Chem.* **1995**, *397*, 321-324.
- (56) Groves, J.T.; Quinn, R. U.S. Patent 4,822,899, April 18, 1989.

- (57) Anding, B.J.; Ellern, A.; Woo, L.K. *Organometallics* **2012**, *31*, 3628-3635.
- (58) Anding, B.J.; Woo, L.K. *Organometallics* **2013**, *32*, 2599-2607.
- 59.) Anding, B.J.; Brgoch, J.; Miller, G.J.; Woo, L.K. *Organometallics* **2012**, *31*, 5586-5590.
- (60) López-Sánchez, C.; Álvarez-Corral, M.; Muñoz-Dorado, M.; Rodríguez-García, I. *Synlett* **2012**, *23*, 2469-2472.
- (61) Wang, J.-C.; Zhang, Y.; Xu, Z.-J.; Lo, V. K.-Y.; Che, C.-M. *ACS Catal.* **2013**, *3*, 1144-1148.
- (62) Lazar, M.; Zhu, B.; Angelici, R.J. *J. Phys. Chem. C* **2007**, *111*, 4074-4076.
- (63) Zhu, B.; Angelici, R.J. *Chem. Commun.* **2007**, 2157-2159.
- (64) Zhou, Y.; Angelici, R.J.; Woo, L.K. *Catal. Lett.* **2010**, *137*, 8-15.
- (65) Klobukowski, E.R.; Angelici, R.J.; Woo, L.K. *Catal. Lett.* **2012**, *142*, 161-167.
- (66) Klobukowski, E.R.; Angelici, R.J.; Woo, L.K. *Organometallics* **2012**, *31*, 2785-2792.
- (67) Shi, F.; Zhang, Q.; Ma, Y.; He, Y.; Deng, Y. *J. Am. Chem. Soc.* **2005**, *127*, 4182-4183.
- (68) Yang, X.; Shen, Y.; Wang, D.; Sun, Y. *React. Kinet. Catal. Lett.* **2008**, *95*, 123-128.
- (69) Sahu, N.; Parida, K. M.; Tripathi, A. K.; Kamble, V. S. *Appl. Catal., A* **2011**, *399*, 110-116.
- (70) Miao, Y.-X.; Li, W.-C.; Sun, Q.; Shi, L.; He, L.; Wang, J.; Deng, G.-M.; Lu, A.-H. *Chem. Commun.* **2015**, *51*, 17728-17731.
- (71) Reina, T. R.; Ivanova, S.; Idakiev, V.; Tabakova, T.; Centeno, M. A.; Deng, Q.-F.; Yuan, Z.-Y.; Odriozola, J. A. *J. Mol. Catal. A: Chem.* **2016**, *414*, 62-71.
- (72) Siddiqui, M.; Rafiq, H.; Warad, I.; Adil, S. F.; Mahfouz, R. M.; Al-Arifi, A. *Oxid. Commun.* **2012**, *35*, 476-481.
- (73) Bujak, P.; Bartczak, P.; Polanski, J. *J. Catal.* **2012**, *295*, 15-21.
- (74) Gawande, M. B.; Rathi, A. K.; Tucek, J.; Safarova, K.; Bundaleski, N.; Teodoro, O. M. N. D.; Kvitek, L.; Varma, R. S.; Zboril, R. *Green Chem.* **2014**, *16*, 4137-4143.

- (75) Choudhary, V. R.; Dumbre, D. K.; Bhargava, S. K. *Ind. Eng. Chem. Res.* **2009**, *48*, 9471-9478.
- (76) Dar, B. A.; Farooqui, M. *Orbital: Electron. J. Chem.* **2011**, *3*, 89-93.
- (77) Samoilova, N. A.; Krayukhina, M. A.; Klimova, T. P.; Babushkina, T. A.; Vyshivannaya, O. V.; Blagodatskikh, I. V.; Yamskov, I. A. *Russ. Chem. Bull.* **2014**, *63*, 1009-1016.
- (78) Preedasuriyachai, P.; Kitahara, H.; Chavasiri, W.; Sakurai, H. *Chem. Lett.* **2010**, *39*, 1174-1176.
- (79) Freakley, S.J.; He, Q.; Kiely, C.J.; Hutchings, G.J. *Catal. Lett.* **2015**, *145*, 71-79.
- (80) Chen, B.; Wang, L.; Gao, S. *ACS Catal.* **2015**, *5*, 5851-5876.

**CHAPTER 2. ADDITION OF AMINES TO A CARBONYL LIGAND:
SYNTHESES, CHARACTERIZATION, AND REACTIVITIES OF IRIDIUM(III)
PORPHYRIN CARBAMOYL COMPLEXES**

Modified from *Organometallics* **2014**, *33*, 2266-2276. Copyright © 2014 American
Chemical Society.

Taiwo O. Dairo, Arkady Ellern, Robert J. Angelici, and L. Keith Woo

Abstract

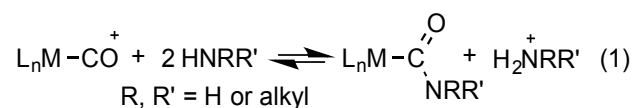
Treatment of (carbonyl)chloro(*meso*-tetra-*p*-tolylporphyrinato)iridium(III), (TTP)Ir(CO)Cl (**1**) with excess primary amines, at 23 °C, in the presence of Na₂CO₃, produces *trans*-amine-coordinated iridium carbamoyl complexes, (TTP)Ir(NH₂R)[C(O)NHR], where R = Bn (**2a**), *n*-Bu (**2b**), *i*-Pr (**2c**) and *t*-Bu (**2d**), with isolated yields up to 94%. The *trans* amine ligand is labile and can be replaced with quinuclidine (1-azabicyclo[2.2.2]octane, ABCO), 1-methylimidazole (1-MeIm), triethylphosphite [P(OEt)₃], and dimethylphenylphosphine (PMe₂Ph), at 23 °C, to afford hexacoordinated carbamoyl complexes, (TTP)Ir(L)[C(O)NHR] (for R = Bn: L = ABCO, **3a**; 1-MeIm, **4a**; P(OEt)₃, **5a**; PMe₂Ph, **6a**). Based on ligand displacement reactions and equilibrium studies, ligand binding strengths to the iridium metal center were found to decrease in the following order: PMe₂Ph > P(OEt)₃ > 1-MeIm > ABCO > BnNH₂ > Et₃N, PCy₃. The carbamoyl complexes (TTP)Ir(L)[C(O)NHR], where L = RNH₂ (**2a-b**) or 1-MeIm (**4a**), undergo protonolysis with HBF₄ to give the cationic carbonyl complexes

[(TTP)Ir(NH₂R)(CO)]BF₄ (**7a-b**) and [(TTP)Ir(1-MeIm)(CO)]BF₄ (**8**), respectively. In contrast, the carbamoyl complexes (TTP)Ir(L)[C(O)NHR], where L = P(OEt)₃ (**5a**) and PMe₂Ph (**6a** and **6c**), reacted with HBF₄ to afford the complexes [(TTP)Ir(PMe₂Ph)]BF₄ (**9**) and [(TTP)IrP(OEt)₃]BF₄ (**10**), respectively. The carbamoyl complexes (TTP)Ir(L)[C(O)NHR], where L = RNH₂ (**2a-d**), 1-MeIm (**4a**), P(OEt)₃ (**5b**) and PMe₂Ph (**6c**), reacted with methyl iodide to give the iodo complexes (TTP)Ir(L)I (L = RNH₂, **11a-d**; 1-MeIm, **12**; P(OEt)₃ **13**; and PMe₂Ph, **14**). Reactions of the complexes [(TTP)Ir(PMe₂Ph)]BF₄ (**9**) and [(TTP)IrP(OEt)₃]BF₄ (**10**) with [Bu₄N]I, benzylamine (BnNH₂) and PMe₂Ph afforded (TTP)Ir(PMe₂Ph)I (**14**), (TTP)Ir[P(OEt)₃]I (**13**), [(TTP)Ir(PMe₂Ph)(NH₂Bn)]BF₄ (**16**) and *trans*-[(TTP)Ir(PMe₂Ph)₂]BF₄ (**17**), respectively. Metrical details for the molecular structures of **4a** and **17** are reported.

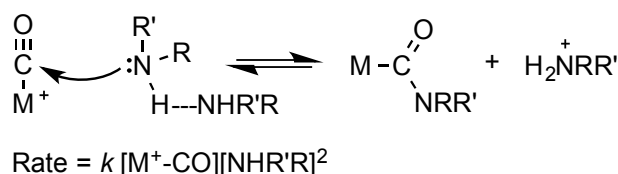
Introduction

Metal carbonyl complexes play a significant role in industrial and organometallic chemistry, serving as important starting materials and catalysts.¹ A key reaction for these complexes is the addition of nucleophiles to the carbonyl ligand. This reactivity provides access to useful organic molecules such as dimethylformamide, methanol, etc.² Furthermore, the nucleophilic addition of the hydroxide anion to the CO ligand in metal carbonyl complexes has been identified as a key step in the water gas shift reaction.³

Addition of amines to a transition metal-bound carbonyl ligand is a convenient route to the synthesis of metal carbamoyl (or carboxamido) complexes (eq 1).⁴ In general, metal carb-

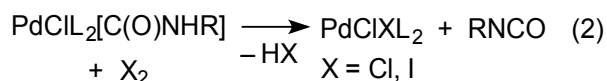


-onyl complexes that are susceptible to nucleophilic amine addition to form metal carbamoyl complexes have $\nu(\text{CO})$ above 2000 cm^{-1} , an indication of the electrophilicity of the CO ligand.^{5,6} Some of the earliest reported examples of carbamoyl complexes prepared by this route include those of Mn, Ru, Pt, and Fe.⁴ Kinetic studies involving the reaction of amines with *trans*-[M(CO)₄L₂]PF₆ (where M = Mn, Re and L = PPh₃, PMePh₂, PMe₂Ph), have revealed that the rate of formation of carbamoyl complexes has a second order dependence on the amine concentration. To rationalize this rate dependence, a mechanism involving amine assisted nucleophilic attack at the carbonyl carbon atom was proposed (Scheme 1).⁷

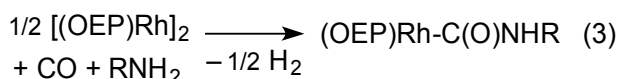


Scheme 1. Carbamoyl complexes via nucleophilic attack of amine on M-CO

Subsequently, metal carbamoyl complexes were either observed or suggested to be involved in several catalytic and stoichiometric chemical transformations. For example, the catalytic oxidative carbonylation of *n*-butylamine to the 1,3-substituted urea, using [(CO)₂W(NPh)I₂]₂ as a catalyst, was proposed to involve the tungsten carbamoyl complex, (CO)W[C(O)NHBu](NH₂R)₂(NPh)I, as an intermediate.⁸ This was supported further by IR spectroscopic studies with stoichiometric reactions of excess secondary and primary amines with [(CO)₂W(NPh)I₂]₂ which produced formamides and 1,3-disubstituted ureas, respectively, in the presence of air as an oxidizing agent.⁹ In addition, treatment of palladium carbamoyl complexes with halogens or other oxidizing agents produced isocyanates, in quantitative yields (eq 2).¹⁰



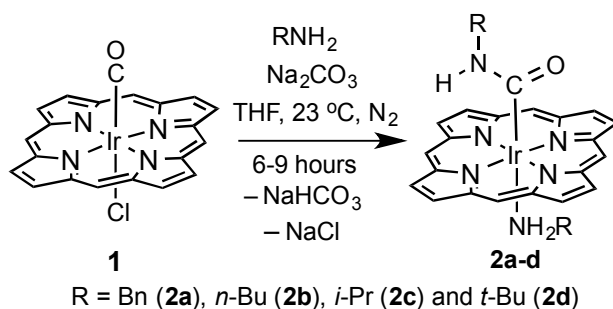
Despite the diversity of metal carbamoyl complexes that exist,¹¹⁻¹⁷ reports on the synthesis and isolation of metalloporphyrin carbamoyl complexes are rare. One example involves the formation of the carbamoyl complex, (TPP)Rh[C(O)NEt₂], from the reaction of (TPP)Rh(CO)Cl with LiNEt₂ in HNEt₂. Treatment of the Rh carbamoyl product with HCl reformed the starting chlorocarbonyl complex.¹⁸ In addition, octaethyl- and tetraphenylporphyrinato rhodium carbamoyl complexes, (OEP)Rh[C(O)NHR] and (TPP)Rh[C(O)NHR], were observed as trace products in reactions of bis(isocyanide) porphyrinato rhodium(III) complexes, [(OEP)Rh(CNR)₂]PF₆ and [(TPP)Rh(CNR)₂]PF₆ with nucleophiles, such as methanol, to form cationic rhodium diaminocarbene species, [(OEP)Rh{=C(NHR)₂}]PF₆ and [(TPP)Rh{=C(NHR)₂}]PF₆.¹⁹ Furthermore, Wayland and co-workers²⁰ isolated pentacoordinate carbamoyl complexes of rhodium octaethylporphyrin, (OEP)Rh[C(O)NHR], by treating [(OEP)Rh]₂ with CO and primary amines (eq 3). In this case, the reaction was proposed to proceed via a hydroxyaminocarbene complex, [(OEP)Rh=C(OH)NHR]⁺.



Although the isolation and characterization of the pentacoordinate octaethylporphyrinato rhodium carbamoyl complexes were described, the reactivities of these metalloporphyrin carbamoyl complexes were not explored. We report herein the syntheses, characterization, and reactivities of novel hexacoordinate porphyrinato iridium carbamoyl complexes.

Results and Discussion

Reactions of (TTP)Ir(CO)Cl with amines: Generally, carbonyl groups react with amines, to give carbamoyl ligands, when $\nu(\text{CO})$ is greater than 2000 cm^{-1} .^{5,6} The $\nu(\text{CO})$ value of (TTP)Ir(CO)Cl (2056 cm^{-1})²¹ suggested that the carbonyl ligand should be susceptible to nucleophilic attack. Thus, treatment of THF-solutions of (TTP)Ir(CO)Cl (**1**) with primary amines, at $23\text{ }^\circ\text{C}$, immediately resulted in a color change from red to brown. $^1\text{H-NMR}$ monitoring of the reactions revealed that product formation was complete within 3 min. Amine-coordinated iridium carbamoyl complexes, (TTP)Ir(NH₂R)[C(O)NHR], were isolated from the reaction mixtures in 73% to 94% yields (Scheme 2). Use of 2 equiv of the amine resulted in quantitative reactions, as monitored by NMR. In order to facilitate product isolation, both excess amine (up to 67 equiv) and excess sodium carbonate were needed. Without Na₂CO₃, work-up resulted in some contamination with (TTP)Ir(CO)Cl, presumably due to reversion of the reaction. Similar observations were reported in the syntheses of the carbamoyl complexes, *cis*-Mn(CNR)[C(O)NHMe](CO)₂(bipy) from fac-[Mn(CNR)(CO)₃(bipy)]⁺ and MeNH₂.¹⁷



Scheme 2. Syntheses of carbamoyl complexes (TTP)Ir(NH₂R)[C(O)NHR] (2a–d**). *Meso*-tolyl groups omitted.**

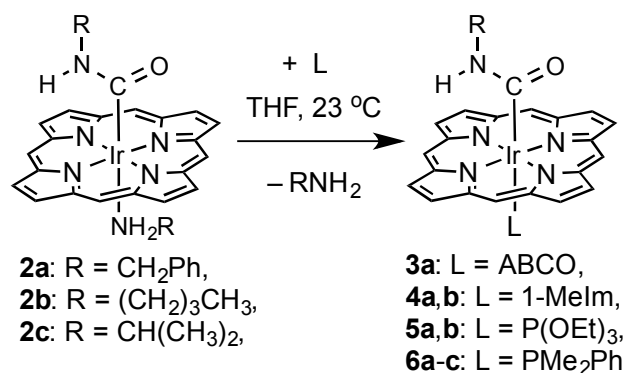
Formation of the carbamoyl complexes was readily followed spectroscopically, as evidenced by the replacement of the ^1H NMR β -pyrrole signal of (TTP)Ir(CO)Cl (**1**), with

the β -pyrrole signal of the corresponding carbamoyl products **2a-d**. The ^1H NMR spectra also showed upfield shifts for the carbamoyl and the *trans*-amine ligands, relative to the free amine chemical shifts. These upfield shifts of the axial ligand signals are attributed to the well-known ring current effect of the porphyrin macrocycle.^{22,19} For example, the methylene protons of free benzylamine resonate at 3.55 ppm, in C_6D_6 . In comparison, the methylene signal of the N-benzylcarbamoyl ligand in complex **2a** appeared as a two-proton doublet at 2.00 ppm, while the methylene protons of the *trans*-benzylamine in **2a** resonated at -1.78 ppm (2H, br), also in C_6D_6 . Generally, the proton signals of the amine ligand are shifted more upfield than those of the carbamoyl fragment, due to the closer proximity of the amine to the porphyrin macrocycle. This is illustrated by $(\text{TTP})\text{Ir}(\text{NH}_2^i\text{Pr})[\text{C}(\text{O})\text{NHPr}^i]$ (**2c**) in which the *i*-propyl methyl signal of the amine ligand resonated at -2.31 ppm, as compared to the *i*-propyl methyl signal of the carbamoyl ligand at -0.75 ppm.

At 26 °C, the amine proton signals in the carbamoyl compounds **2a-d** were notably broadened relative to all other signals (Fig. S1, S5, S7, and S9), suggesting that the amine ligand was labile. Cooling the NMR sample (in CDCl_3) to 0 °C resulted in a sharpening of these signals (Fig. S2). Further evidence of this lability was demonstrated by ^1H NMR experiments with added amine. When ~ 1.5 equiv of benzylamine was added to a C_6D_6 solution of **2a**, at 26 °C, the ^1H NMR spectrum exhibited broad methylene signals for both the coordinated (-1.78 ppm) and free (3.55 ppm) amines. When the temperature of the NMR sample was increased to 45 °C, these signals coalesced into the baseline. Restoring the sample temperature to 26 °C produced the original spectrum in which separate free and coordinated amine signals became visible again.

Ligand replacement reactions: The lability of the coordinated amines was further demonstrated by their ease of substitution at 23 °C, by the ligands L = quinuclidine (1-azabicyclo[2.2.2]octane, ABCO), 1-methylimidazole (1-MeIm), triethylphosphite [P(OEt)₃] and dimethylphenylphosphine (PMe₂Ph), leading to the isolation of the complexes (TTP)Ir(L)[C(O)NHR] (**3-6**) (Scheme 3). Benzylamine in (TTP)Ir(NH₂Bn)[C(O)NHBn] (**2a**) was completely displaced by 1 equiv. of 1-methylimidazole within 3 min. Coordination of the imidazole in complex (TTP)Ir(1-MeIm)[C(O)NHBn] (**4a**) was established by the appearance of sharp proton singlets at 0.43 (3H), 1.63 (1H), 1.74 (1H), and 3.70 ppm (1H), assigned to the methyl and ring protons of the bound 1-MeIm, which are upfield-shifted from 2.51 (methyl protons), 6.26, 6.99, and 7.22 ppm (ring protons), respectively, in the free 1-MeIm. The N-benzylcarbamoyl ligand remained bound to the metal center, as evidenced by ¹H NMR signals of the carbamoyl NH (-1.13 ppm, t) and CH₂ (2.07 ppm, d) in complex **4a**, which were downfield-shifted, in comparison with the carbamoyl NH and CH₂ proton signals (-1.34 ppm and 2.00 ppm respectively) of complex **2a**. In complex **6a**, the ³¹P NMR signal of PMe₂Ph shifted downfield from -46.61 ppm to -41.23 ppm upon coordination to iridium (Table 1). A similar downfield shift in the ³¹P NMR signal for phosphine ligand coordination to the rhodium tetraphenylporphyrin complex, (DPAP)₂Rh(III)TPP, where DPAP is diphenyl(phenylethynyl)phosphine, was observed earlier by Stulz and co-workers.²³ In contrast, coordination of P(OEt)₃ to Ir in **5a-b** resulted in a large upfield shift of the phosphite signal (Table 1). An analogous large upfield shift in the compound η-MeCp(CO)₂Mn(P(OEt)₃) was rationalized by metal d-electron back donation to the π-acid P(OEt)₃ ligand.²⁴

The ¹³C chemical shifts for the α-C of the carbamoyl ligands were readily assigned in the



Scheme 3. Substitution of amine ligands in (TTP)Ir(NH₂R)[C(O)NHR]. *Meso*-tolyl groups omitted.

Table 1. ³¹P NMR data^a for P(OEt)₃ and PMe₂Ph as free ligands and coordinated to carbamoyl complexes, (TTP)Ir(L)[C(O)NHR], L = P(OEt)₃ (**5a-b**); PMe₂Ph (**6a-c**).

³¹ P (δ) Free Ligand	(TTP)Ir(L)[C(O)NHR]	³¹ P (δ) Bound L
138.06 (P(OEt) ₃)	R = Bn (5a)	72.06
	R = ⁿ Bu (5b)	72.88
-46.61 (PMe ₂ Ph)	R = Bn (6a)	-41.23
	R = ⁿ Bu (6b)	-41.32
	R = ⁱ Pr (6c)	-41.27

^aWith C₆D₆ solution of PPh₃ (³¹P NMR δ: -5.53 ppm) as an external standard.

P(OEt)₃ and PMe₂Ph complexes (**5a-b** and **6a-c**, respectively), due to 2-bond ³¹P-¹³C coupling. For example, in **5a**, a low-field ¹³C doublet appeared at 162.72 ppm (²J_{P-C} = 270.3 Hz), while a low-field ¹³C doublet appeared at 163.87 ppm (²J_{P-C} = 184.2 Hz) for **6a** (Table 2).

Relative binding strengths of the ligands: A series of substitution reactions to determine the relative binding affinities of the BnNH₂, ABCO, 1-MeIm, and P(OEt)₃ ligands at the iridium center in the (TTP)Ir(L)[C(O)NHBn] complexes was monitored by ¹H NMR (eq 4). Equilibrium constants determined for ligand exchange reactions in C₆D₆ at 25 °C are

Table 2. ^{13}C NMR data^a for the $\alpha\text{-C}$ of the carbamoyl ligands in $(\text{TTP})\text{Ir}(\text{L})[\text{C}(\text{O})\text{NHR}]$, where $\text{L} = \text{P}(\text{OEt})_3$ (**5a-b**) and PMe_2Ph (**6a-c**)

Complex	R	δ Carbamoyl $\alpha\text{-C}$
5a	Bn	162.72 (d, $^2J_{\text{P-C}} = 270.3$ Hz)
5b	ⁿ Bu	162.73 (d, $^2J_{\text{P-C}} = 267.3$ Hz)
6a	Bn	163.87 (d, $^2J_{\text{P-C}} = 184.2$ Hz)
6b	ⁿ Bu	163.87 (d, $^2J_{\text{P-C}} = 182.7$ Hz)
6c	ⁱ Pr	163.39 (d, $^2J_{\text{P-C}} = 184.2$ Hz)

^aIn CDCl_3

listed in Table 3.

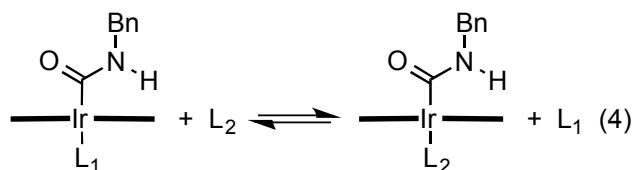


Table 3. Equilibrium constants for ligand exchange reactions involving $(\text{TTP})\text{Ir}(\text{L})[\text{C}(\text{O})\text{NHBn}]$ at 25 °C (eq 4).

Entry	L_1	L_2	K^a
1	BnNH_2	ABCO	9.4 ± 0.2
2	ABCO	BnNH_2	0.11 ± 0.01
3	MeIm	BnNH_2	0.06 ± 0.02
4	ABCO	MeIm	1.9 ± 0.1
5	MeIm	ABCO	0.58 ± 0.05
6	ABCO	$\text{P}(\text{OEt})_3$	14.4 ± 1.0
7	$\text{P}(\text{OEt})_3$	ABCO	0.07 ± 0.004
8	MeIm	$\text{P}(\text{OEt})_3$	5.7 ± 0.5
9	$\text{P}(\text{OEt})_3$	MeIm	0.18 ± 0.01

^aReactions were carried out in C_6D_6 , under air, with 1,3,5-mesitylene as an internal standard, and monitored by ^1H NMR (600 MHz).

The data in Table 3 show that $\text{P}(\text{OEt})_3$ is more strongly bound to the iridium than 1-MeIm, based on the values of the equilibrium constants shown in entries 8 and 9, and 1-

MeIm is more strongly bound to the metal center than ABCO, as indicated by the equilibrium constants in entries 4 and 5.

In general, the more basic amines (conjugate acid pKa values listed in parentheses) *n*-butylamine (10.59), benzylamine (9.34), *i*-propylamine (10.63), and *t*-butylamine (10.55)²⁵ were readily replaced by the less basic 1-MeIm (7.2),²⁶ P(OEt)₃ (3.31),²⁷ and PMe₂Ph (6.50).²⁷ Moreover, only 1 equiv of P(OEt)₃ or PMe₂Ph was required to completely displace 1-MeIm, from the Ir carbamoyl complexes, (TTP)Ir(1-MeIm)[C(O)NHR]. This indicates that factors other than the ligand basicity, such as π -acidity and softness, influence ligand binding. Thus, the d⁶ Ir(III) center, a soft acid²⁸ and electron rich π -donor, prefers 1-methylimidazole and phosphorus ligands (soft bases) over amines (hard bases). Other studies (see below) indicate that the order of neutral ligand binding to (TTP)Ir(L)[C(O)NHBn] decreases in the order: PMe₂Ph > P(OEt)₃ > 1-MeIm > ABCO > BnNH₂ >> Et₃N, PCy₃. The stronger binding of PMe₂Ph compared to P(OEt)₃ is based on the observation that 5 equivalents of P(OEt)₃ failed to displace PMe₂Ph from the carbamoyl complex **6a** at 23 °C. These results are in accord with the higher σ -donating ability of PMe₂Ph, relative to P(OEt)₃.²⁴ In addition to electronic factors, steric hindrance also influences the binding of axial ligands to the iridium center. The reaction with tricyclohexylphosphine, PCy₃, (pKa 9.70, cone angle 170°)²⁷ illustrates the importance of steric hindrance. When 1.5 equivalents of PCy₃ was added to a C₆D₆ solution of **2a** at 23°C, no reaction occurred after 12.5 hours, as monitored by ¹H NMR. Other less basic and less sterically hindered tertiary phosphines, such as P(*n*-Bu)₃ (pKa 8.43, cone angle 136°) and PPh₃ (pKa 2.73, cone angle 145°)²⁷ readily displaced BnNH₂ from complex **2a**. Steric bulk also affects the binding of amines. This was apparent during an attempt to replace the benzylamine ligand (cone angle 106°; pKa 9.34)^{25,29} in complex **2a**

with Et₃N (cone angle 150°; pK_a 10.65)^{25,29} in C₆D₆, at 23 °C. Although Et₃N is more basic than BnNH₂, no reaction was observed, even after heating the reaction at 90 °C for almost 9 hours with 2 equivalents of Et₃N. However, when an excess of the more basic but less sterically hindered tertiary amine, quinuclidine (pK_a 11.0°,³⁰ cone angle 132°²⁹), was added at ambient temperature, to a C₆D₆ solution of complex **2a**, complete displacement of BnNH₂ was observed, affording complex **3a**, in less than 7 minutes. All of these results indicate that both electronic and steric properties of the L ligand contribute to the overall trend in binding strengths in the (TTP)Ir(L)[C(O)NHBn] complexes.

The molecular structure for (TTP)Ir(1-MeIm)[C(O)NHBn] (**4a**) was solved by single-crystal X-ray diffraction analysis (Fig. 1). The benzyl group of the N-benzylcarbamoyl ligand [C(O)NHBn] is anti to the iridium. The sum of the angles at the carbonyl carbon, C(53), is 360.0°, consistent with a trigonal planar carbon atom. In addition, the N-benzylcar-

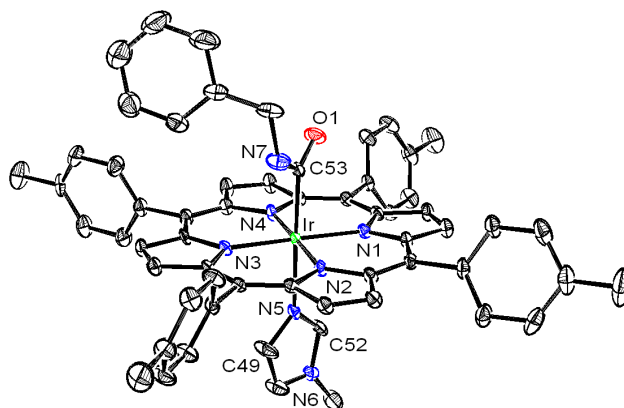


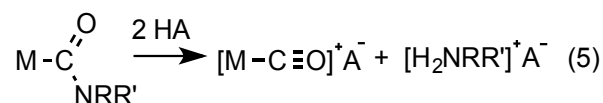
Figure 1. Molecular structure of (TTP)Ir(1-MeIm)[C(O)NHBn] (**4a**) with 30% probability ellipsoids. Selected bond distances (Å) and angles (deg): Ir-C(53) = 2.026(6), Ir-N(5) = 2.208(5), C(53)-O(1) = 1.217(7), C(53)-N(7) = 1.355(8); C(53)-Ir-N(5) = 178.86(19), N(3)-Ir-N(1) = 178.92(18), N(2)-Ir-N(4) = 178.44(18), O(1)-C(53)-N(7) = 119.0(6), O(1)-C(53)-Ir = 124.3(5), N(7)-C(53)-Ir = 116.7(4).

-bamoyl and the axial 1-MeIm ligands are collinear, with a C(53)-Ir-N(5) bond angle of 178.89(19). The C(53)-N(7) bond distance (1.355(8) Å) of the carbamoyl ligand is similar to

that of secondary organic amides, RC(O)NHR' (1.334 Å),³¹ and the C=O bond distance (1.217(7) Å) of the carbamoyl ligand is comparable to that of secondary organic amides (1.231 Å).³¹ The C(53)-N(7) bond distance (1.355(8) Å) of the carbamoyl ligand is also analogous to that (1.341(5) Å)²⁰ reported for the pentacoordinate rhodium complex, [(OEP)Rh[C(O)NH(C₆H₃Me₂)], and that (1.34(1) Å)³² for a hexacoordinate ruthenium biscarbamoyl complex [Ru(dppe)(CO)₂[C(O)NHCHMe₂]₂. However, the Ir-N(5) bond distance of 2.208(5) Å in the 1-methylimidazole complex is longer than that reported for Ir-NMe₃ in Ir(TTP)Cl(NMe₃) [2.174(2) Å]³³. The Ir-C(53) length of 2.026(6) Å is comparable to the Ir-C length reported for the pentacoordinate Ir(TTP)[C(O)Ph] [2.038(12) Å],³⁴ but is longer than the Rh-C bond length [1.988(5)] Å in (OEP)Rh[C(O)NH(C₆H₃Me₂)].²⁰

Reactions of the carbamoyl ligand with electrophiles

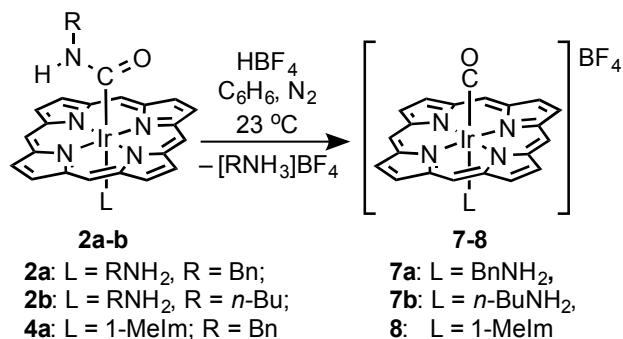
a. Reactions with HBF₄: Metal carbamoyl complexes generally react with acids to form metal carbonyl complexes, a process that also serves as a supporting test for the presence of a carbamoyl ligand⁴ (eq 5). When 2 equiv of HBF₄•Et₂O were added, at 23 °C, to benzene



solutions of the amine-coordinated carbamoyl complexes, (TTP)Ir(NH₂R)[C(O)NHR] (**2a-b**), the corresponding cationic amine-coordinated carbonyl complexes, [(TTP)Ir(NH₂R)(CO)]BF₄ (**7a-b**), were produced, as shown in Scheme 4. The carbonyl ligands of complexes **7a-b** exhibited CO stretching frequencies at 2075 and 2078 cm⁻¹, respectively.

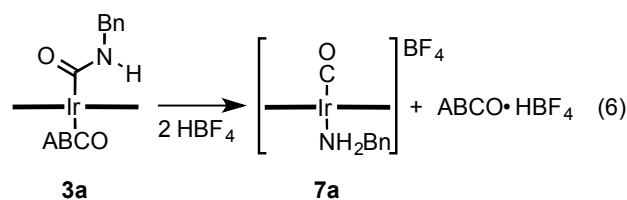
Characterization of complex **7a** was representative of these new cationic carbonyl compounds. A low-intensity peak at 138.96 ppm was assigned as the carbonyl ¹³C NMR

resonance (Fig. S33). This is similar to the assignment for the carbonyl of $[(\text{TTP})\text{Ir}(\text{CO})]\text{BF}_4$ (131.3 ppm) reported by Chan.³⁴ Moreover, the parent ion peak ($m/z = 996.3275$) observed by HRMS for $[(\text{TTP})\text{Ir}(\text{NH}_2\text{Bn})(\text{CO})]^+$, and satisfactory elemental analysis provided confirmation of the composition and purity of complex **7a**. This represents the second account of a cationic iridium porphyrinato carbonyl complex. The first report was for the ins-

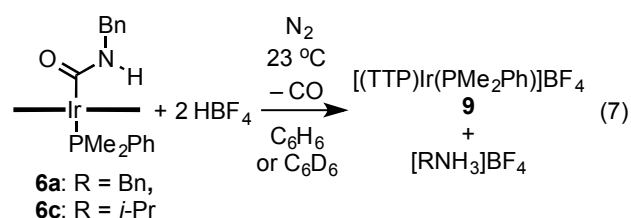


Scheme 4. Reaction of carbamoyl complexes $(\text{TTP})\text{Ir}(\text{L})[\text{C}(\text{O})\text{NHR}]$ (2-4) with HBF_4 . *Meso*-tolyl groups omitted.

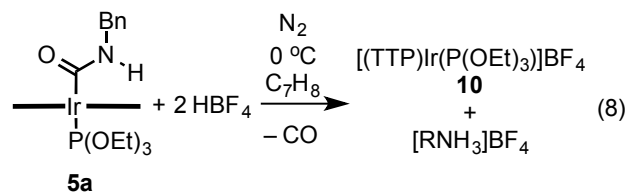
-eparable mixture of cations, $[(\text{TTP})\text{Ir}(\text{CO})]\text{BF}_4/[(\text{TTP})\text{Ir}]\text{BF}_4$, described by Chan and co-workers.³⁴ While a similar reaction between 2 equiv of $\text{HBF}_4 \cdot \text{Et}_2\text{O}$ and the 1-Melm-coordinated carbamoyl complex (**4a**) led to the formation of the cationic 1-Melm-coordinated carbonyl complex, $[(\text{TTP})\text{Ir}(1\text{-Melm})(\text{CO})]\text{BF}_4$ (**8**) (Scheme 4), the quinuclidine-coordinated carbamoyl complex (**3a**) reacted with acid (eq 6) to give the cationic benzylamine-coordinated carbonyl complex, $[(\text{TTP})\text{Ir}(\text{NH}_2\text{Bn})(\text{CO})]\text{BF}_4$ (**7a**), as the major porphyrin product (56%, by ¹H NMR), with the co-formation of a mixture of other unidentified porphyrin products. The formation of **7a**, and not $[(\text{TTP})\text{Ir}(\text{ABCO})(\text{CO})]\text{BF}_4$, is in accord with the higher basicity of quinuclidine over benzylamine, and its thermodynamic preference for the ammonium form.



In contrast to the reactions of the amine (**2a** and **b**) and 1-MeIm (**4a**) complexes, the ambient temperature reactions between excess $\text{HBF}_4 \cdot \text{Et}_2\text{O}$ (3-4 equiv) and each of the two PMe_2Ph -coordinated carbamoyl complexes, **6a** and **6c**, resulted in loss of the entire carbamoyl ligand, as monitored by IR and NMR. The formation of $[(\text{TTP})\text{Ir}(\text{PMe}_2\text{Ph})]\text{BF}_4$ (**9**) was observed by ^1H NMR in each case (eq 7). The appearance of **9** was manifested by a β -pyrrole proton signal at 8.83 ppm (in C_6D_6) and the upfield shift of the dimethyl resonance of the phosphine ligand from -2.66 ppm in the carbamoyl complex **6a**, to -2.90 ppm in **9**.



Moreover, the *ortho* and *meta* aryl proton signals of the phosphine ligand (in C_6D_6) were shifted upfield from 4.07 (2H) and 6.34 (2H) ppm, in **6a**, to 3.74 (2H) and 6.26 (2H) ppm, in **9**, respectively. Temperature was an important factor in the protonolysis of the $\text{P}(\text{OEt})_3$ -coordinated carbamoyl complex **5a**. When a C_6D_6 solution of **5a** was treated with 2 equivalents of $\text{HBF}_4 \cdot \text{Et}_2\text{O}$, at 23 °C, the formation of $[(\text{TTP})\text{IrP}(\text{OEt})_3]\text{BF}_4$ (**10**) was accompanied by 2 other unidentified porphyrin products (5.5% and 11.5%), none of which, contained a CO ligand, as revealed by IR analysis. However, when the same reaction was carried out in toluene at 0 °C, complex **10** was formed as the only porphyrin product (eq 8).

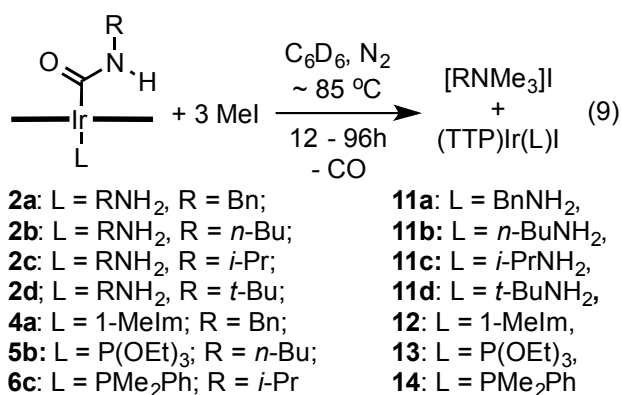


The failure of the phosphine-coordinated complexes **6a** and **6c** to form the cationic carbonyl complex, [(TTP)Ir(PMe₂Ph)(CO)]BF₄, is presumably due to the trans influence of the PMe₂Ph ligand. In an analogous case, the trans effect of PPh₃ was proposed as a reason for the failure to isolate phosphine-coordinated ruthenium(II) tetraarylporphyrinato carbonyl complexes, of the form (PR₃)Ru(II)(CO)(DPP), which were only observed in solution by IR spectroscopy.³⁵ Similarly, the π acidity of P(OEt)₃²⁴ may have contributed to the dissociation of the CO ligand (eq 8).

It is not clear whether complexes **9** and **10** are pentacoordinate with a non-coordinating counter anion or whether the BF₄⁻ is coordinating to the iridium metal center through a fluoride atom. Examples of metal-ligation by weakly-coordinating ligands such as BF₄⁻, SbF₆⁻ and PF₆⁻ have been studied by variable temperature solution NMR experiments.^{36,37} A bound BF₄ anion was established in *mer*-(*cis*-PMe₃)(*trans*-NO)(CO)₃W(μ -F)BF₃ through a ³¹P NMR doublet at 192 K, as a result of ³¹P-¹⁹F coupling. Upon warming a CD₂Cl₂ solution of the *mer*-(*cis*-PMe₃)(*trans*-NO)(CO)₃W(μ -F)BF₃ to 262 K, the doublet ³¹P NMR signal became a pentet, due to exchange of the four fluorine atoms of the BF₄⁻ into the bridging position.³⁶ However, solution ³¹P NMR spectra of [(TTP)Ir(PMe₂Ph)]BF₄ (**9**) acquired in CD₂Cl₂ at 223 K, 200 K, and 190 K, revealed only a ³¹P NMR singlet peak at -39.61 ppm. This suggests that the BF₄⁻ anion is not coordinated to the metal center in complex **9** or is rapidly dissociating on the NMR time scale.

b. Reactions with methyl iodide. When a C₆D₆ solution of a carbamoyl complex (**2a-d**, **4a**, **5b**, or **6c**) was heated to ~ 85 °C with 3-6 equiv of MeI for 12-96 h, the iodo complex, (TTP)Ir(L)I was produced as the main porphyrin product with purities ranging from 88 to 94% (eq 9), as identified by ¹H NMR. For example, the β-pyrrole signal of the *t*-butylamine-coordinated carbamoyl complex **2d**, at 8.88 ppm, was replaced by a new resonance at 8.94 ppm, upon formation of the iodo complex, (TTP)Ir(NH₂Bu^{*t*})I (**11d**). In addition, the complete loss of the proton resonances for the *t*-butylcarbamoyl ligand was observed. Of the amine-carbamoyl complexes (**2a-d**), the *n*-butyl analog (**2b**) reacted with MeI the fastest (12 hours), an indication that a less sterically bulky carbamoyl substituent increases the reaction rate.

In the reactions of **2a**, **2b** and **6c** with MeI, ammonium iodide co-products were detected in the precipitate from the reaction mixtures. For example, the only ammonium salt produced from the reaction of (TTP)Ir(PMe₂Ph)[C(O)NH^{*i*}Pr] (**6c**) with methyl iodide was identified as [*i*-PrNMe₃]I. This characterization was accomplished by comparing the ¹H NMR spectrum

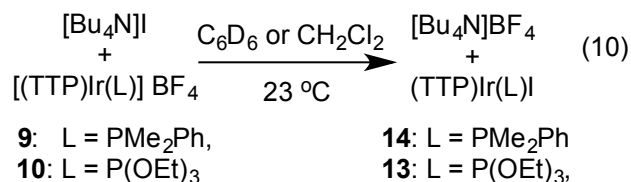


(in D₂O) and ¹³C NMR spectrum (in CDCl₃) of the precipitate from the reaction mixture with that of an authentic sample of [*i*-PrNMe₃]I (see Fig. S69-S70), prepared by treating (*i*-Pr)NMe₂ with a 2-fold excess of methyl iodide, at 23 °C. Similarly, [*n*-BuNMe₃]I was the only ammonium salt produced from the treatment of (TTP)Ir(NH₂^{*n*}Bu)[C(O)NH^{*n*}Bu] (**2b**)

with MeI. In the reaction of (TTP)Ir(NH₂Bn)[C(O)NHBn] (**2a**) with 2 equiv of MeI, three ammonium salts were identified, [BnNMe₃]I (66%), [BnNH₃]I (25%), and [Me(Bn)NH₂]I (9%). One-bond ¹³C-¹⁴N coupling was observed for the N-Me carbon atoms in the ¹³C NMR spectra of [BnNMe₃]I, [*n*-BuNMe₃]I, and [*i*-PrNMe₃]I. Similar coupling in the ¹³C NMR spectra of quaternary ammonium halide salts was reported earlier.^{38,39} Increasing the scale of reaction 9, up to three-fold, failed to provide cleanly isolable iodo products. However, complexes **13** and **14** were conveniently synthesized by an independent method (*vide infra*). Although the formation of the (TTP)Ir(L)I complexes could proceed via a transient [(TTP)Ir(L)CO]⁺ intermediate, treatment of a C₆D₆ solution of the cationic iridium carbonyl complex [(TTP)Ir(NH₂Bn)(CO)]BF₄ (**7a**) with [Bu₄N]I, for 3.5 hours under refluxing conditions resulted in a mixture that contained 63% (TTP)Ir(NH₂Bn)I (**11a**), 36% (TTP)Ir(CO)I³³ and 1% (TTP)Ir(NH₂Bn)[C(O)NHBn] (**2a**), as revealed by ¹H NMR, rather than pure **11a**.

Reactions of [(TTP)Ir(L)]BF₄ and [(TTP)Ir(L)CO]BF₄ with other ligands

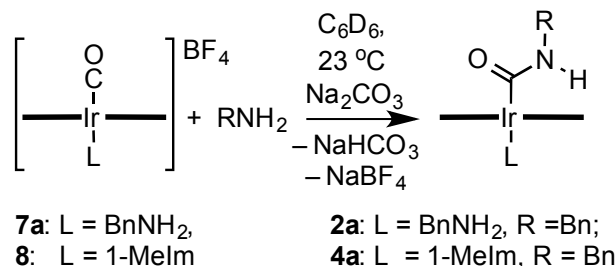
a. Reactions with [Bu₄N]I: Treatment of a CH₂Cl₂ solution of [(TTP)Ir(PMe₂Ph)]BF₄ (**9**) with ~ 2 equiv of [Bu₄N]I at 23 °C for 8 min, yielded the iodo complex **14** in 69% isolated yield (eq 10). The ¹H NMR spectrum (in C₆D₆) of (TTP)Ir(PMe₂Ph)I (**14**) exhibited a β-pyrrole proton resonance at 8.84 ppm and a doublet peak at -3.06 ppm for the methyl pro-



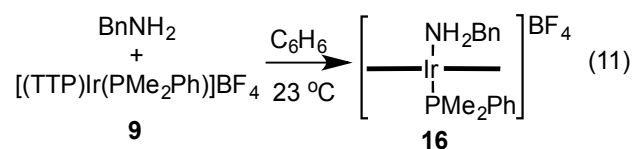
-tons of the coordinated PMe_2Ph . These spectral properties matched those for the product of the reaction of MeI with $(\text{TTP})\text{Ir}(\text{PMe}_2\text{Ph})[\text{C}(\text{O})\text{NHPr}^r]$ (**6c**) (eq 9). In addition, the ^{31}P NMR signal, for $(\text{TTP})\text{Ir}(\text{PMe}_2\text{Ph})\text{I}$ (**14**), appeared at -43.55 ppm, which is different from the ^{31}P NMR signal (-41.28 ppm) for $[(\text{TTP})\text{Ir}(\text{PMe}_2\text{Ph})]\text{BF}_4$ (**9**). Similarly, a 2.2-mg scale synthesis of the $\text{P}(\text{OEt})_3$ analogue (**13**), was carried out by treating a C_6D_6 solution of $[(\text{TTP})\text{Ir}(\text{P}(\text{OEt})_3)]\text{BF}_4$ (**10**) with ~ 3 equiv of $[\text{Bu}_4\text{N}]\text{I}$ (eq 10). The formation of $(\text{TTP})\text{Ir}[\text{P}(\text{OEt})_3]\text{I}$ (**13**) (43.5% isolated yield) was observed by ^1H NMR, as evidenced by the shifts of the CH_3 and CH_2 ^1H NMR signals (in C_6D_6) from -0.53 and 0.55 ppm to -0.38 and 0.70 ppm, respectively, in going from reactant **10** to product **13**. The ^{31}P NMR signal of the reactant **10** at 35.16 ppm, was also replaced by a signal at -0.01 ppm, upon formation of product, **13**. An independent synthesis was carried out by treating a benzene solution of $[(\text{TTP})\text{Ir}(\text{P}(\text{OEt})_3)(\text{NH}_2\text{Bn})]\text{BF}_4$ (**15**) with 5 equiv of $[\text{Bu}_4\text{N}]\text{I}$, resulting in a 49% isolated yield of $(\text{TTP})\text{Ir}[\text{P}(\text{OEt})_3]\text{I}$ (**13**).

b. Reactions of $[(\text{TTP})\text{Ir}(\text{L})\text{CO}]\text{BF}_4$ and $[(\text{TTP})\text{Ir}(\text{L})]\text{BF}_4$ with primary amines: The cationic CO complexes could be used in alternative syntheses of carbamoyl compounds. When C_6D_6 solutions of each of the cationic CO complexes **7a** and **8**, were treated with 1 equivalent of BnNH_2 , in the presence of Na_2CO_3 , the carbamoyl complexes **2a** and **4a**, were formed quantitatively (Scheme 5).

An amine Ir phosphine complex, $[(\text{TTP})\text{Ir}(\text{PMe}_2\text{Ph})(\text{NH}_2\text{Bn})]\text{BF}_4$ (**16**), was prepared by treatment of a C_6H_6 solution of phosphine complex **9** with BnNH_2 . After the reaction mixture was stirred, at 23 °C, for 30 minutes, complex **16** was isolated in 90 % yield (eq 11). The ^{31}P



Scheme 5. Reactions of [(TTP)Ir(L)CO]BF₄ (L = BnNH₂, **7a; L = 1-Melm, **8**) with primary amines RNH₂**



NMR signal for [(TTP)Ir(PMe₂Ph)(NH₂Bn)]BF₄ (**16**), which appeared at -41.49 ppm, was very similar to that of the starting complex [(TTP)Ir(PMe₂Ph)]BF₄ (**9**) (-41.28 ppm). However, the formulation of **16** was supported by the presence of an m/z peak at 1106.3899, corresponding to [16-BF₄]⁺, in the high-resolution mass spectrum. Moreover, the coordination of BnNH₂ in complex **16** was established by ¹H NMR spectroscopy, with the appearance, of upfield multiplet signals at -3.42 (2H) and -1.72 (2H) ppm, assigned to the NH₂ and CH₂ protons, respectively. In addition, a doublet at -3.17 ppm (6H, CH₃, ²J_{P-H} = 12 Hz) was assigned to the methyl protons of the PMe₂Ph ligand.

c. Reactions of [(TTP)Ir(PMe₂Ph)]BF₄ (9**) with PMe₂Ph:** The addition of 1.1 equiv of PMe₂Ph to a CDCl₃ solution of monophosphine complex [(TTP)Ir(PMe₂Ph)]BF₄ (**9**) resulted in a rapid reaction. The most notable change in the ¹H NMR spectrum, observed 10 minutes after initial addition of PMe₂Ph, was the replacement of the 6-H methyl doublet of the monophosphine ligand at -2.75 ppm with a 12-H virtual triplet at -2.77 ppm assigned to the bisphosphines in *trans*-[(TTP)Ir(PMe₂Ph)₂]BF₄ (**17**). This virtual coupling is diagnostic of a

trans arrangement of methylphosphines.⁴⁰⁻⁴⁴ The apparent J_{P-H} measured for **17** was 4.0 Hz and is similar to the values for the coupling constants in *trans*-PdI₂(PMe₂Ph)₂ (4.4 Hz), and, for the *trans*-PMe₂Ph ligands in IrCl₃(PMe₂Ph)₃ (4.5 Hz).⁴⁵ Analogous rhodium and ruthenium porphyrinato bisphosphine complexes have also been reported including [(DPAP)₂Rh^{III}(TPP)]I and (DPPA)₂Ru^{II}(DPP), where DPAP is diphenyl(phenylethynyl)phosphine and DPPA is bis(diphenylphosphino)acetylene.^{23,35} The composition of complex **17** was confirmed further by the m/z peak at 1137.3752 for [17-BF₄]⁺ by HRMS. The ³¹P NMR signal (in C₆D₆) for **17** (-32.35 ppm) was also markedly different from that for **9** (-41.28 ppm).

The molecular structure of **17** was confirmed by single-crystal X-ray diffraction (Fig. 2). The two axial PMe₂Ph ligands are collinear with a P(1)-Ir-P(2) bond angle of 179.20(11).

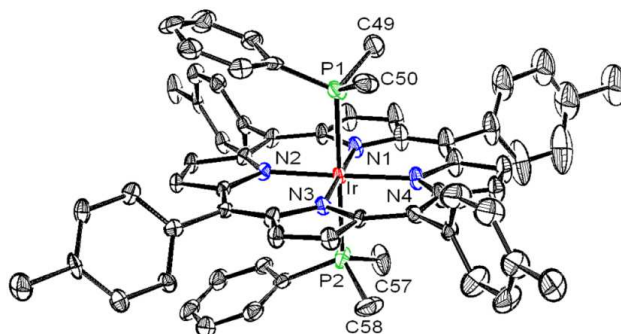


Figure 2. Molecular structure of *trans*-[(TTP)Ir(PMe₂Ph)₂]₂BF₄ (**17**) with 30% probability ellipsoids. Selected bond distances (Å) and angles (deg): Ir-P(1) = 2.354(3), Ir-P(2) = 2.348(3); P(1)-C(49) = 1.783(13), P(1)-C(50) = 1.800(12), P(1)-C(51) = 1.794(12), P(2)-C(57) = 1.822(13), P(2)-C(58) = 1.805(13), P(2)-C(59) = 1.808(12); P(1)-Ir-P(2) = 179.20(11).

The iridium-phosphorus bond distances of Ir-P(1) = 2.354(3) Å and Ir-P(2) = 2.348(3) Å are comparable to the Ir-P distances reported for non-porphyrinic mono-, bis-, tris- and tetrakisphosphino iridium complexes (2.2044 – 2.3927 Å).⁴⁶⁻⁵¹ However, the iridium-phosphorus bonds in complex **17** are both shorter than the Ir-P bond distance (2.537 Å)

reported for the porphyrinic iridium phosphine complex (OEP)Ir(C₃H₇)(PPh₃).⁵² This unusually long Ir-P bond length was attributed to the trans influence of the alkyl ligand, and to steric repulsion between the bulky PPh₃ ligand and the octaethylporphyrin ligand.

Conclusions

The reaction (Scheme 2) of (TTP)Ir(CO)Cl (**1**) with primary amines readily generates the amine-coordinated carbamoyl complexes, (TTP)Ir(NH₂R)[C(O)NHR], **2a-d**, under ambient conditions. A possible first step in the mechanism of this reaction is amine attack on the CO ligand to give a carbamoyl group (eq 1); such a reaction is expected, based on the high CO stretching frequency (2056 cm⁻¹) in **1**. Also supporting this step is the known reaction³³ of **1** with O-NMe₃ to give (TTP)Ir(Cl)(NMe₃) and CO₂, which presumably involves nucleophilic attack of O-NMe₃ on the CO ligand in **1**. This is a reaction typical of O-NMe₃ with CO ligands in a variety of metal carbonyl complexes.⁵³⁻⁵⁵ Following carbamoyl ligand formation in the first step, the Cl⁻ ligand could be rapidly substituted by an amine to give the (TTP)Ir(NH₂R)[C(O)NHR] product. Although this mechanism for the reactions of **1** with amines is entirely plausible, it is not possible to exclude an alternate pathway in which the first step involves amine substitution of the Cl⁻ ligand to give the cationic (TTP)Ir(NH₂R)(CO)⁺, which would be expected to react rapidly with amine to give the final carbamoyl product **2**.

The amine ligand in **2** is labile on the NMR timescale at 23 °C, allowing substitution with a variety of ligands. This has led to the preparation of phosphine-, phosphite-, 1-MeIm- and ABCO-coordinated (TTP)Ir(L)[C(O)NHR] carbamoyl complexes. Equilibrium studies of ligand displacement reactions of these complexes show that the binding affinities of the L

ligands decrease in the following order: $\text{PMe}_2\text{Ph} > \text{P}(\text{OEt})_3 > 1\text{-MeIm} > \text{ABCO} > \text{BnNH}_2 \gg \text{Et}_3\text{N}, \text{PCy}_3$. Reactions of these carbamoyl complexes $(\text{TTP})\text{Ir}(\text{L})[\text{C}(\text{O})\text{NHR}]$ with HBF_4 either at room temperature [for $\text{L} = \text{RNH}_2$ and 1-MeIm (Scheme 4) and $\text{L} = \text{PMe}_2\text{Ph}$ (eq 7)] or at $0\text{ }^\circ\text{C}$ [for $\text{L} = \text{P}(\text{OEt})_3$] (eq 8) give products that depend on the nature of the axial L ligand. When this ligand is an amine (**2a-b**, **4a**), the reactions produce cationic Ir carbonyl complexes of the form $[(\text{TTP})\text{Ir}(\text{L})(\text{CO})]\text{BF}_4$ (**7a-b**, **8**). With complexes containing phosphite (**5a**) or phosphine (**6a**, **6c**) ligands, treatment with HBF_4 results in complete loss of the carbamoyl ligand and production of complexes **9** and **10**, $[(\text{TTP})\text{Ir}(\text{L})]\text{BF}_4$, where L is PMe_2Ph or $\text{P}(\text{OEt})_3$ respectively. Reactions of MeI with all of the carbamoyl complexes require a higher temperature ($85\text{ }^\circ\text{C}$) and afford the neutral iodo complexes, $(\text{TTP})\text{Ir}(\text{L})\text{I}$ (**11a-d**, **12-14**), regardless of the L ligand. All of these results demonstrate that carbamoyl complexes of Ir(III) porphyrin complexes are easily formed and show a broad range of reactivity.

Experimental Section

All manipulations were performed under a dry nitrogen atmosphere, either in a glovebag, a glovebox, or using Schlenk techniques, except where otherwise stated. $\text{Ir}(\text{TTP})\text{Cl}(\text{CO})$ (**1**), was prepared according to a literature procedure⁵⁶. Benzylamine and isopropylamine were distilled from CaH_2 and stored over 4\AA molecular sieves prior to use. Dimethylphenylphosphine was stored in an inert-atmosphere glovebox. Tetrahydrofuran and toluene were deoxygenated and dried by passage through columns of reduced copper and alumina, respectively. All other chemicals were reagent grade and used without further purification. NMR spectra were collected using Varian VXR 300 MHz, Varian VXR 400

MHz, Bruker DRX 400 MHz, Varian MR 400 MHz and Bruker AVIII 600 MHz spectrometers. IR spectra were acquired in the solid state on NaCl salt plates, using a Bruker IFS66V FTIR instrument. ^1H NMR peak positions were referenced against residual proton resonances of deuterated solvents (δ , ppm: CDCl_3 , 7.26; C_6D_6 , 7.15; D_2O , 4.79), while ^{13}C NMR peaks were referenced to CDCl_3 (δ 77.36 ppm). When multiple porphyrin products were obtained in NMR-tube reactions, the purity of the major product was determined by the ratio of its β -pyrrole proton area to that of the total β -pyrrole integration. A solution of PPh_3 in C_6D_6 (^{31}P NMR δ : -5.53 ppm) was used as an external standard during ^{31}P NMR data collection.

(TTP)Ir(NH₂Bn)[C(O)NHBn] (2a): In a nitrogen-filled glove bag, a 100-mL round-bottomed flask, was charged with (TTP)Ir(CO)(Cl) (**1**) (91 mg, 0.099 mmol), Na_2CO_3 (682 mg, 6.43 mmol), a stir bar and 30 mL of THF. Benzylamine (610 μL , 5.6 mmol, 57 equiv) was added by syringe into the flask, the flask was capped with a rubber septum, and the mixture was stirred under N_2 for 6 hours. The reaction mixture was then opened to air, and solids were removed via filtration. Solvent and excess benzylamine were removed under reduced pressure. The residue was washed with 60 mL of hexanes, and **2a** was obtained. Yield: 87% (95 mg, 0.086 mmol). Anal. Calcd for $\text{C}_{63}\text{H}_{53}\text{IrN}_6\text{O}\cdot 0.7\text{H}_2\text{O}$: C, 67.87; H, 4.91; N, 7.54. Found: C, 67.90; H, 4.74; N, 7.37. ^1H NMR (299 K, 300 MHz, C_6D_6) δ : -5.14 (br, 2H, NH_2), -1.78 (br, 2H, amine- CH_2), -1.34 (t, 1H, $J = 6$ Hz, carbamoyl- NH), 0.41 (s, 1.40H, H_2O), 2.00 (d, 2H, $J = 6$ Hz, carbamoyl- CH_2), 2.38 (s, 12H, $-\text{C}_6\text{H}_4-\text{CH}_3$), 4.52 (br, 2H, amine- o -H), 5.27 (d, 2H, $J = 6$ Hz, carbamoyl- o -H), 6.22 (br, 2H, amine- m -H), 6.39 (br, 1H, amine- p -H), 6.79 (m, 3H, carbamoyl- m,p -H), 7.21 (dd, 4H, $J = 6$ Hz, 3 Hz, $-\text{C}_6\text{H}_4-\text{CH}_3$), 7.28

(dd, 4H, $J = 6$ Hz, 3 Hz, $-C_6H_4-CH_3$), 7.94 (dd, 4H, $J = 6$ Hz, 3 Hz, $-C_6H_4-CH_3$), 8.15 (dd, 4H, $J = 9$ Hz, 3 Hz, $-C_6H_4-CH_3$), 8.91 (s, 8H, pyrrole- H). 1H NMR (273 K, 400 MHz, $CDCl_3$) δ : -5.01 (t, 2H, $J = 8$ Hz, NH_2), -2.00 (t, 2H, $J = 8$ Hz, amine- CH_2), -1.83 (t, 1H, $J = 8$ Hz, carbamoyl- NH), 1.76 (d, 2H, $J = 8$ Hz, carbamoyl- CH_2), 2.68 (s, 12H, $-C_6H_4-CH_3$), 5.03 (d, 2H, 8 Hz amine- $o-H$), 5.17 (d, 2H, $J = 8$ Hz, carbamoyl- $o-H$), 6.52 (t, 2H, $J = 8$ Hz, amine- $m-H$), 6.65 (t, 1H, $J = 8$ Hz, amine- $p-H$), 6.83 (t, 2H, $J = 8$ Hz, carbamoyl- $m-H$), 6.93 (t, 1H, $J = 8$ Hz, carbamoyl- $p-H$), 7.49 (dd, 8H, $J = 16$ Hz, 8 Hz, $-C_6H_4-CH_3$), 7.85 (dd, 4H, $J = 8$ Hz, 4 Hz, $-C_6H_4-CH_3$), 7.99 (dd, 4H, $J = 8$ Hz, 4 Hz, $-C_6H_4-CH_3$), 8.62 (s, 8H, pyrrole- H). ^{13}C NMR (151 MHz, $CDCl_3$) δ : 21.87, 40.36, 41.64 (low intensity peak assigned by 2D HSQC), 122.91, 125.89, 126.03, 127.17, 127.47, 127.82, 127.84, 128.30, 128.60, 128.92, 131.83, 133.82, 134.68, 137.40, 139.19, 139.56, 142.80, 143.64 (CO Carbon). UV-vis (C_6H_6) λ_{max} nm (log ϵ): 414 (5.24), 521 (4.21). HRMS (+ESI): Calcd for $[MH]^+$ ($C_{63}H_{54}IrN_6O$) $^+$ m/z 1103.3988; found m/z 1103.3921.

(TTP)Ir(NH $_2$ n Bu)[C(O)NH n Bu] (2b): This compound was prepared similarly to **2a**, using complex **1**, (161 mg, 0.174 mmol), Na_2CO_3 (958 mg, 9.04 mmol), n -butylamine (960 μ L, 9.62 mmol, 55 equiv), and 40 mL of THF. Yield: 84.2% (152 mg, 0.147 mmol). 1H NMR (400 MHz, C_6D_6) δ : -5.79 (br, 2H, amine- NH_2), -2.80 (br, 2H, amine- αCH_2), -2.22 (br, 2H, amine- βCH_2), -1.68 (t, 1H, $J = 8$ Hz, carbamoyl- NH), -0.85 (m, 2H, amine- γCH_2), -0.41 (m, 2H, carbamoyl- βCH_2), -0.30 to -0.23 (m, 5H, amine- Me /carbamoyl- γCH_2), 0.17 (t, 3H, $J = 8$ Hz, carbamoyl- Me), 0.82 (m, 2H, carbamoyl- αCH_2), 2.38 (s, 12H, $-C_6H_4-CH_3$), 7.24 (d, 4H, $J = 8$ Hz, $-C_6H_4-CH_3$), 7.31 (d, 4H, $J = 8$ Hz, $-C_6H_4-CH_3$), 8.10 (d, 4H, $J = 8$ Hz, $-C_6H_4-CH_3$), 8.21 (d, 4H, $J = 8$ Hz, $-C_6H_4-CH_3$), 8.92 (s, 8H, pyrrole- H). ^{13}C NMR (151 MHz,

CDCl₃) δ : 12.74, 13.60, 18.43, 18.50, 21.87, 30.88, 30.92, 35.80, 37.11, 122.77, 127.50, 127.81, 131.67, 133.90, 134.60, 137.36, 139.38, 142.78, 144.35 (CO Carbon). UV-vis (C₆H₆) λ_{\max} nm (log ϵ): 414 (5.34), 521 (4.23). HRMS (+ESI): Calcd for [MH]⁺ (C₅₇H₅₈IrN₆O)⁺ m/z 1035.4301; found m/z 1035.4238

(TTP)Ir(NH₂^{*i*}Pr)[C(O)NH^{*i*}Pr] (2c): This compound was prepared similarly to **2a**, using complex **1**, (334 mg, 0.36 mmol), Na₂CO₃ (1.99 g, 19.0 mmol), *i*-propylamine (1.95 mL, 24.0 mmol, 67 equiv), and 80 mL of THF. Yield: 94% (340 mg, 0.34 mmol). Anal. Calcd for C₅₅H₅₃IrN₆O: C, 65.65; H, 5.31; N, 8.35. Found: C, 65.71; H, 5.05; N, 8.07. ¹H NMR (300 MHz, C₆D₆) δ : -5.74 (br, 2H, amine-NH₂), -2.48 (br, 1H, amine-CH), -2.31 (br, 6H, amine-Me), -1.99 (d, 1H, *J* = 6 Hz, carbamoyl-NH), -0.75 (d, 6H, *J* = 6 Hz, carbamoyl-Me), 1.59 (m, 1H, carbamoyl-CH), 2.38 (s, 12H, -C₆H₄-CH₃), 7.22 (d, 4H, *J* = 6 Hz, -C₆H₄-CH₃), 7.32 (d, 4H, *J* = 6 Hz, -C₆H₄-CH₃), 8.08 (dd, 4H, *J* = 6 Hz, 3 Hz, -C₆H₄-CH₃), 8.20 (dd, 4H, *J* = 6 Hz, 3 Hz, -C₆H₄-CH₃), 8.89 (s, 8H, pyrrole-H). ¹³C NMR (151 MHz, CDCl₃) δ : 21.47, 21.88, 22.10, 37.36, 39.39, 122.83, 127.48, 127.82, 131.69, 133.95, 134.55, 137.36, 139.38, 142.73. UV-vis (C₆H₆) λ_{\max} nm (log ϵ): 412 (5.27), 519 (4.17). HRMS (+ESI): Calcd for [MH]⁺ (C₅₅H₅₄IrN₆O)⁺ m/z 1007.3988; found m/z 1007.3916.

(TTP)Ir(NH₂^{*t*}Bu)[C(O)NH^{*t*}Bu] (2d): This compound was prepared similarly to **2a**, using complex **1** (152 mg, 0.164 mmol), Na₂CO₃ (899 mg, 8.48 mmol), *t*-butylamine (970 μ L, 9.05 mmol, 55.2 equiv), and 40 mL of THF. Yield: 72.8% (124 mg, 0.119 mmol). ¹H NMR (300 MHz, C₆D₆) δ : -5.35 (br, 2H, amine-NH₂), -2.17 (br s, 9H, amine-Me), -0.52 (s, 9H, carbamoyl-Me), 2.38 (s, 12H, -C₆H₄-CH₃), 7.24 (d, 4H, *J* = 6 Hz, -C₆H₄-CH₃), 7.32 (d,

4H, $J = 6$ Hz, $-C_6H_4-CH_3$), 8.12 (d, 4H, $J = 6$ Hz, $-C_6H_4-CH_3$), 8.20 (d, 4H, $J = 6$ Hz, $-C_6H_4-CH_3$), 8.88 (s, 8H, pyrrole- H). ^{13}C NMR (151 MHz, $CDCl_3$) δ : 21.89, 27.44, 27.81, 45.35, 48.04, 123.08, 127.49, 127.79, 131.74, 134.07, 134.42, 137.36, 139.36, 141.49 (CO Carbon), 142.76. UV-vis (C_6H_6) λ_{max} nm (log ϵ): 409 (5.31), 513 (4.30). HRMS (+ESI): Calcd for $[MH]^+$ ($C_{57}H_{58}IrN_6O$) $^+$ m/z 1035.4301; found m/z 1035.4220.

(TTP)Ir(ABCO)[C(O)NHBn] (3a): In a nitrogen-filled glove bag, a 20-mL scintillation vial was charged with complex **2a** (71 mg, 0.064 mmol), quinuclidine [ABCO] (112 mg, 1.0 mmol, 15.6 equiv), and 10 mL of C_6H_6 . After the mixture was stirred at 23 °C, for 20 min, volatile materials were removed under reduced pressure and the residues were washed with 50 mL of hexanes to remove free benzylamine. Additional treatment under reduced pressure at 85 °C for 2.5 days was needed to remove excess quinuclidine, to afford complex **3a**. Yield: 52% (37 mg, 0.034 mmol). 1H NMR (400 MHz, C_6D_6) δ : -2.73 (br t, 6H, $J = 8$ Hz, ABCO- NCH_2), -1.56 (t, 1H, $J = 8$ Hz, carbamoyl- NH), -0.8 (br, 6H, ABCO- CCH_2), -0.27 (br, 1H, ABCO- CH), 1.90 (d, 2H, $J = 8$ Hz, carbamoyl- CH_2), 2.37 (s, 12H, $-C_6H_4-CH_3$), 5.22 (d, 2H, $J = 8$ Hz, carbamoyl- oH), 6.77 (m, 3H, carbamoyl- m/pH), 7.20 (d, 4H, $J = 8$ Hz, $-C_6H_4-CH_3$), 7.32 (d, 4H, $J = 8$ Hz, $-C_6H_4-CH_3$), 7.92 (dd, 4H, $J = 8$ Hz, 4 Hz, $-C_6H_4-CH_3$), 8.20 (dd, 4H, $J = 8$ Hz, 4 Hz, $-C_6H_4-CH_3$), 8.87 (s, 8H, pyrrole- H). ^{13}C NMR (101 MHz, $CDCl_3$) δ : 17.94, 21.87, 24.20, 40.47, 43.73, 123.26, 125.89, 126.00, 127.36, 127.80, 127.83, 131.79, 134.00, 134.41, 137.37, 137.68, 139.26, 139.36, 142.78. UV-vis (C_6H_6) λ_{max} nm (log ϵ): 415 (5.19), 519 (4.19). HRMS (+ESI): Calcd for $[MH]^+$ ($C_{63}H_{58}IrN_6O$) $^+$ m/z 1107.4301; found m/z 1107.4299.

(TTP)Ir(1-MeIm)[C(O)NHBn] (4a): In air, a 20-mL scintillation vial was charged with complex **2a** (85 mg, 0.077 mmol), 1-methylimidazole (40 μ L, 0.50 mmol, 6.5 equiv), and 15 mL of THF. After the solution was stirred at 23 °C for 1 hour, volatile materials were removed under reduced pressure. Recrystallization was then done by adding hexanes to a concentrated THF solution of the dried product, to afford complex **4a**. Yield: 89% (74 mg, 0.069 mmol). Anal. Calcd for $C_{60}H_{50}IrN_7O \cdot 1.25H_2O$: C, 65.52; H, 4.81; N, 8.91. Found: C, 65.36; H, 4.35; N, 8.63. 1H NMR (300 MHz, C_6D_6) δ : -1.13 (t, 1H, $J = 6$ Hz, carbamoyl-NH), 0.40 (s, 1.40H, H_2O peak), 0.43 (s, 3H; 1-MeIm-Me), 1.63 (s, 1H, 1-MeIm-arylH), 1.74 (s, 1H, 1-MeIm-arylH), 2.07 (d, 2H, $J = 6$ Hz, carbamoyl- CH_2), 2.35 (s, 12H, $-C_6H_4-CH_3$), 3.70 (s, 1H, 1-MeIm-arylH), 5.32 (d, 2H, $J = 3$ Hz, carbamoyl-oH), 6.79 (m, 3H, carbamoyl-m/pH), 7.22 (d, 4H, $J = 9$ Hz, $-C_6H_4-CH_3$), 7.25 (d, 4H, $J = 9$ Hz, $-C_6H_4-CH_3$), 7.98 (d, 4H, $J = 9$ Hz, $-C_6H_4-CH_3$), 8.13 (d, 4H, $J = 9$ Hz, $-C_6H_4-CH_3$), 8.91 (s, 8H, pyrrole-H). ^{13}C NMR (151 MHz, $CDCl_3$) δ : 21.76, 32.93, 39.99, 117.76, 122.60, 122.98, 125.63, 125.92, 127.15, 127.60, 127.67, 131.35, 131.62, 133.74, 134.55, 137.06, 139.39, 139.78, 142.48, 146.83 (CO Carbon). UV-vis (C_6H_6) λ_{max} nm (log ϵ): 416 (5.23), 523 (4.22). HRMS (+ESI): Calcd for $[MH]^+$ ($C_{60}H_{51}IrN_7O$) $^+$ m/z 1078.3784; found m/z 1078.3780.

(TTP)Ir(1-MeIm)[C(O)NHⁿBu] (4b): This compound was prepared similarly to **4a**, using complex **2b** (40 mg, 0.037 mmol), 1-methylimidazole (20.5 μ L, 0.255 mmol, 6.9 equiv), and 10 mL of THF. Recrystallization was done by adding hexanes to a concentrated THF solution of the dried product, to afford complex **4b**. Yield: 98% (38 mg, 0.036 mmol). 1H NMR (300 MHz, C_6D_6) δ : -1.44 (t, 1H, $J = 6$ Hz, carbamoyl-NH), -0.35 (m, 2H, carbamoyl- βCH_2), -0.20 (m, 2H, carbamoyl- γCH_2), 0.20 (t, 3H, $J = 6$ Hz, carbamoyl- CH_3),

0.42 (s, 3H, 1-MeIm-*Me*), 0.89 (q, 2H, $J = 6$ Hz, carbamoyl- α CH₂), 1.63 (s, 1H, 1-MeIm-aryl*H*), 1.75 (s, 1H, 1-MeIm-aryl*H*), 2.36 (s, 12H, -C₆H₄-CH₃), 3.71 (s, 1H, 1-MeIm-aryl*H*), 7.25 (d, 8H, $J = 6$ Hz, -C₆H₄-CH₃), 8.16 (t, 8H, $J = 12$ Hz, -C₆H₄-CH₃), 8.92 (s, 8H, pyrrole-*H*). ¹³C NMR (151 MHz, CDCl₃) δ : 13.65, 18.54, 21.87, 30.98, 32.96, 35.66, 117.78, 122.65, 123.13, 127.30, 127.71, 131.40, 131.77, 133.98, 134.59, 137.17, 139.63, 142.61, 146.97 (CO Carbon). UV-vis (C₆H₆) λ_{\max} nm (log ϵ): 415 (5.31), 523 (4.22). HRMS (+ESI): Calcd for [MH]⁺ (C₅₇H₅₃IrN₇O)⁺ m/z 1044.3941; found m/z 1044.3933.

(TTP)IrP(OEt)₃[C(O)NHBn] (5a): In air, a 20-mL scintillation vial was charged with complex **2a** (85 mg, 0.077 mmol), triethylphosphite (70 μ L, 0.40 mmol, 5.2 equiv), and 15 mL of THF. After the solution was stirred at 23 °C for 40 minutes, volatile materials were removed under reduced pressure. After washing with hexanes, and further drying under reduced pressure, **5a** was obtained. Yield: 46% (42 mg, 0.036 mmol). ¹H NMR (400 MHz, C₆D₆) δ : -1.48 (t, 1H, $J = 8$ Hz, carbamoyl-NH), -0.18 (t, 9H, $J = 8$ Hz, PCH₂-*Me*), 0.85 (p, 6H, $J = 8$ Hz, PCH₂), 1.93 (d, 2H, $J = 8$ Hz, carbamoyl-CH₂), 2.38 (s, 12H, -C₆H₄-CH₃), 5.18 (d, 2H, $J = 8$ Hz, carbamoyl-*oH*), 6.77 (m, 3H, carbamoyl-*m,pH*), 7.21 (d, 4H, $J = 8$ Hz, -C₆H₄-CH₃), 7.33 (d, 4H, $J = 8$ Hz, -C₆H₄-CH₃), 7.96 (dd, 4H, $J = 8$ Hz, 4 Hz, -C₆H₄-CH₃), 8.20 (dd, 4H, $J = 8$ Hz, 4 Hz, -C₆H₄-CH₃), 8.93 (s, 8H, pyrrole-*H*). ¹³C NMR (151 MHz, CDCl₃) δ : 15.50 (d, $J = 4.5$ Hz), 21.77, 39.32 (d, $J = 4.5$ Hz), 56.66 (d, $J = 4.5$ Hz), 122.25, 125.64, 125.94, 127.17, 127.59, 127.65, 131.36, 133.89, 134.60, 137.07, 139.56, 139.61, 142.28, 162.72 (² $J_{P-C} = 270.3$ Hz, CO Carbon). ³¹P{¹H} NMR (162 MHz, C₆D₆) δ : 72.06 ppm. UV-vis (C₆H₆) λ_{\max} nm (log ϵ): 396 (5.07), 429 (4.75), 546 (3.96), 593 (3.80). HRMS (+ESI): Calcd for [MH]⁺ (C₆₂H₆₀IrN₅O₄P)⁺ m/z 1162.4012; found m/z 1162.4009.

(TTP)IrP(OEt)₃[C(O)NHⁿBu] (5b): This compound was prepared similarly to **5a**, using complex **2b** (41 mg, 0.040 mmol), triethylphosphite (36.0 μ L, 0.205 mmol, 5.1 equiv), and 10 mL of THF. Yield: 29% (13 mg, 0.012 mmol). ¹H NMR (400 MHz, C₆D₆) δ : -1.81 (t, 1H, $J = 4$ Hz, carbamoyl-NH), -0.48 (m, 2H, carbamoyl- β CH₂), -0.33 (m, 2H, carbamoyl- γ CH₂), -0.17 (t, 9H, $J = 8$ Hz, PCH₂-Me), 0.15 (t, 3H, $J = 8$ Hz, carbamoyl-Me), 0.74 (q, 2H, $J = 8$ Hz, 4 Hz, carbamoyl- α CH₂), 0.85 (p, 6H, $J = 8$ Hz, PCH₂), 2.38 (s, 12H, -C₆H₄-CH₃), 7.24 (d, 4H, $J = 8$ Hz, -C₆H₄-CH₃), 7.33 (d, 4H, $J = 8$ Hz, -C₆H₄-CH₃), 8.15 (dd, 4H, $J = 8$ Hz, 4 Hz, -C₆H₄-CH₃), 8.20 (dd, 4H, $J = 8$ Hz, 4 Hz, -C₆H₄-CH₃), 8.94 (s, 8H, pyrrole-H). ¹³C NMR (151 MHz, CDCl₃) δ : 13.61, 15.63 (d, $J = 4.5$ Hz), 18.50, 21.88, 30.94, 35.00 (d, $J = 4.5$ Hz), 56.69 (d, $J = 4.5$ Hz), 122.30, 127.33, 127.71, 131.41, 134.14, 134.65, 137.18, 139.82, 142.41, 162.73 (d, ²J_{P-C} = 267.3 Hz, CO Carbon). ³¹P {¹H} NMR (162 MHz, C₆D₆) δ : 72.88 ppm. UV-vis (C₆H₆) λ_{\max} nm (log ϵ): 398 (5.04), 410 (5.00), 432 (4.74) 528 (3.87), 592 (3.67). HRMS (+ESI): Calcd for [M-H+K] (C₅₉H₆₀IrN₅O₄PK)⁺ m/z 1165.3649; found m/z 1165.3747.

(TTP)Ir(PMe₂Ph)[C(O)NHBn] (6a): In a glovebox, a 20-mL scintillation vial was charged with complex **2a** (101 mg, 0.091 mmol), dimethylphenylphosphine (70 μ L, 0.49 mmol, 5.4 equiv), and 15 mL of THF. After the solution was stirred at 23 °C for 30 minutes, volatile materials were removed under reduced pressure. After washing with hexanes, and further drying under reduced pressure, **6a** was obtained. Yield: 45% (46 mg, 0.041 mmol). Anal. Calcd for C₆₄H₅₅IrN₅OP·2.5H₂O: C, 65.23; H, 5.13; N, 5.94. Found: C, 65.05; H, 4.82; N, 5.78. ¹H NMR (400 MHz, C₆D₆) δ : -2.66 (d, 6H, $J = 8$ Hz, PMe), -1.38 (t, 1H, $J = 8$ Hz, carbamoyl-NH), 0.44 (s, 5H, H₂O), 1.97 (d, 2H, $J = 8$ Hz, carbamoyl-CH₂), 2.40 (s, 12H, -

$C_6H_4-CH_3$), 4.07 (t, 2H, $J = 8$ Hz, *o*-PPh), 5.20 (d, 2H, $J = 8$ Hz, carbamoyl-*oH*), 6.34 (t, 2H, $J = 8$ Hz, *m*-PPh), 6.58 (t, 1H, $J = 8$ Hz, *p*-PPh), 6.76 (m, 3H, carbamoyl-*m/pH*), 7.20 (d, 4H, $J = 8$ Hz, $-C_6H_4-CH_3$), 7.37 (d, 4H, $J = 8$ Hz, $-C_6H_4-CH_3$), 7.92 (d, 4H, $J = 8$ Hz, $-C_6H_4-CH_3$), 8.02 (d, 4H, $J = 8$ Hz, $-C_6H_4-CH_3$), 8.80 (s, 8H, pyrrole-*H*). ^{13}C NMR (151 MHz, $CDCl_3$) δ : 5.34 (d, $J = 18.1$ Hz), 21.87, 39.62, 122.37, 125.75, 126.05, 126.41 (d, $J = 10.6$ Hz), 127.18 (d, $J = 7.6$ Hz), 127.24, 127.70, 127.76, 127.81, 130.94 (d, $J = 30.2$ Hz), 131.60, 133.97, 134.67, 137.26, 139.37, 139.80, 142.19, 163.87 (d, $^2J_{P-C} = 184.2$ Hz, CO Carbon). $^{31}P\{^1H\}$ NMR (162 MHz, C_6D_6) δ : -41.23 ppm. UV-vis (C_6H_6) λ_{max} nm (log ϵ): 398 (5.09), 419 (4.80), 440 (4.62), 548 (3.86), 601 (3.81). HRMS (+APCI): Calcd for $[MH]^+$ ($C_{64}H_{56}IrN_5OP$) $^+$ m/z 1134.3852; found m/z 1134.3852.

(TTP)Ir(PMe₂Ph)[C(O)NH^{*n*}Bu] (6b): This compound was prepared similarly to **6a**, using complex **2b** (48 mg, 0.046 mmol), dimethylphenylphosphine (33.0 μ L, 0.232 mmol, 5.0 equiv), and 8 mL of THF. Yield: 23.1% (12 mg, 0.011 mmol). 1H NMR (300 MHz, C_6D_6) δ : -2.66 (d, 6H, $J = 6$ Hz, *PMe*), -1.70 (t, 1H, $J = 6$ Hz, carbamoyl-*NH*), -0.44 (m, 2H, carbamoyl- βH), -0.30 (m, 2H, carbamoyl- γH), 0.15 (t, 3H, $J = 6$ Hz, carbamoyl-*Me*), 0.80 (m, 2H, carbamoyl- αH), 2.40 (s, 12H, $-C_6H_4-CH_3$), 4.07 (t, 2H, $J = 9$ Hz, *o*-PPh), 6.34 (t, 2H, $J = 9$ Hz, *m*-PPh), 6.58 (t, 1H, $J = 9$ Hz, *p*-PPh), 7.23 (d, 4H, $J = 6$ Hz, $-C_6H_4-CH_3$), 7.37 (d, 4H, $J = 6$ Hz, $-C_6H_4-CH_3$), 8.02 (d, 4H, $J = 6$ Hz, $-C_6H_4-CH_3$), 8.09 (d, 4H, $J = 6$ Hz, $-C_6H_4-CH_3$), 8.82 (s, 8H, pyrrole-*H*). ^{13}C NMR (151 MHz, $CDCl_3$) δ : 5.40 (d, $J = 18.1$ Hz), 13.60, 18.52, 21.88, 30.96, 35.14 (d, $J = 3.0$ Hz), 122.30, 126.43 (d, $J = 10.6$ Hz), 127.17 (d, $J = 7.6$ Hz), 127.29, 127.73, 131.21 (d, $J = 28.7$ Hz), 131.55, 132.05, 134.11, 134.60, 137.26, 139.51, 142.21, 163.87 (d, $^2J_{P-C} = 182.7$ Hz, CO Carbon). $^{31}P\{^1H\}$ NMR (162 MHz, C_6D_6) δ :

-41.32 ppm (s). UV-vis (C_6H_6) λ_{max} nm ($\log \mathcal{E}$): 401 (5.13), 410 (5.11), 451 (4.53), 522 (3.99), 599 (3.71). HRMS (+ESI): Calcd for $[MH]^+$ ($C_{61}H_{58}IrN_5OP$) $^+$ m/z 1100.4008; found m/z 1100.4028.

(TTP)Ir(PMe₂Ph)[C(O)NH^tPr] (6c): This compound was prepared similarly to **6a**, using complex **2c** (211 mg, 0.21 mmol), dimethylphenylphosphine (150 μ L, 1.1 mmol, 5.2 equiv), and 30 mL of THF. Yield: 59% (135 mg, 0.12 mmol). 1H NMR (400 MHz, C_6D_6) δ : -2.63 (d, 6H, $J = 8$ Hz, *PMe*), -1.98 (d, 1H, $J = 8$ Hz, carbamoyl-NH), -0.74 (d, 6H, $J = 4$ Hz, carbamoyl-Me), 1.61 (m, 1H, carbamoyl-CH), 2.40 (s, 12H, $-C_6H_4-CH_3$), 4.09 (t, 2H, $J = 8$ Hz, *o*-PPh), 6.35 (t, 2H, $J = 8$ Hz, *m*-PPh), 6.59 (t, 1H, $J = 8$ Hz, *p*-PPh), 7.21 (d, 4H, $J = 8$ Hz, $-C_6H_4-CH_3$), 7.37 (d, 4H, $J = 8$ Hz, $-C_6H_4-CH_3$), 8.04 (t, 8H, $J = 4$ Hz, $-C_6H_4-CH_3$), 8.81 (s, 8H, pyrrole-H). ^{13}C NMR (151 MHz, $CDCl_3$) δ : 5.48 (d, $J = 16.6$ Hz), 21.88, 22.22, 36.70, 122.23, 126.41 (d, $J = 9.1$ Hz), 127.14 (d, $J = 7.6$ Hz), 127.29, 127.72, 131.26 (d, $J = 28.7$ Hz), 131.52, 134.08, 134.63, 137.24, 139.51, 142.13, 163.39 ($^2J_{P-C} = 184.2$ Hz, CO Carbon). $^{31}P\{^1H\}$ NMR (162 MHz, C_6D_6) δ : -41.27 ppm (s). UV-vis (C_6H_6) λ_{max} nm ($\log \mathcal{E}$): 399 (5.20), 421 (4.76), 531 (3.82), 602 (3.76). HRMS (+ESI): Calcd for $[MH]^+$ ($C_{60}H_{56}IrN_5OP$) $^+$ m/z 1086.3852; found m/z 1086.3845.

[(TTP)Ir(CO)(NH₂Bn)]BF₄ (7a): In a nitrogen-filled glove bag, a 20-mL scintillation vial was charged with complex **2a** (51 mg, 0.047 mmol), 6 mL of C_6H_6 , and $HBf_4 \cdot Et_2O$ (11 μ L, 0.092 mmol, 2 equiv). After the solution was stirred at 23 °C for 20 minutes, the reddish porphyrin product solution was separated, via vacuum filtration, from the insoluble precipitate. Thereafter, volatile materials were removed from the filtrate under reduced

pressure. After recrystallization of the porphyrin product by adding excess hexanes to a concentrated benzene-solution of the dried product, **7a** was obtained. Yield: 36% (18 mg, 0.017 mmol). Anal. Calcd for $C_{56}H_{45}BF_4IrN_5O$: C, 62.10; H, 4.19; N, 6.47. Found: C, 62.03; H, 4.10; N, 6.29. 1H NMR (400 MHz, C_6D_6) δ : -2.98 (br, 2H, amine- NH_2), -1.89 (t, 2H, $J = 8$ Hz, amine- CH_2), 2.41 (s, 12H, $-C_6H_4-CH_3$), 4.76 (d, 2H, $J = 8$ Hz, amine- oH), 6.25 (t, 2H, $J = 8$ Hz, amine- mH), 6.39 (t, 1H, $J = 8$ Hz, amine- pH), 7.25 (d, 4H, $J = 8$ Hz, $-C_6H_4-CH_3$), 7.34 (d, 4H, 8 Hz, $-C_6H_4-CH_3$), 7.92 (d, 4H, $J = 8$ Hz, $-C_6H_4-CH_3$), 8.37 (d, 4H, $J = 8$ Hz, $-C_6H_4-CH_3$), 9.09 (s, 8H, pyrrole- H). ^{13}C NMR (151 MHz, $CDCl_3$) δ : 21.84, 40.52, 123.03, 125.77, 127.43, 127.80, 127.99, 128.40, 132.92, 133.08, 134.12, 134.98, 137.55, 138.48, 138.96 (CO Carbon), 141.63. IR (NaCl, cm^{-1}) ν ($C\equiv O$) = 2078 (s). UV-vis (C_6H_6) λ_{max} nm ($\log \epsilon$): 420 (5.33), 529 (4.33), 564 (3.73). HRMS (+ESI): Calcd for $[M-BF_4]^+$ ($[C_{56}H_{45}IrN_5O]^+$) m/z 996.3253; found m/z 996.3275.

[(TTP)Ir(CO)(NH₂ⁿBu)]BF₄ (7b**):** In a nitrogen-filled glove bag, 0.65 mL of C_6D_6 was added, via syringe, into an NMR tube containing complex **2b** (6.8 mg, 0.0066 mmol). The C_6D_6 -solution of **2b** was then treated with 2.8 μ L (0.024 mmol, 3.6 equiv) of $HBF_4 \cdot Et_2O$. After the complete consumption of **2b** (within 4 minutes), as monitored by 1H NMR, the reaction mixture was filtered through Celite® to remove insoluble precipitates. After volatile components were removed from the filtrate under reduced pressure, **7b** was obtained. Yield: 59% (4.1 mg, 0.0039 mmol; 94% pure by NMR) 1H NMR (300 MHz, C_6D_6) δ : -3.51 (br, m, 4H, amine- $NH_2/\alpha CH_2$), -1.69 (m, 2H, amine- βCH_2), -0.84 (m, 2H, amine- γH), -0.35 (t, 3H, $J = 6$ Hz, amine- Me), 2.40 (s, 12H, $-C_6H_4-CH_3$), 7.26 (d, 4H, $J = 6$ Hz, $-C_6H_4-CH_3$), 7.36 (d, 4H, $J = 6$ Hz, $-C_6H_4-CH_3$), 7.95 (dd, 4H, $J = 9$ Hz, $J = 3$ Hz, $-C_6H_4-CH_3$), 8.45 (dd,

4H, 9 Hz, 3 Hz, -C₆H₄-CH₃), 9.14 (s, 8H, pyrrole-*H*). ¹³C NMR (101 MHz, CDCl₃) δ: 12.30, 18.16, 21.93, 27.79, 36.77, 123.14, 127.90, 128.53, 132.97, 134.14, 135.09, 137.74, 138.60, 139.52 (CO Carbon), 141.75. IR (NaCl, cm⁻¹) ν (C≡O) = 2075 (s). UV-vis (CH₂Cl₂) λ_{max} nm (log ε): = 418 (5.64), 528 (4.45), 564 (3.83). HRMS (+ESI): Calcd for [M-BF₄]⁺ ([C₅₃H₄₇IrN₅O]⁺) m/z 962.3410; found m/z 962.3408.

[(TTP)Ir(CO)(1-MeIm)]BF₄ (8): This compound was prepared similarly to **7a**, using complex **4a** (33 mg, 0.031 mmol), 5 mL of C₆H₆, and HBF₄·Et₂O (7.4 μL, 0.062 mmol, 2 equiv). Recrystallization from CH₂Cl₂-hexanes afforded complex **8**. Yield: 58% (19 mg, 0.018 mmol; ¹H NMR (400 MHz, CDCl₃) δ: 0.19 (s, 1H, Im-*H*), 0.97 (s, 1H, Im-*H*), 2.19 (s, 3H, Im-*Me*), 2.73 (s, 12H, -C₆H₄-CH₃), 4.96 (s, 1H, Im-*H*), 7.62 (m, 8H, -C₆H₄-CH₃), 8.09 (m, 8H, -C₆H₄-CH₃), 9.06 (s, 8H, pyrrole-*H*). ¹³C NMR (101 MHz, CDCl₃) δ: 21.91, 34.13, 119.00, 120.33, 123.21, 128.13, 128.49, 129.95, 133.04, 134.38, 134.81, 137.42, 138.85, 139.65 (CO Carbon), 141.52. IR (NaCl, cm⁻¹) ν (C≡O) = 2079 (s). UV-vis (CH₂Cl₂) λ_{max} nm (log ε): UV-vis (CH₂Cl₂) λ_{max} nm (log ε): 416 (5.61), 528 (4.39), 564 (3.75). HRMS (+ESI): Calcd for [M-BF₄]⁺ ([C₅₃H₄₂IrN₆O]⁺) m/z 971.3049; found m/z 971.3050.

[(TTP)Ir(PMe₂Ph)]BF₄ (9): In a nitrogen-filled glove bag, a 20-mL scintillation vial was charged with complex **6a** (35 mg, 0.030 mmol), 6 mL of C₆H₆, and HBF₄·Et₂O (14.5 μL, 0.12 mmol, 4 equiv). After stirring at 23 °C for 20 minutes, the reaction mixture was decanted, to separate it from the precipitates. Volatile materials were then removed from the mother liquor under reduced pressure. Recrystallization by adding excess hexanes to a concentrated benzene-solution of the dried product, afforded the product **9**. Yield: 81% (27

mg, 0.024 mmol). ^1H NMR (400 MHz, CDCl_3) δ : -2.75 (d, 6H, $J = 12$ Hz, *PMe*), 2.71 (s, 12H, $-\text{C}_6\text{H}_4\text{-CH}_3$), 3.84 (m, 2H, *o*-PPh), 6.53 (t, 2H, $J = 8$ Hz, *m*-PPh), 6.96 (t, 1H, $J = 8$ Hz, *p*-PPh), 7.57 (t, 8H, $J = 8$ Hz, $-\text{C}_6\text{H}_4\text{-CH}_3$), 7.91 (d, 4H, $J = 8$ Hz, $-\text{C}_6\text{H}_4\text{-CH}_3$), 8.12 (d, 4H, $J = 8$ Hz, $-\text{C}_6\text{H}_4\text{-CH}_3$), 8.78 (s, 8H, pyrrole-*H*). ^{13}C NMR (151 MHz, CDCl_3) δ : 5.05 (d, $J = 45.3$ Hz), 21.90, 123.41, 125.90 (d, $J = 7.6$ Hz), 127.58, 127.71 (d, $J = 12.1$ Hz), 128.45, 130.43, 132.44, 133.64, 135.03, 138.17, 138.26, 142.27. $^{31}\text{P}\{^1\text{H}\}$ NMR (162 MHz, C_6D_6) δ : -41.28 ppm. UV-vis (CH_2Cl_2) λ_{max} nm (log ϵ): 414 (5.38), 520 (4.41), 551 (3.66). HRMS (+ESI): Calcd for $[\text{M-BF}_4]^+$ ($[\text{C}_{56}\text{H}_{47}\text{IrN}_4\text{P}]^+$) m/z 999.3168; found m/z 999.3141.

[(TTP)IrP(OEt)₃]BF₄ (10): A nitrogen-purged 5-mL round-bottomed flask containing a 1-mL toluene solution of complex **5a** (2.7 mg, 0.0023 mmol) at 0 °C, was charged with 0.8 μL of $\text{HBF}_4\cdot\text{Et}_2\text{O}$. While the solution was stirred at 0 °C for 3 minutes, the color of the reaction mixture quickly changed from brown-black to bright red. After volatile materials were removed under reduced pressure, the residues were washed by hexane, and further dried under reduced pressure to afford **10** (88%, 2.2 mg, 0.0020 mmol). ^1H NMR (400 MHz, C_6D_6) δ : -0.53 (t, 9H, $J = 8$ Hz, $\text{PCH}_2\text{-Me}$), 0.55 (p, 6H, $J = 8$ Hz, PCH_2), 2.42 (s, 12H, $-\text{C}_6\text{H}_4\text{-CH}_3$), 7.31 (d, 4H, 8 Hz, $-\text{C}_6\text{H}_4\text{-CH}_3$), 7.36 (d, 4H, 8 Hz, $-\text{C}_6\text{H}_4\text{-CH}_3$), 8.05 (d, 4H, $J = 8$ Hz, $-\text{C}_6\text{H}_4\text{-CH}_3$), 8.30 (d, 4H, $J = 8$ Hz, $-\text{C}_6\text{H}_4\text{-CH}_3$), 8.98 (s, 8H, pyrrole-*H*). $^{31}\text{P}\{^1\text{H}\}$ NMR (162 MHz, C_6D_6) δ : 35.16 ppm (s). HRMS (+ESI): Calcd. for $[\text{M-BF}_4]^+$ ($[\text{C}_{54}\text{H}_{51}\text{IrN}_4\text{O}_3\text{P}]^+$) m/z 1027.3328; found m/z 1027.3326.

(TTP)Ir(NH₂Bn)I (11a): In the glovebox, 0.65 mL of C_6D_6 was added to an NMR tube containing **2a** (6 mg, 0.0056 mmol). This was followed by the addition of 11 μL (0.011

mmol, 2 equiv) of a C₆D₆ stock solution containing 0.11 mM of MeI. The NMR tube was sealed with a rubber septum and heated at 85 °C for 72 hours, while monitored by ¹H NMR spectroscopy for the consumption of **2a**. The reaction mixture was filtered through Celite® to remove insoluble precipitates. Removal of volatile components from the filtrate under reduced pressure yielded **11a** (61%, 3.8 mg, 0.0035 mmol, 92% purity). ¹H NMR (300 MHz, C₆D₆) δ: -4.87 (t, 2H, *J* = 6 Hz, NH₂), -2.32 (t, 2H, *J* = 9 Hz, CH₂), 2.38 (s, 12H, -C₆H₄-CH₃), 4.21 (d, 2H, *J* = 6 Hz, amine-*oH*), 6.05 (t, 2H, *J* = 6 Hz, amine-*mH*), 6.28 (t, 1H, *J* = 6 Hz, amine-*pH*), 7.20 (d, 4H, *J* = 9 Hz, -C₆H₄-CH₃), 7.30 (d, 4H, *J* = 9 Hz, -C₆H₄-CH₃), 8.02 (d, 4H, *J* = 9 Hz, -C₆H₄-CH₃), 8.16 (d, 4H, *J* = 9 Hz, -C₆H₄-CH₃), 8.96 (s, 8H, pyrrole-*H*). ¹³C NMR (101 MHz, CDCl₃) δ: 21.89, 42.68, 122.95, 126.31, 127.48, 128.00, 128.11, 128.54, 132.32, 133.74, 134.37, 135.05, 137.62, 139.09, 142.89. UV-vis (C₆H₆) λ_{max} (log ε): 418 (5.42), 528 (4.27), 562 (3.65). HRMS (+ESI): Calcd for [M+H]⁺ ([C₅₅H₄₆IrN₅I])⁺ m/z 1096.2427; found m/z 1096.2448.

(TTP)Ir(NH₂ⁿBu)I (11b): This compound was prepared similarly to **11a** using **2b** (9 mg, (0.0084 mmol), 0.65 mL of C₆D₆, and 1.2 μL (0.019 mmol, 2.3 equiv) of MeI. The septum-sealed NMR tube was heated at 90 °C for 12 hours and monitored by ¹H NMR spectroscopy for the consumption of **2b**. Yield of **11b**: 51% (4.5mg, 0.0042 mmol 93% purity). ¹H NMR (300 MHz, C₆D₆) δ: -5.46 (br t, 2H, *J* = 6 Hz, NH₂), -3.46 (m, 2H, amine-αCH₂), -2.55 (m, 2H, βCH₂), -1.11 (m, 2H, γCH₂), -0.44 (t, 3H, *J* = 9 Hz, amine-*Me*), 2.38 (s, 12H, -C₆H₄-CH₃), 7.20 (d, 4H, *J* = 6 Hz, -C₆H₄-CH₃), 7.33 (d, 4H, *J* = 6 Hz, -C₆H₄-CH₃), 8.02 (dd, 4H, *J* = 6 Hz, 3 Hz, -C₆H₄-CH₃), 8.24 (dd, 4H, *J* = 9 Hz, 3 Hz, -C₆H₄-CH₃), 8.96 (s, 8H, pyrrole-*H*). ¹³C NMR (101 MHz, CDCl₃) δ: 12.38, 18.17, 21.89, 29.22, 38.20, 122.87, 127.47,

127.98, 132.20, 133.67, 135.03, 137.58, 139.15, 142.88. UV-vis (C_6H_6) λ_{max} ($\log \epsilon$): 418 (5.43), 528 (4.26), 562 (3.61). HRMS (+ESI): Calcd for $[M+H]^+$ ($[C_{52}H_{48}IrN_5I]^+$) m/z 1062.2584; found m/z 1062.2573.

(TTP)Ir(NH₂ⁱPr)I (11c): This compound was prepared similarly to **11b**, using complex **2c** (9 mg, 0.0086 mmol) of **2c**, 0.65 mL of C_6D_6 , and MeI (2.4 μ L, 0.039 mmol, 4.5 equiv). The reaction was heated at 90 °C for 55 hours while monitored by 1H NMR for the consumption of **2c**. Yield **11c**: 73% (6.6 mg, 0.0063 mmol, 90% purity). 1H NMR (300 MHz, C_6D_6) δ : -5.51 (d, 2H, $J = 6$ Hz, NH_2), -3.58 (m, 1H, amine- CH), -2.56 (d, 6H, $J = 6$ Hz, amine- Me), 2.38 (s, 12H, $-C_6H_4-CH_3$), 7.20 (d, 4H, $J = 9$ Hz, $-C_6H_4-CH_3$), 7.34 (d, 4H, $J = 9$ Hz, $-C_6H_4-CH_3$), 8.01 (dd, 4H, $J = 6$ Hz, 3 Hz, $-C_6H_4-CH_3$), 8.20 (dd, 4H, $J = 6$ Hz, 3 Hz, $-C_6H_4-CH_3$), 8.94 (s, 8H, pyrrole- H). ^{13}C NMR (101 MHz, $CDCl_3$) δ : 20.63, 21.88, 41.25, 122.89, 127.43, 127.96, 132.21, 133.76, 134.90, 137.56, 139.15, 142.87. UV-vis (C_6H_6) λ_{max} ($\log \epsilon$): 418 (5.40), 528 (4.24), 562 (3.60). HRMS (+ESI): Calcd for $[M+H]^+$ ($[C_{51}H_{46}IrN_5I]^+$) m/z 1048.2427; found m/z 1048.2407.

(TTP)Ir(NH₂ⁱBu)I (11d): This compound was prepared similarly to **11b**, using complex **2d** (9 mg, 0.0084 mmol), 0.65 mL of C_6D_6 , and MeI (1.8 μ L, 0.029 mmol, 3.5 equiv) of. The reaction was heated at 90 °C for 112 hours while monitored by 1H NMR for the consumption of **2d**. Yield **11d**: 64% (5.7 mg, 0.0054 mmol, 94% purity). 1H NMR (300 MHz, C_6D_6) δ : -5.25 (s, 2H, amine- NH_2), -2.62 (s, 9H, amine- Me), 2.38 (s, 12H, $-C_6H_4-CH_3$), 7.20 (d, 4H, $J = 9$ Hz, $-C_6H_4-CH_3$), 7.34 (d, 4H, $J = 9$ Hz, $-C_6H_4-CH_3$), 8.00 (dd, 4H, $J = 9$ Hz, 3 Hz, $-C_6H_4-CH_3$), 8.21 (dd, 4H, $J = 9$ Hz, 3 Hz, $-C_6H_4-CH_3$), 8.94 (s, 8H, pyrrole- H). UV-vis (CH_2Cl_2)

λ_{\max} (log ϵ): 418 (5.36), 528 (4.24), 562 (3.70). HRMS (+ESI): Calcd for $[M+H]^+$ ($[C_{52}H_{48}IrN_5I]^+$) m/z 1062.2584; found m/z 1062.2559.

(TTP)Ir(1-MeIm)I (12): In a glovebox, a 20-mL scintillation vial was charged with **4a** (27 mg, 0.025 mmol), 5 mL of C_6H_6 , and MeI (3.4 μ L, 0.055 mmol, 2.2 equiv). After refluxing the contents of the vial at 80 °C for 36 hours, the solution was vacuum-filtered through Celite® on a fritted funnel. After removal of volatile components from the filtrate under reduced pressure, followed by recrystallization of the residue from C_6H_6 -hexanes, **12** was obtained, in 88% purity, as determined by 1H NMR. Yield: 61% (16 mg, 0.015 mmol). 1H NMR (400 MHz, C_6D_6) δ : 0.16 (s, 3H, 1-MeIm-Me), 1.14 (t, 1H, $J = 4$ Hz, 1-MeIm-arylH), 1.28 (t, 1H, $J = 4$ Hz, 1-MeIm-arylH), 2.35 (s, 12H, $-C_6H_4-CH_3$), 3.39 (t, 1H, $J = 4$ Hz, 1-MeIm-arylH), 7.19 (dd, 4H, $J = 8$ Hz, 4 Hz, $-C_6H_4-CH_3$), 7.27 (d, 4H, $J = 8$ Hz, 4 Hz, $-C_6H_4-CH_3$), 8.06 (dd, 4H, $J = 8$ Hz, 4 Hz, $-C_6H_4-CH_3$), 8.17 (dd, 4H, $J = 8$ Hz, 4 Hz, $-C_6H_4-CH_3$), 8.97 (s, 8H, pyrrole-H). ^{13}C NMR (151 MHz, $CDCl_3$) δ : 21.88, 33.67, 117.61, 122.25, 122.72, 127.25, 127.86, 130.45, 131.86, 133.76, 135.02, 137.36, 139.44, 142.62. UV-vis (C_6H_6): λ_{\max} (log ϵ) 420 (5.38), 528 (4.27), 563 (3.71). HRMS (+ESI): Calcd for $[M]^+$ ($[C_{52}H_{42}IrN_6I]^+$) m/z 1070.2145; found m/z 1070.2162.

(TTP)Ir[P(OEt)₃]I (13): In air, a 20-mL scintillation vial was charged with 28 mg of crude (~60% pure) compound **15** (0.013 mmol), 6 mL of benzene, and 24.5 mg (0.065 mmol, 5 equiv) of $[Bu_4N]I$. The mixture was then stirred, at 23 °C, for 30 hours. The *n*-butyl ammonium salts were extracted from the organic layer, using water. After volatile components were removed under reduced pressure, followed by a hexane wash, complex **13**

was obtained. Yield: 49% (8 mg, 0.0065 mmol). ^1H NMR (400 MHz, C_6D_6) δ : -0.38 (t, 9H, $J = 8$ Hz, $\text{PCH}_2\text{-Me}$), 0.70 (p, 6H, $J = 8$ Hz, PCH_2), 2.38 (s, 12H, $-\text{C}_6\text{H}_4\text{-CH}_3$), 7.19 (d, 4H, $J = 8$ Hz, $-\text{C}_6\text{H}_4\text{-CH}_3$), 7.36 (d, 4H, $J = 8$ Hz, $-\text{C}_6\text{H}_4\text{-CH}_3$), 8.03 (dd, 4H, $J = 8$ Hz, 4 Hz, $-\text{C}_6\text{H}_4\text{-CH}_3$), 8.19 (dd, 4H, $J = 8$ Hz, 4 Hz, $-\text{C}_6\text{H}_4\text{-CH}_3$), 8.99 (s, 8H, pyrrole- H). ^{13}C NMR (151 MHz, CDCl_3) δ : 15.22 (d, $J = 6.0$ Hz), 21.87, 59.39 (d, $J = 7.6$ Hz), 122.80, 127.29, 127.96, 131.67, 133.75, 135.17, 137.45, 139.56, 142.29. $^{31}\text{P}\{^1\text{H}\}$ NMR (162 MHz, C_6D_6) δ : -0.01 ppm. UV-vis (CH_2Cl_2) λ_{max} nm (log ϵ): 370 (4.55), 433 (5.17), 539 (4.20), 576 (3.89). HRMS (+ESI): Calcd for $[\text{M-I}]^+$ ($[\text{C}_{54}\text{H}_{51}\text{IrN}_4\text{O}_3\text{P}]^+$) m/z 1027.3328; found m/z 1027.3302.

(TTP)Ir(PMe₂Ph)I (14): In air, a 20-mL scintillation vial was charged with complex **9** (34 mg, 0.031 mmol), $[\text{Bu}_4\text{N}]\text{I}$ (23.1 mg, 0.061 mmol, 2 equiv), and CH_2Cl_2 (5 mL). After stirring the mixture at 23 °C for 8 min, the *n*-butyl ammonium salts were extracted from the organic phase using water. Volatile components were then removed from the organic phase under reduced pressure. After washing with hexanes and drying under reduced pressure, complex **14** was obtained. Yield: 69% (24 mg, 0.021 mmol) Anal. Calcd for $\text{C}_{56}\text{H}_{47}\text{IrN}_4\text{PI}\cdot 0.12\text{C}_6\text{H}_{14}$: C, 59.95; H, 4.32; N, 4.93. Found: C, 60.25; H, 4.16; N, 4.79. ^1H NMR (400 MHz, C_6D_6) δ : -3.06 (d, 6H, $J = 8$ Hz, PMe), 0.89 (t, 0.73H, C_6H_{14}), 1.24 (m, 0.96H, C_6H_{14}), 2.40 (s, 12H, $-\text{C}_6\text{H}_4\text{-CH}_3$), 3.86 (m, 2H, $\text{PPh-}o\text{H}$), 6.23 (td, 2H, $J = 8$ Hz, 4 Hz, $\text{PPh-}m\text{H}$), 6.57 (m, 1H, $\text{PPh-}p\text{H}$), 7.18 (d, 4H, $J = 8$ Hz, $-\text{C}_6\text{H}_4\text{-CH}_3$), 7.39 (d, 4H, $J = 8$ Hz, $-\text{C}_6\text{H}_4\text{-CH}_3$), 7.95 (dd, 4H, $J = 8$ Hz, 4 Hz, $-\text{C}_6\text{H}_4\text{-CH}_3$), 8.04 (dd, 4H, $J = 8$ Hz, 4 Hz, $-\text{C}_6\text{H}_4\text{-CH}_3$), 8.84 (s, 8H, pyrrole- H). ^{13}C NMR (151 MHz, CDCl_3) δ : 3.69 (d, $J = 37.8$ Hz), 21.88, 122.93, 125.27 (d, $J = 55.9$ Hz), 126.36 (d, $J = 9.1$ Hz), 127.27, 127.42 (d, $J = 9.1$ Hz), 127.95, 129.55, 131.93, 133.66, 135.15, 137.52, 139.20, 142.05. $^{31}\text{P}\{^1\text{H}\}$ NMR (162

MHz, C₆D₆) δ : -43.55 ppm. UV-vis (C₆H₆): λ_{\max} nm (log \mathcal{E}) 385 (4.82), 439 (5.14), 545 (4.18), 582 nm (4.02). HRMS (+ESI): Calcd for [M-I]⁺ ([C₅₆H₄₇IrN₄P]⁺) m/z 999.3168; found m/z 999.3139.

[(TTP)Ir[P(OEt)₃](NH₂Bn)]BF₄ (15): In a nitrogen-filled glove bag, a 50-mL round-bottomed flask was charged with **5a** (53 mg, 0.046 mmol) and 25 mL of toluene. The flask was capped with a septum, then cooled to 0 °C. HBF₄·Et₂O (11 μ L, 0.093 mmol, 2.0 equiv) to the flask via a gas-tight syringe. While the solution was stirred at 0 °C for 3 min, the color of the reaction mixture quickly changed from brown-black to a red solution. The solution was then decanted from the precipitates and volatile components were removed from the mother liquor under reduced pressure to afford crude **15**. Yield: 90% (50 mg, 0.041 mmol, 59% purity). In air, a 20-mL scintillation vial was then charged with 17.6 mg of the crude compound **15** (0.014 mmol), 5 mL of dichloromethane, and 10 μ L (0.091 mmol, 6.5 equiv) of benzylamine. The reaction mixture was stirred, at 23 °C, for 10 min, then volatile components were removed under reduced pressure. After a hexane wash, and then further drying of the product under reduced pressure, 13.3 mg of **15** was obtained. Yield: 78% (13 mg, 0.011 mmol, 83% purity). ¹H NMR (400 MHz, C₆D₆) δ : -3.50 (m, 2H, NH₂), -1.78 (q, 2H, J = 4 Hz, CH₂-NH₂), -0.48 (t, 9H, J = 8 Hz, PCH₂-CH₃), 0.55 (p, 6H, J = 8 Hz, PCH₂), 2.42 (s, 12H, -C₆H₄-CH₃), 4.92 (d, 2H, J = 8 Hz, amine-*o*-H), 6.31 (t, 2H, J = 8 Hz, amine-*m*-H), 6.41 (t, 1H, J = 8 Hz amine-*p*-H), 7.34 (d, 4H, J = 8 Hz, -C₆H₄-CH₃), 7.37 (d, 4H, J = 8 Hz, -C₆H₄-CH₃), 8.08 (d, 4H, J = 8 Hz, -C₆H₄-CH₃), 8.41 (d, 4H, J = 8 Hz, -C₆H₄-CH₃), 9.01 (s, 8H, pyrrole-H). ¹³C NMR (101 MHz, CDCl₃) δ : 15.11 (d, J = 6.1 Hz), 21.90, 40.69 (d, J = 3.0 Hz), 60.09 (d, J = 9.1 Hz), 123.07, 125.95, 127.47, 127.94, 128.23, 128.35, 132.52,

134.11, 134.75, 138.27, 138.31, 138.41, 142.32. $^{31}\text{P}\{^1\text{H}\}$ NMR (162 MHz, C_6D_6) δ : 18.75 ppm. UV-vis (C_6H_6): λ_{max} ($\log \epsilon$) 420 (5.32), 529 (4.28), 562 nm (3.65). HRMS (+ESI): Calcd for $[\text{M-BF}_4]^+$ ($[\text{C}_{61}\text{H}_{60}\text{IrN}_5\text{O}_3\text{P}]^+$) m/z 1134.4063; found m/z 1134.4059.

[(TTP)Ir(PMe₂Ph)(NH₂Bn)]BF₄ (16): In air, a 20-mL scintillation vial was charged with complex **9** (30 mg, 0.028 mmol), benzylamine (7.5 μL , 0.068 mmol, 2.4 equiv), and 10 mL of C_6H_6 . After stirring the mixture at 23 °C for 30 minutes, volatile materials were removed under reduced pressure. Recrystallization of the residues from THF-hexanes afforded complex **16** (90%, 30 mg, 0.025 mmol). ^1H NMR (400 MHz, C_6D_6) δ : -3.42 (m, 2H, amine- NH_2), -3.17 (d, 6H, $J = 12$ Hz, PMe), -1.72 (m, 2H, amine- CH_2), 2.44 (s, 12H, - $\text{C}_6\text{H}_4\text{-CH}_3$), 3.64 (m, 2H, $\text{PPh-}o\text{H}$), 4.89 (d, 2H, $J = 8$ Hz, amine- $o\text{H}$), 6.17 (t, 2H, $J = 8$ Hz, $\text{PPh-}m\text{H}$), 6.25 (t, 2H, $J = 8$ Hz, amine- $m\text{H}$), 6.37 (t, 1H, $J = 8$ Hz, $\text{PPh-}p\text{H}$), 6.51 (t, 1H, $J = 8$ Hz, amine- $p\text{H}$), 7.32 (d, 4H, $J = 8$ Hz, - $\text{C}_6\text{H}_4\text{-CH}_3$), 7.41 (d, 4H, $J = 8$ Hz, - $\text{C}_6\text{H}_4\text{-CH}_3$), 7.95 (dd, 4H, $J = 8$ Hz, 4 Hz, - $\text{C}_6\text{H}_4\text{-CH}_3$), 8.34 (dd, 4H, $J = 8$ Hz, 4 Hz, - $\text{C}_6\text{H}_4\text{-CH}_3$), 8.86 (s, 8H, pyrrole- H). ^{13}C NMR (151 MHz, CDCl_3) δ : 4.90 (d, $J = 42.3$ Hz), 21.92, 41.37, 123.18, 125.15 (d, $J = 58.9$ Hz), 125.96, 126.06 (d, $J = 9.1$ Hz), 127.32, 127.71 (d, $J = 10.6$ Hz), 127.78, 128.13, 128.38, 130.00, 132.76, 133.97, 134.91, 135.15, 138.03, 138.29, 142.19. $^{31}\text{P}\{^1\text{H}\}$ NMR (162 MHz, C_6D_6) δ : -41.49 ppm. UV-vis (C_6H_6): λ_{max} ($\log \epsilon$) 419 (5.36), 528 (4.32), 561 nm (3.71). HRMS (+ESI): Calcd for $[\text{M-BF}_4]^+$ ($[\text{C}_{63}\text{H}_{56}\text{IrN}_5\text{P}]^+$) m/z 1106.3903; found m/z 1106.3899.

trans-[(TTP)Ir(PMe₂Ph)₂]BF₄ (17): In a glovebox, an NMR tube was charged with 20 mg (0.0185 mmol) of **9**, 1.0 mL of CDCl_3 and 2.9 μL (0.020 mmol, 1.1 equiv) of PMe_2Ph .

Analysis, by ^1H NMR, after 6.5 hours showed quantitative formation of **17**. After volatile components were removed under reduced pressure, compound **17** was obtained. Yield: 80% (18 mg, 0.015 mmol). ^1H NMR (400 MHz, CDCl_3) δ : -2.77 (t, 12H, $J = 4$ Hz, *PMe*), 2.73 (s, 12H, $-\text{C}_6\text{H}_4\text{-CH}_3$), 3.82 (m, 4H, *o*-PPh), 6.51 (t, 4H, $J = 8$ Hz, *m*-PPh), 6.91 (t, 2H, $J = 8$ Hz, *p*-PPh), 7.60 (d, 8H, $J = 8$ Hz, $-\text{C}_6\text{H}_4\text{-CH}_3$), 7.87 (d, 8H, $J = 8$ Hz, $-\text{C}_6\text{H}_4\text{-CH}_3$), 8.73 (s, 8H, pyrrole-*H*). ^{13}C NMR (151 MHz, CDCl_3) δ : 4.20 (t, $J = 16.6$ Hz), 21.89, 123.23, 125.34 (t, $J = 24.2$ Hz), 126.35 (t, $J = 4.5$ Hz), 127.80 (t, $J = 4.5$ Hz), 128.22, 129.86, 132.92, 134.33, 137.63, 138.66, 141.92. $^{31}\text{P}\{^1\text{H}\}$ NMR (162 MHz, C_6D_6) δ : -32.35 ppm. UV-vis (CH_2Cl_2) λ_{max} nm (log \mathcal{E}): 312 (sh, 4.13), 333 (sh, 4.33), 356 (4.50), 432 (5.21), 541 (4.14), 578 (4.09). HRMS (+ESI): Calcd for $[\text{M-BF}_4]^+$ ($[\text{C}_{64}\text{H}_{58}\text{IrN}_4\text{P}_2]^+$) m/z 1137.3766; found m/z 1137.3752.

[BnNMe₃]I: ^1H NMR (400 MHz, D_2O) δ : 3.08 (s, 9H, *N-Me*), 4.48 (s, 2H, *CH*₂), 7.53 – 7.59 (m, 5H, C_6H_5). ^{13}C NMR (101 MHz, CDCl_3): 53.29 (t, $^1J_{\text{C-N}} = 4$ Hz), 69.31 (t, $^1J_{\text{C-N}} = 2$ Hz), 127.42, 129.70, 131.37, 133.44. HRMS (+ESI): Calcd for $[\text{M-I}]^+$ ($[\text{C}_{10}\text{H}_{16}\text{N}]^+$) m/z 150.1283; found m/z 150.1281.

[*i*-PrNMe₃]I: ^1H NMR (400 MHz, D_2O): 1.38 (dt, 6H, *CH-Me*, $J = 8$ Hz, 4 Hz), 3.04 (s, 9H, *N-Me*), 3.64 (h, 1H, *CH*, $J = 8$ Hz). ^{13}C NMR (101 MHz, CDCl_3): 17.50, 51.64 (t, $^1J_{\text{C-N}} = 4$ Hz), 67.81.

[*n*-BuNMe₃]I: ^1H NMR (400 MHz, CDCl_3) δ : 1.03 (t, 3H, $J = 8$ Hz), 1.48 (m, 2H), 1.7 (m, 2H), 3.44 (s, 9H), 3.59 (m, 2H). ^{13}C NMR (101 MHz, CDCl_3) δ : 14.07, 19.93, 25.51,

54.18 (t, $^1J_{C-N} = 3$ Hz), 67.63 (t, $^1J_{C-N} = 3$ Hz). HRMS (+ESI): Calcd for $[M-I]^+$ ($[C_7H_{18}N]^+$)
m/z 116.1439; found m/z 116.1434.

General procedure for the determination of equilibrium constants: Stock solutions of each carbamoyl complex (**2a**, **3a**, **4a** and **5a**) were made in 5.0 mL of C_6H_6 , with concentrations ranging between 3.9 and 6.4 mM. Additional stock solutions of the free ligands were made in 5.0 mL of C_6D_6 . A single 5.0 ml C_6D_6 stock solution (91.7 mM) of mesitylene was used for the internal standard in all the reactions. A known volume of the carbamoyl complex solution was added to an NMR tube equipped with a high-vacuum Teflon stopcock, and the C_6H_6 was removed under reduced pressure. A known volume (typically 0.6 mL) of C_6D_6 was added to the solid carbamoyl complex, followed by either 10. μ L (0.92 μ mol) or 20. μ L (1.83 μ mol) of the internal standard solution. After analysis of the mixture by 1H NMR, the actual molarity of the metal carbamoyl complex was calculated from its β -pyrrole peak integration versus the mesitylene aliphatic proton peak integration. The actual molarity of the stock solution of each free ligand was similarly determined by the 1H NMR analysis of a mixture of a known volume of the ligand and internal standard. For the equilibrium measurements, a fresh volume of the free ligand solution, was transferred by syringe into the NMR tube containing a C_6D_6 solution of both the complex and the internal standard. Each reaction was then monitored by NMR, over a period of up to 1 h (Note that the reaction of **5a** with quinuclidine took 10 h to reach equilibrium). Concentrations of reactants and products were determined by 1H NMR analysis, monitored at 10 – 15 min intervals for each mixture.

X-ray crystal structure determination of complexes 4a and 17: X-ray quality crystals of (TTP)Ir(1-MeIm)[C(O)NHBn] (**4a**) and *trans*-[(TTP)Ir(PMe₂Ph)₂]BF₄ (**17**) were obtained by layering a saturated THF-solution of the complex with hexanes, and allowing the hexane to slowly diffuse into the THF solution at -21 °C over a period of 24 hours (for **4a**) and 10 days (for **17**).

A red needle-like single crystal of **4a** and brown plate-like crystal of **17** were selected under the microscope, and covered with PARATONE oil. The samples were mounted in a Bruker APEX2 diffractometer under a stream of cold nitrogen. Full sphere X-ray intensity data were measured to a resolution of 0.71 Å (0.5 deg. width ω -scan, 15 sec per frame, Mo K α radiation. $\lambda = 0.71073$ Å, graphite monochromator). The frames were integrated using a narrow-frame algorithm. Data were corrected for absorption effects using the multi-scan method.^{57,58} Structures were solved by direct methods. All non-hydrogen atoms were refined in a full-matrix anisotropic approximation based on F². All expected hydrogen atoms were placed on calculated positions and were refined in an isotropic approximation using a "riding" model. The $U_{\text{iso}}(\text{H})$ values were set at 1.2 - 1.5 times the U_{eq} value of the carrier atom. All calculations were performed using the APEX II Software Suite.⁵⁹

One molecule of **4a** and three THF solvent molecules were found in the asymmetric unit of the triclinic cell. Although additional THF molecules may partially occupy observed voids, attempts to apply SQUEEZE were not able to improve the refinement significantly. Thus, the original dataset was used for final results. Similarity constraints on geometrical parameters and on displacement parameters were used to treat solvent molecules.

Three chemically equivalent, but crystallographically non-equivalent molecules were observed in the structure refinement of **17**. One molecule, two halves of the same molecule

lying on an inversion center, two BF_4^- counter-ions (one of them disordered by two equivalent positions) and two solvent THF molecules were found in the asymmetric unit of the triclinic cell. Similarity constraints on geometrical parameters and on displacement parameters were used to obtain a reasonable molecular geometry and displacement coefficients for the atoms of the BF_4^- counter ions and THF solvent molecules.

References

- (1) Hartwig, J. F. *Organotransition Metal Chemistry: From Bonding to Catalysis*; University Science Books: Mill Valley, CA, 2010.
- (2) Doxsee, K. M.; Grubbs, R. H. *J. Am. Chem. Soc.* **1981**, *103*, 7696-7698.
- (3) Darensbourg, D. J.; Baldwin, B. J.; Froelich, J. A. *J. Am. Chem. Soc.* **1980**, *102*, 4688-4694.
- (4) Angelici, R. J. *Acc. Chem. Res.* **1972**, *5*, 335-337.
- (5) Darensbourg, D. J.; Darensbourg, M. Y. *Inorg. Chem.* **1970**, *9*, 1691-1694.
- (6) Angelici, R. J.; Blacik, L. J. *Inorg. Chem.* **1972**, *11*, 1754-1757.
- (7) Angelici, R. J.; Brink, R. W. *Inorg. Chem.* **1973**, *12*, 1067-1071.
- (8) McCusker, J. E.; Logan, J.; McElwee-White, L. *Organometallics* **1998**, *17*, 4037-4041.
- (9) McCusker, J. E.; Abboud, K. A.; McElwee-White, L. *Organometallics* **1997**, *16*, 3863-3866.
- (10) Aresta, M.; Giannecaro, P.; Tommasi, I.; Dibenedetto, A.; Lanfredi, A. M. M.; Ugozzoli, F. *Organometallics* **2000**, *19*, 3879-3889.
- (11) Huang, T. M.; Chen, J. T.; Lee, G. H.; Wang, Y. *Organometallics* **1991**, *10*, 175-179.
- (12) Fernandez, M. J.; Modrego, J.; Rodriguez, M. J.; Santamaria, M. C.; Oro, L. A. *J. Organomet. Chem.* **1992**, *441*, 155-158.
- (13) Liao, W. J.; Wang, Y. J.; Chen, J. D.; Lin, Y. C.; Liu, L. K. *J. Chin. Chem. Soc.* **1992**, *39*, 311-317.

- (14) Giannoccaro, P.; Tommasi, I.; Aresta, M. *J. Organomet. Chem.* **1994**, *476*, 13-18.
- (15) Anderson, S.; Cook, D. J.; Hill, A. F. *Organometallics* **1997**, *16*, 5595-5597.
- (16) Aballay, A.; Buono-Core, G. E.; Godoy, F.; Klahn, A. H.; Ibanez, A.; Garland, M. T. *J. Organomet. Chem.* **2009**, *694*, 3749-3752.
- (17) Ruiz, J.; Garcia, L.; Mejuto, C.; Perandonos, B. F.; Vivanco, M. *Organometallics* **2012**, *31*, 6420-6427.
- (18) Cohen, I. A.; Chow, B. C. *Inorg. Chem.* **1974**, *13*, 488-489.
- (19) Boschi, T.; Licoccia, S.; Paolesse, R.; Tagliatesta, P.; Pelizzi, G.; Vitali, F. *Organometallics* **1989**, *8*, 330-336.
- (20) Poszmik, G.; Carroll, P. J.; Wayland, B. B. *Organometallics* **1993**, *12*, 3410-3417.
- (21) Sugimoto, H.; Ueda, N.; Mori, M. *J. Chem. Soc., Dalton Trans.* **1982**, 1611-1615.
- (22) Djukic, J. P.; Young, V. G.; Woo, L. K. *Organometallics* **1994**, *13*, 3995-4003.
- (23) Stulz, E.; Scott, S. M.; Bond, A. D.; Otto, S.; Sanders, J. K. M. *Inorg. Chem.* **2003**, *42*, 3086-3096.
- (24) Golovin, M. N.; Rahman, M.; Belmonte, J. E.; Giering, W. P. *Organometallics* **1985**, *4*, 1981-1991.
- (25) Hall, H. K. *J. Am. Chem. Soc.* **1957**, *79*, 5441-5444.
- (26) Taoka, S.; Tu, C. K.; Kistler, K. A.; Silverman, D. N. *J. Biol. Chem.* **1994**, *269*, 17988-17992.
- (27) Liu, H. Y.; Eriks, K.; Prock, A.; Giering, W. P. *Organometallics* **1990**, *9*, 1758-1766.
- (28) Tsang, J. Y. K.; Chan, K. S. *Can. J. Chem.* **2011**, *89*, 1506-1511.
- (29) Seligson, A. L.; Trogler, W. C. *J. Am. Chem. Soc.* **1991**, *113*, 2520-2527.
- (30) Hext, N. M.; Hansen, J.; Blake, A. J.; Hibbs, D. E.; Hursthouse, M. B.; Shishkin, O. V.; Mascal, M. *J. Org. Chem.* **1998**, *63*, 6016-6020.
- (31) Allen, F. H.; Kennard, O.; Watson, D. G.; Brammer, L.; Orpen, A. G.; Taylor, R. *J. Chem. Soc., Perkin Trans. 2* **1987**, S1-S19.
- (32) Gargulak, J. D.; Gladfelter, W. L. *Inorg. Chem.* **1994**, *33*, 253-257.

- (33) Anding, B. J.; Ellern, A.; Woo, L. K. *Organometallics* **2012**, *31*, 3628-3635.
- (34) Song, X.; Chan, K. S. *Organometallics* **2007**, *26*, 965-970.
- (35) Stulz, E.; Maue, M.; Feeder, N.; Teat, S. J.; Ng, Y. F.; Bond, A. D.; Darling, S. L.; Sanders, J. K. M. *Inorg. Chem.* **2002**, *41*, 5255-5268.
- (36) Honeychuck, R. V.; Hersh, W. H. *Inorg. Chem.* **1989**, *28*, 2869-2886.
- (37) Hersh, W. H. *J. Am. Chem. Soc.* **1985**, *107*, 4599-4601.
- (38) Taylor, M. J.; Calvert, D. J.; Hobbs, C. M. *Magn. Reson. Chem.* **1988**, *26*, 619-621.
- (39) Liu, A. T.; Nag, M.; Carroll, W. R.; Roberts, J. D. *Magn. Reson. Chem.* **2013**, *51*, 701-704.
- (40) Crabtree, R. H. In *The Organometallic Chemistry of the Transition Metals*; John Wiley & Sons, Inc.: 2005, p 235-273.
- (41) Bancroft, G. M.; Libbey, E. T. *Can. J. Chem.* **1973**, *51*, 1482-1484.
- (42) Brookes, P. R.; Shaw, B. L. *J. Chem. Soc. A* **1967**, 1079-1084.
- (43) Shaw, B. L.; Smithies, A. C. *J. Chem. Soc. A* **1968**, 2784-2787.
- (44) Haines, L. M. *Inorg. Chem.* **1971**, *10*, 1685-1692.
- (45) Jenkins, J. M.; Shaw, B. I. *Proc. Chem. Soc. London* **1963**, 279.
- (46) Yamamoto, Y.; Sugawara, K.; Kakeya, M. *Inorg. Chim. Acta* **2002**, *340*, 21-28.
- (47) Dube, T.; Faller, J. W.; Crabtree, R. H. *Inorg. Chem.* **2002**, *41*, 5561-5565.
- (48) Dutta, D. K.; Deb, B.; Sarmah, B. J.; Woollins, J. D.; Slawin, A. M. Z.; Fuller, A. L.; Randall, R. A. M. *Eur. J. Inorg. Chem.* **2011**, 835-841.
- (49) Xu, C.; Dong, X. M.; Wang, Z. Q.; Hao, X. Q.; Li, Z.; Duan, L. M.; Ji, B. M.; Song, M. *P. J. Organomet. Chem.* **2012**, *700*, 214-218.
- (50) Souza, F. E. S.; Nguyen, P.; Marder, T. B.; Scott, A. J.; Clegg, W. *Inorg. Chim. Acta* **2005**, *358*, 1501-1509.
- (51) Langer, J.; Imhof, W.; Fabra, M. J.; Garcia-Orduna, P.; Górls, H.; Lahoz, F. J.; Oro, L. A.; Westerhausen, M. *Organometallics* **2010**, *29*, 1642-1651.

- (52) Kadish, K. M.; Cornillon, J. L.; Mitaine, P.; Deng, Y. J.; Korp, J. D. *Inorg. Chem.* **1989**, *28*, 2534-2542.
- (53) Shvo, Y.; Hazum, E. *J. Chem. Soc., Chem. Commun.* **1975**, 829-830.
- (54) Kelly, A. M.; Rosini, G. P.; Goldman, A. S. *J. Am. Chem. Soc.* **1997**, *119*, 6115-6125.
- (55) Shen, J. K.; Gao, Y. C.; Shi, Q. Z.; Basolo, F. J. *Organomet. Chem.* **1991**, *401*, 295-303.
- (56) Yeung, S. K.; Chan, K. S. *Organometallics* **2005**, *24*, 6426-6430.
- (57) Blessing, R. H. *Acta Crystallogr., Sect. A* **1995**, *51*, 33-38.
- (58) Sheldrick, G. M. *Acta Crystallogr., Sect. A* **2008**, *64*, 112-122.
- (59) *APEX2 Version 4.1* and *APEX2 Version 4.1*; Bruker AXS Inc., Madison, WI, USA, 2013.

Supporting Information

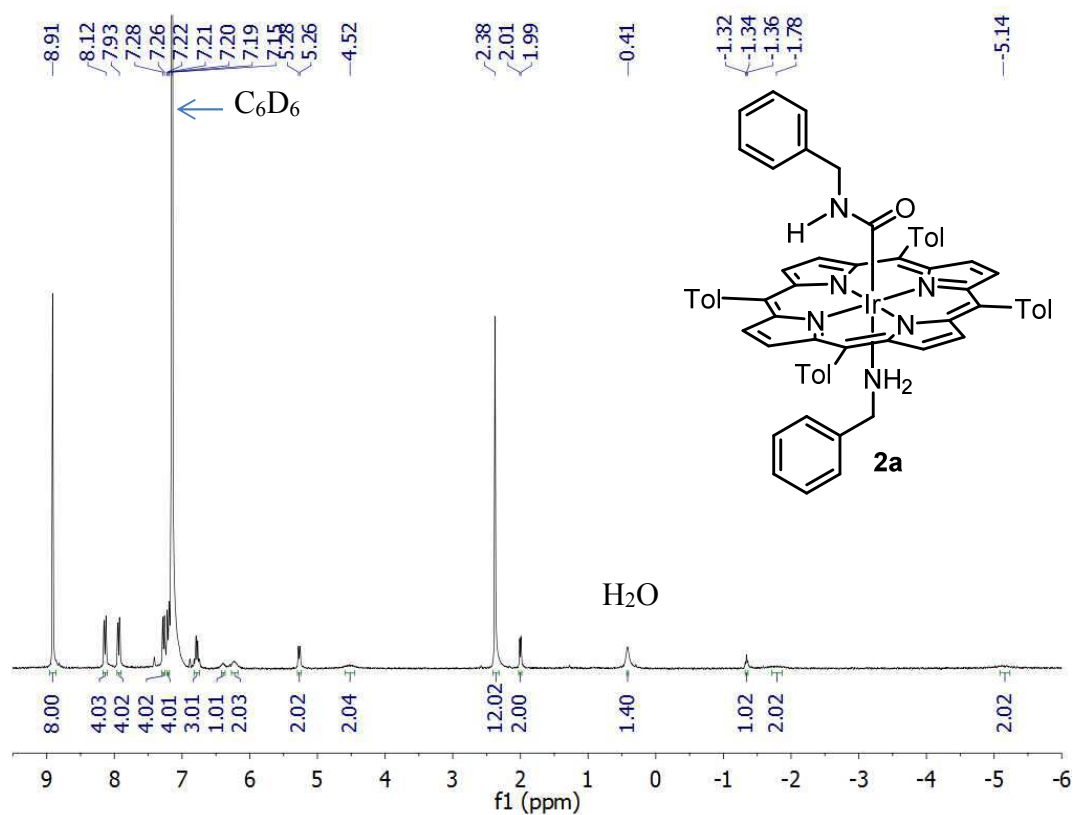


Fig. S1. ^1H NMR spectrum for (TTP)Ir(NH₂Bn)[C(O)NHBn] (**2a**) in C₆D₆ at 299 K

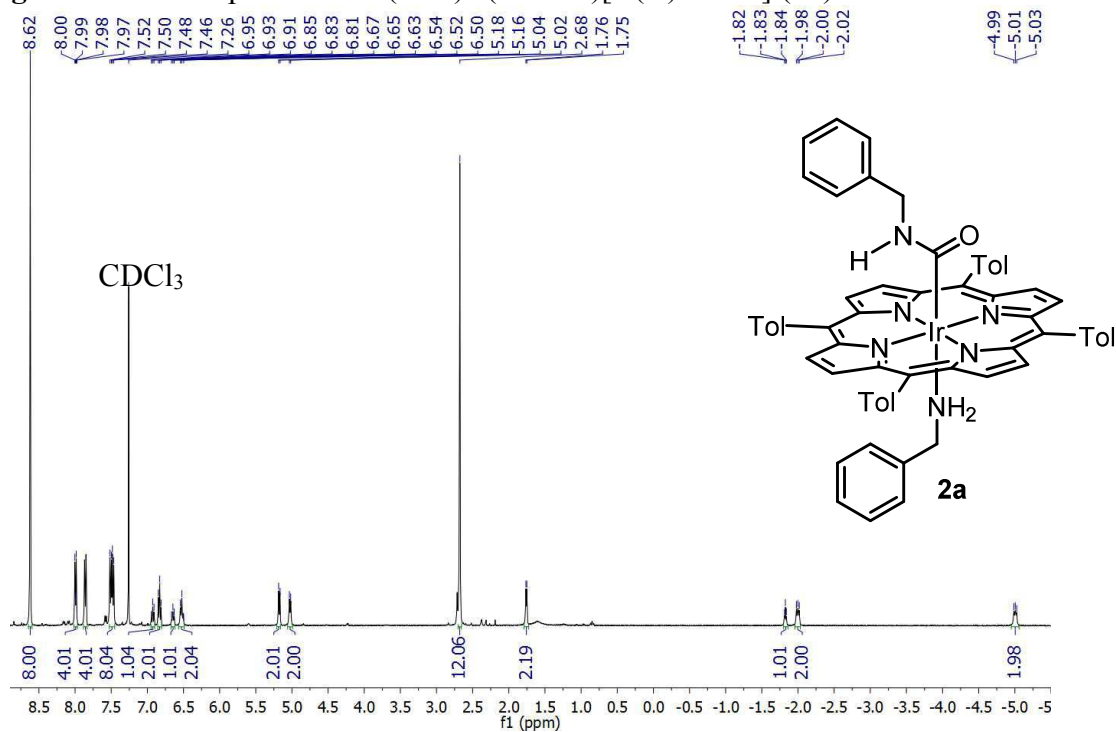


Fig. S2. ^1H NMR spectrum for (TTP)Ir(NH₂Bn)[C(O)NHBn] (**2a**) in CDCl₃ at 273 K

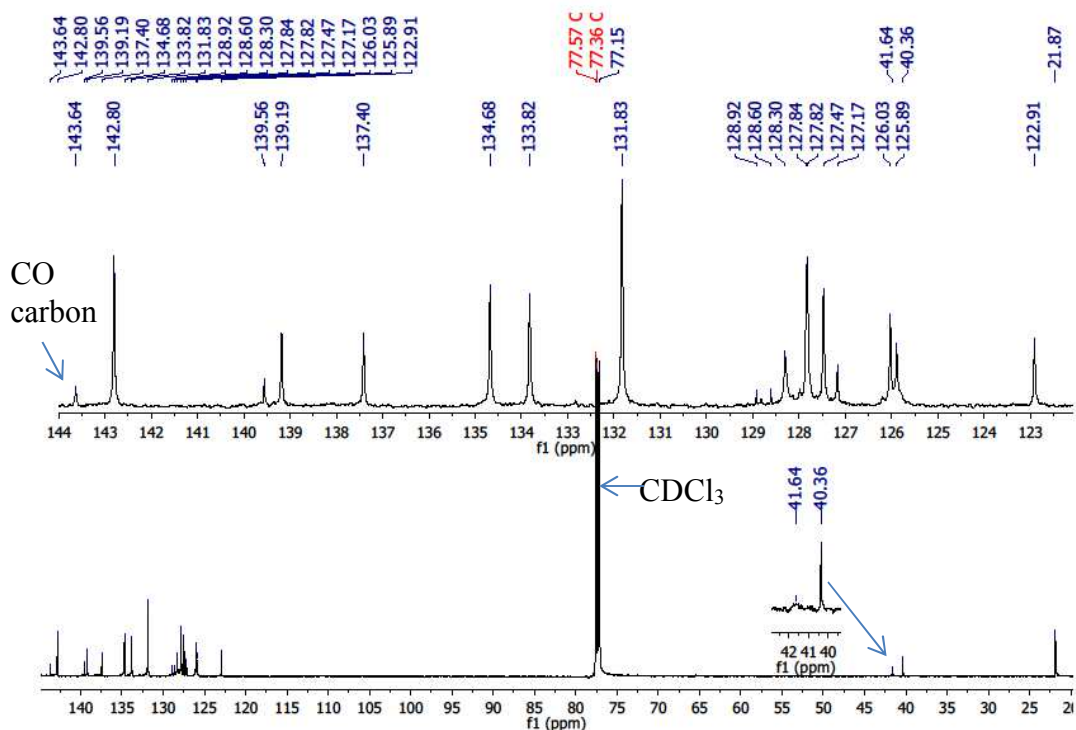


Fig. S3. ^{13}C NMR spectrum for $(\text{TTP})\text{Ir}(\text{NH}_2\text{Bn})[\text{C}(\text{O})\text{NHBn}]$ (**2a**) in CDCl_3

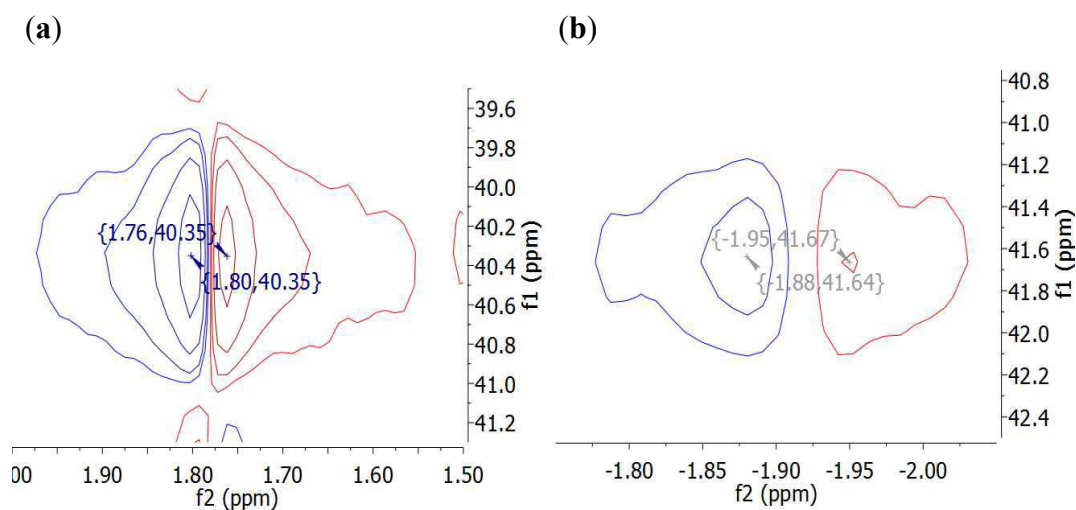


Fig. S4. Partial 2D gHSQC spectrum for $(\text{TTP})\text{Ir}(\text{NH}_2\text{Bn})[\text{C}(\text{O})\text{NHBn}]$ (**2a**) in CDCl_3 showing correlations for: (a) ^1H and ^{13}C signals of carbamoyl- CH_2 , (b) ^1H and ^{13}C signals of amine- CH_2

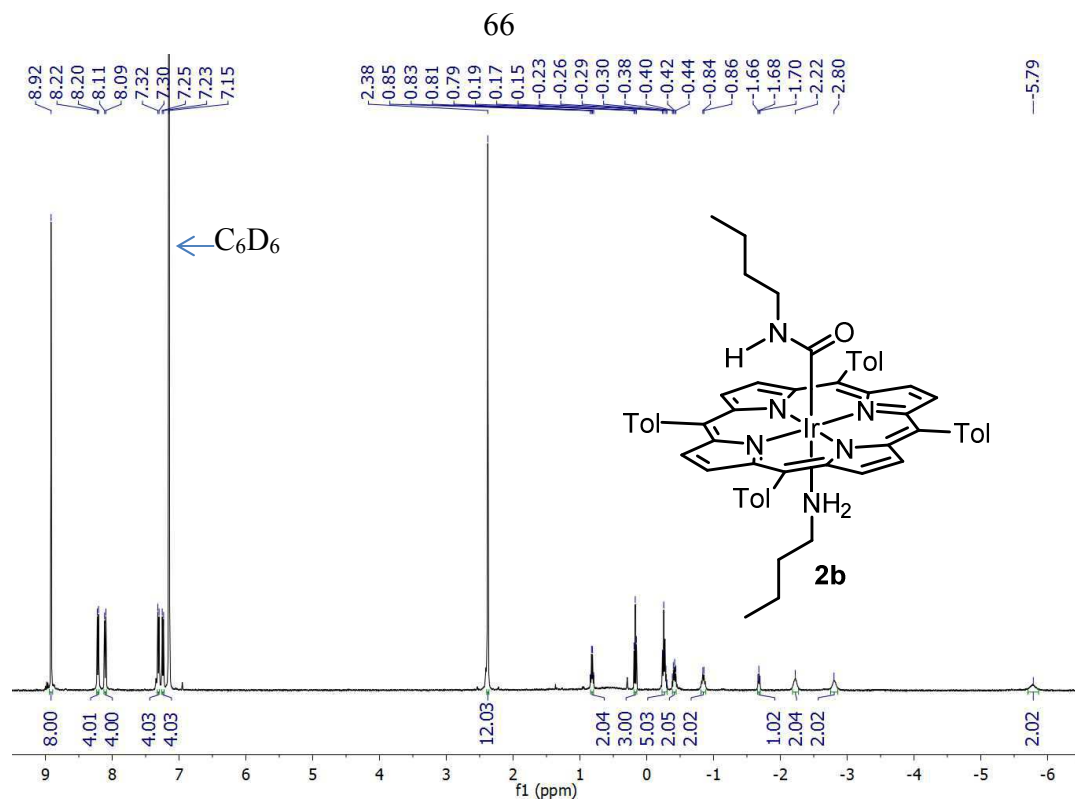


Fig. S5. ¹H NMR spectrum for (TTP)Ir(NH₂ⁿBu)[C(O)NHⁿBu] (**2b**) in C₆D₆

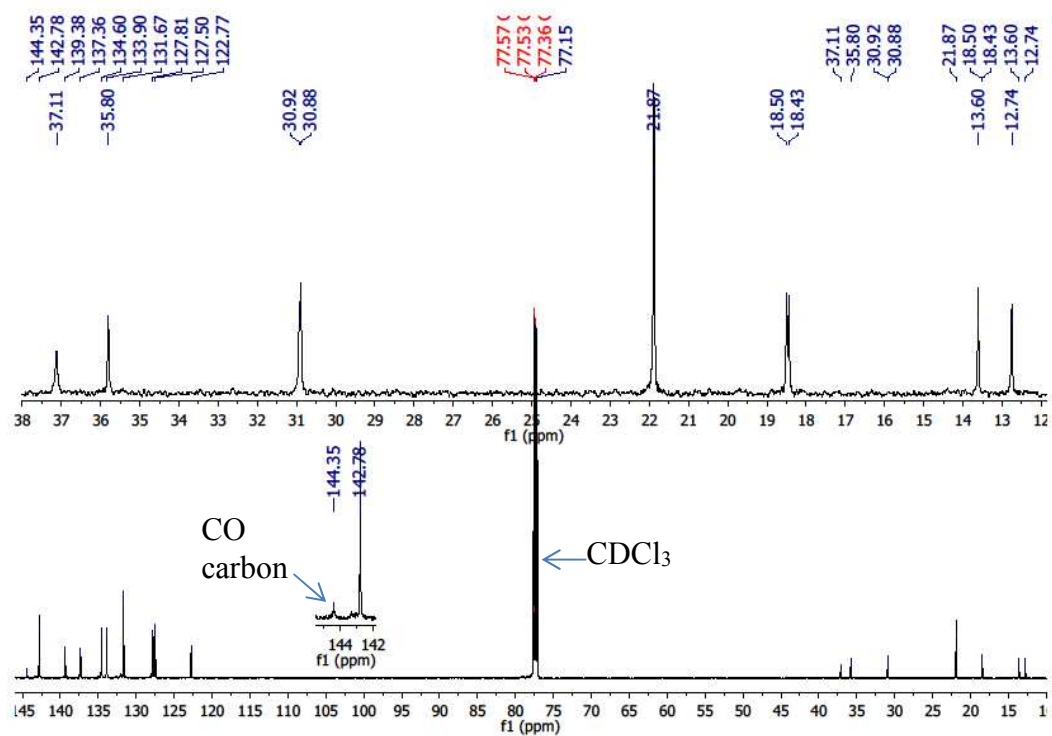


Fig. S6. ¹³C NMR spectrum for (TTP)Ir(NH₂ⁿBu)[C(O)NHⁿBu] (**2b**) in CDCl₃

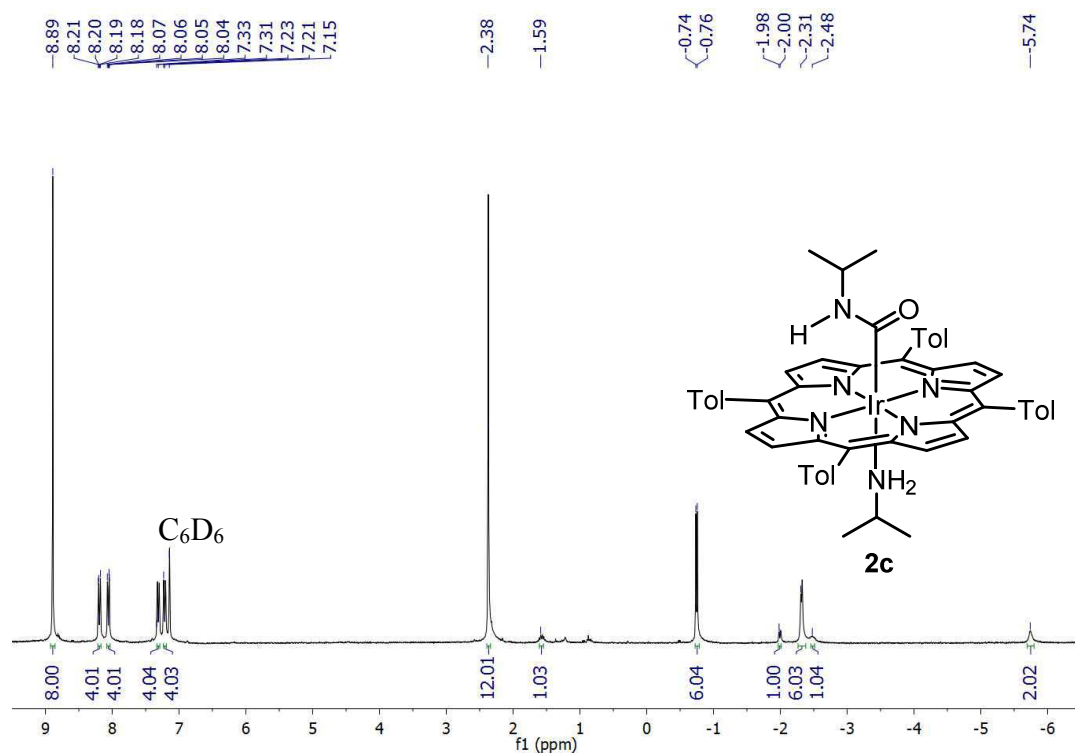


Fig. S7. ¹H NMR spectrum for (TTP)Ir(NH₂ⁱPr)[C(O)NHⁱPr] (**2c**) in C₆D₆

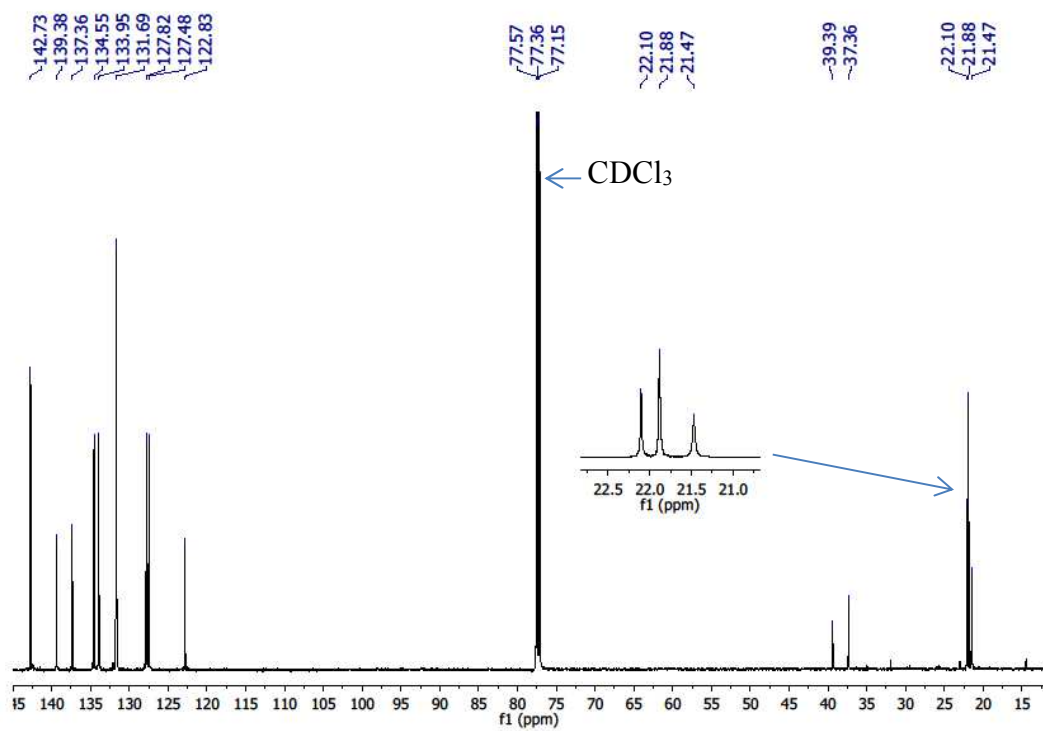


Fig. S8. ¹³C NMR spectrum for (TTP)Ir(NH₂ⁱPr)[C(O)NHⁱPr] (**2c**) in CDCl₃

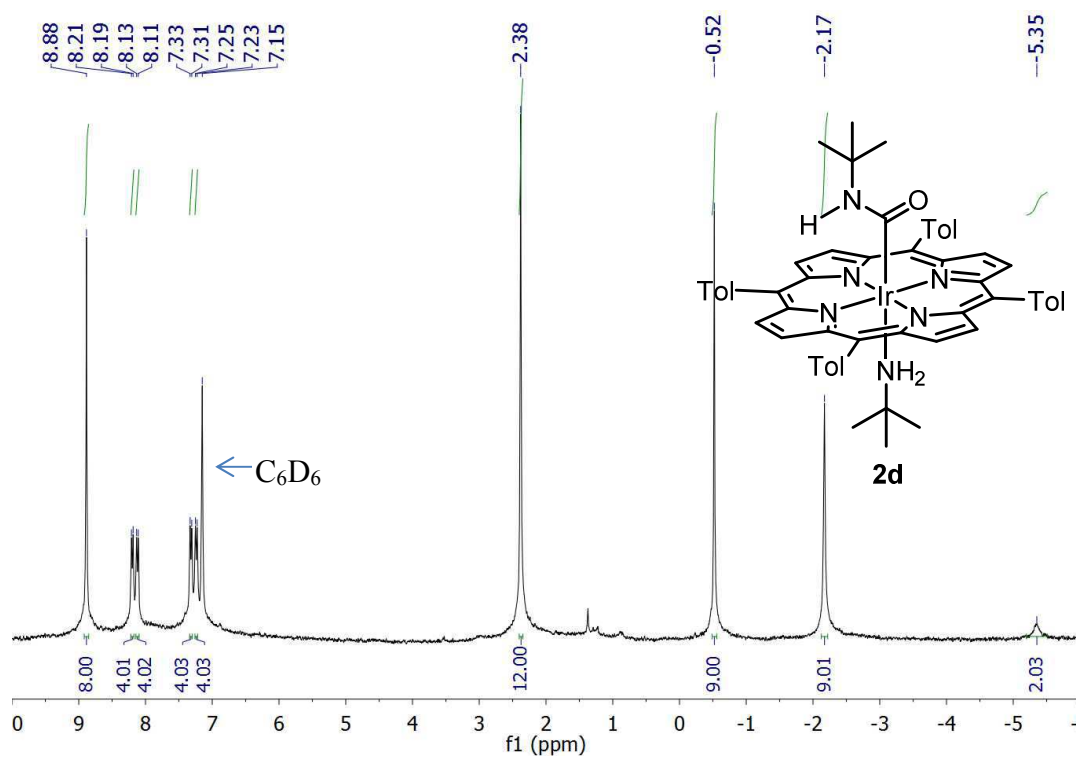


Fig. S9. ^1H NMR spectrum for $(\text{TTP})\text{Ir}(\text{NH}_2'\text{Bu})[\text{C}(\text{O})\text{NH}'\text{Bu}]$ (**2d**) in C_6D_6

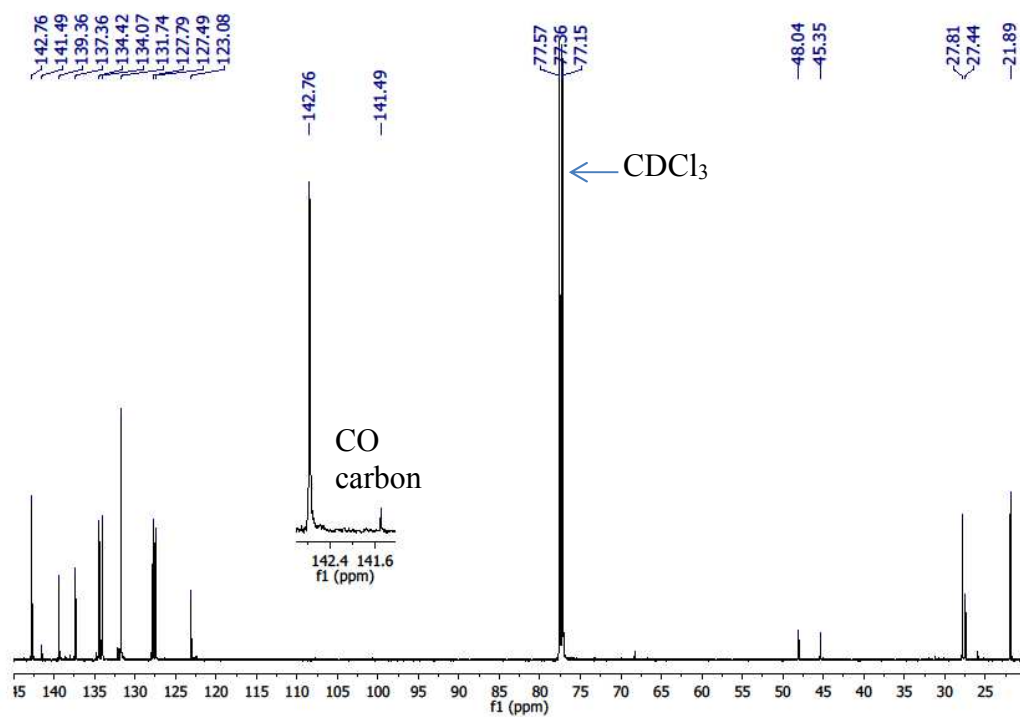


Fig. S10. ^{13}C NMR spectrum for $(\text{TTP})\text{Ir}(\text{NH}_2'\text{Bu})[\text{C}(\text{O})\text{NH}'\text{Bu}]$ (**2d**) in CDCl_3

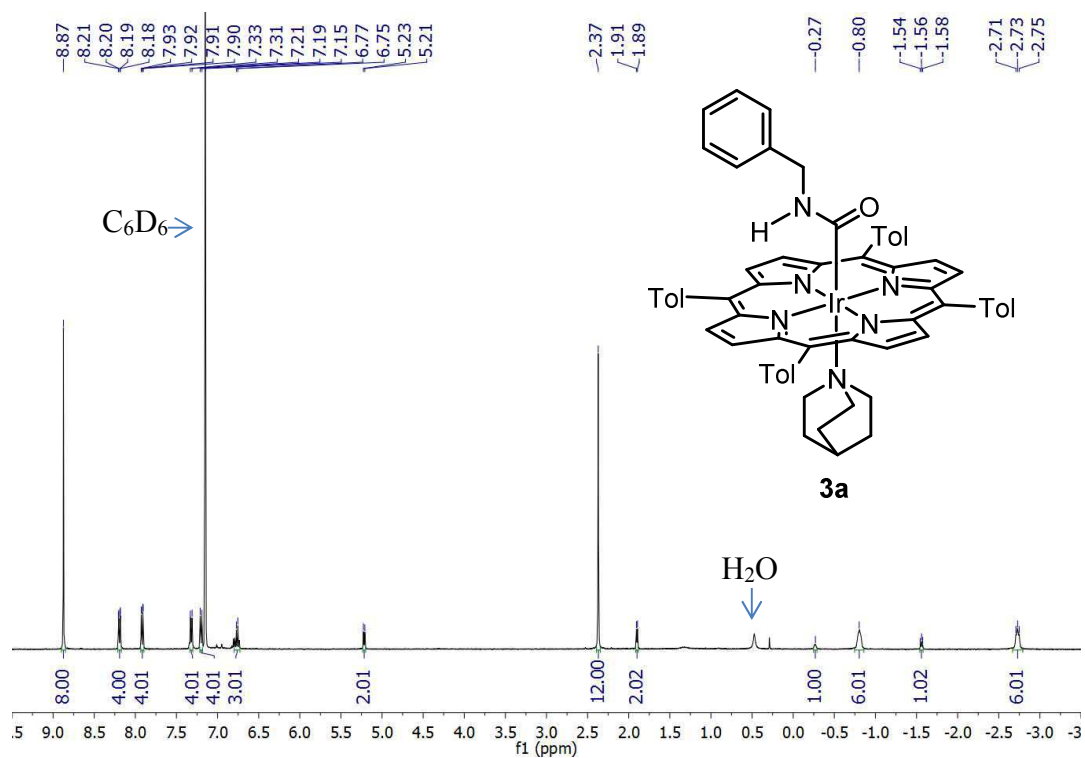


Fig. S11. ¹H NMR spectrum for (TTP)Ir(ABCO)[C(O)NHBn] (**3a**) in C₆D₆

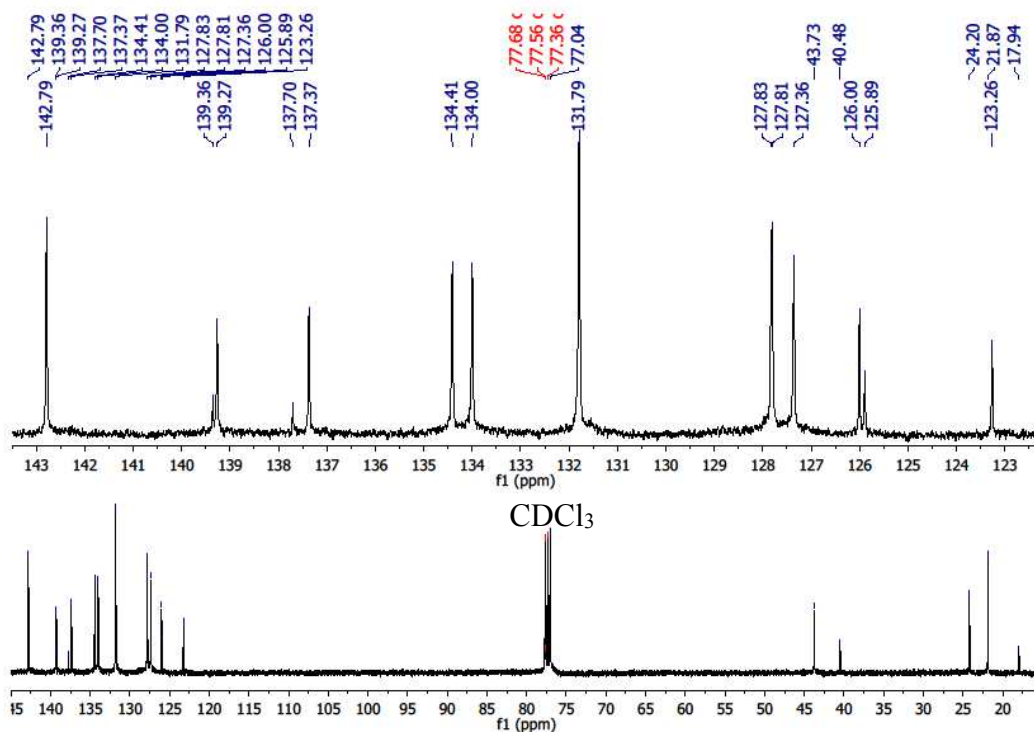


Fig. S12. ¹³C NMR spectrum for (TTP)Ir(ABCO)[C(O)NHBn] (**3a**) in CDCl₃

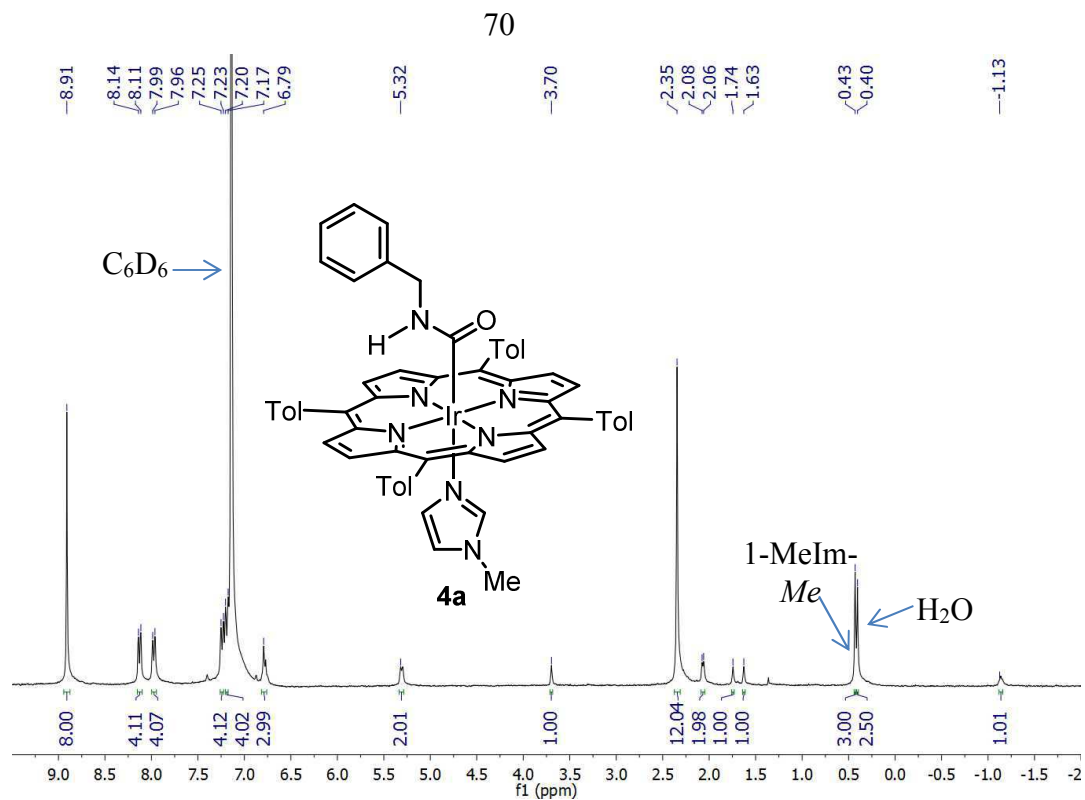


Fig. S13. ¹H NMR spectrum for (TTP)Ir(1-MeIm)[C(O)NHBn] (**4a**) in C₆D₆

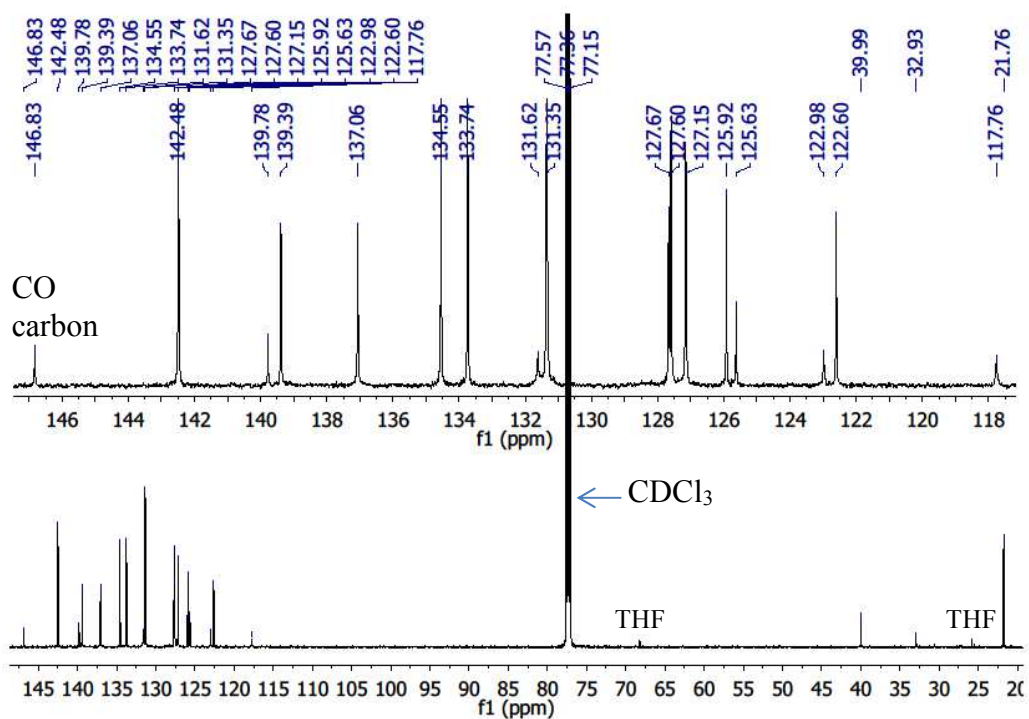
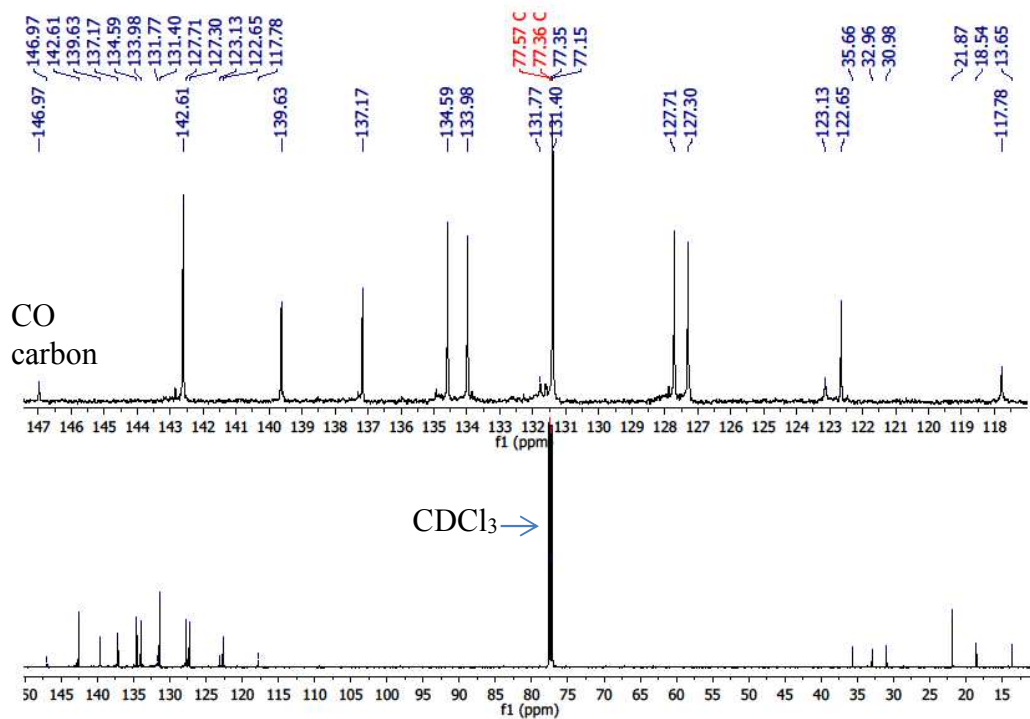
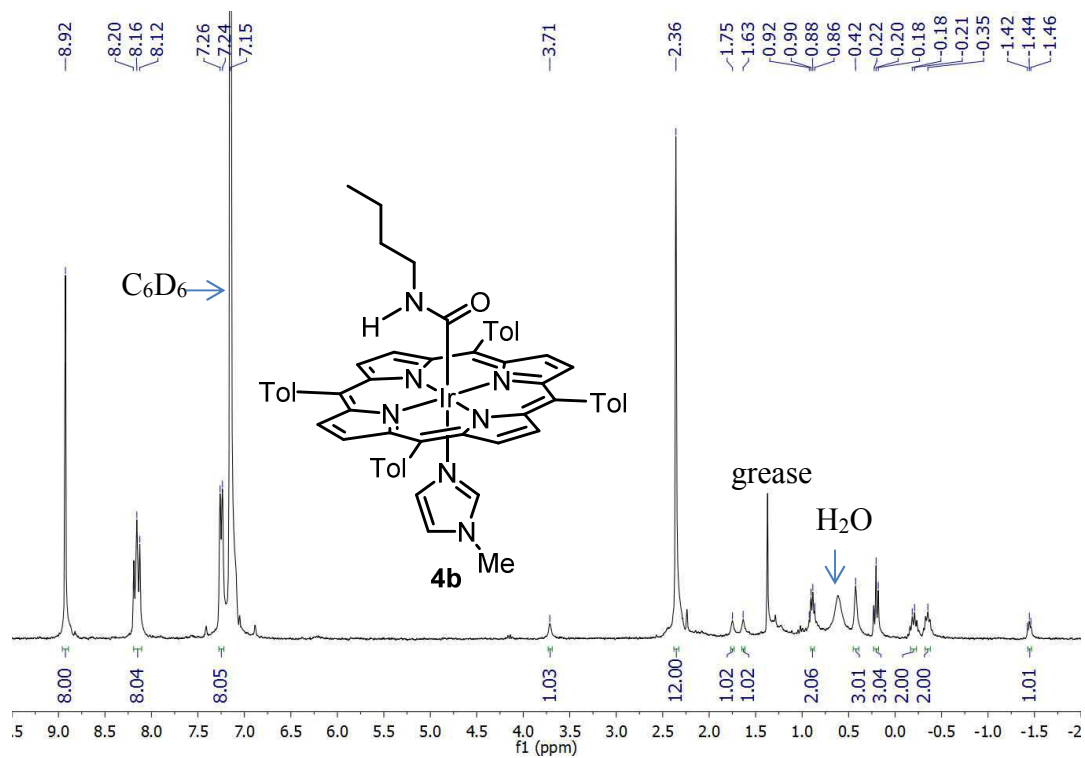
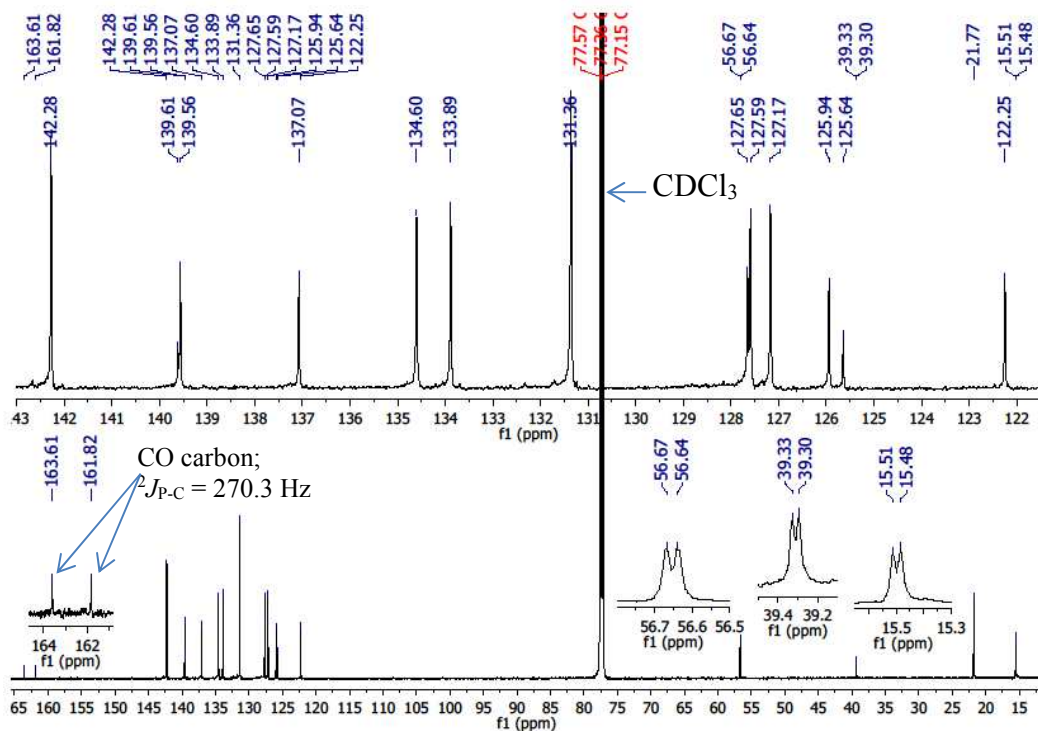
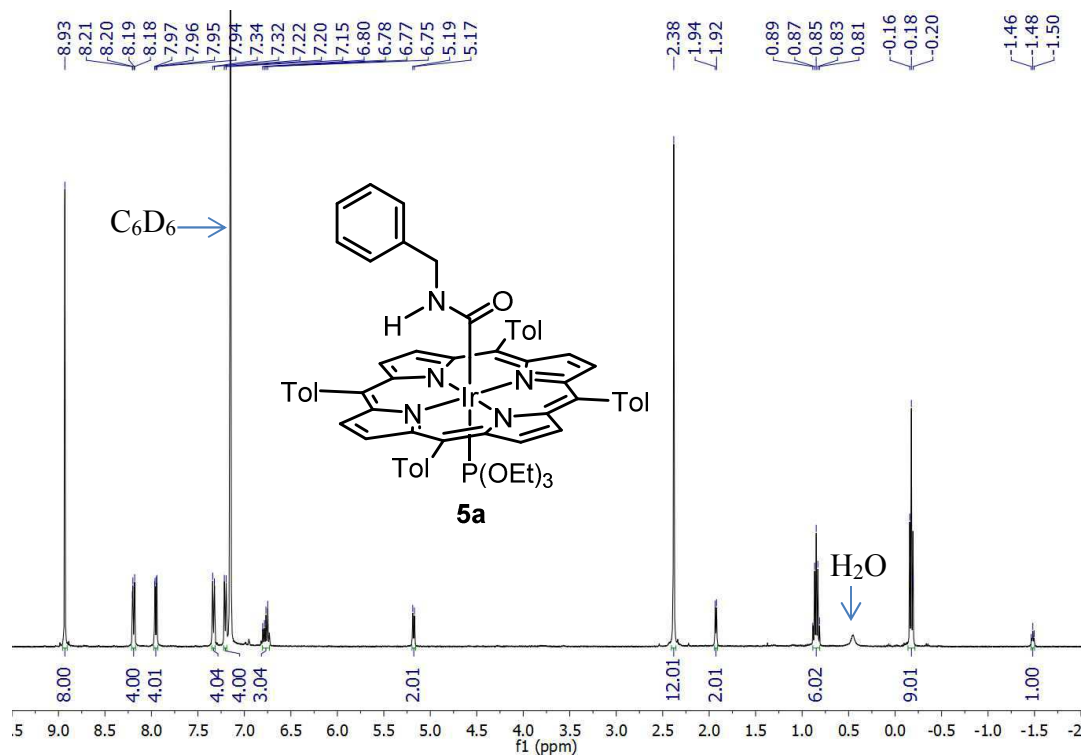


Fig. S14. ³¹C NMR spectrum for (TTP)Ir(1-MeIm)[C(O)NHBn] (**4a**) in CDCl₃





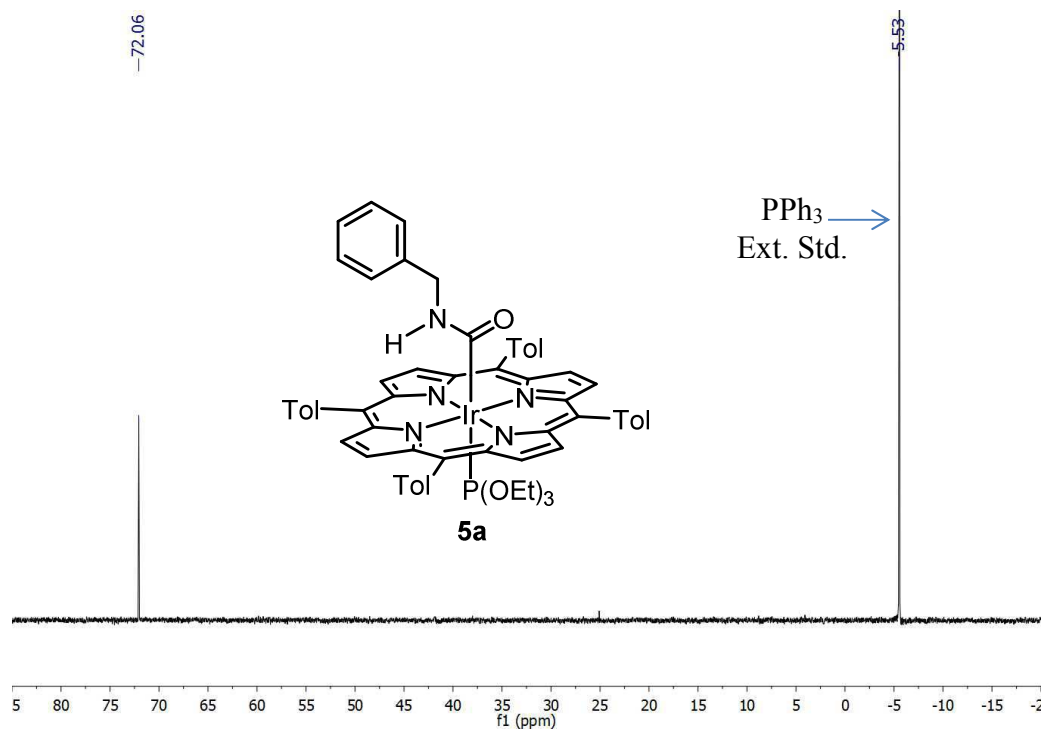


Fig. S19. ³¹P NMR spectrum for $(\text{TTP})\text{Ir}[\text{P}(\text{OEt})_3][\text{C}(\text{O})\text{NHBn}]$ (**5a**) in C₆D₆

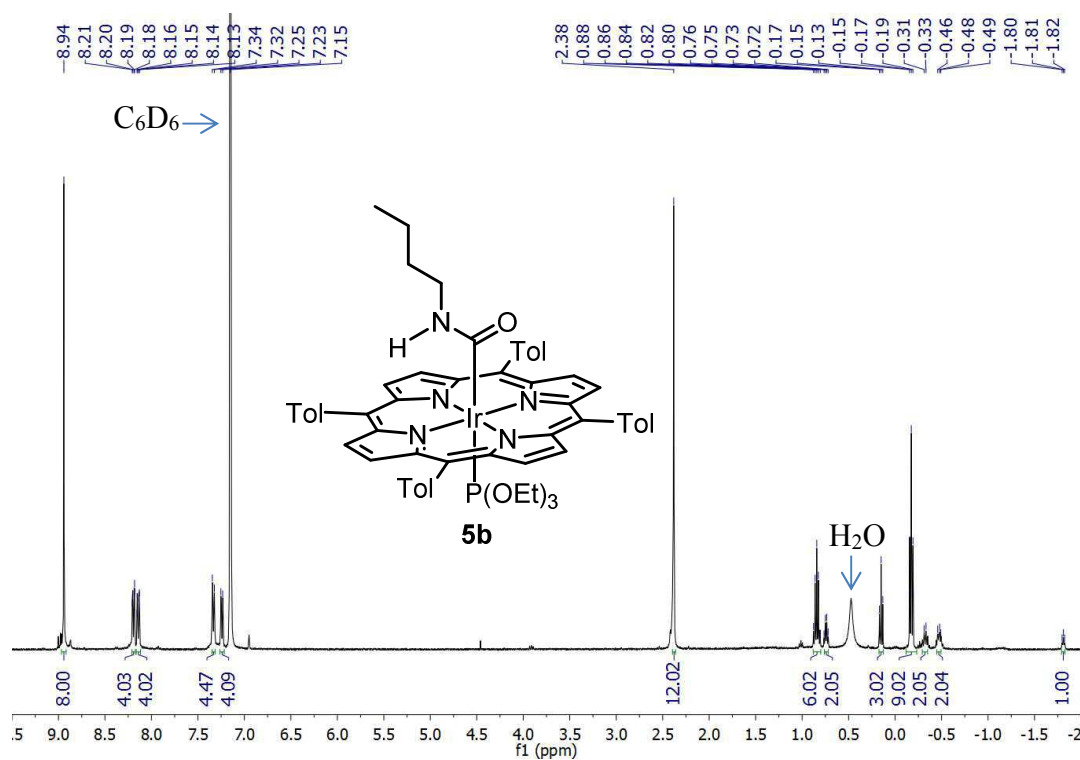


Fig. S20. ¹H NMR spectrum for $(\text{TTP})\text{Ir}[\text{P}(\text{OEt})_3][\text{C}(\text{O})\text{NH}^n\text{Bu}]$ (**5b**) in C₆D₆

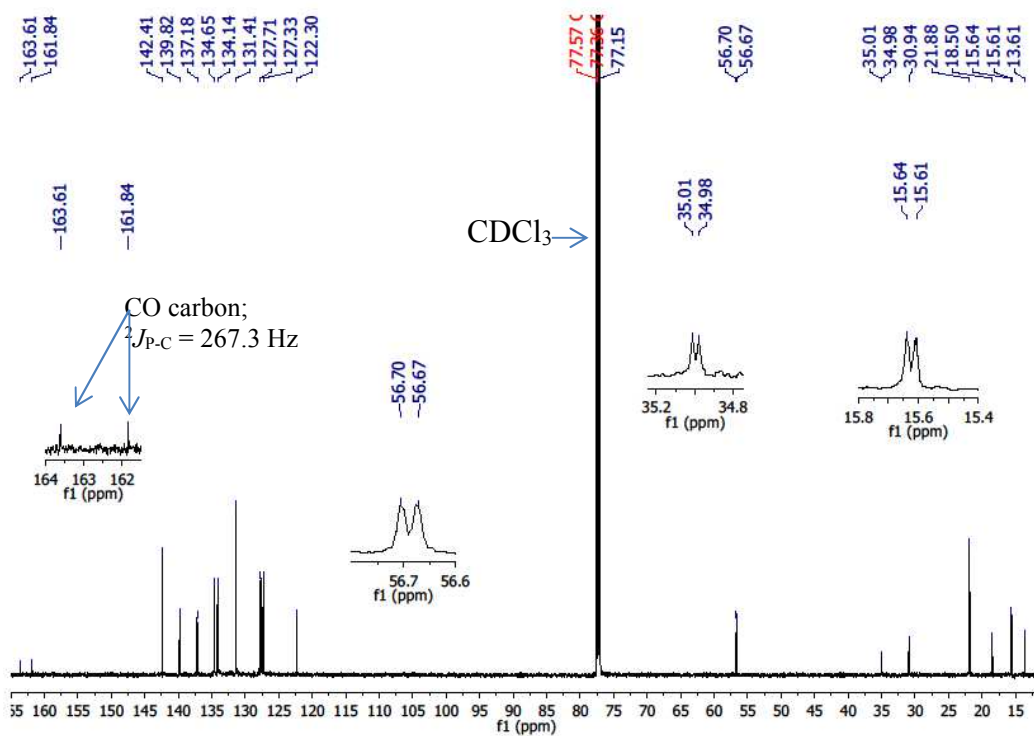


Fig. S21. ¹³C NMR spectrum for (TTP)Ir[P(OEt)₃][C(O)NHⁿBu] (**5b**) in CDCl₃

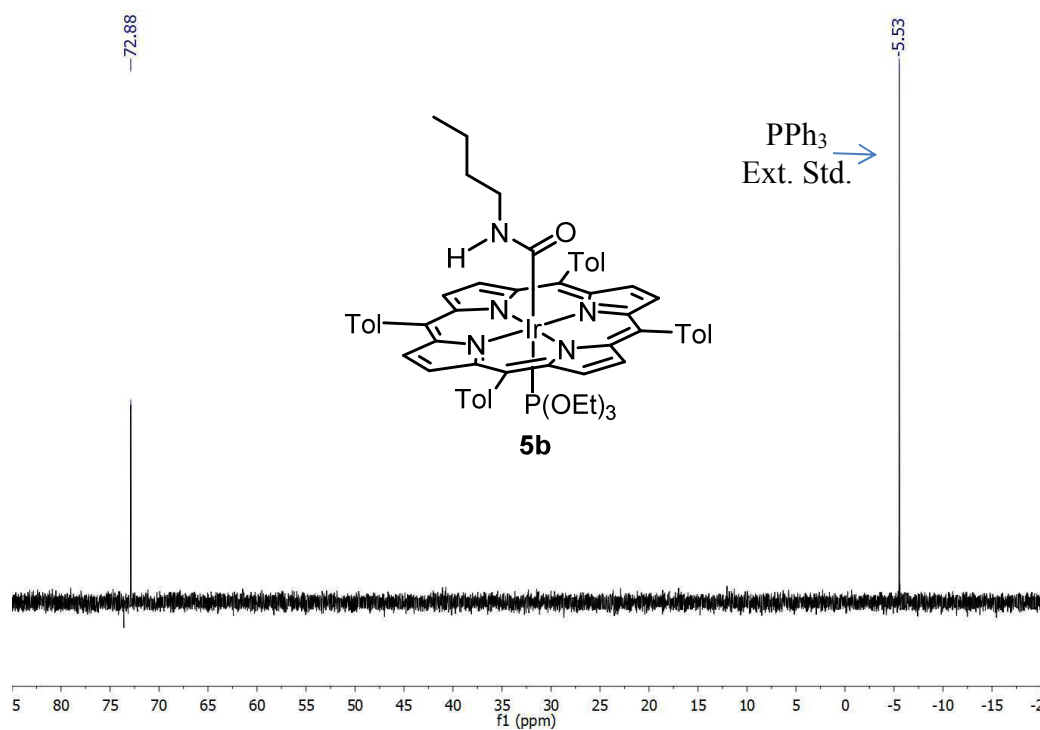


Fig. S22. ³¹P NMR spectrum for (TTP)Ir[P(OEt)₃][C(O)NHⁿBu] (**5b**) in C₆D₆

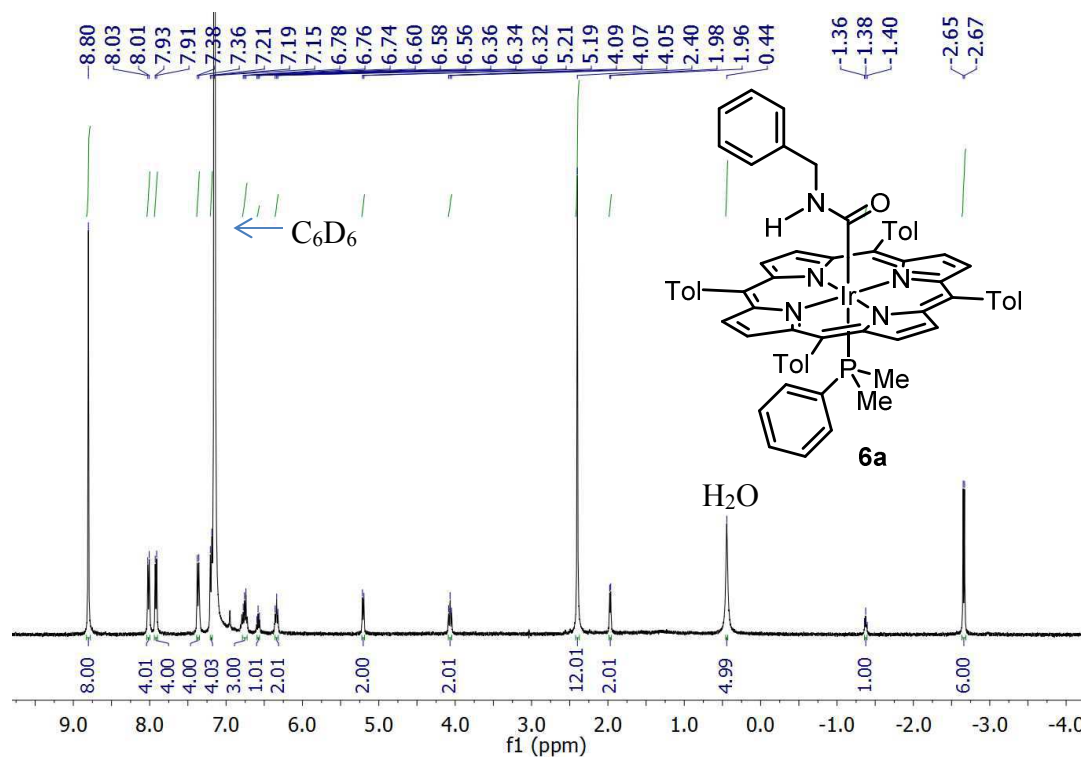


Fig. S23. ¹H NMR spectrum for (TTP)Ir(PMe₂Ph)[C(O)NHBn] (**6a**) in C₆D₆

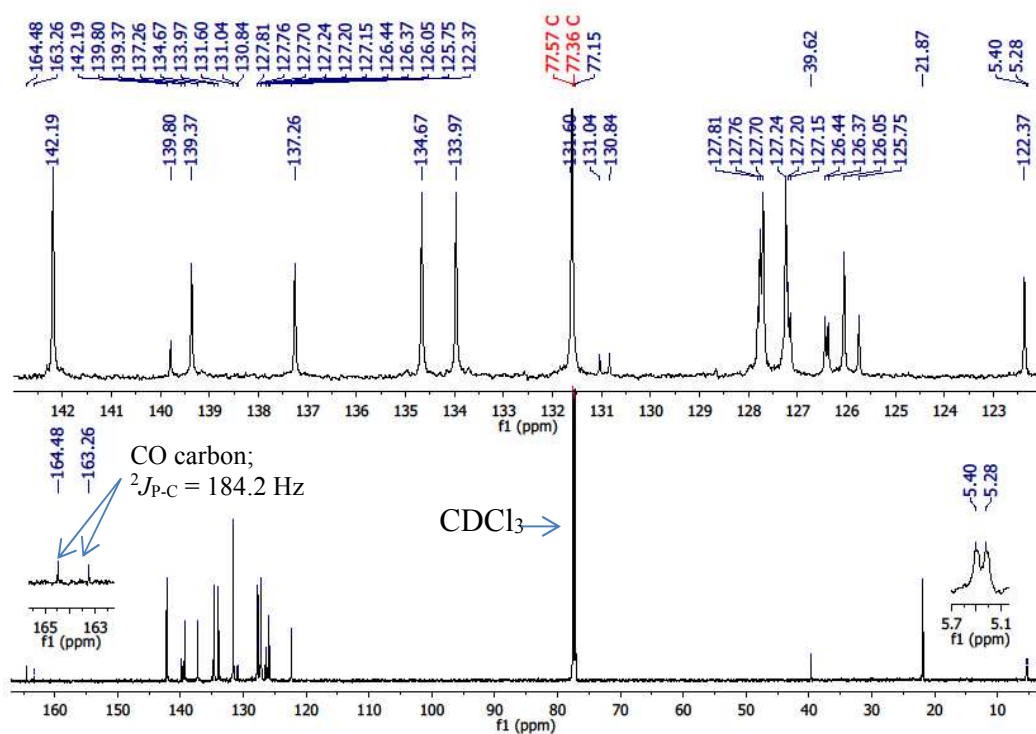


Fig. S24. ¹³C NMR spectrum for (TTP)Ir(PMe₂Ph)[C(O)NHBn] (**6a**) in CDCl₃

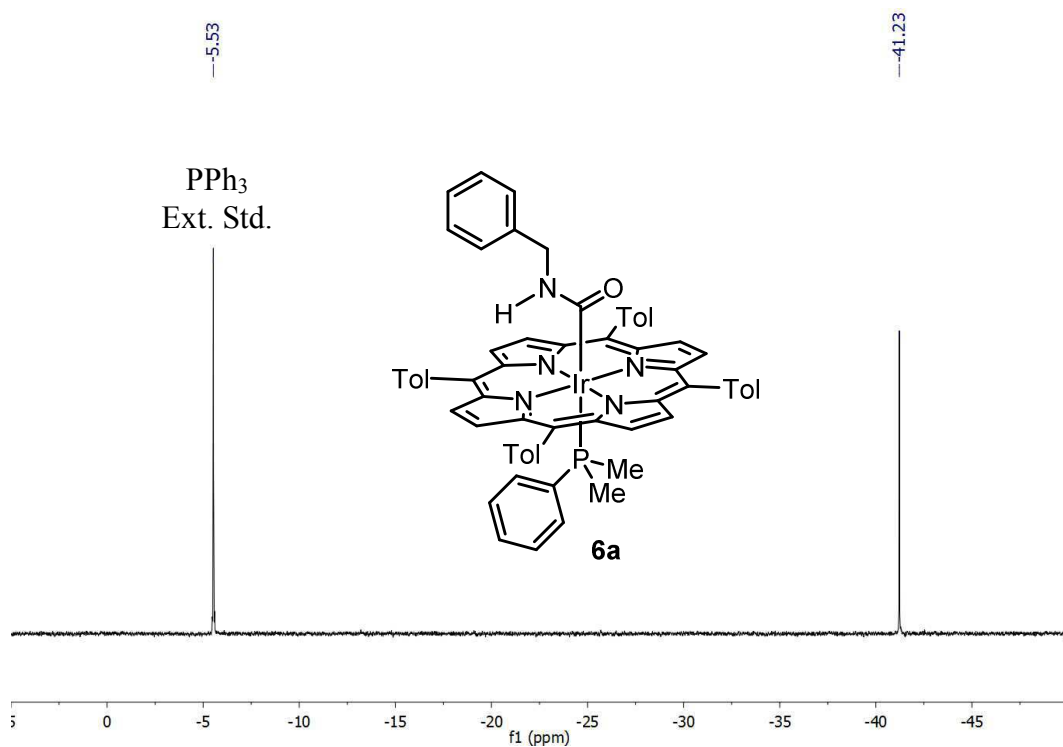


Fig. S25. ^{31}P NMR spectrum for $(\text{TTP})\text{Ir}(\text{PMe}_2\text{Ph})[\text{C}(\text{O})\text{NHBn}]$ (**6a**) in C_6D_6

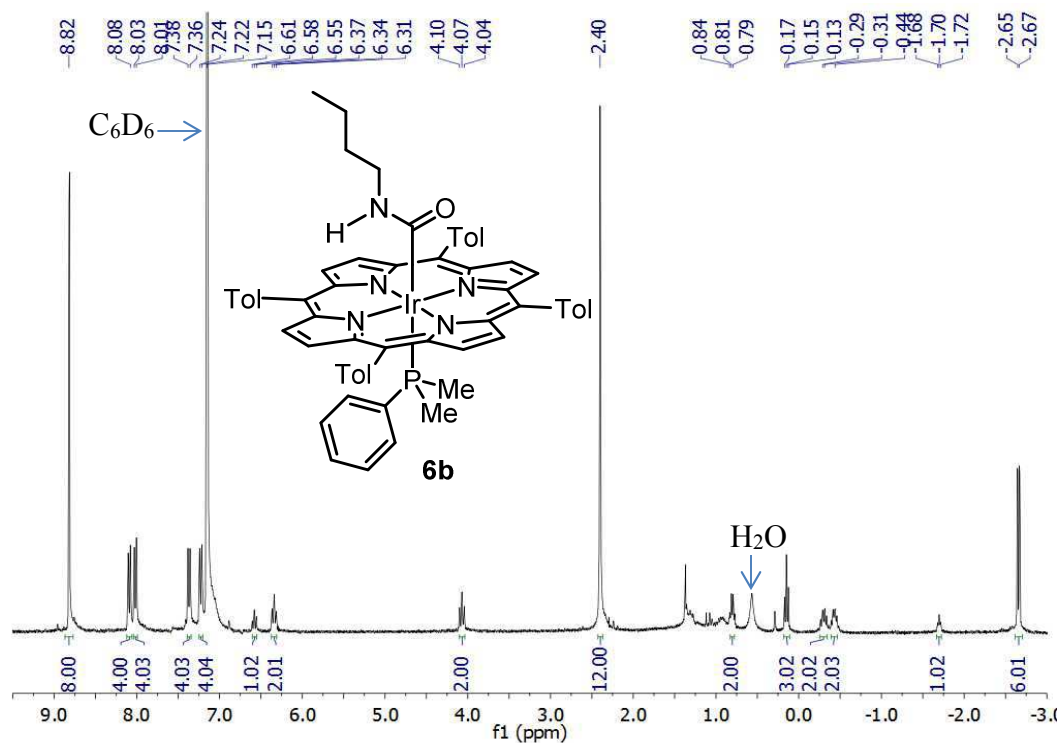


Fig. S26. ^1H NMR spectrum for $(\text{TTP})\text{Ir}(\text{PMe}_2\text{Ph})[\text{C}(\text{O})\text{NH}^n\text{Bu}]$ (**6b**) in C_6D_6

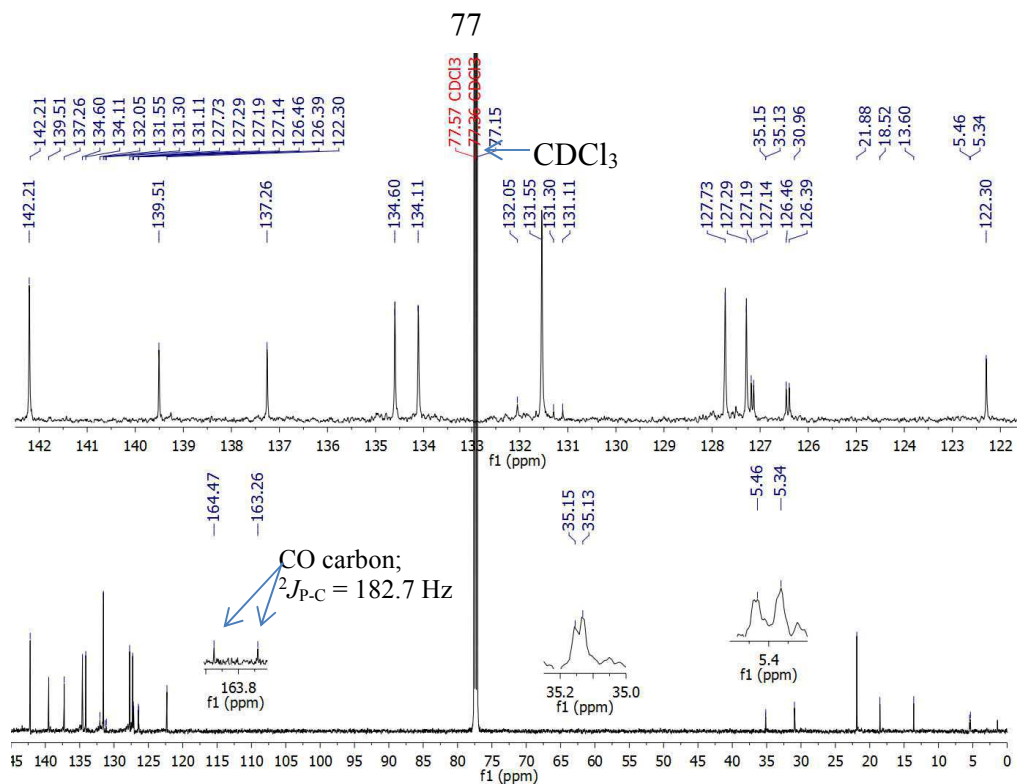


Fig. S27. ^{13}C NMR spectrum for $(\text{TTP})\text{Ir}(\text{PMe}_2\text{Ph})[\text{C}(\text{O})\text{NH}^n\text{Bu}]$ (**6b**) in CDCl_3

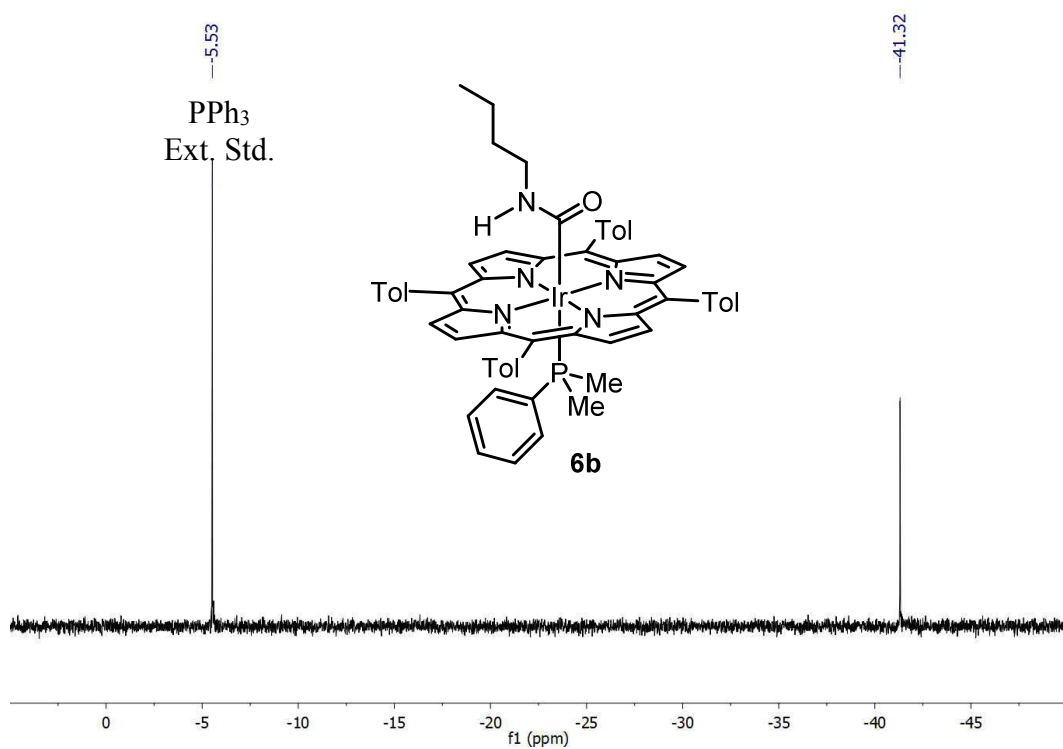


Fig. S28. ^{31}P NMR spectrum for $(\text{TTP})\text{Ir}(\text{PMe}_2\text{Ph})[\text{C}(\text{O})\text{NH}^n\text{Bu}]$ (**6b**) in C_6D_6

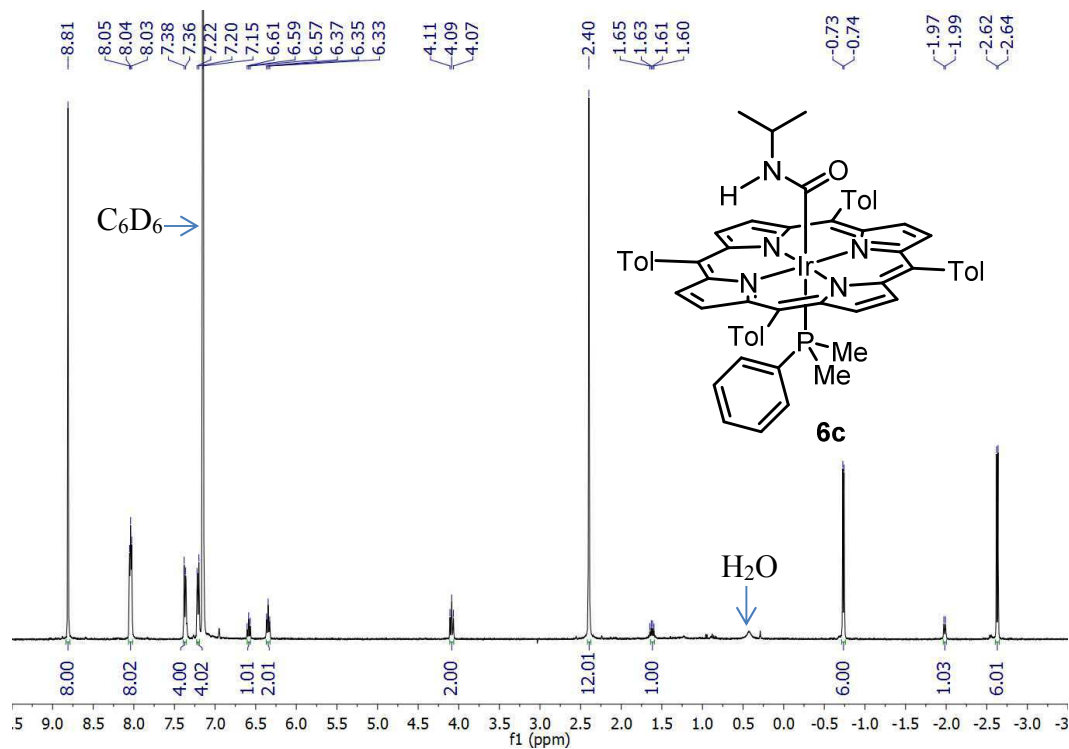


Fig. S29. ¹H NMR spectrum for (TTP)Ir(PMe₂Ph)[C(O)NH^tPr] (**6c**) in C₆D₆

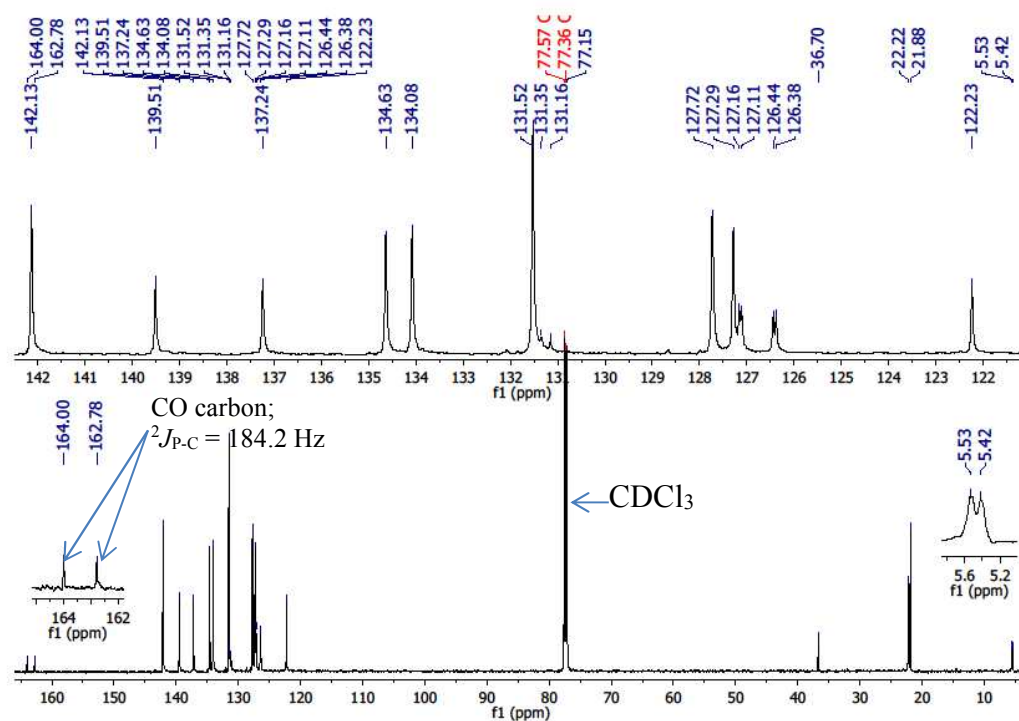


Fig. S30. ¹³C NMR spectrum for (TTP)Ir(PMe₂Ph)[C(O)NH^tPr] (**6c**) in CDCl₃

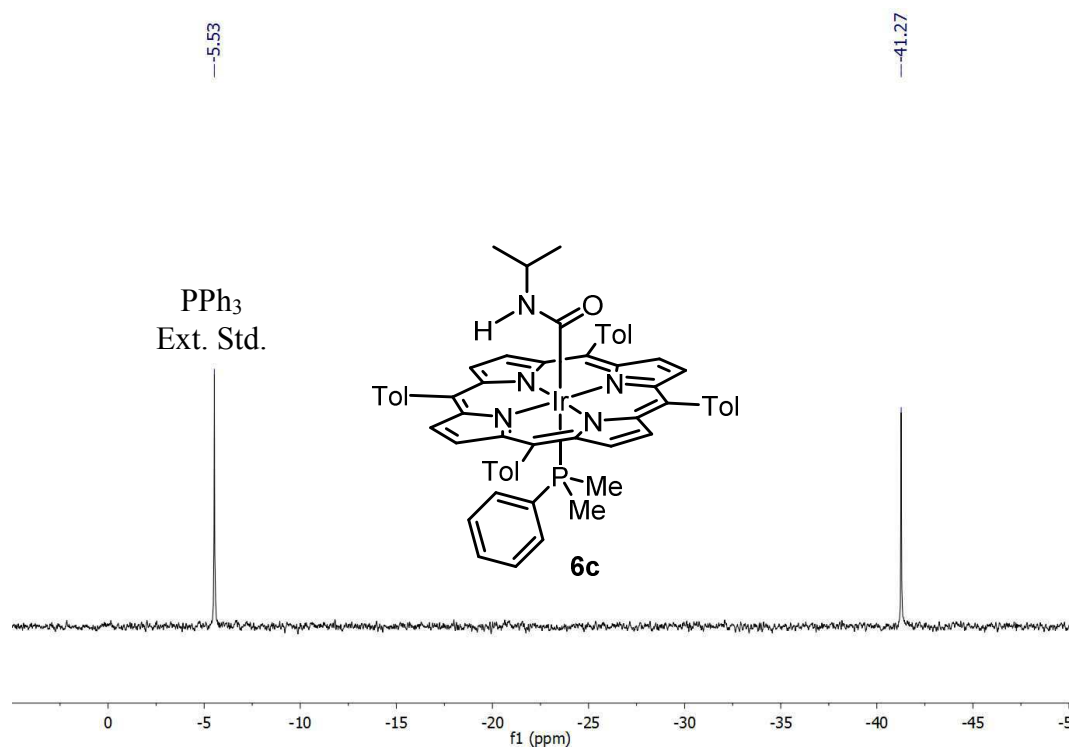


Fig. 31. ^{31}P NMR spectrum for $(\text{TTP})\text{Ir}(\text{PMe}_2\text{Ph})[\text{C}(\text{O})\text{NH}^i\text{Pr}]$ (**6c**) in C_6D_6

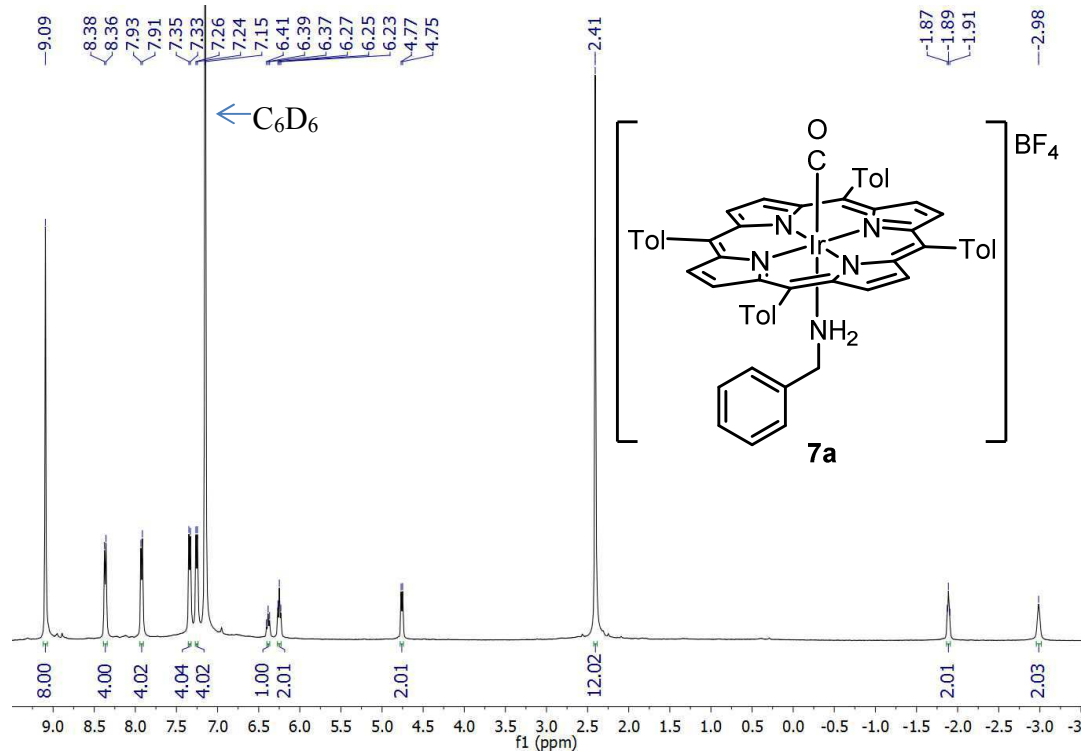
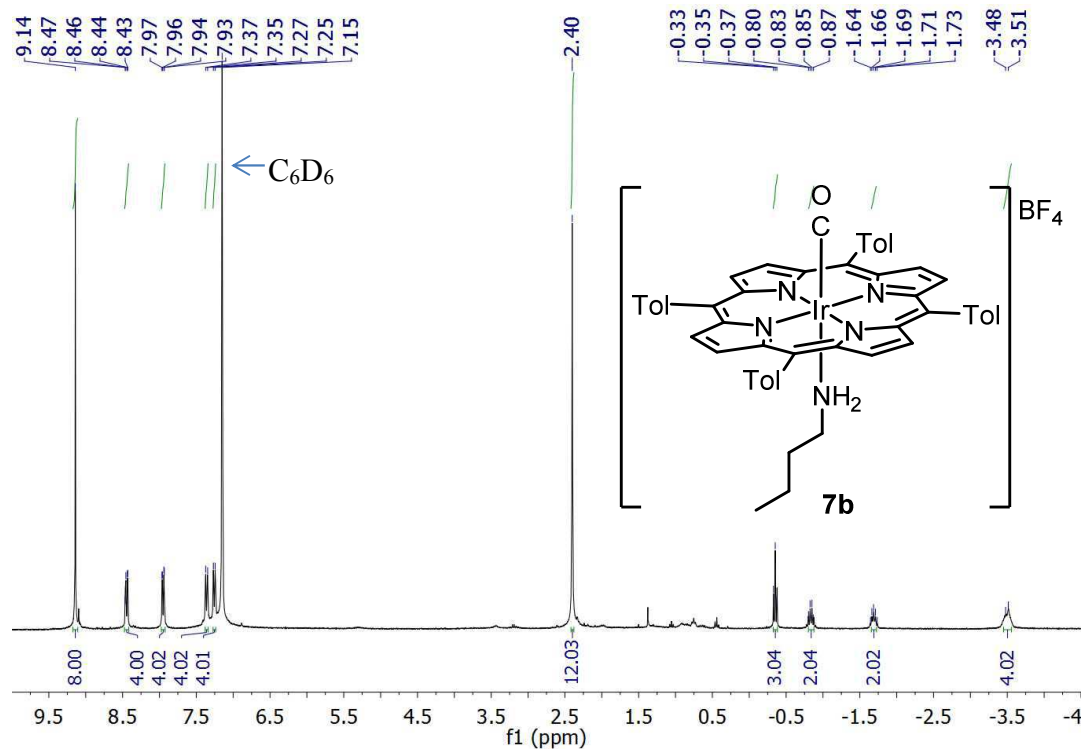
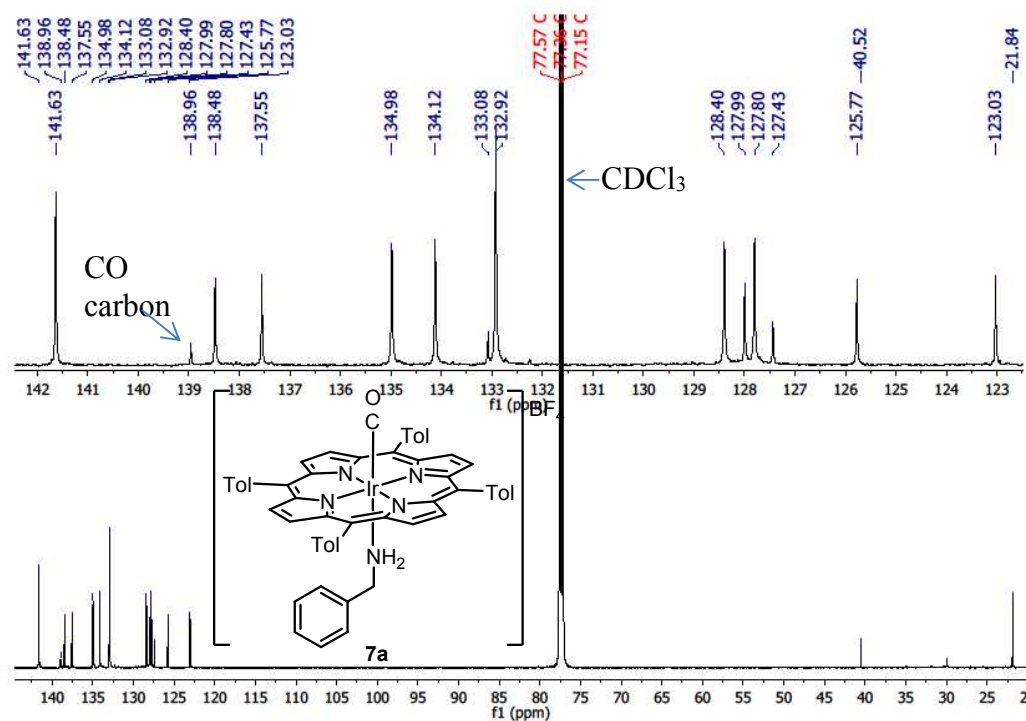


Fig. 32. ^1H NMR spectrum for $[(\text{TTP})\text{Ir}(\text{NH}_2\text{Bn})(\text{CO})]\text{BF}_4$ (**7a**) in C_6D_6



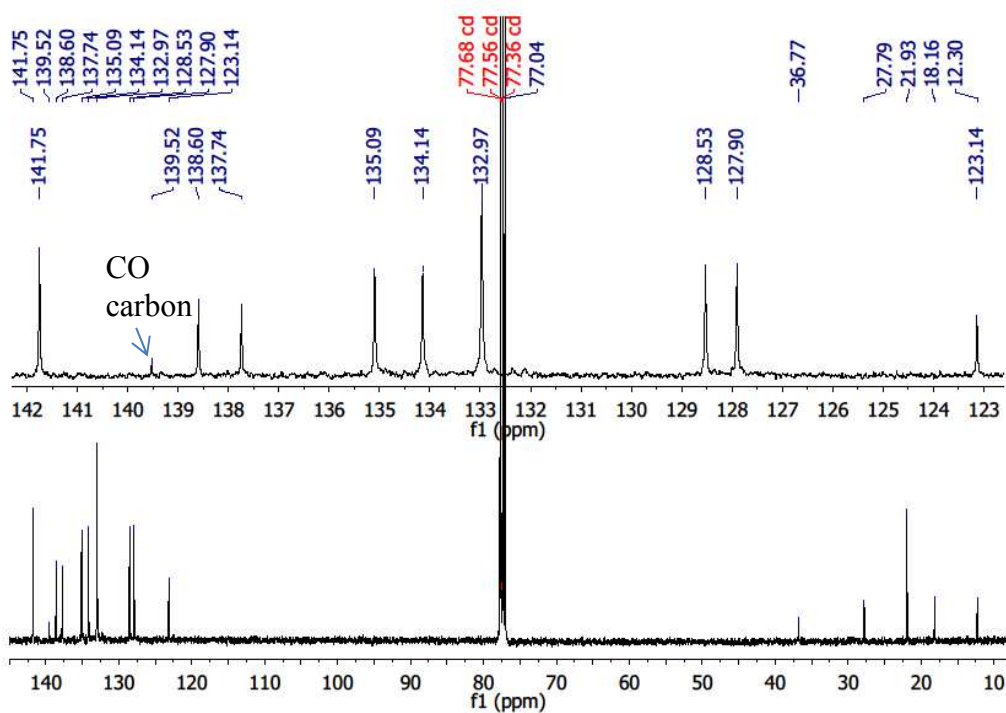


Fig. S35. ¹³C NMR spectrum for [(TTP)Ir(NH₂ⁿBu)(CO)]BF₄ (**7b**) in CDCl₃

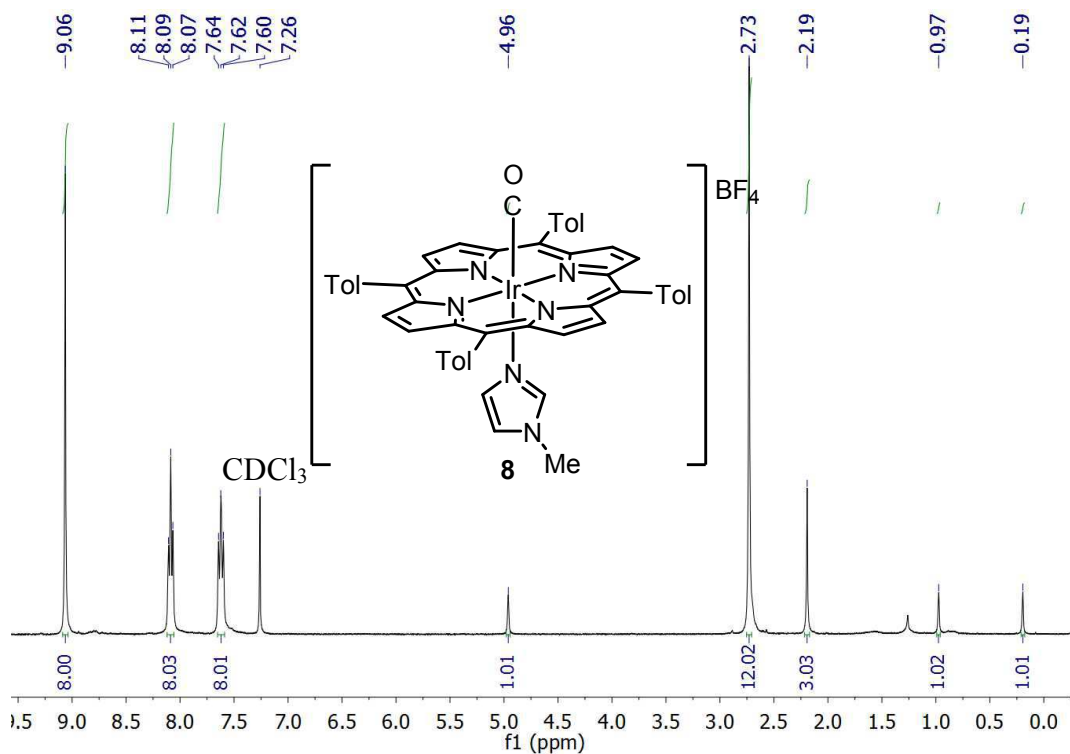
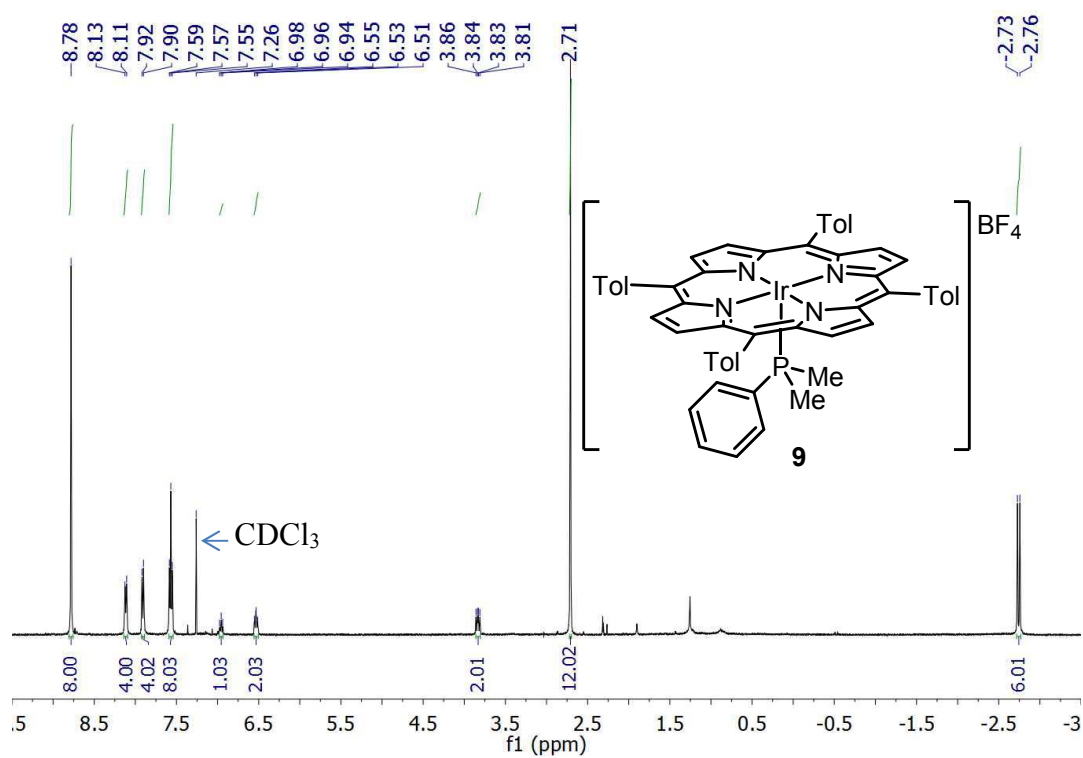
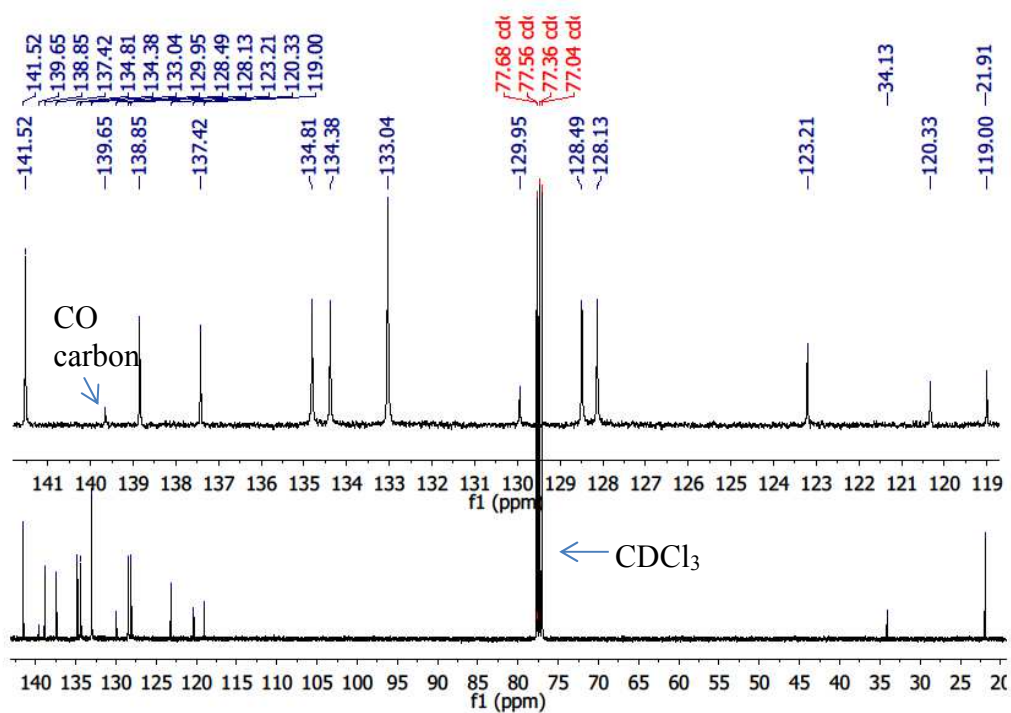


Fig. S36. ¹H NMR spectrum for [(TTP)Ir(1-MeIm)(CO)]BF₄ (**8**) in CDCl₃



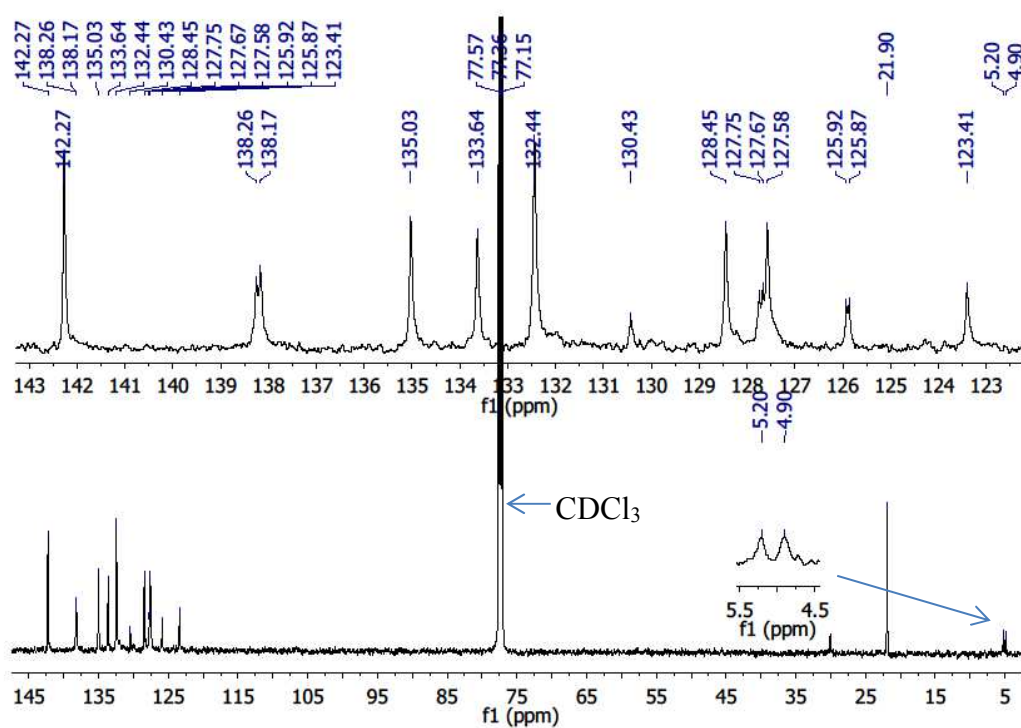


Fig. S39. ^{13}C NMR spectrum for $[(\text{TTP})\text{Ir}(\text{PMe}_2\text{Ph})]\text{BF}_4$ (**9**) in CDCl_3

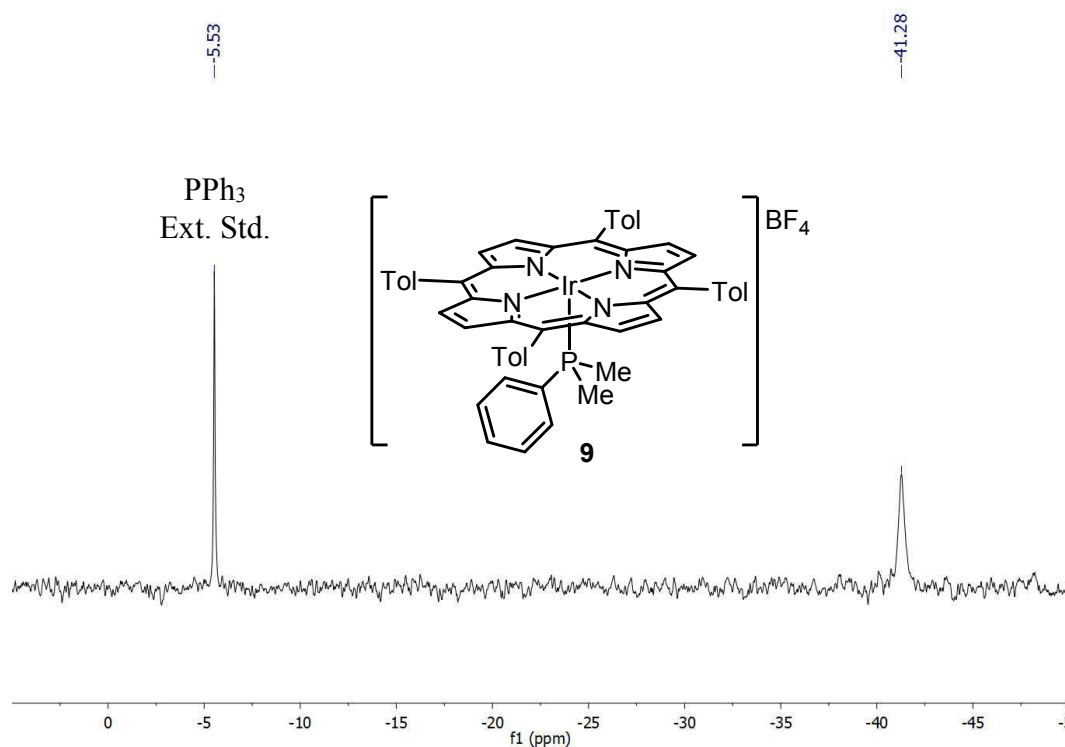


Fig. S40. ^{31}P NMR spectrum for $[(\text{TTP})\text{Ir}(\text{PMe}_2\text{Ph})]\text{BF}_4$ (**9**) in C_6D_6

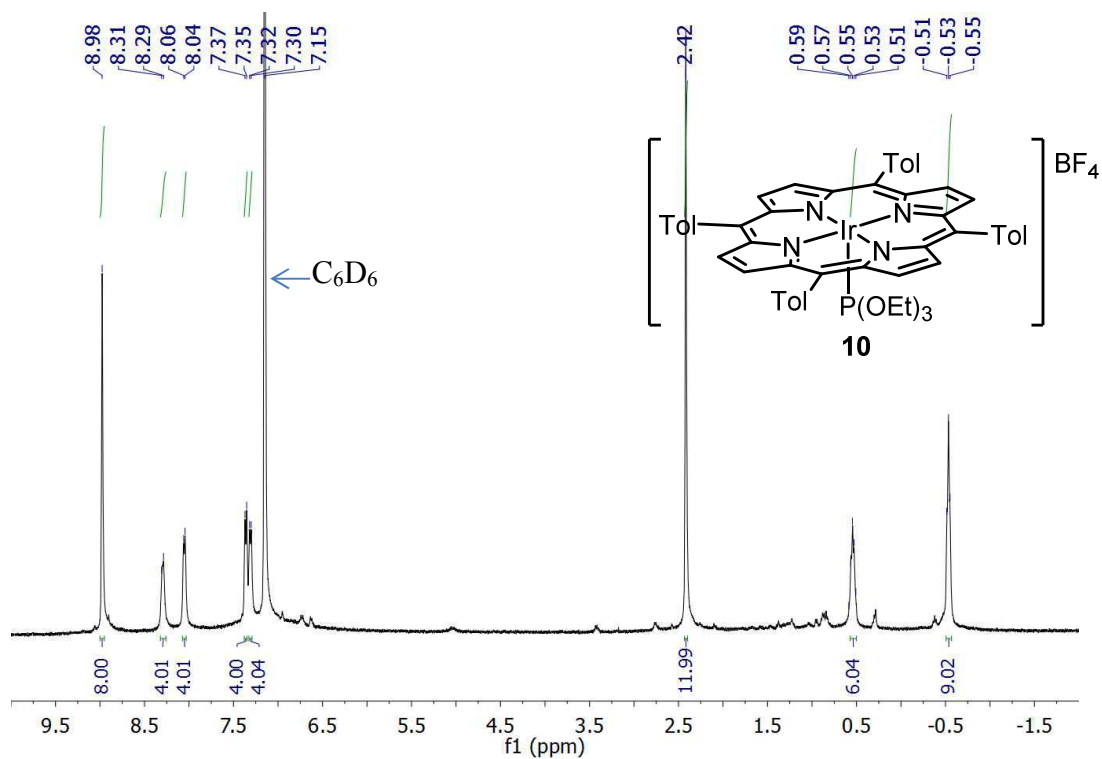


Fig. S41. ^1H NMR spectrum for $[(\text{TTP})\text{Ir}\{\text{P}(\text{OEt})_3\}]\text{BF}_4$ (**10**) in C_6D_6

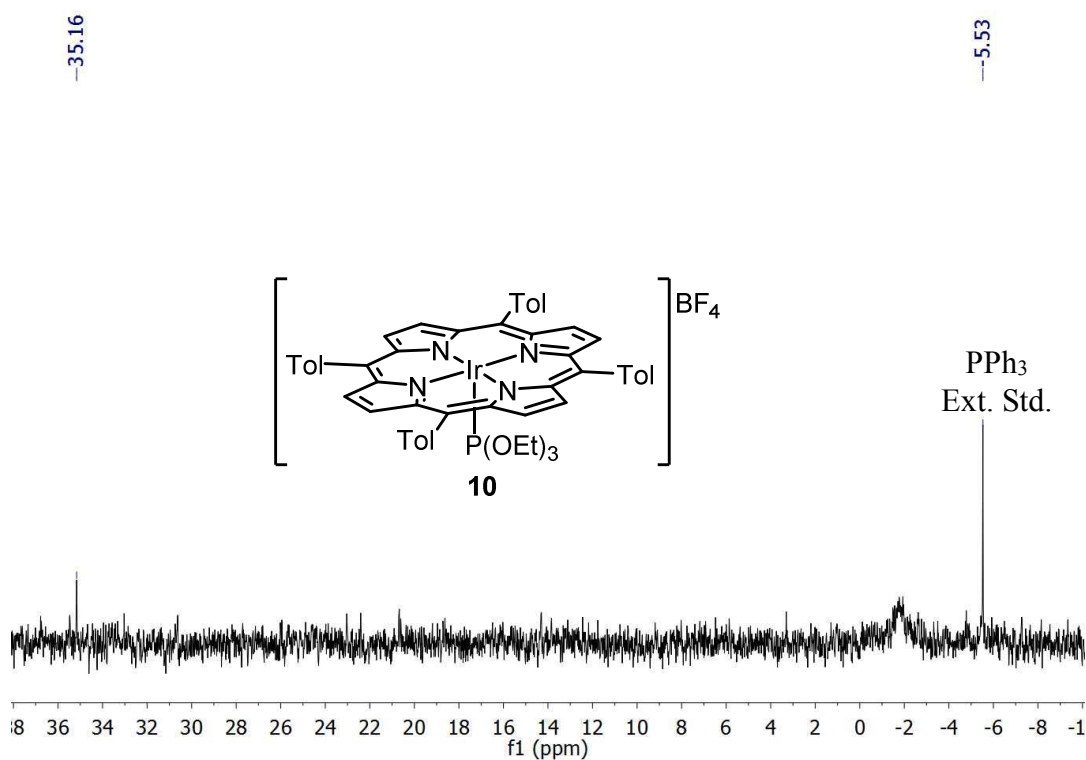


Fig. S42. ^{31}P NMR spectrum for $[(\text{TTP})\text{Ir}\{\text{P}(\text{OEt})_3\}]\text{BF}_4$ (**10**) in C_6D_6

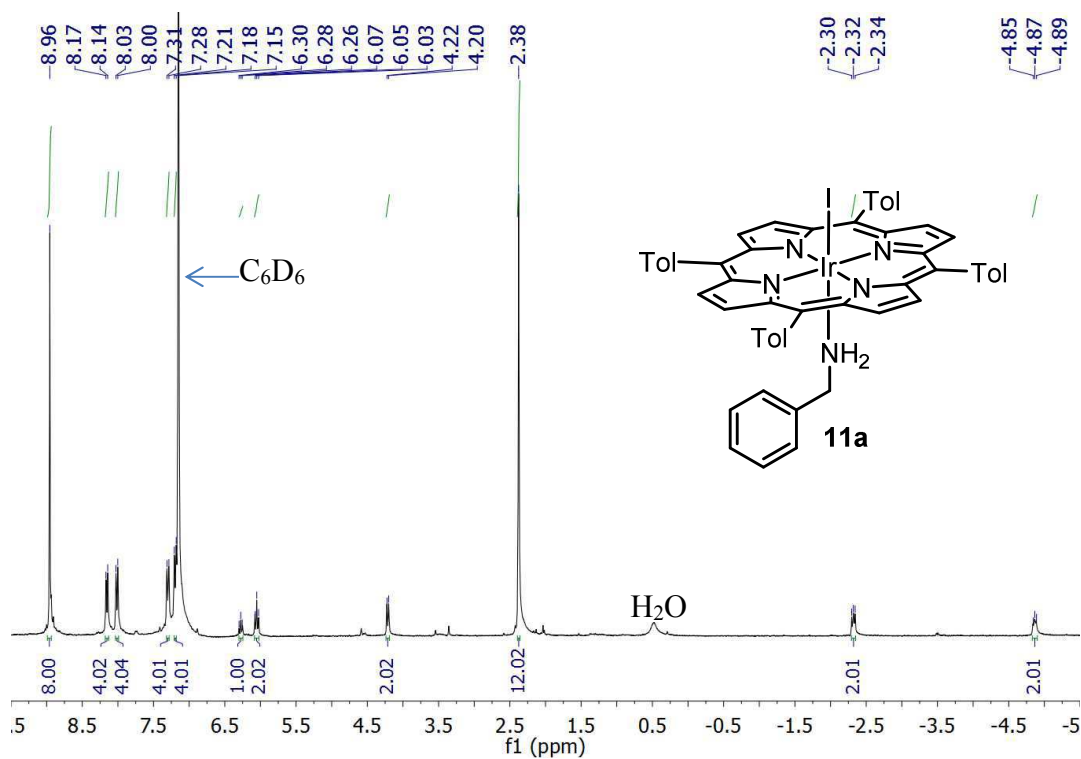


Fig. S43. ^1H NMR spectrum for (TTP)Ir(NH₂Bn)I (**11a**) in C₆D₆

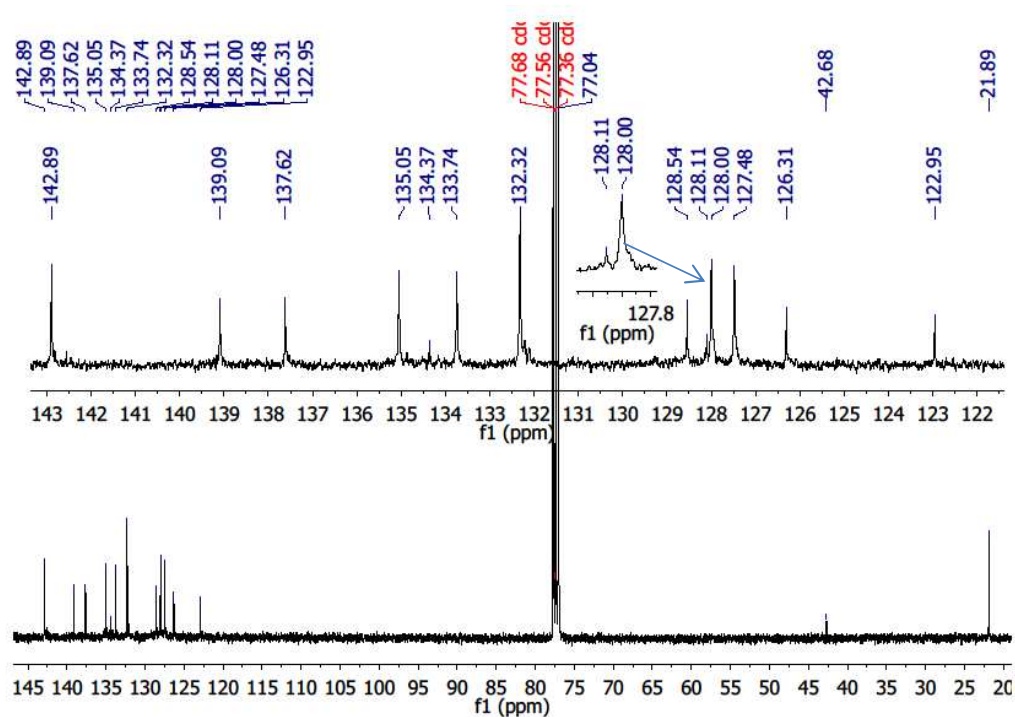
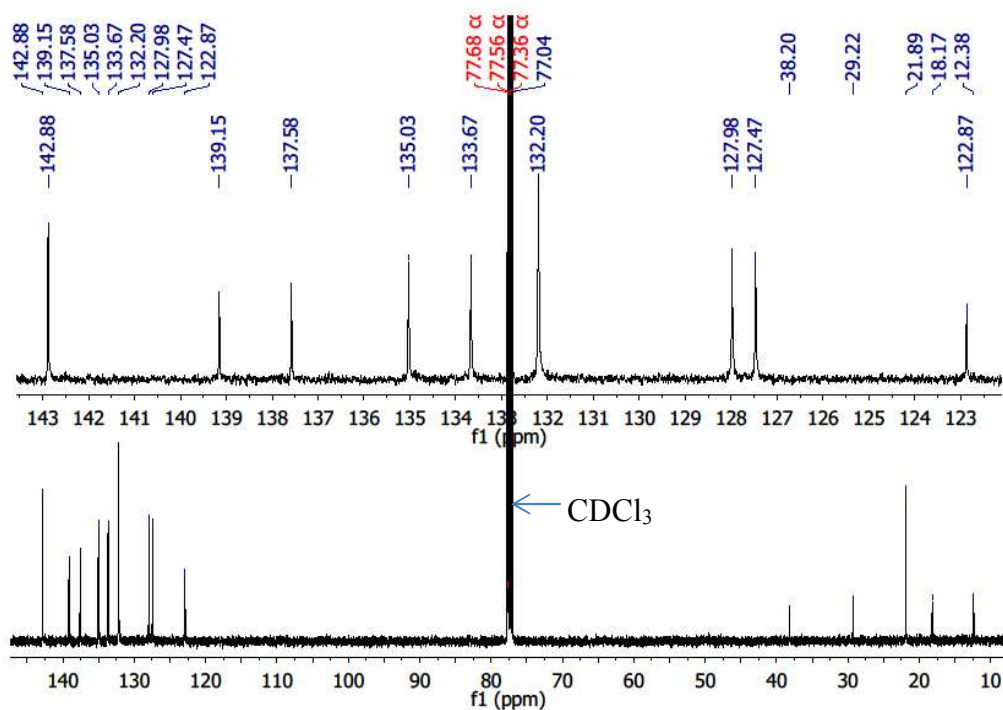
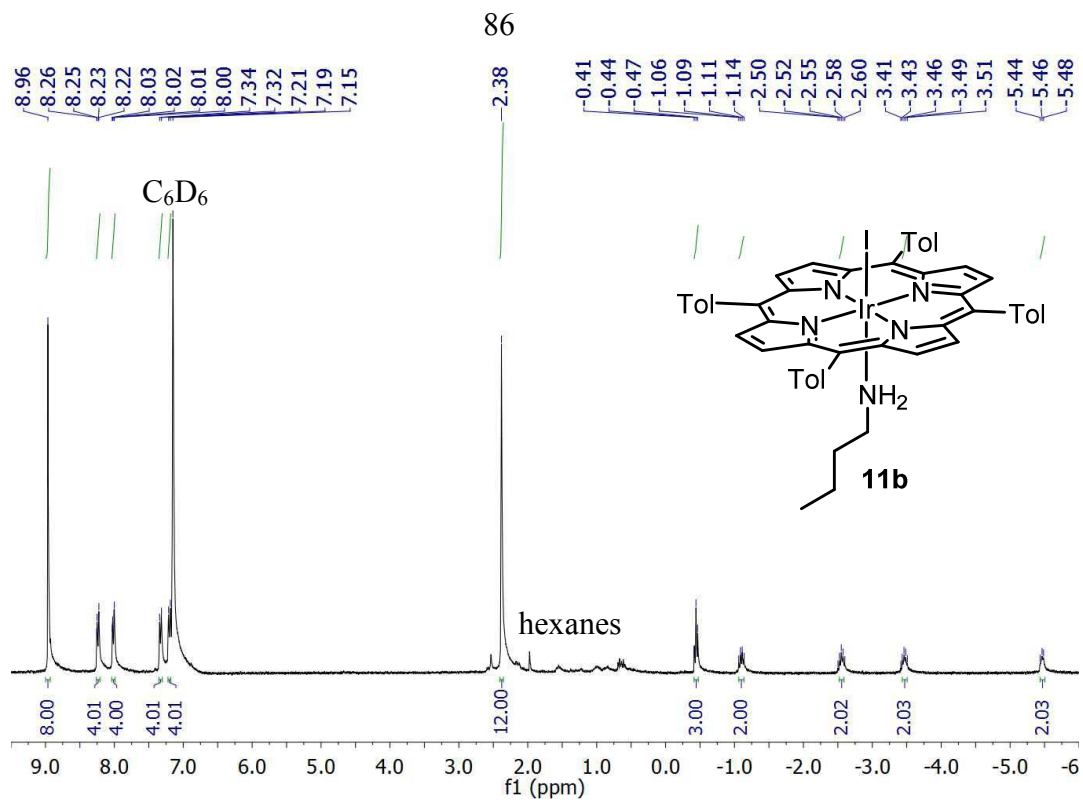


Fig. S44. ^{13}C NMR spectrum for (TTP)Ir(NH₂Bn)I (**11a**) in CDCl₃



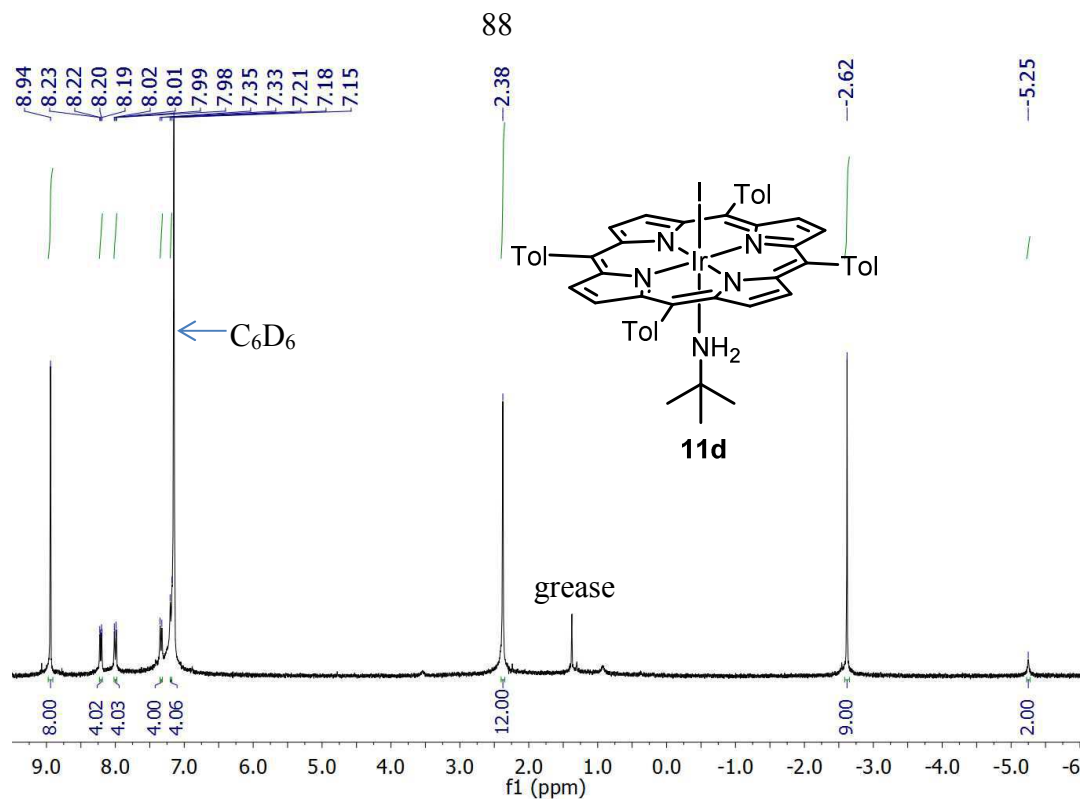


Fig. S49. ¹H NMR spectrum for (TTP)Ir(NH₂Bu'^t)I (**11d**) in C₆D₆

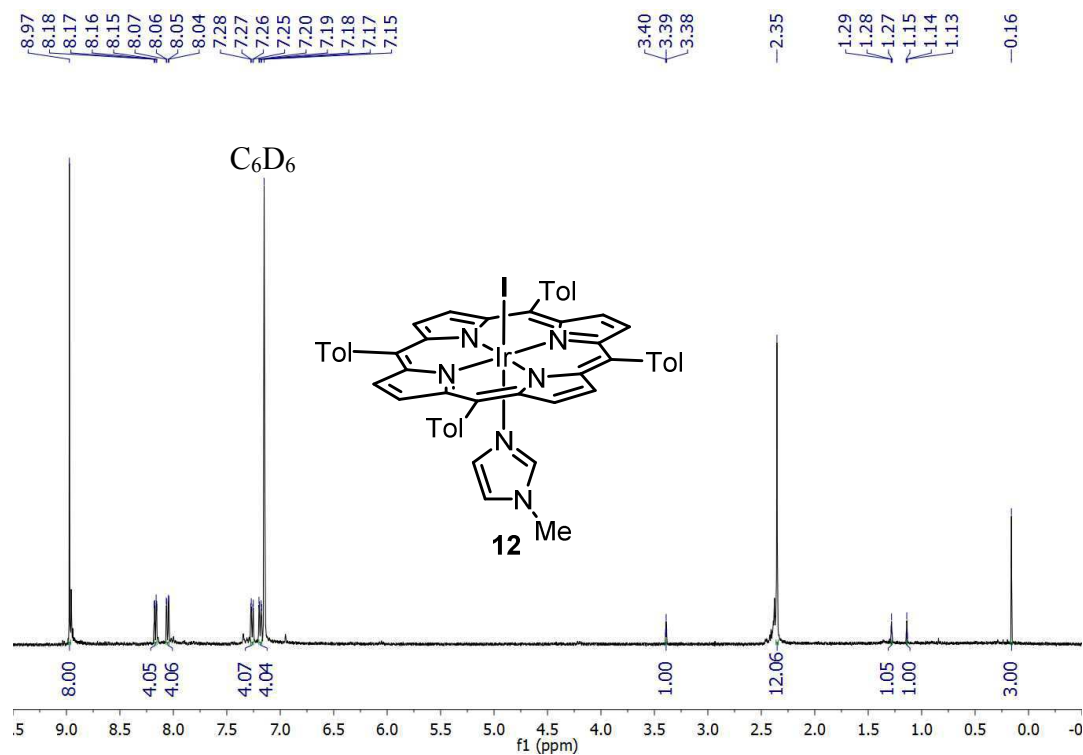


Fig. S50. ¹H NMR spectrum for (TTP)Ir(1-MeIm)I (**12**) in C₆D₆

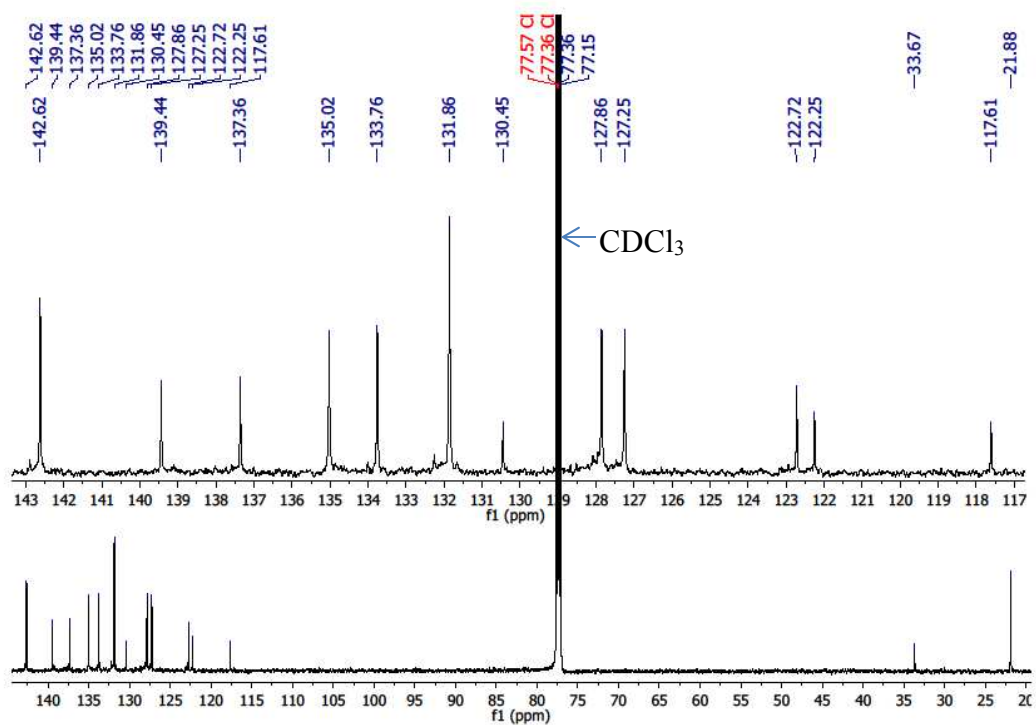


Fig. S51. ^{13}C NMR spectrum for $(\text{TTP})\text{Ir}(1\text{-MeIm})\text{I}$ (**12**) in CDCl_3

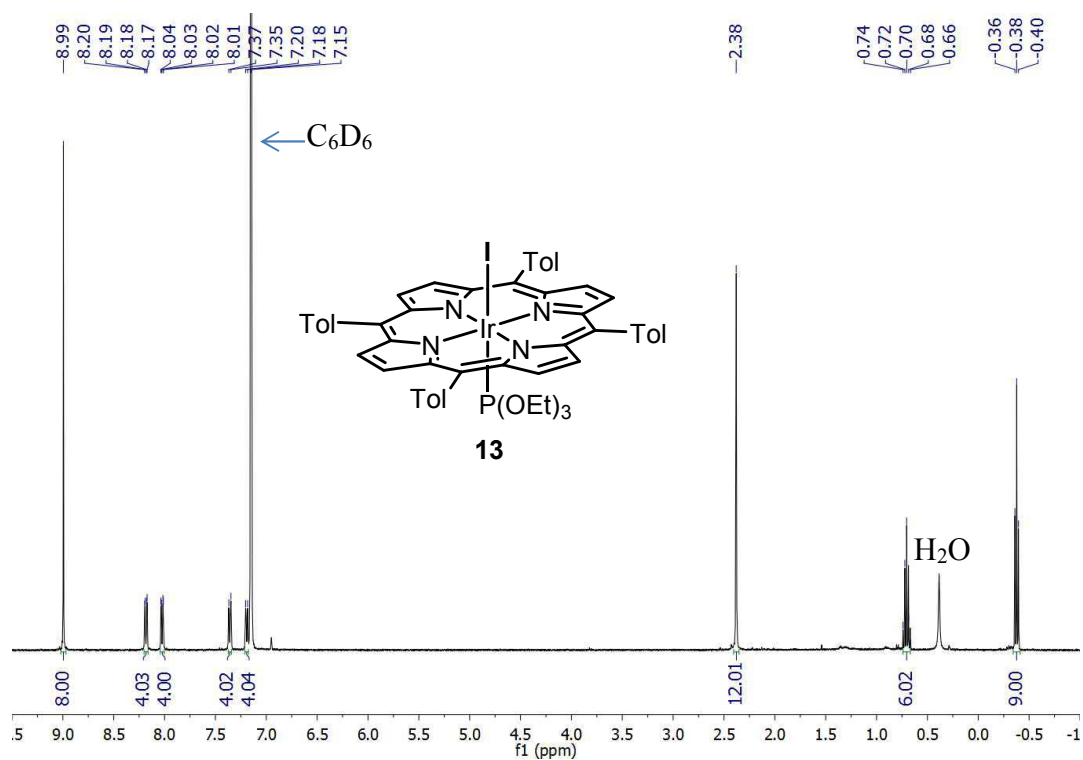


Fig. S52. ^1H NMR spectrum for $(\text{TTP})\text{Ir}[\text{P}(\text{OEt})_3]\text{I}$ (**13**) in C_6D_6

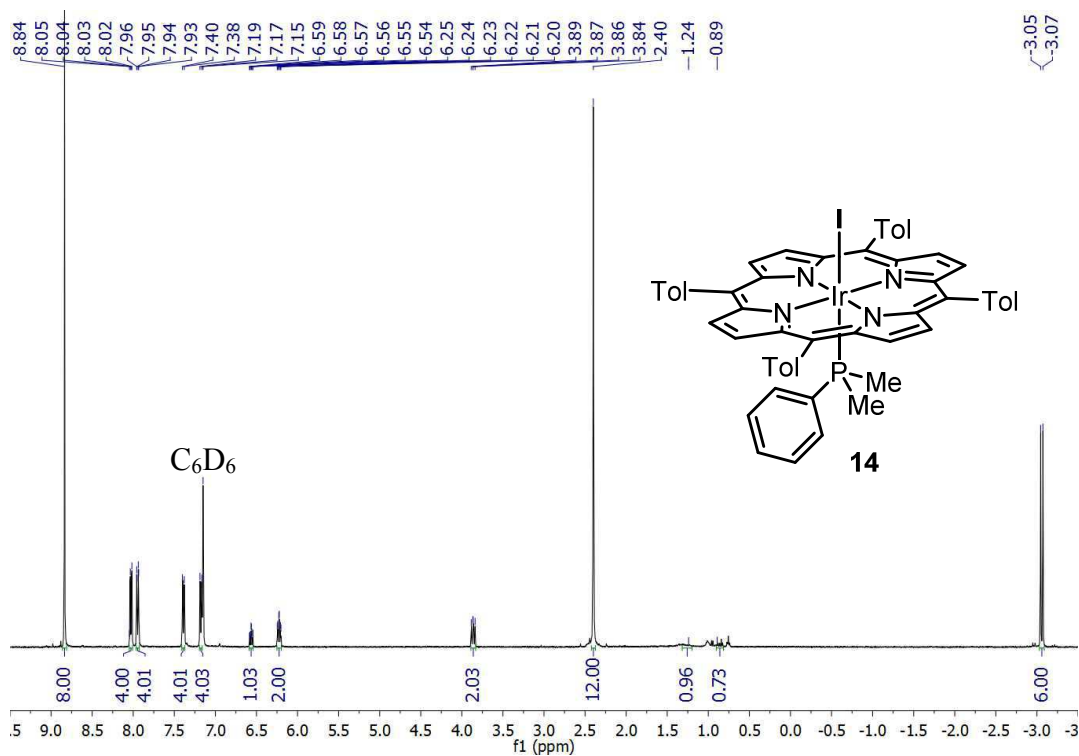


Fig. S55. ¹H NMR spectrum for (TTP)Ir(PMe₂Ph)I (**14**) in C₆D₆

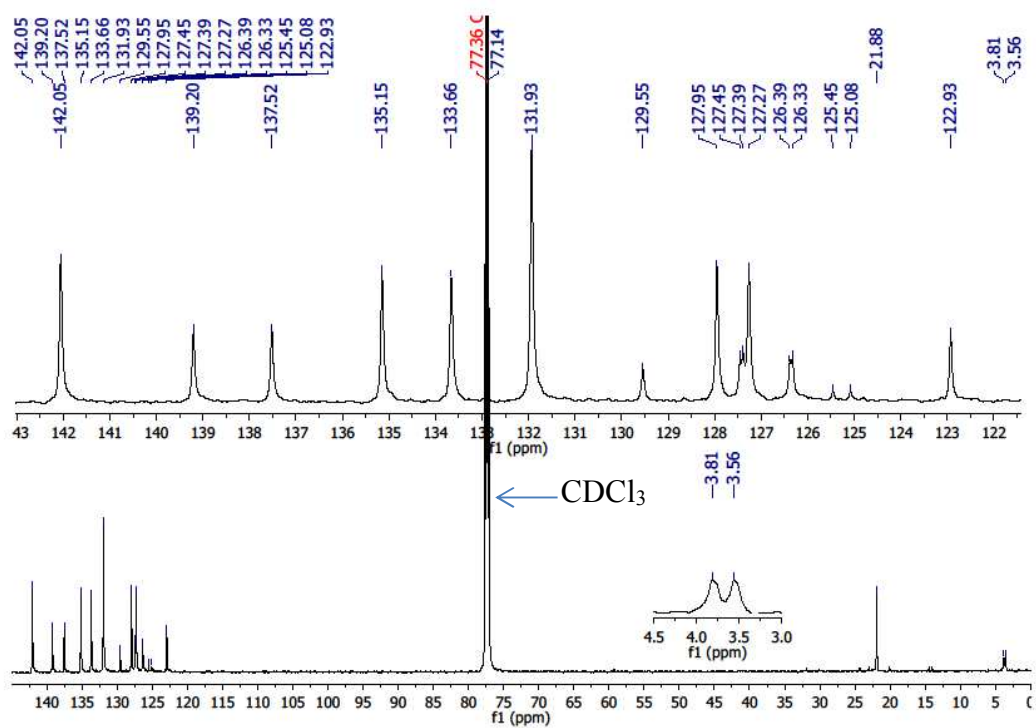


Fig. S56. ¹³C NMR spectrum for (TTP)Ir(PMe₂Ph)I (**14**) in CDCl₃

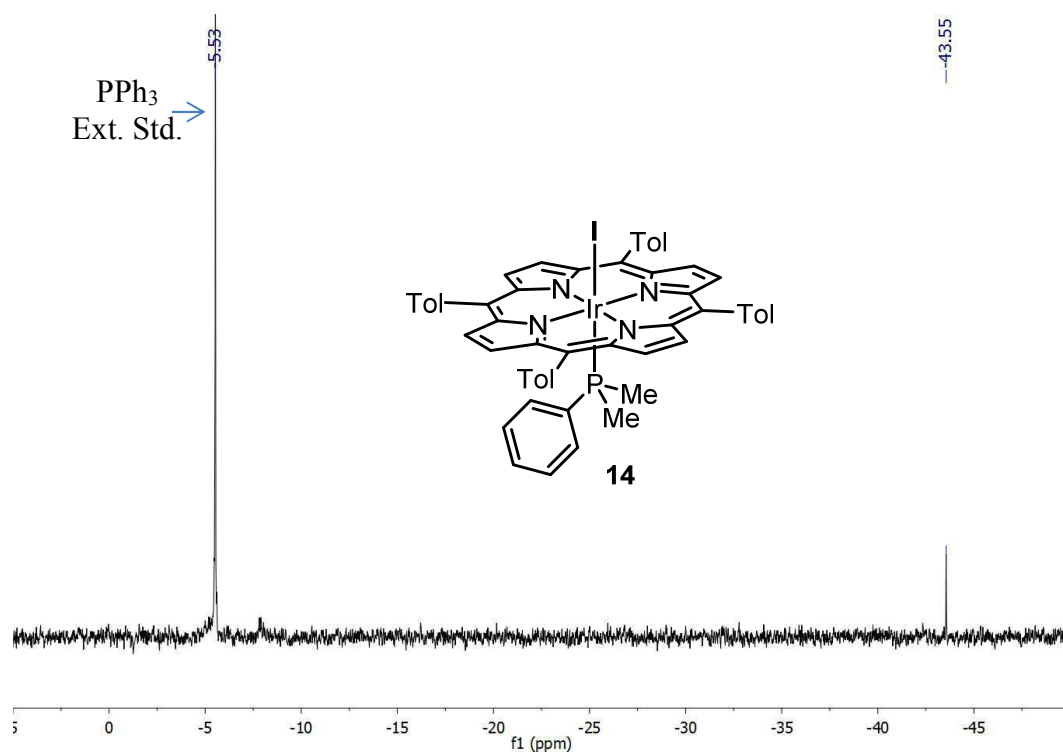


Fig. S57. ^{31}P NMR spectrum for $(\text{TTP})\text{Ir}(\text{PMe}_2\text{Ph})\text{I}$ (**14**) in C_6D_6

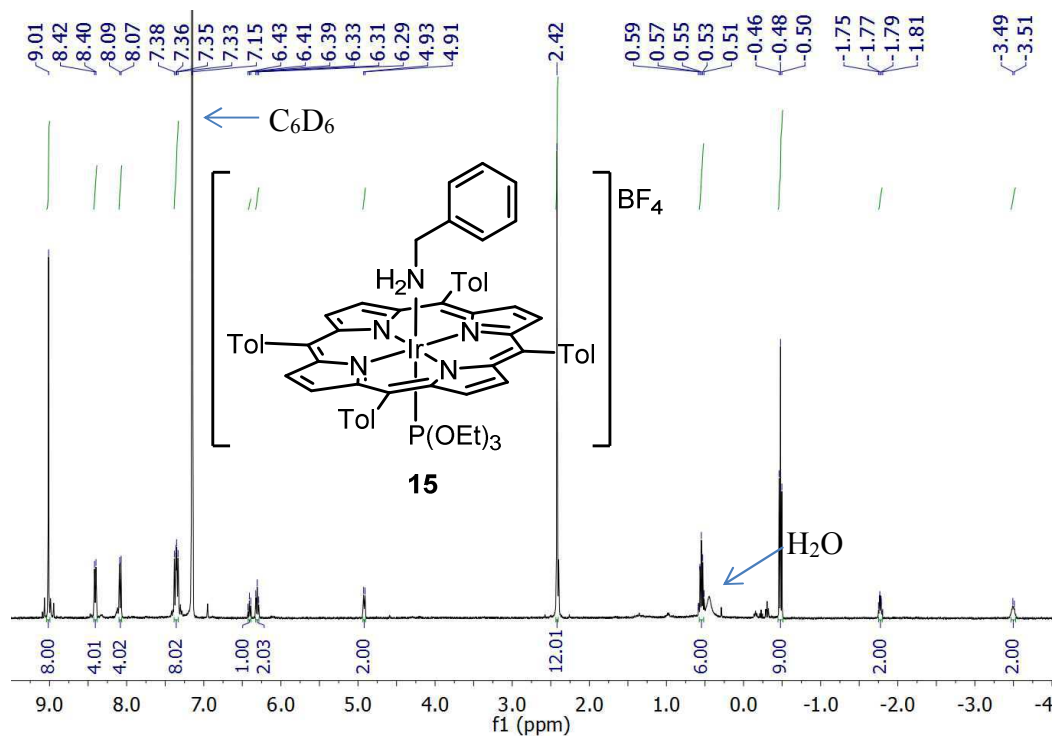


Fig. S58. ^1H NMR spectrum for $[(\text{TTP})\text{Ir}[\text{P}(\text{OEt})_3](\text{NH}_2\text{Bn})]\text{BF}_4$ (**15**) in C_6D_6

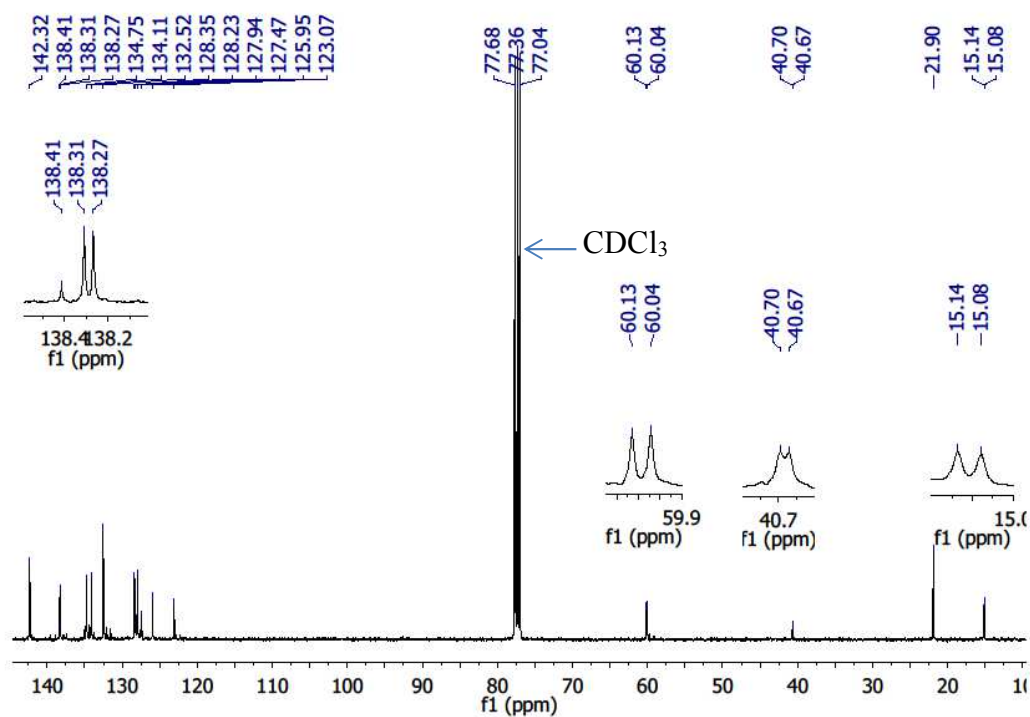


Fig. S59. ^{13}C NMR spectrum for $[(\text{TTP})\text{Ir}[\text{P}(\text{OEt})_3](\text{NH}_2\text{Bn})]\text{BF}_4$ (**15**) in CDCl_3

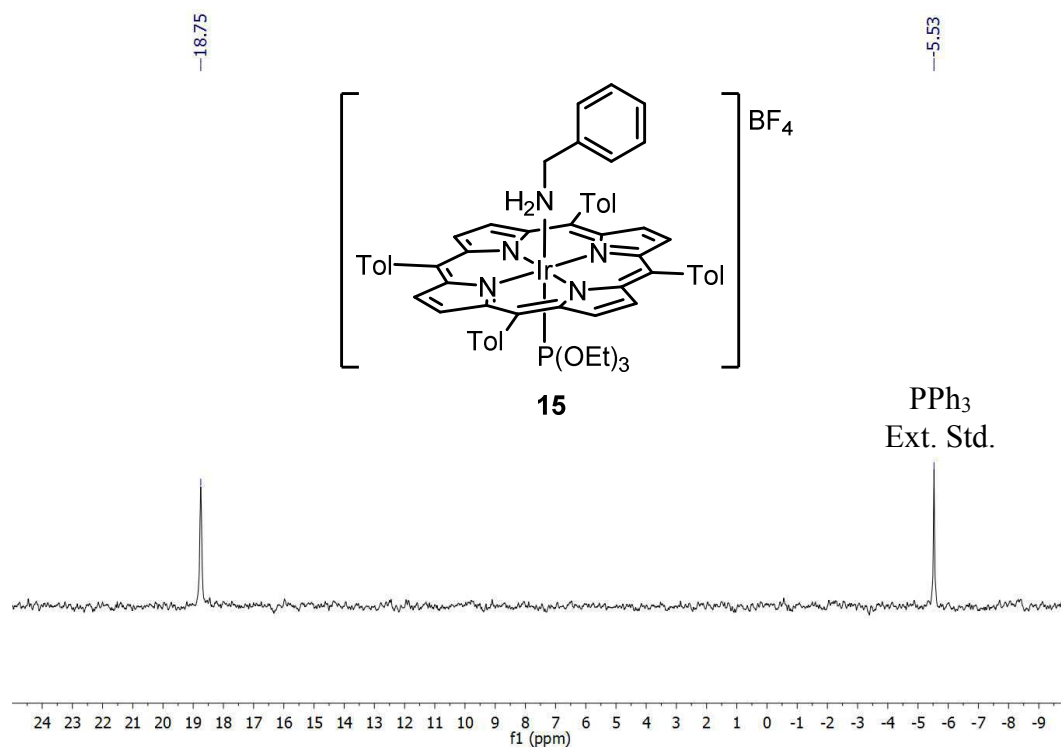
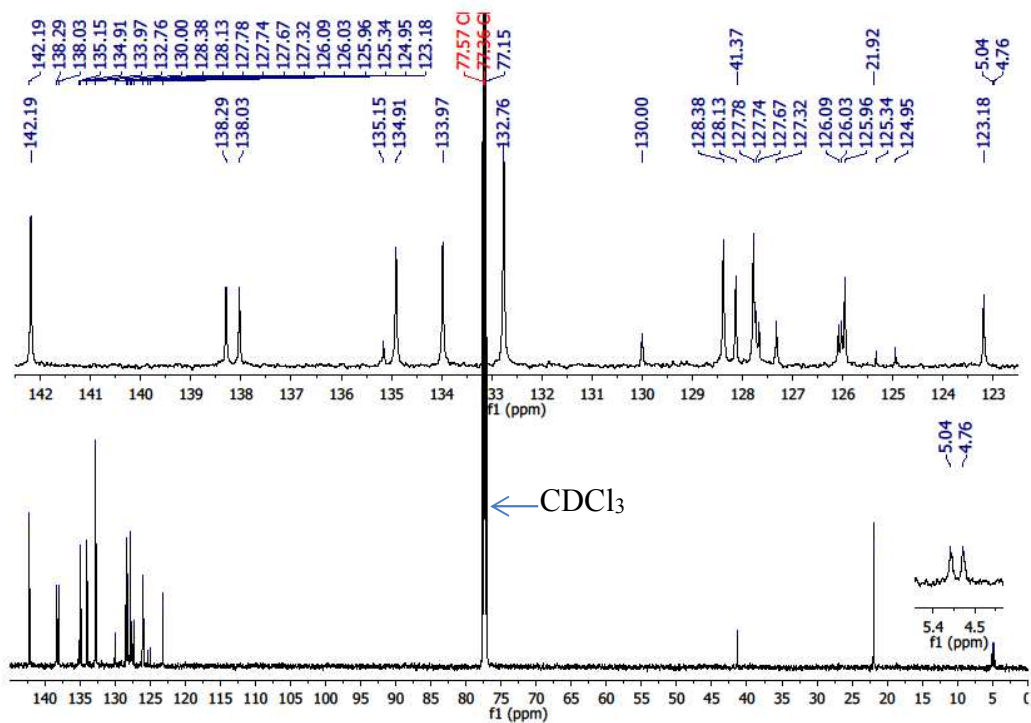
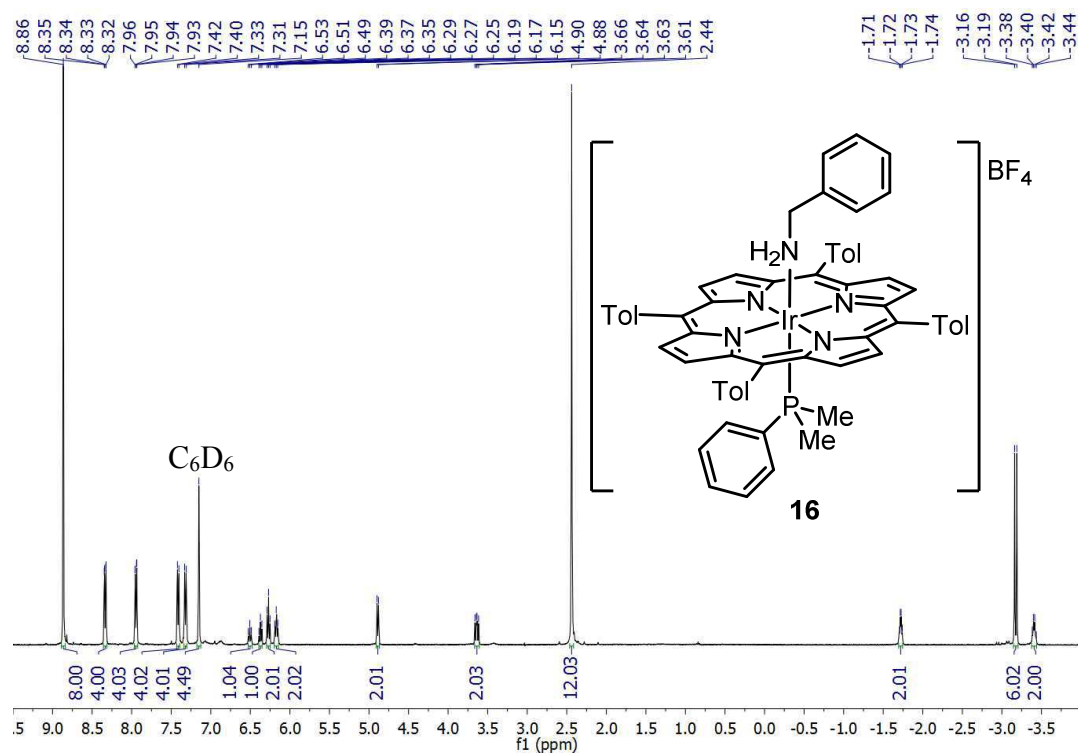


Fig. S60. ^{31}P NMR spectrum for $[(\text{TTP})\text{Ir}[\text{P}(\text{OEt})_3](\text{NH}_2\text{Bn})]\text{BF}_4$ (**15**) in C_6D_6



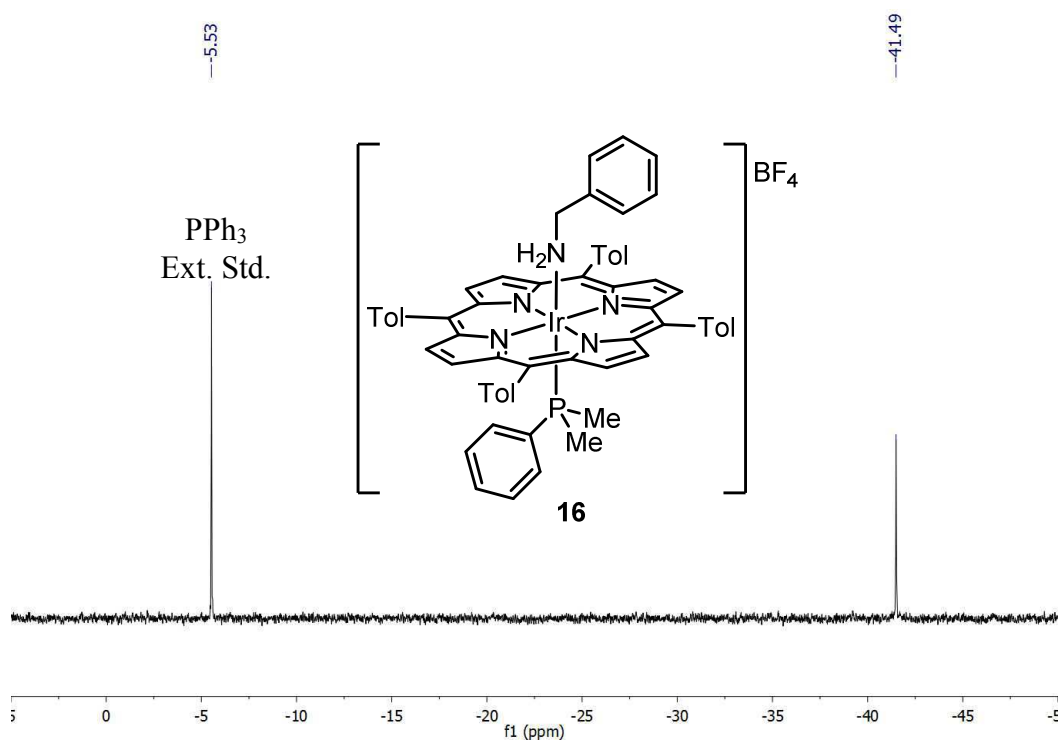


Fig. 63. ³¹P NMR spectrum for [(TTP)Ir(PMe₂Ph)(NH₂Bn)]BF₄ (**16**) in C₆D₆

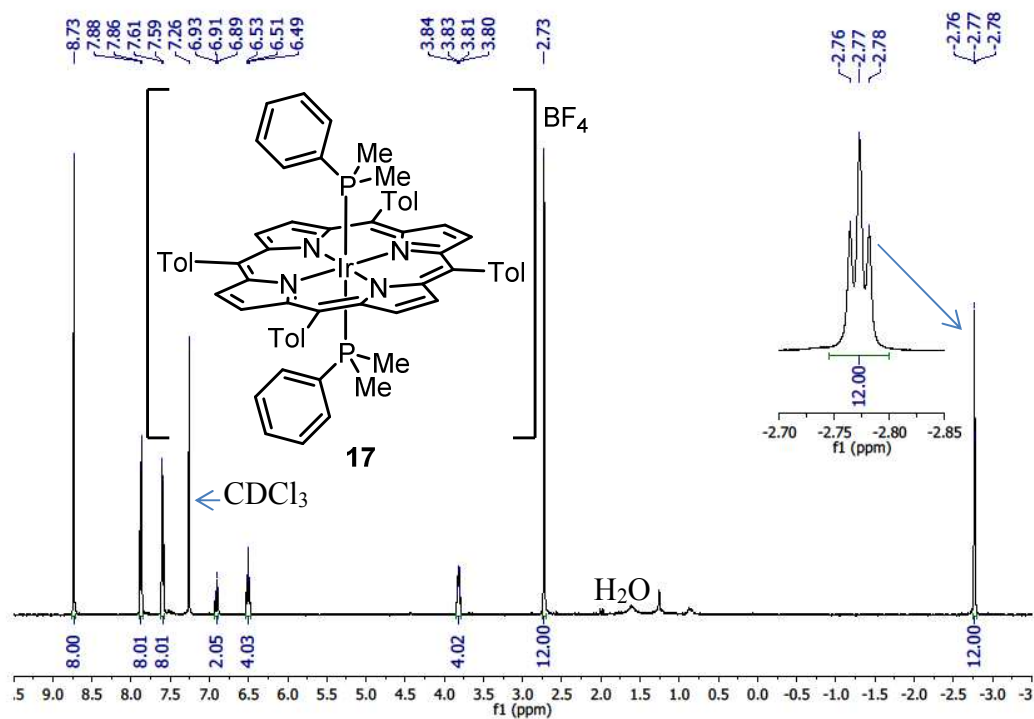


Fig. S64. ¹H NMR spectrum for *trans*-[(TTP)Ir(PMe₂Ph)₂]BF₄ (**17**) in CDCl₃

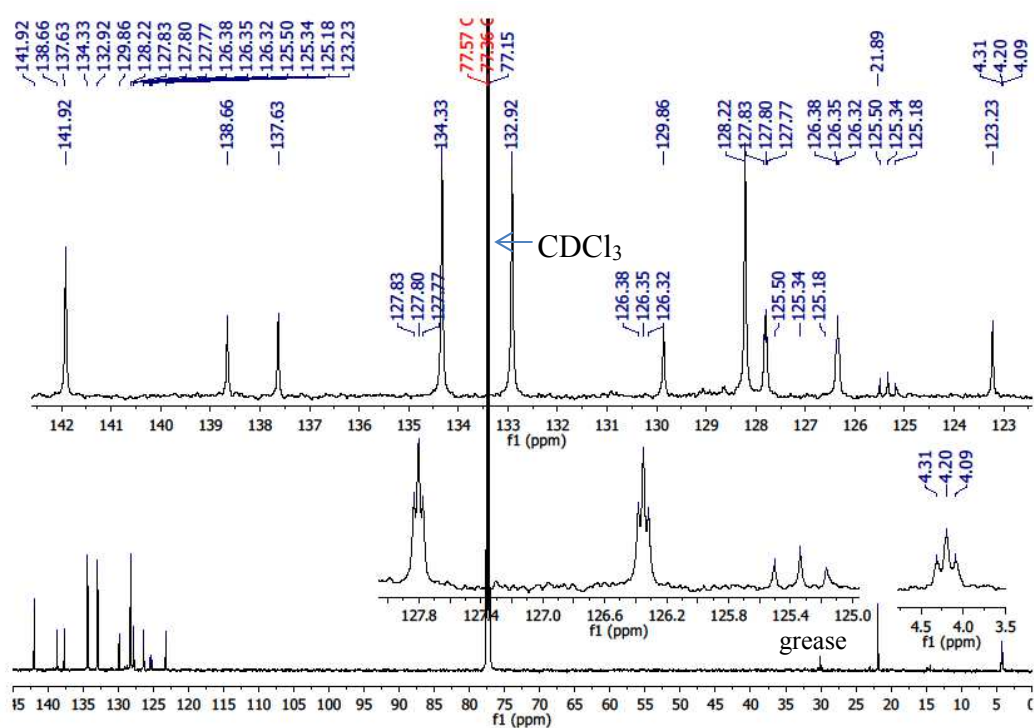


Fig. S65. ^{13}C NMR spectrum for *trans*-[(TTP)Ir(PMe₂Ph)₂]BF₄ (**17**) in CDCl₃

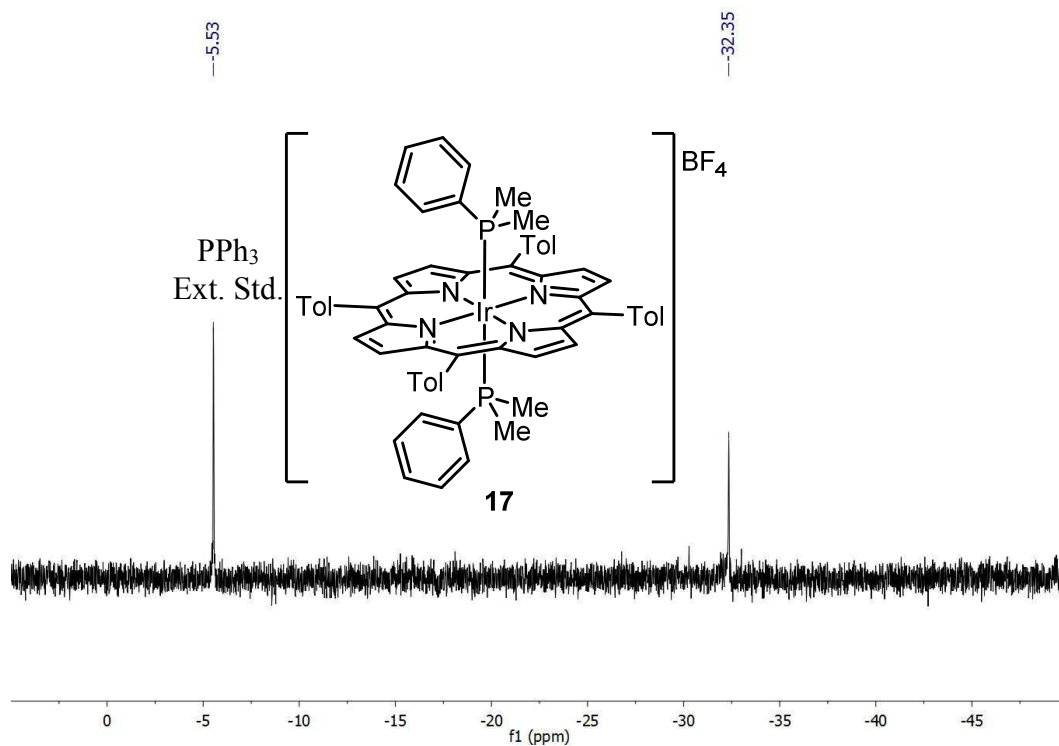


Fig. S66. ^{31}P NMR spectrum for *trans*-[(TTP)Ir(PMe₂Ph)₂]BF₄ (**17**) in C₆D₆

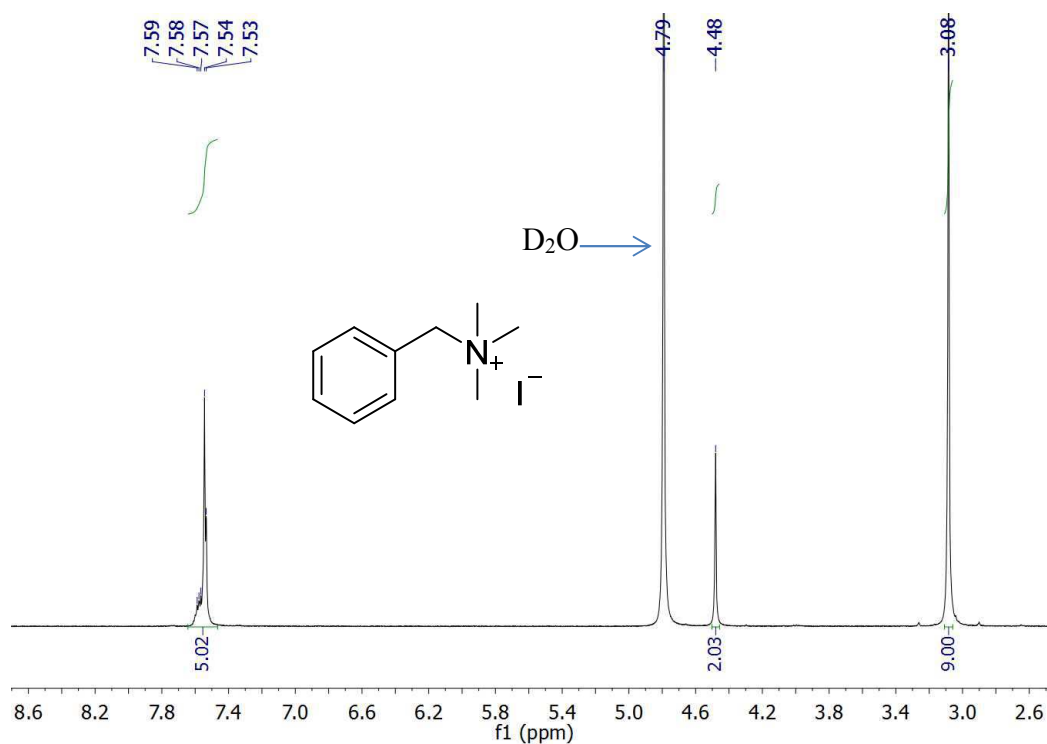


Fig. S67. ^1H NMR spectrum for $[\text{BnNMe}_3]\text{I}$ in D_2O

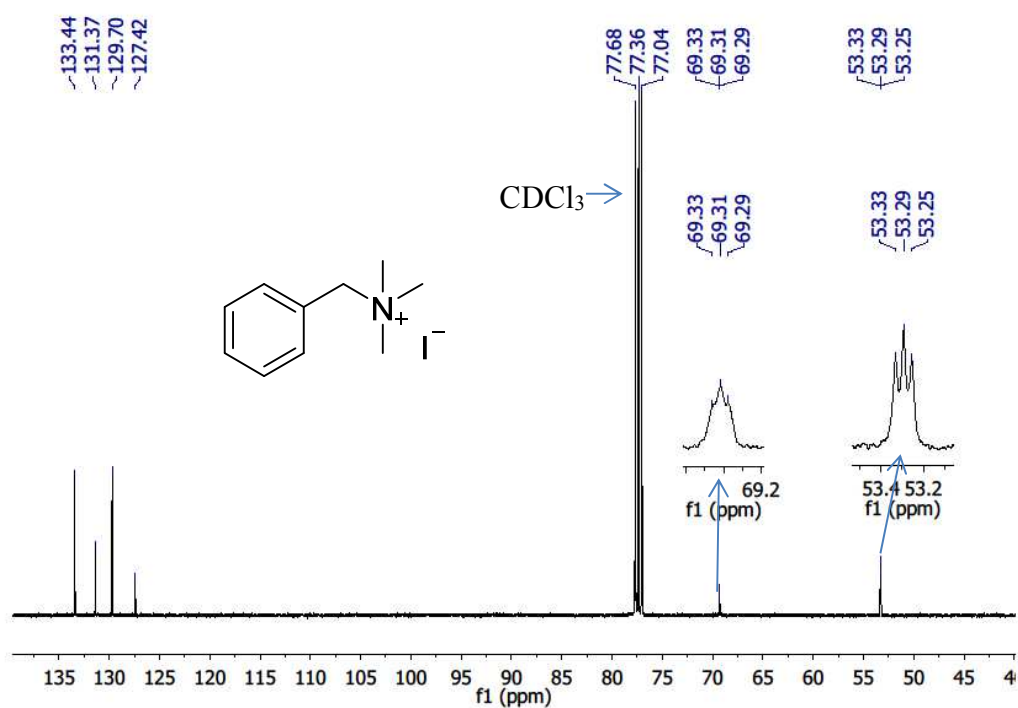


Fig. S68. ^{13}C NMR spectrum for $[\text{BnNMe}_3]\text{I}$ in CDCl_3

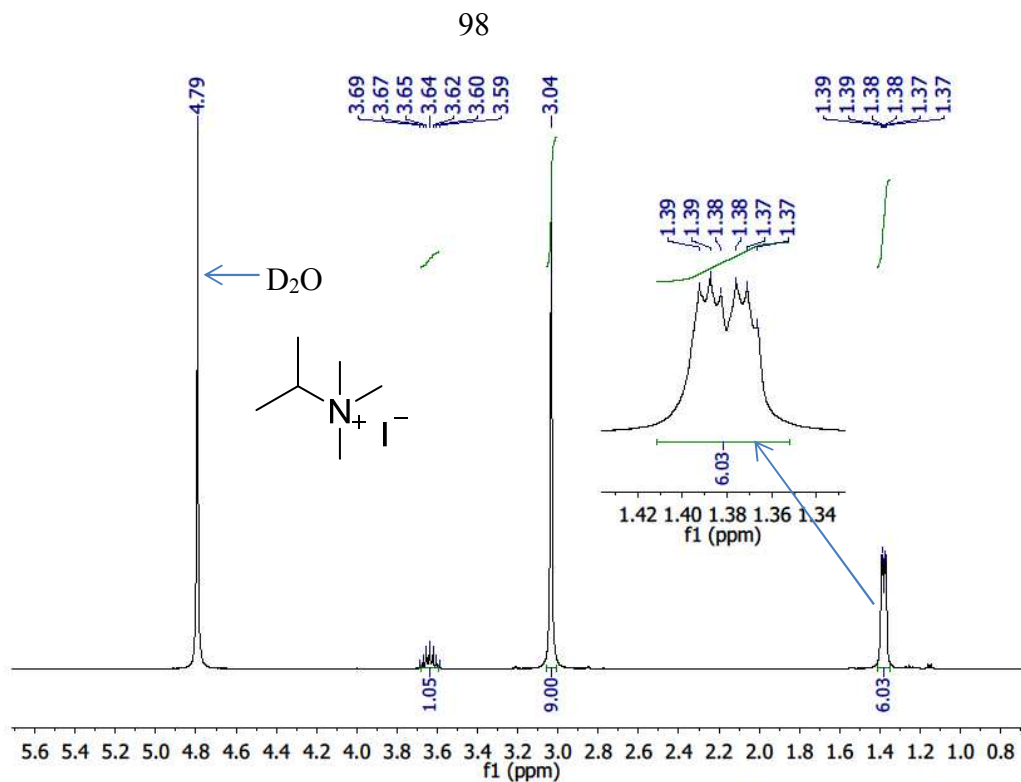


Fig. S69. ^1H NMR spectrum for $[i\text{-PrNMe}_3]\text{I}$ in D_2O

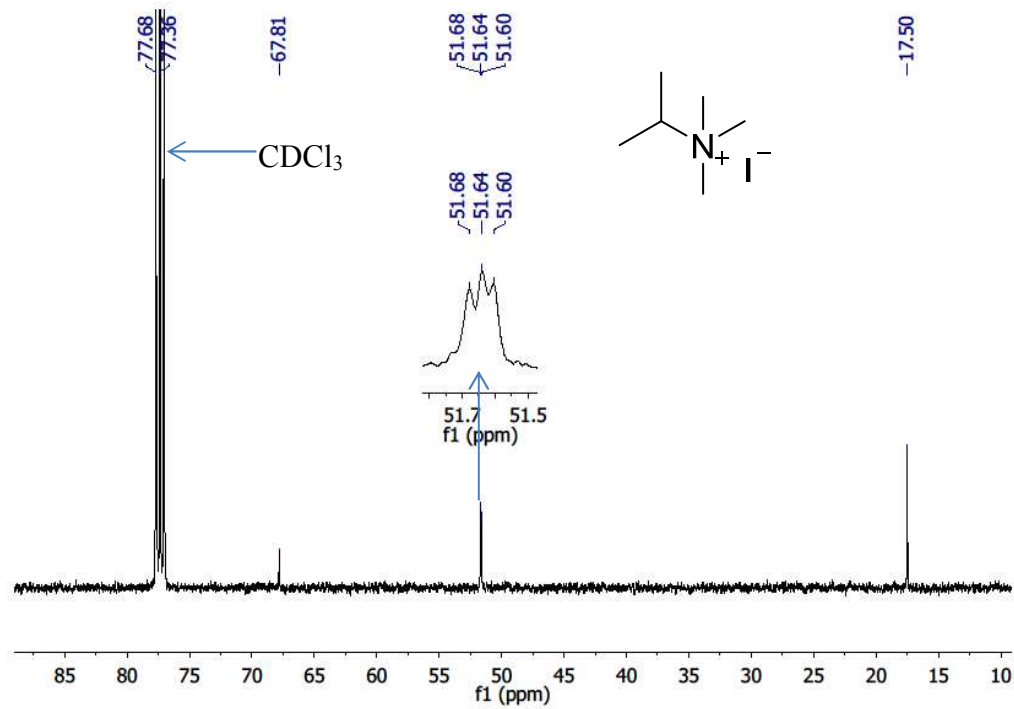


Fig. S70. ^{13}C NMR spectrum for $[i\text{-PrNMe}_3]\text{I}$ in CDCl_3

Table S1. Crystallographic and Structure Refinement Data for **4a** and **17**

Compound	(TTP)Ir(MeIm)[C(O)NHBn] (4a)	[(TTP)Ir(PMe ₂ Ph) ₂]BF ₄ (17)
Empirical Formula	C ₇₂ H ₇₄ Ir N ₇ O ₄	C ₆₈ H ₆₆ B F ₄ Ir N ₄ O P ₂
Formula weight (g mol ⁻¹)	1293.58	1296.19
Temperature (K)	173(2)	173(2)
Wavelength (Å)	0.71073	0.71073
Crystal system	Triclinic	Triclinic
Space group (no.)	P -1	P -1
<i>a</i> (Å)	9.833(3)	16.528(4)
<i>b</i> (Å)	16.673(5)	16.705(4)
<i>c</i> (Å)	20.164(7)	25.722(5)
α (°)	77.200(5)	82.678(4)
β (°)	86.527(5)	72.836(4)
γ (°)	81.073(5)	61.732(4)
<i>V</i> (Å ³)	3183.4(18)	5976(2)
<i>Z</i>	2	4
<i>D</i> _{calc} (g cm ⁻³)	1.350	1.441
μ (mm ⁻¹)	2.151	2.347
<i>F</i> (000)	1328	2632
θ range for data collection	1.27-27.72°	2.43-18.98°
Index ranges	-12 ≤ <i>h</i> ≤ 12, -21 ≤ <i>k</i> ≤ 21, -26 ≤ <i>l</i> ≤ 25	-18 ≤ <i>h</i> ≤ 18, -18 ≤ <i>k</i> ≤ 18, -28 ≤ <i>l</i> ≤ 28
Absorption corrections (<i>T</i> _{min} / <i>T</i> _{max})	0.55 / 0.74	0.63 / 0.74
Reflections collected	31174	55875
Completeness to θ_{\max}	98.5%	100%
Data/restraints/parameters	14716 / 150 / 757	17163 / 451 / 1498
Final <i>R</i> indices [<i>I</i> > 2σ(<i>I</i>)]	<i>R</i> ₁ = 0.0534, <i>wR</i> ₂ = 0.1369	<i>R</i> ₁ = 0.0580, <i>wR</i> ₂ = 0.1454
<i>R</i> indices (all data)	<i>R</i> ₁ = 0.0725, <i>wR</i> ₂ = 0.1463	<i>R</i> ₁ = 0.0979, <i>wR</i> ₂ = 0.1685
Goodness-of-fit on <i>F</i> ²	1.084	1.037
Largest diff. peak and hole	2.252 and -2.513 eÅ ⁻³	1.696 and -1.339 eÅ ⁻³

Table S2. Selected bond distances and angles for **4a** and **17**

(TTP)Ir(MeIm)[C(O)NHBn] (4a)		[(TTP)Ir(PMe ₂ Ph) ₂] ₂ BF ₄ (17)	
Ir-C(53)	2.026(6)	Ir-P(1)	2.354(3)
Ir-N(5)	2.208(5)	Ir-P(2)	2.348(3)
C(53)-O(1)	1.217(7)	P(1)-C(49)	1.783(13)
C(53)-N(7)	1.355(8)	P(1)-C(50)	1.800(12)
Ir-N(1)	2.034(4)	P(1)-C(51)	1.794(12)
Ir-N(2)	2.040(4)	P(2)-C(57)	1.822(13)
Ir-N(3)	2.045(4)	P(2)-C(58)	1.805(13)
Ir-N(4)	2.043(5)	P(2)-C(59)	1.808(12)
C(53)-Ir-N(5)	178.86(19)	Ir-N(1)	2.049(9)
O(1)-C(53)-N(7)	119.0(6)	Ir-N(2)	2.035(8)
O(1)-C(53)-Ir	124.3(5)	Ir-N(3)	2.035(8)
N(7)-C(53)-Ir	116.7(4)	Ir-N(4)	2.045(9)
N(1)-Ir-N(2)	89.57(17)	P(1)-Ir-P(2)	179.20(11)
N(1)-Ir-N(3)	178.92(18)	N(1)-Ir-N(2)	90.4(3)
N(1)-Ir-N(4)	90.68(18)	N(1)-Ir-N(3)	179.2(4)
N(2)-Ir-N(3)	90.12(17)	N(1)-Ir-N(4)	89.3(3)
N(2)-Ir-N(4)	178.44(18)	N(2)-Ir-N(3)	90.4(3)
N(3)-Ir-N(4)	89.59(18)	N(2)-Ir-N(4)	179.2(4)
C(53)-Ir-N(1)	88.9(2)	N(3)-Ir-N(4)	89.9(3)
C(53)-Ir-N(2)	91.7(2)	Ir-P(1)-C(49)	114.3(5)
C(53)-Ir-N(3)	92.2(2)	Ir-P(1)-C(50)	113.2(4)
C(53)-Ir-N(4)	89.8(2)	Ir-P(1)-C(51)	114.5(4)
		Ir-P(2)-C(57)	112.8(6)
		Ir-P(2)-C(58)	114.0(5)
		Ir-P(2)-C(59)	113.9(4)

CHAPTER 3. SCOPE AND MECHANISM OF IRIDIUM PORPHYRIN- CATALYZED S-H INSERTION REACTIONS

To be submitted to *Organometallics* for publication

Taiwo O. Dairo and L. Keith Woo

Abstract

The insertion of carbenes from ethyl diazoacetate (EDA), methyl diazoacetate (MDA), methyl phenyldiazoacetate (MPDA) or methyl (*p*-tolyl)diazoacetate (MTDA) into the S-H bonds of aromatic and aliphatic thiols was catalyzed by (5,10,15,20-tetratolylporphyrinato)methyliridium(III), Ir(TTP)CH₃, under ambient temperatures. Yields of the resulting thioether products were as high as 97% for aromatic thiols, with catalyst loadings as low as 0.07 mol%. Thiol binding to Ir(TTP)CH₃ was measured by titration studies and provided equilibrium constants, K_b, ranging from 4.25 x 10² - 1.69 x 10³, for *p*-nitrobenzenethiol, *p*-chlorobenzenethiol, benzenethiol, *p*-methylbenzenethiol, *p*-methoxybenzenethiol, and benzyl mercaptan. Hammett plots generated from substrate competition experiments with different *para* substituted benzenethiols, in the presence of MDA and MTDA, had slopes of -0.12 ± 0.01 and -0.78 ± 0.11, respectively. These data are consistent with nucleophilic attack of thiols on an iridium-carbene species. Control experiments showed that thioether product inhibition on the catalyst was not significant. Kinetic studies also suggested that the nature of the rate-limiting step was determined by the thiol concentration.

Introduction

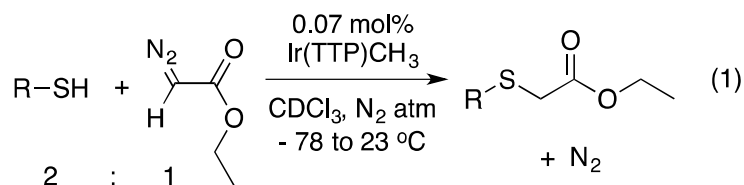
The biological and medicinal importance of thioethers^{1,2} drives the search for convenient and efficient strategies of forming C–S bonds. Over the years, thioethers have been synthesized by several methods, including metal-free conditions, in the presence of acid and base catalysts.³⁻⁵ Other approaches involved the use of iron(III) porphyrin catalysts in the addition of disulfides to olefins,^{6,7} while alternative routes to thioethers included the palladium-catalyzed coupling of organic halides with thiols.^{8,9} Furthermore, thioethers have been produced from the copper-catalyzed reactions between diaryl disulfides and β -dicarbonyl compounds.¹⁰ An atom-economic method of forming new C-S bonds is the insertion of the carbene fragment of diazo compounds into the S-H bond of thiols, releasing N_2 as the only by-product.¹¹ One of the earliest examples of a diazo reaction with an S-H bond was reported by Yates, wherein copper was found to catalyze the production of 1-phenyl-2-(phenylthio)ethan-1-one in 67% yield from the treatment of benzenethiol with 2-diazoacetophenone at 70 °C.¹² Subsequently, transition metal salts and complexes containing rhenium,¹³ iron,¹⁴ ruthenium,¹⁵ scandium,¹⁶ indium,¹⁷ and rhodium^{18,19} have been reported to catalyze S-H insertion reactions. The catalytic activity of porphyrin complexes of iron and ruthenium has also been demonstrated.²⁰⁻²⁴

Our group has recently reported the synthesis and catalytic utility of iridium(III)porphyrinato complexes in carbene transfer reactions.²⁵⁻²⁹ Notably, we have demonstrated that tetratolylporphyrinatomethyliridium(III) $[Ir(TTP)CH_3]$ efficiently catalyzed the N-H insertion reactions of aliphatic and aromatic amines with different diazoesters.²⁷ High catalyst turnover numbers (TON) up to 10^5 were achieved with aromatic amine substrates, and a mechanistic investigation of the reaction pathway was also carried

out. Furthermore, chiral and achiral iridium(III) porphyrin complexes were shown to be active catalysts for C-H and Si-H insertion reactions involving diazo compounds.³⁰⁻³² Despite the vast effectiveness of transition metal complexes as catalysts in S-H insertion reactions between diazo compounds and thiols, a more detailed mechanistic investigation is lacking in the literature. We show that Ir(TTP)CH₃ efficiently catalyzes the insertion of carbene moieties into the S-H bond of thiols. In order to gain further insight into the reaction pathway, we undertook kinetic studies, and our findings are reported herein.

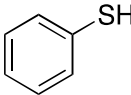
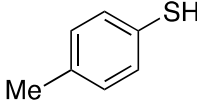
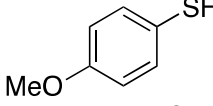
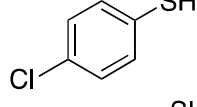
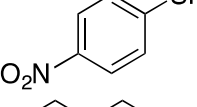
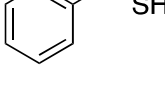
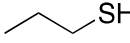
Results and Discussion

When a CDCl₃ solution of benzenethiol was treated with ethyl diazoacetate (EDA) in the presence of a catalytic amount of Ir(TTP)CH₃ (0.07 mol% relative to EDA), the carbene fragment from EDA readily inserted into the S-H bond, to generate ethyl 2-(phenylthio)acetate in 87% yield, within 15 minutes of reaction (Table 1, entry 1). The only observed byproducts were diethyl maleate and diethyl fumarate, resulting from carbene dimerization. The optimal stoichiometric ratio was found to be a 2:1 mole ratio of thiol:EDA. In contrast, the use of a 1:1 substrate ratio required longer reaction times to afford a comparable product yield (Table 1, entry 2). Typically, reactions were started at -78 °C, allowed to warm to 23 °C (eq 1), and maintained at this temperature for 15 minutes. This reaction protocol is similar to the recently reported optimized reaction conditions for the Ir(TTP)CH₃-catalyzed single insertion of EDA into the N-H bond of aromatic amines.²⁷ Control experiments showed that no reaction occurred in the absence of Ir(TTP)CH₃.



The same conditions employed for the S-H insertion reaction between benzenethiol and EDA were applied to other aromatic thiols. For example, the yields of sulfides from the reaction of EDA with the electron-rich *p*-methyl- and *p*-methoxybenzenethiols were 79% and

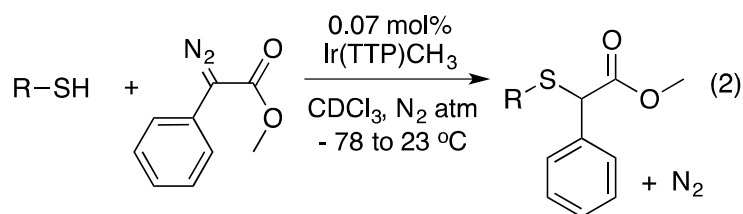
Table 1. Reaction of EDA with aromatic and aliphatic thiols catalyzed by Ir(TTP)CH₃^a.

Entry	Thiol	Time (min)	Insertion (%) ^b	Carbene Dimers (%) ^b
1		15	87	10
2	"	45 ^c	81	11
3		15	79	13
4		25	80	19
5		35	70	27
6		15	85	14
7		15	83	15
8		75	80	19

^aIr(TTP)CH₃ (0.031 μmol; 0.07 mol%), EDA (42.6 μmol; 73 mM), thiol (87.0; 150 mM), in 0.58 mL CDCl₃. ^bYields were determined by NMR, with Ph₃CH as internal standard. ^cEDA:thiol = 1:1 (73 mM each)

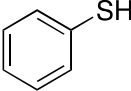
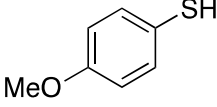
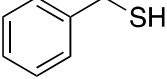
80%, respectively (Table 1, entries 3 and 4). Similarly, ethyl 2-[(4-chlorophenyl)thio]acetate and ethyl 2-[(4-nitrophenyl)thio]acetate were obtained in 70% and 85% yields from the electron-poor *p*-chloro- and *p*-nitrobenzenethiols, respectively (Table 1, entries 5 and 6). Furthermore, Ir(TTP)CH₃ efficiently catalyzed the reaction of EDA with aliphatic substrates, benzyl mercaptan and propanethiol, with high S-H insertion yields (Table 1, entries 7 and 8). In each case, the organic side products were the carbene dimers of EDA, diethyl maleate and diethyl fumarate.

When the bulkier and less active methyl phenyldiazoacetate (MPDA) was used as the carbene source for a selection of the thiol compounds (eq 2), a reduction in carbene dimerization was observed.²⁵ Thus, treatment of MPDA in separate reactions with twofold e-



xcesses of benzenethiol or *p*-methoxybenzenethiol and Ir(TTP)CH₃ produced the corresponding S-H insertion products in near-quantitative yields (Table 2, entries 1 and 2). However, the yield of methyl 2-(benzylthio)-2-phenylacetate obtained from the 2-h reaction of MPDA with benzyl mercaptan was much lower (21%), using the same reaction protocol (Table 2, entry 3). Extending the reaction time to 6 h increased the yield to 47%. Furthermore, a similarly low product yield (21%) was obtained, when equal amounts of the substrates were used (Table 2, entry 4). When MPDA was added first to the catalyst, followed by the addition of benzyl mercaptan to avoid catalyst poisoning by the thiol,²⁷ the yield dropped to 5% (Table 2, entry 5). However, use of excess amounts of MPDA (2.5 and

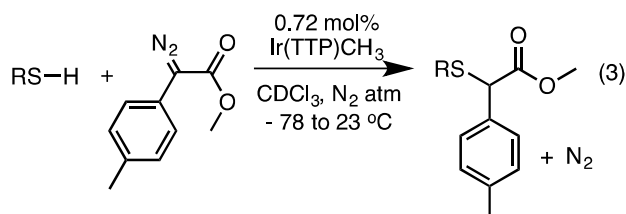
Table 2. Reaction of MPDA with aromatic and aliphatic thiols catalyzed by Ir(TTP)CH₃.

Entry	Thiol	Time	Insertion (%)
1		90 min	94 ^a
2		75 min	97 ^a
3		2 h	21 ^a
4	"	2 h	21 ^b
5	"	2 h	5 ^{a,c}
6	"	1 h	80 ^d
7	"	30 min	83 ^e
8	"	1 h	Trace ^{c,d}

^aIr(TTP)CH₃ (0.031 μmol), MPDA (42.6 μmol), thiol (87.0 μmol), in 0.58 mL CDCl₃. ^bIr(TTP)CH₃ (0.031 μmol), MPDA (42.6 μmol), Thiol (42.6 μmol), in 0.58 mL CDCl₃. ^cMPDA was added first to Ir(TTP)CH₃. ^dIr(TTP)CH₃ (0.031 μmol), MPDA (87.8 μmol), thiol (35.4 μmol), in 0.50 mL CDCl₃. ^eIr(TTP)CH₃ (0.031 μmol), MPDA (227 μmol), thiol (35.4 μmol), in 0.50 mL CDCl₃. Yields were determined by NMR, with Ph₃CH as an internal standard.

6.4 equivalents relative to benzyl mercaptan) was found to improve the product yields to 80% and 83% (Table 2, entries 6 and 7).

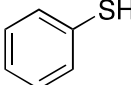
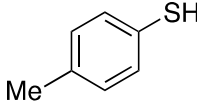
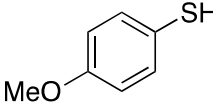
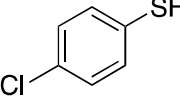
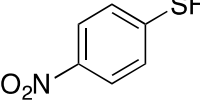
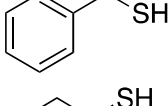

The carbene moiety of methyl (*p*-tolyl)diazoacetate (MTDA) also inserts into the S-H bond of the thiol compounds, albeit with a higher catalyst loading than was used with MDA and MPDA (eq 3). Using the same reaction protocol that was employed above, methyl 2-(*p*-



-enylthio)-2-(*p*-tolyl)acetate was obtained from the reaction between benzenethiol and MTDA in 61% yield within 1 hour (Table 3, entry 1). Similar treatment of the other aromatic and aliphatic thiols with MTDA in the presence of catalytic amount of Ir(TTP)CH₃ gave the corresponding thioethers in yields up to 81% (Table 3, entries 2 – 7).

Since five-coordinate metalloporphyrins have a vacant coordination site, equilibrium binding between the thiol substrates and Ir(TTP)CH₃ was studied by titration experiments, usi-

Table 3. Reaction of MTDA with aromatic and aliphatic thiols catalyzed by Ir(TTP)CH₃.^a

Entry	Thiol	Time (min)	Insertion (%)
1		60	61
2		30	54
3		30	81(74) ^b
4		30	51
5		25	80(57) ^b
6		45	74
7		45	70

^aIr(TTP)CH₃ (0.306 μmol; 0.72 mol%), MTDA (42.6 μmol; 73 mM), thiol (87.0; 150 mM), in 0.58 mL CDCl₃. Yields were determined by NMR, with Ph₃CH as internal standard. ^bIsolated yields based on the amount of MTDA.

-ng UV-visible spectrophotometry (eq 4; see experimental section for details). The equilibrium binding constants (Table 4) were used to generate a Hammett plot (Figure 1) that

provided a correlation constant, ρ^+ , of -0.18 ± 0.01 . The negative ρ^+ value indicates that electron-rich thiols are more tightly bound to iridium than electron-poor thiols. This trend is similar to that reported earlier for anilines,²⁷ although primary aromatic amines were more strongly bound ($K_b = 2.4 \times 10^3 - 2.3 \times 10^5$) to Ir(TTP)CH₃ than were thiols. A consequence of

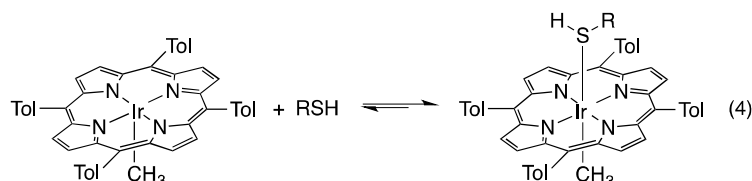


Table 4. Equilibrium binding constants for the coordination of thiols to Ir(TTP)CH₃ at 23 °C.

Entry	Thiol	K
1	<i>p</i> -methoxybenzenethiol	$7.98 \pm 0.02 \times 10^2$
2	<i>p</i> -methylbenzenethiol	$6.76 \pm 0.24 \times 10^2$
3	benzenethiol	$5.78 \pm 0.33 \times 10^2$
4	<i>p</i> -chlorobenzenethiol	$5.26 \pm 0.35 \times 10^2$
5	<i>p</i> -nitrobenzenethiol	$4.25 \pm 0.44 \times 10^2$
6	benzyl mercaptan	$1.69 \pm 0.029 \times 10^3$

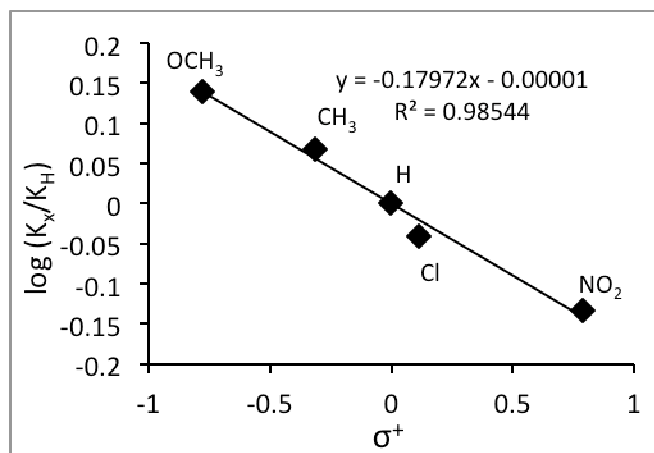


Figure 1. Hammett correlation for the equilibrium binding of *para*-substituted benzenethiols to Ir(TTP)CH₃.

strong thiol binding to iridium is apparent in the reaction of MPDA with benzyl mercaptan (Table 2). The strong affinity of benzyl mercaptan for iridium (Table 4, entry 6) inhibits coordination of the bulky MPDA, requiring an excess of the diazo reagent to afford higher yields of the insertion product.

Competition experiments involving benzenethiol and various *para*-substituted benzenethiols were carried out to determine relative rates (eq. 5).

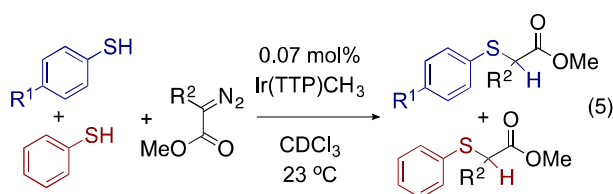


Table 5. Substrate competition reactions catalyzed by Ir(TTP)CH₃.

Substrate A	Substrate B	Diazo reagent	k_A / k_B
		MDA	1.09 ^a
"	"	MTDA	1.99 ^a
	"	MDA	1.03 ^a
"	"	MTDA	1.58 ^a
	"	MDA	0.910 ^a
"	"	MTDA	1.08 ^a
	"	MDA	0.802 ^a
"	"	MTDA	0.283 ^a

^aIr(TTP)CH₃ (0.031 μmol), Substrate A (42.6 μmol), Substrate B (42.6 μmol), diazo reagent (46.8 μmol), in 0.58 mL CDCl₃. Product ratios were determined by NMR, with Ph₃CH as internal standard.

With MDA, a Hammett correlation of $\rho = -0.12 \pm 0.01$ was obtained, while a correlation of $\rho = -0.78 \pm 0.11$ was obtained for reactions with MTDA (Figure 2). A value of $\rho = -0.66$ was previously observed during insertion reactions of EDA into the N-H bond of amines, catalyzed

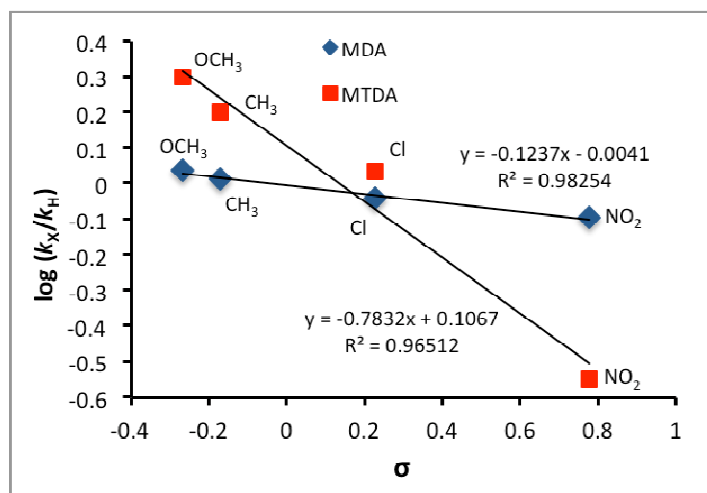
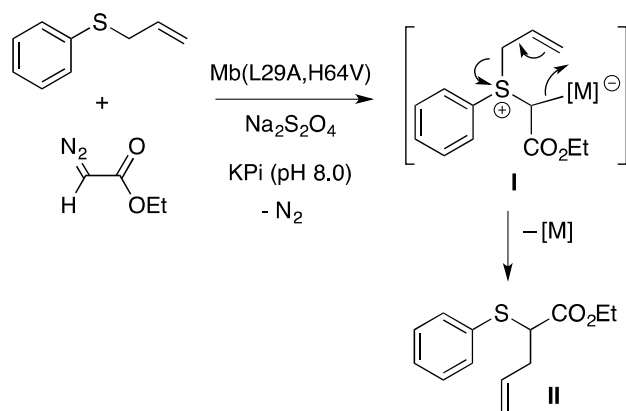


Figure 2. Hammett correlations for substrate competition reactions between benzenethiol and *p*-substituted benzenethiols in the presence a catalytic amount of Ir(TTP)CH₃ and either MDA or MTDA.

ed by iron(III)tetraphenylporphyrin chloride [Fe(TPP)Cl],³³ while a ρ^+ value of -0.56 was observed during the Ir(TTP)CH₃-catalyzed insertion reactions of MPDA into the N-H bond of amines.²⁷

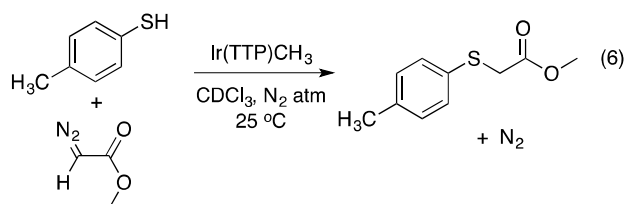
In the Ir(TTP)CH₃ system, the slightly negative values of ρ suggest a small build-up of positive charge on the sulfur atom during the S-H insertion reactions, consistent with the formation of a metal-ylide species. In analogy, a metal-bound ylide intermediate was recently suggested for a dirhodium-catalyzed S-H insertion system.³⁴ During a recently-reported myoglobin-catalyzed insertion of carbenes from diazo esters into the S-H bonds of thiols, Fasan and co-workers trapped a sulfonium ylide intermediate, using allyl phenyl sulfide.³⁵

The allyl moiety can trap metal–ylide intermediates by a rapid intramolecular 2,3-sigmatropic rearrangement via intermediate **I** (Scheme 1).³⁵ Similarly, treatment of a catalytic amount of Ir(TTP)CH₃ with a CDCl₃ solution of allyl phenyl sulfide and EDA (see experimental section for details) resulted in the formation of 2-(phenylthio)pent-4-enoate (**II**) in 85% yield, in addition to carbene dimers of EDA (4%).



Scheme 1. Allyl sulfide trapping of ylide intermediate I

Kinetic studies were undertaken to gain further mechanistic insights into the S-H insertion reaction. For ease of monitoring by ¹H NMR, *p*-methylbenzenethiol was used as the thiol substrate and methyl diazoacetate (MDA) was the carbene source (eq 6). The initial reaction rate (first 10% of reaction) was determined for each kinetic run from a plot of the concentration of the S-H insertion product [methyl 2-(*p*-tolylthio)acetate] versus time (see SI).



The catalyst concentration was varied with the same initial concentrations of the thiol (0.207 M) and MDA (0.072 M). When the catalyst concentration was halved from 1.23×10^{-5} M to 6.15×10^{-6} M, the reaction rate also reduced by approximately half, from 7.72×10^{-5} M/s (Table 6, entry 4) to 4.02×10^{-5} M (Table 6, entry 3). Similarly, doubling the catalyst concentration at the same concentrations of thiol and MDA approximately doubled the reaction rate (Table 6, entries 4 and 5). Consequently, the order of reaction with respect to catalyst concentration was derived from a plot of $\log(\text{reaction rate})$ versus the $\log[\text{Ir}(\text{TTP})\text{CH}_3]$. The slope of this plot (Figure S8) showed the rate order with respect to catalyst concentration was 1.12 ± 0.17 .

Table 6. Variation of initial S-H insertion rates with Ir(TTP)CH₃ concentration, at 297.8 ± 0.4 K.^a

Entry	[Ir(TTP)CH ₃] (M)	Rate (M/s)
1	0.00000308	0.0000152
2	0.00000484	0.0000164
3	0.00000615	0.0000402
4	0.0000123	0.0000772
5	0.0000246	0.000133

^a[MDA]₀ = 0.072 M and [*p*-methylbenzenethiol]₀ = 0.207 M

The reaction rate dependence on MDA concentration was explored in a similar manner (Table 7) with $[\text{Ir}(\text{TTP})\text{CH}_3]_0 = 1.23 \times 10^{-5}$ M and $[\text{thiol}]_0 = 0.207$ M. The plot of the $\log(\text{reaction rate})$ versus $\log[\text{MDA}]$ exhibited a slope of 1.12 ± 0.14 , consistent with a rate law that is first order in [MDA] (Figure S9). A similar first order dependence was found previously during the Ir(TTP)CH₃-catalyzed cyclopropanation of 1-hexene with MDA.²⁵

Table 7. Variation of initial S-H insertion rate with MDA concentration at 297.6 ± 0.51 K.^a

Entry	[MDA] (M)	Rate (M/s)
1	0.036	0.00002999
2	0.072	0.00007722
3	0.144	0.00014189

^a[Ir(TTP)CH₃]₀ = 1.23×10^{-5} M and [*p*-methylbenzenethiol]₀ = 0.207 M.

Furthermore, a series of kinetic runs were performed with various *p*-methylbenzenethiol concentrations, with the same initial concentrations of MDA (7.20×10^{-2} M) and Ir(TTP)CH₃ (1.23×10^{-5} M) at 298 K (Table 8). For thiol concentrations up to 0.827 M, the reaction rates increased, but in a relationship that was less than first order with respect to the thiol concentration (Table 8). At much higher concentrations of *p*-methylbenzenethiol, the rate of S-H insertion began to decrease (Table 7, entries 7 – 9).

Table 8. Variation of initial rates of S-H insertion with thiol concentration^a

Entry	[Thiol] : [MDA]	[Thiol] (M)	[Rxn rate] (M/s)
1	0.71 : 1	0.0513	0.0000590
2	1.44 : 1	0.104	0.0000634
3	2.88 : 1	0.207	0.0000772
4	5.79 : 1	0.414	0.000111
5	7.92 : 1	0.570	0.000124
6	11.5 : 1	0.827	0.000189
7	16.9 : 1	1.22	0.000177
8	22.9 : 1	1.65	0.000151
9	29.0 : 1	2.09	0.000104

^aMDA (0.072 M), Ir(TTP)CH₃ (0.0000123 M) in CDCl₃ at 298.0 ± 0.36 K.

Hammett plots, kinetic data, and ylide-trapping experiments support the proposed catalytic cycle shown in Scheme 2, which is similar to that proposed for the iridium-catalyzed N-H insertion with amines and diazo compounds.²⁷ Reversible thiol ligation to the iridium metal center, as demonstrated by binding experiments, forms an inactive hexacoordinated (thiol)Ir(TTP)CH₃. On dissociation of thiol, diazo binding to the five-coordinate iridium form generates an iridium-carbene complex. Nucleophilic attack of the thiol on the metal-carbene complex produces a ylide species, which then undergoes tautomerization, to form the S-H insertion product and regenerate the Ir(TTP)CH₃ catalyst. Ylide formation is supported by the build-up of positive charge on sulfur, as demonstrated with competition experiments and by ρ values of -0.12 and -0.78, obtained from the Hammett plots (Figure 2).

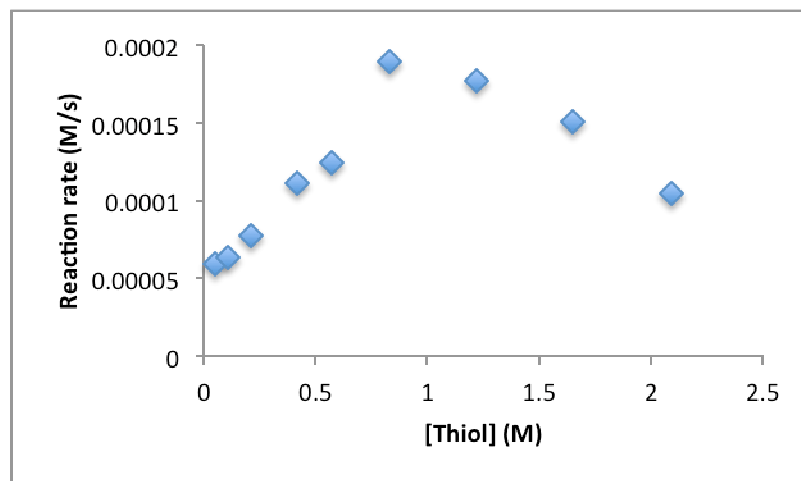
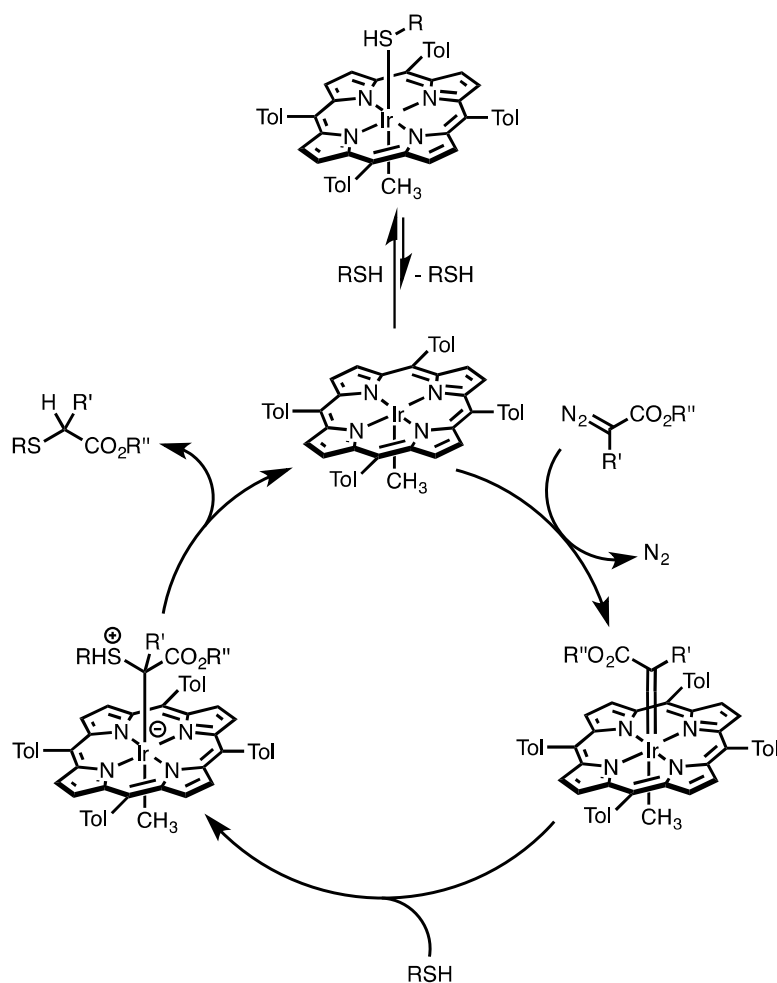


Figure 3. Initial rate variation of S-H insertion with thiol concentration^a.

^a*p*-Methylbenzenethiol (0.0513 – 2.09 M), MDA (0.072 M), Ir(TTP)CH₃ (0.0000123 M) in CDCl₃ at 298.0 ± 0.36 K.

The initial rate dependence on thiol concentration (Figure 3) shows two regimes. Approximate orders of reaction with respect to thiol concentration derived from the slopes of

the $\log(\text{reaction rate})$ versus $\log[\text{thiol}]$ plots (Figures S10 and S11) gave rate orders of 0.4 and -0.6 in the two regimes. This behavior is consistent with dual roles of the thiol substrate that offset each other. These involve attack of the thiol at the carbene carbon and binding to the Ir center. Attack at carbon drives product formation and is dominant at low thiol concentration. However, at higher thiol concentration, binding to Ir inhibits the catalyst and begins to decrease the reaction rate. The subsequent catalyst inhibition (Figure 3) at $[\text{thiol}] > 0.827 \text{ M}$ is similar to the deactivation of $\text{Ir}(\text{TTP})\text{CH}_3$ by aniline during the N-H insertion with MDA.²⁷ However, the S-H insertion rates for *p*-methylbenzenethiol ($\sim 10^{-4} \text{ M/s}$) are faster



Scheme 2. Proposed catalytic cycle for the $\text{Ir}(\text{TTP})\text{CH}_3$ -catalyzed insertion of carbenes from diazoesters into S-H bonds.

than those for N-H insertion with aniline ($\sim 10^{-5}$ M/s). This reflects the binding strengths of amines vs. thiols for Ir(TTP)CH₃. Aniline has a binding constant of $K = 2.7 \pm 0.2 \times 10^4$,²⁷ which is more than an order of magnitude greater than that for *p*-methylbenzenethiol.

The relatively high binding constant of allyl phenyl sulfide to Ir(TTP)CH₃ ($K = 9.01 \pm 0.12 \times 10^3$; Figure S7) suggested that product inhibition might pose a complication. Thus, methyl 2-(*p*-tolylthio)acetate was probed as a possible inhibitor. The addition of 28.2 mM of the sulfide product to a reaction mixture containing 0.207 and 0.072 M of thiol and MDA, respectively, had no effect on the initial reaction rate (Table 9, entries 1 and 2). However, increased amounts of the sulfide at the onset of the reaction did reduce the reaction rate, but

Table 9. Effect of added methyl 2-(*p*-tolylthio)acetate product on initial rates of S-H insertion.^a

Entry	Thiol (M)	MDA (M)	Added pdt (M)	Rate (M/s)
1	0.207	0.072	0	0.0000772
2	0.207	0.072	0.0282	0.0000779
3	0.207	0.072	0.0423	0.0000537
4	0.207	0.072	0.0564	0.0000536

^a0.0000123 M of Ir(TTP)CH₃ at 297.7 ± 0.25 K

reached a point of saturation (Table 9, entries 3 and 4; Figure S11).

Conclusions

This work demonstrates the effectiveness of (5,10,15,20-tetratolylporphyrinato)methyliridium(III) [Ir(TTP)CH₃] in the catalytic insertion of carbenes from diazo esters into the S-H bond of aromatic and aliphatic thiols. Equilibrium binding studies revealed that the thiol substrates reversibly bind to iridium, to generate an inactive

hexacoordinated complex, (thiol)Ir(TTP)CH₃. Competition and trapping experiments also provide evidence for a ylide intermediate, which would be formed from a nucleophilic attack of the thiol substrate on a putative iridium-carbene complex. A rearrangement of the free or metal-bound ylide then undergoes a rearrangement to form the thioether product. Kinetic studies revealed that the thiol binding to the metal center of the catalyst, and the nucleophilic attack of the thiol on the metal carbene to generate the product, offset each other, to give the observed rate behavior illustrated in Figure 3. At lower thiol concentrations, nucleophilic attack at the carbene carbon is more dominant, leading to faster reaction rates, as the thiol concentration is increased to 0.827 M. At the higher thiol concentration regime, greater than 0.827 M, thiol binding to iridium is more dominant, causing a reduction in the rate of S-H insertion.

Experimental Section

Ir(TTP)CH₃, MDA, MPDA and MTDA were prepared according to literature procedures.³⁶⁻³⁹ CDCl₃ and C₆H₆ were stored over 4 Å molecular sieves prior to use, while acetonitrile and dichloromethane were deoxygenated and dried by passage through columns of reduced copper and alumina, respectively. All other chemicals were reagent grade and used without further purification. Absorption spectra were acquired on Agilent Cary 8454 UV-Vis Spectrophotometer. Kinetic NMR spectra were acquired using Bruker DRX 400 MHz spectrometer, while other NMR spectra were collected using Varian MR 400 MHz and Bruker AVIII 600 MHz spectrometers. ¹H NMR peak positions were referenced against residual proton resonances of deuterated CDCl₃ (δ, 7.26 ppm). Products of S-H insertion reactions were identified by comparing their ¹H NMR spectra with those found in the

literature.^{10,13,34,35,40-42} Previously unreported S-H insertion products obtained from reactions with MTDA were isolated and characterized by NMR, elemental analysis, and HR-MS.

General procedure for carbene insertion into S-H bonds: In air, Ir(TTP)CH₃ (0.0310 μmol) was transferred via syringe (130. μL) from a 0.236 mM stock solution of catalyst in CH₂Cl₂ into an NMR tube, then dried under a flow of nitrogen gas. Triphenylmethane (31.1 μmol) was then added as an internal standard, using 50.0 μL of a CDCl₃ solution (622 mM), followed by addition of the thiol (87.0 μmol) from 0.410 mL of a CDCl₃ solution (212 mM). The NMR tube was then capped with a rubber septum, and it was cooled with its contents to -78 °C in a dry ice/acetone bath. After about 10 minutes, EDA (42.6 μmol) was added using 0.120 mL of a CDCl₃ solution (355 mM) by injection into the NMR tube through the rubber septum. After an additional 5 minutes at -78 °C, the reaction mixture was allowed to warm to ambient temperature. ¹H NMR was used to monitor the reaction and to determine product yields. When the diazo compound was MPDA or MTDA, the same procedure was followed, using the appropriate reagent amounts shown in the footnotes of Table 2 or 3.

General procedure for substrate competition experiments using benzenethiol and *p*-substituted benzenethiols: The same procedure above was followed, but the benzenethiol and *p*-substituted benzenethiol for each reaction were premixed in a 1:1 mol ratio, and introduced into the NMR tube, as a single solution containing 42.6 μmol of each thiol. The amount of diazo reagent added, after the NMR tube and its contents had been cooled to -78 °C, was also 46.8 μmol.

General procedure for the preparation of unreported thioethers: From a 2.32 mM stock solution of Ir(TTP)CH₃ in CH₂Cl₂, a 0.590-mL aliquot containing 1.37 μmol of catalyst was transferred via syringe into a 25-mL round-bottomed flask. The flask was charged with the thiol substrate (0.370 mmol), 1.1 mL of CH₂Cl₂, and a stir bar, then capped with a rubber septum, through which, a syringe needle attached to a nitrogen-filled balloon was inserted. The flask and its contents were then cooled to -78 °C in a dry ice/acetone bath. After about 10 minutes, a CHCl₃ solution (0.85 mL) containing 0.181 mmol of MTDA was injected into the flask through the rubber septum. After an additional 5 minutes at -78 °C, the reaction mixture was allowed to warm to ambient temperature, and stirring was continued at this temperature for the specified time below. After purification by silica gel chromatography, the volatiles were removed under reduced pressure, to afford the thioether product.

Methyl 2-((4-methoxyphenyl)thio)-2-(*p*-tolyl)acetate: The reaction mixture was stirred at ambient temperature for 30 minutes, then purified by silica gel chromatography (16.0 cm length x 0.15 cm diameter), using 30:1 hexanes/ethyl acetate as eluent. The product was obtained as an orange solid. Yield: 74% (40.7 mg, 0.135 mmol). Anal. Calcd for C₁₇H₁₈O₃S: C, 67.52; H, 6.00. Found: C, 67.68; H, 5.87. ¹H NMR (600 MHz, CDCl₃) δ: 2.33 (s, 3H), 3.66 (s, 3H), 3.79 (s, 3H), 4.75 (s, 1H), 6.81 (m, 2H), 7.13 (d, 2H, *J* = 6.0 Hz), 7.30 (d, 2H, *J* = 6.0 Hz), 7.34 (m, 2H). ¹³C NMR (151 MHz, CDCl₃) δ: 21.47, 52.84, 55.59, 57.45, 114.78, 124.17, 128.72, 129.60, 133.02, 136.38, 138.33, 160.45, 171.44. HRMS (+ESI): Calcd for [MH]⁺ (C₁₇H₁₉O₃S)⁺ m/z 303.1055; found m/z 303.1043.

Methyl 2-((4-nitrophenyl)thio)-2-(*p*-tolyl)acetate: The reaction mixture was stirred at ambient temperature for 30 minutes, then purified by silica gel chromatography (17.0 cm length x 0.15 cm diameter), using 30:1 hexanes/ethyl acetate as eluent. The product was obtained as a yellow solid. Yield: 57% (33.0 mg, 0.104 mmol). ^1H NMR (600 MHz, CDCl_3) δ : 2.35 (s, 3H), 3.73 (s, 3H), 5.10 (s, 1H), 7.18 (d, 2H, $J = 6.0$ Hz), 7.38 (m, 4H), 8.10 (d, 2H, $J = 12.0$ Hz). ^{13}C NMR (151 MHz, CDCl_3) δ : 21.50, 53.51, 54.51, 124.31, 128.59, 129.10, 130.11, 131.43, 139.28, 144.92, 146.42, 170.44. HRMS (+ESI): Calcd for $[\text{MH}]^+$ ($\text{C}_{16}\text{H}_{16}\text{NO}_4\text{S}$) $^+$ m/z 318.0800; found m/z 318.0793.

Reaction between allyl phenyl sulfide and EDA in the presence of $\text{Ir}(\text{TTP})\text{CH}_3$: A procedure similar to those used for carbene insertion into S-H bonds was followed, but with the use of 0.031 μmol of $\text{Ir}(\text{TTP})\text{CH}_3$, 44.1 μmol (65.8 mM) of EDA, 147 μmol (219 mM) of allyl phenyl sulfide, and 6.58 μmol of mesitylene as an internal standard.

General procedure for kinetic experiments: From a 0.236 mM stock solution of $\text{Ir}(\text{TTP})\text{CH}_3$ in CH_2Cl_2 , a 32.5- μL aliquot containing 0.00767 μmol of $\text{Ir}(\text{TTP})\text{CH}_3$ catalyst was transferred via syringe into an NMR tube, then dried under a flow of nitrogen gas. To the dried catalyst, 50.0 μL of a CDCl_3 solution (622 mM) containing triphenylmethane (31.1 μmol) was then added, followed by an aliquot of *p*-methylbenzenethiol (33.3 μmol – 1.36 mmol) in CDCl_3 . The NMR tube was then capped with a rubber septum and a syringe needle attached to a nitrogen-filled balloon was inserted through the septum. Immediately prior to insertion of the sample into a shimmed NMR probe that was equilibrated to 298 K, MDA

(46.8 μmol) was added using 50 μL of a CDCl_3 solution (936 mM). After rapid and thorough mixing, the NMR tube was inserted into the NMR instrument, and acquisition of spectra at 16-second intervals began as quickly as possible.

Determination of binding constants of thiols and allyl phenyl sulfide to $\text{Ir}(\text{TTP})\text{CH}_3$:

Binding constants were measured using an adapted method of a previously-published procedure.²⁷ All absorbance spectra were acquired in quartz sample cells with a 1 mm path length, and freshly prepared benzene solutions of thiols and allyl phenyl sulfide were used in all measurements. The extinction coefficients of $\text{Ir}(\text{TTP})\text{CH}_3$ were determined at 400 and 425 nm from the absorbance spectrum of an 80 μM benzene solution. A 200-fold excess of ligand was used to obtain the extinction coefficients for the hexacoordinated $(\text{RSH})\text{Ir}(\text{TTP})\text{CH}_3$ or $(\text{RSR}')\text{Ir}(\text{TTP})\text{CH}_3$ complexes, using solutions containing 80 μM of $\text{Ir}(\text{TTP})\text{CH}_3$ and 17 mM of the desired thiol or sulfide. Equilibrium constants were measured from absorbance spectra of solutions with known initial concentrations of $\text{Ir}(\text{TTP})\text{CH}_3$ (80 μM) and thiols or sulfide (25.3 μM – 7.21 mM).

References

- (1) Clayden, J.; MacLellan, P. *Beilstein J. Org. Chem.* **2011**, *7*, 582-595.
- (2) Landelle, G.; Panossian, A.; Leroux, F. R. *Curr. Top. Med. Chem.* **2014**, *14*, 941-951.
- (3) Screttas, C.; Micha-Screttas, M. *J. Org. Chem.* **1979**, *44*, 713 - 719.
- (4) Yin, J. M.; Pidgeon, C. *Tetrahedron Lett.* **1997**, *38*, 5953-5954.
- (5) Couch, E. D.; Auvil, T. J.; Mattson, A. E. *Chem. Eur. J.* **2014**, *20*, 8283-8287.

- (6) Kano, K.; Takeuchi, M.; Hashimoto, S.; Yoshida, Z. *Chem. Lett.* **1990**, 1381-1384.
- (7) Takeuchi, M.; Shimakoshi, H.; Kano, K. *Organometallics* **1994**, *13*, 1208-1213.
- (8) Li, G. *Angew. Chem. Int. Ed.* **2001**, *40*, 1513 - 1516.
- (9) Fernandez-Rodriguez, M. A.; Shen, Q. L.; Hartwig, J. F. *J. Am. Chem. Soc.* **2006**, *128*, 2180-2181.
- (10) Zou, L. H.; Priebbenow, D. L.; Wang, L.; Mottweiler, J.; Bolm, C. *Adv. Synth. Catal.* **2013**, *355*, 2558-2563.
- (11) P. Doyle, M.; McKervey, M. A.; Ye, T. *Modern Catalytic Methods for Organic Synthesis with Diazo Compounds: From Cyclopropanes to Ylides*; Wiley, New York, 1998.
- (12) Yates, P. *J. Am. Chem. Soc.* **1952**, *74*, 5376-5381.
- (13) Zhu, Z. L.; Espenson, J. H. *J. Am. Chem. Soc.* **1996**, *118*, 9901-9907.
- (14) Zhu, S.-F.; Zhou, Q.-L. *Natl. Sci. Rev.* **2014**, *1*, 580 - 603.
- (15) Zotto, A. D.; Baratta, W.; Rigo, P. *J. Chem. Soc., Perkin Trans. 1* **1999**, *21*, 3079-3081.
- (16) Pansare, S. V.; Jain, R. P.; Bhattacharyya, A. *Tetrahedron Lett.* **1999**, *40*, 5255-5258.
- (17) Sengupta, S.; Mondal, S. *Tetrahedron Lett.* **1999**, *40*, 8685-8688.
- (18) Yao, W. G.; Liao, M. Y.; Zhang, X. M.; Xu, H.; Wang, J. B. *Eur. J. Org. Chem.* **2003**, 1784-1788.
- (19) Zhang, X.; Ma, M.; Wang, J. *ARKIVOC* **2003**, 84 - 91.
- (20) Anding, B. J.; Woo, L. K. In *Handbook of porphyrins*; Kadish, K. M., Guillard, R., Smith, K., Eds.; World Scientific: Hackensack, New Jersey, 2012; Vol. 21, p 145-319.
- (21) Galardon, E.; LeMaux, P.; Simonneaux, G. *J. Chem. Soc., Perkin Trans. 1* **1997**, 2455-2456.
- (22) Galardon, E.; Le Maux, P.; Simonneaux, G. *Tetrahedron* **2000**, *56*, 615-621.
- (23) Aviv, I.; Gross, Z. *Chem. Eur. J.* **2008**, *14*, 3995-4005.
- (24) Chan, K.-H.; Guan, X.; Lo, V. K. Y.; Che, C. M. *Angew. Chem. Int. Ed.* **2014**, *53*.
- (25) Anding, B. J.; Ellern, A.; Woo, L. K. *Organometallics* **2012**, *31*, 3628-3635.

- (26) Anding, B. J.; Brgoch, J.; Miller, G. J.; Woo, L. K. *Organometallics* **2012**, *31*, 5586-5590.
- (27) Anding, B. J.; Woo, L. K. *Organometallics* **2013**, *32*, 2599-2607.
- (28) Dairo, T. O.; Ellern, A.; Angelici, R. J.; Woo, L. K. *Organometallics* **2014**, *33*, 2266-2276.
- (29) Anding, B.; Ellern, A.; Woo, L. K. *Organometallics* **2014**, *33*, 2219 - 2229
- (30) Wang, J. C.; Xu, Z. J.; Guo, Z.; Deng, Q. H.; Zhou, C. Y.; Wan, X. L.; Che, C. M. *Chem. Commun.* **2012**, *48*, 4299-4301.
- (31) Lopez-Sanchez, C.; Alvarez-Corral, M.; Munoz-Dorado, M.; Rodriguez-Garcia, I. *Synlett* **2012**, 2469-2472.
- (32) Wang, J. C.; Zhang, Y.; Xu, Z. J.; Lo, V. K. Y.; Che, C. M. *ACS Catal.* **2013**, *3*, 1144-1148.
- (33) Baumann, L. K.; Mbuvi, H. M.; Du, G.; Woo, L. K. *Organometallics* **2007**, *26*, 3995-4002.
- (34) Xu, B.; Zhu, S. F.; Zhang, Z. C.; Yu, Z. X.; Ma, Y.; Zhou, Q. L. *Chem. Sci.* **2014**, *5*, 1442-1448.
- (35) Tyagi, V.; Bonn, R. B.; Fasan, R. *Chem. Sci.* **2015**, *6*, 2488-2494.
- (36) Yeung, S. K.; Chan, K. S. *Organometallics* **2005**, *24*, 6426-6430.
- (37) Zhao, W. J.; Yan, M.; Huang, D.; Ji, S. J. *Tetrahedron* **2005**, *61*, 5585-5593.
- (38) Mao, H. B.; Lin, A. J.; Shi, Y.; Mao, Z. J.; Zhu, X. B.; Li, W. P.; Hu, H. W.; Cheng, Y. X.; Zhu, C. J. *Angew. Chem. Int. Ed.* **2013**, *52*, 6288-6292.
- (39) Davies, H. M. L.; Hansen, T.; Churchill, M. R. *J. Am. Chem. Soc.* **2000**, *122*, 3063-3070.
- (40) Hamed, E. A.; El-Bardan, A. A.; Moussa, A. M. *Phosphorus, Sulfur Silicon Relat. Elem.* **1991**, *62*, 269-273.
- (41) Wang, X. L.; Xue, Z. Y.; Ma, Y. Y.; Yang, F. *J. Chem. Res.* **2014**, 493-495.
- (42) Nakamura, S.; Nakagawa, R.; Watanabe, Y.; Toru, T. *J. Am. Chem. Soc.* **2000**, *122*, 11340-11347.

Supporting Information

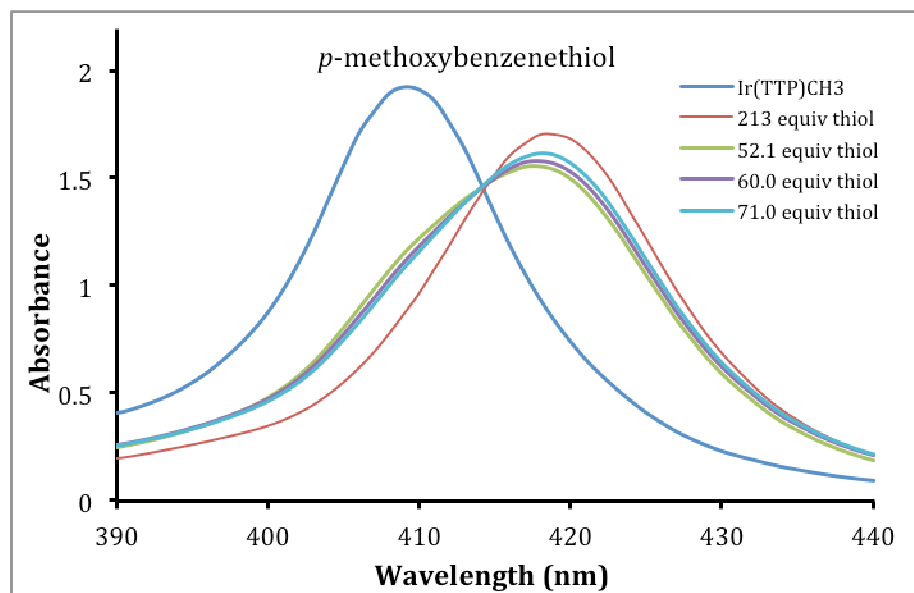
Equilibrium binding studies

Figure S1. Overlaid absorbance spectra for binding of *p*-methoxybenzenethiol to 80 μM Ir(TTP)CH₃ in benzene: 17.0 mM (213 equiv) thiol, 4.17 mM (52.1 equiv) thiol, 4.80 mM (60.0 equiv) thiol, 5.68 mM (71.0 equiv) thiol. $K = 7.98 \pm 0.02 \times 10^2$

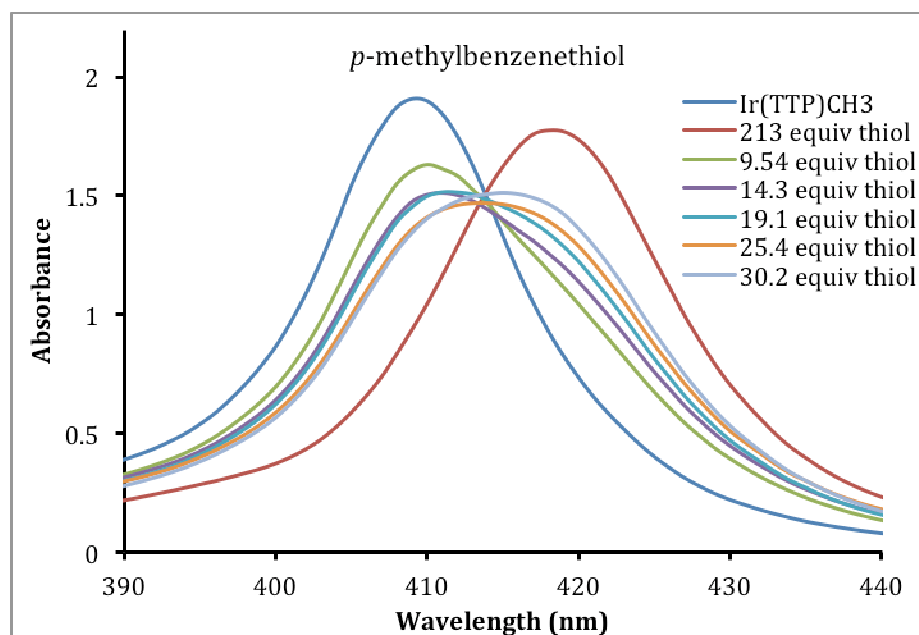


Figure S2. Overlaid absorbance spectra for binding of *p*-methylbenzenethiol to 80 μM Ir(TTP)CH₃ in benzene: 17.0 mM (213 equiv) thiol, 0.763 mM (9.54 equiv) thiol, 1.15 mM

(14.3 equiv) thiol, 1.53 mM (19.1 equiv) thiol, 2.04 mM (25.4 equiv) thiol, 2.42 mM (30.2 equiv) thiol in benzene. $K = 6.76 \pm 0.24 \times 10^2$

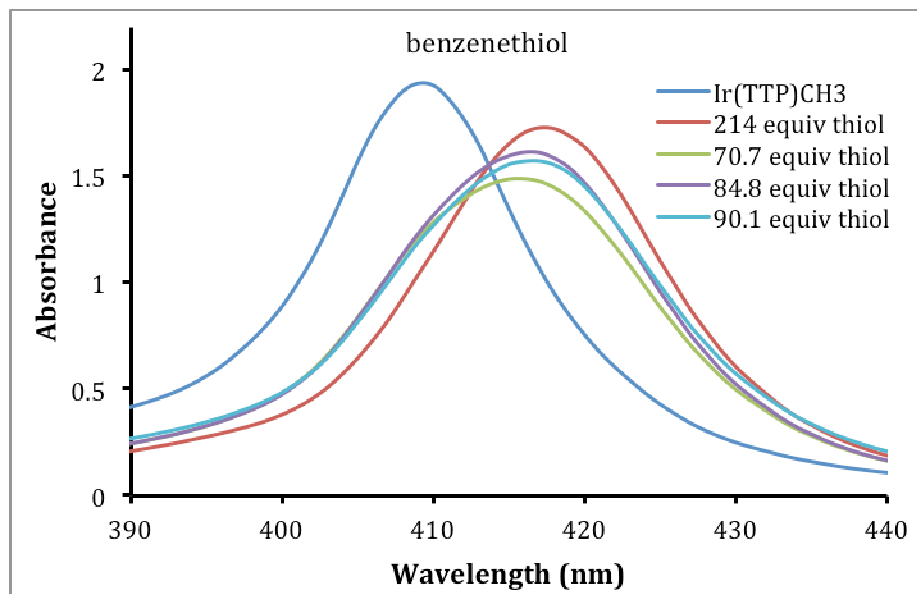


Figure S3. Overlaid absorbance spectra for binding of benzenethiol to 80 μM $\text{Ir}(\text{TTP})\text{CH}_3$ in benzene: 17.1 mM (214 equiv) thiol, 5.65 mM (70.7 equiv) thiol, 6.79 mM (84.8 equiv) thiol, 7.21 mM (90.1 equiv) thiol. $K = 5.78 \pm 0.33 \times 10^2$

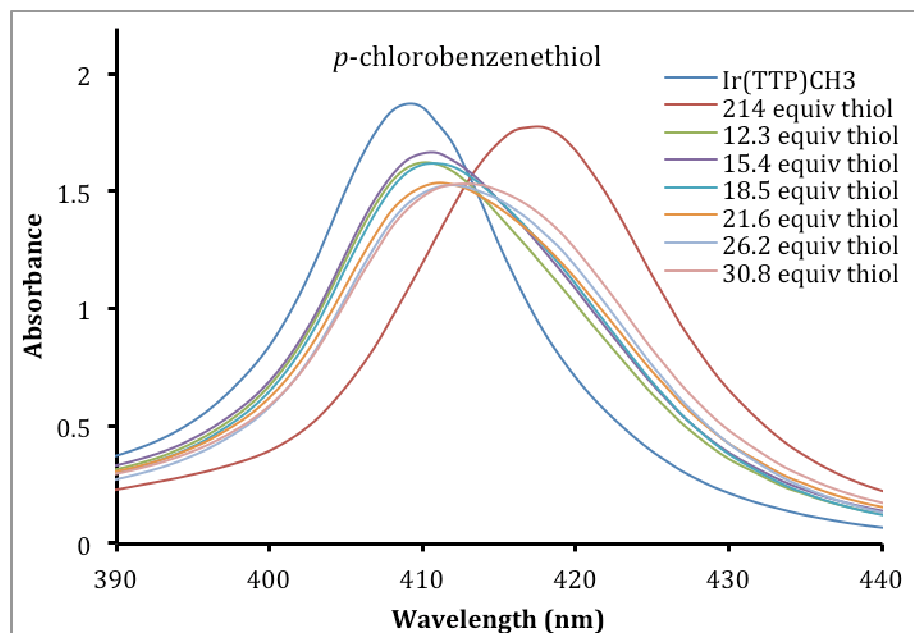


Figure S4. Overlaid absorbance spectra for binding of *p*-chlorobenzenethiol to 80 μM $\text{Ir}(\text{TTP})\text{CH}_3$ in benzene: 17.1 mM (214 equiv) thiol, 0.986 mM (12.3 equiv) thiol, 1.23 mM

(15.4 equiv) thiol, 1.48 mM (18.5 equiv) thiol, 1.72 mM (21.6 equiv) thiol in benzene, 2.09 mM (26.2 equiv) thiol, 2.46 mM (30.8 equiv) thiol. $K = 5.26 \pm 0.35 \times 10^2$

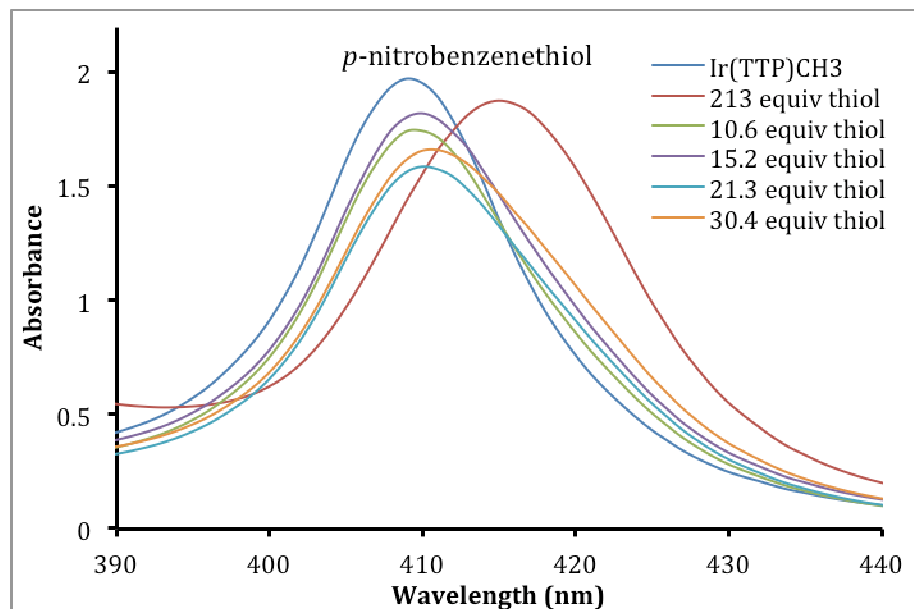


Figure S5. Overlaid absorbance spectra for binding of *p*-nitrobenzenethiol to 80 μM Ir(TTP)CH₃ in benzene: 17.0 mM (213 equiv) thiol, 0.851 mM (10.6 equiv) thiol, 1.22 mM (15.2 equiv) thiol, 1.70 mM (21.3 equiv) thiol, 2.43 mM (30.4 equiv) thiol in benzene. $K = 4.25 \pm 0.44 \times 10^2$

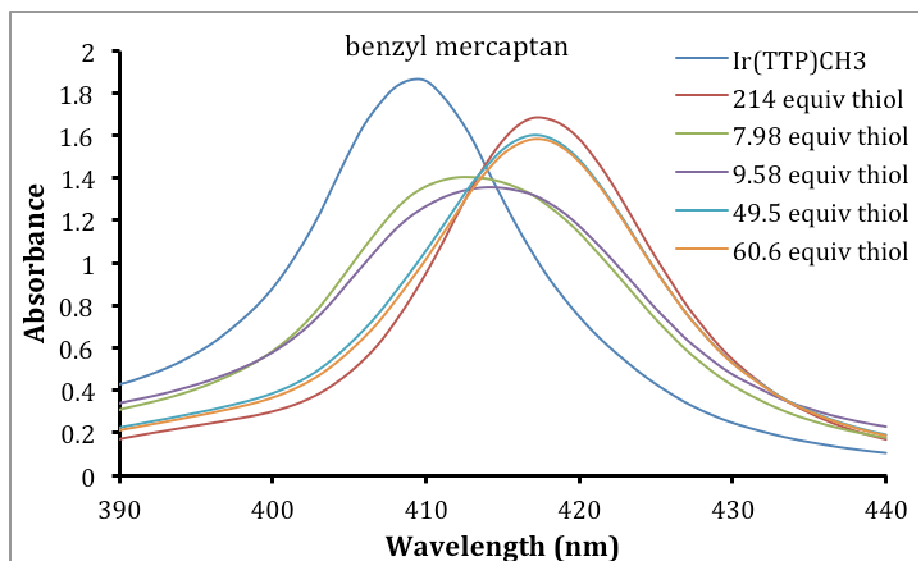


Figure S6. Overlaid absorbance spectra for binding of benzyl mercaptan to 80 μM Ir(TTP)CH₃ in benzene: 17.1 mM (214 equiv) thiol, 0.638 mM (7.98 equiv) thiol, 0.766

mM (9.58 equiv) thiol, 3.96 mM (49.5 equiv) thiol, 4.85 mM (60.6 equiv) thiol. $K = 1.69 \pm 0.029 \times 10^3$

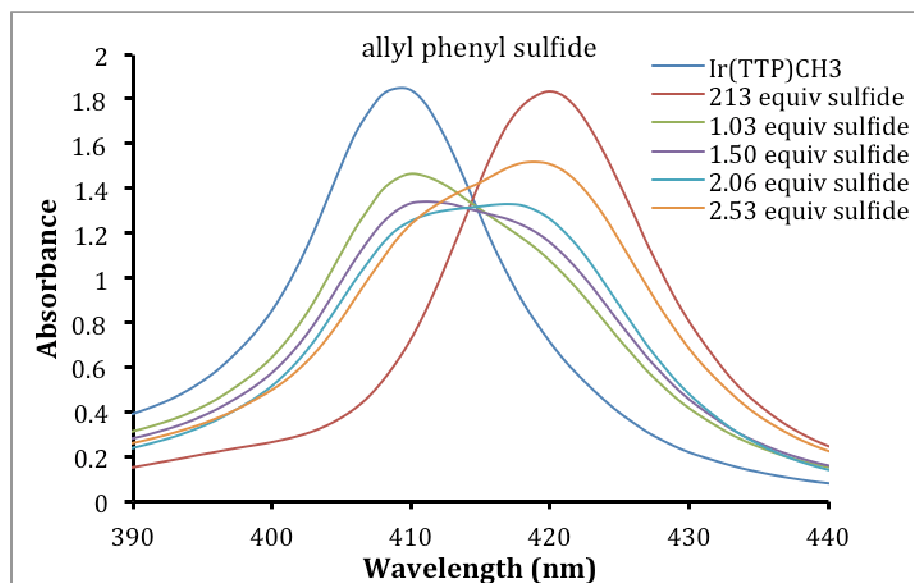


Figure S7. Overlaid absorbance spectra for binding of allyl phenyl sulfide to 80 μ M Ir(TTP)CH₃ in benzene: 17.0 mM (213 equiv) sulfide, 82.2 μ M (1.03 equiv) sulfide, 120. μ M (1.50 equiv) sulfide, 164 μ M (2.06 equiv) sulfide, 202 μ M (2.53 equiv) sulfide. $K = 9.01 \pm 0.12 \times 10^3$.

Kinetic Studies

Reaction rates shown are initial rates determined as the rate of formation of S-H insertion product from the first 10% of reaction.

$$\text{Rate} = k[\text{Ir(TTP)CH}_3]^a[\text{MDA}]^b[\text{Thiol}]^c \quad (1)$$

$$\text{Rate} = [\text{Pdt}]/\text{time} = k'[\text{Ir(TTP)CH}_3]^a \quad (2)$$

$$\text{Log(Rate)} = \text{Log}(k') + a\text{Log}[\text{Ir(TTP)CH}_3] \quad (3)$$

$$\text{Rate} = [\text{Pdt}]/\text{time} = k'[\text{MDA}]^b \quad (4)$$

$$\text{Log(Rate)} = \text{Log}(k') + b\text{Log}[\text{MDA}] \quad (5)$$

$$\text{Rate} = [\text{Pdt}]/\text{time} = k'[\text{Thiol}]^c \quad (6)$$

$$\text{Log(Rate)} = \text{Log}(k') + c\text{Log}[\text{Thiol}] \quad (7)$$

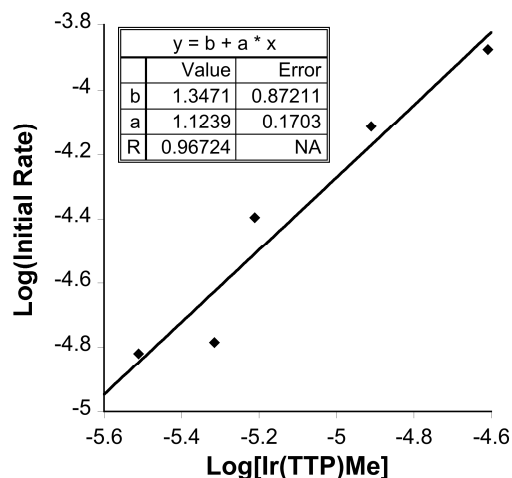


Figure S8. Data for Rate Law Order of [Ir(TTP)CH₃]. [MDA]₀ = 0.072 M and [*p*-methylbenzenethiol]₀ = 0.207 M, [Ir(TTP)CH₃] = 3.08 × 10⁻⁶, 4.84 × 10⁻⁶, 6.15 × 10⁻⁶, 12.3 × 10⁻⁶ and 24.6 × 10⁻⁶ M, T = 297.8±0.13 K

At constant initial thiol and MDA concentrations, the [Ir(TTP)CH₃] was varied for five different reactions. The order of reaction with respect to [Ir(TTP)CH₃] was determined from eq. 3.

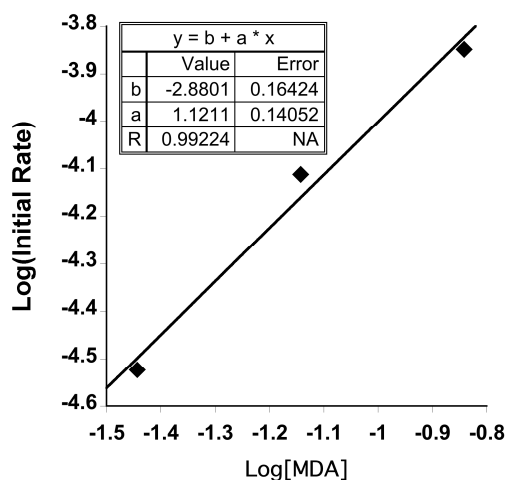


Figure S9. Data for Rate Law Order of [MDA]. [Ir(TTP)CH₃]₀ = 1.23 × 10⁻⁵ M, [*p*-methylbenzenethiol]₀ = 0.207, MDA = 0.036, 0.072, and 0.144 M, T = 297.4±0.14 K

At constant initial thiol and Ir(TTP)CH₃ concentrations, the [MDA] was varied for three different reactions. The order of reaction with respect to [MDA] was determined from eq. 5.

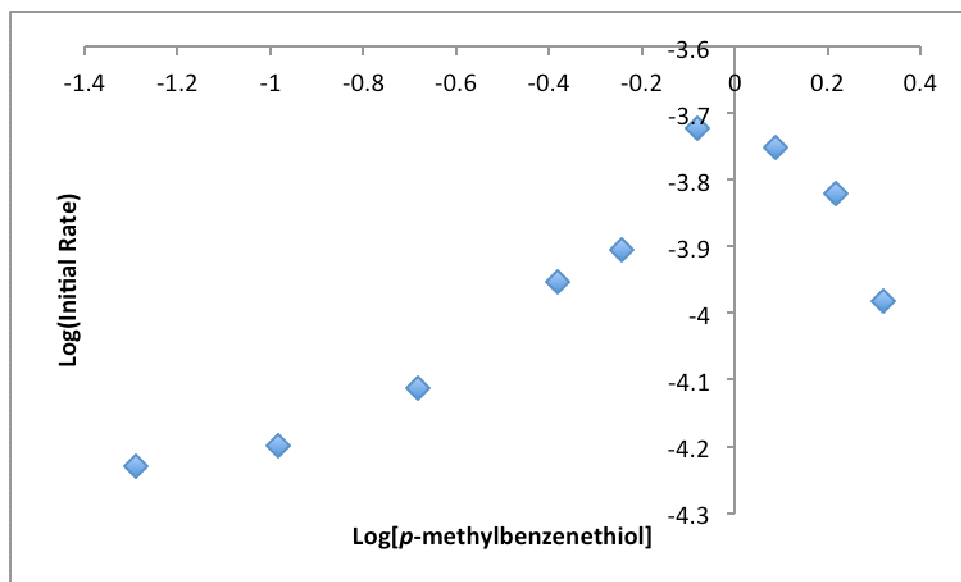


Figure S10. Log(rate) vs log[*p*-methylbenzenethiol]. Thiol = (0.0513 – 2.09 M), MDA (0.072 M), Ir(TTP)CH₃ (0.0000123 M) in CDCl₃ at 298.0±0.36 K.

The order of reaction in [thiol] was derived from the slope of a plot of log(initial rate) versus log[thiol], eq. 7. Reactions were carried out at constant initial concentrations of MDA and Ir(TTP)CH₃.

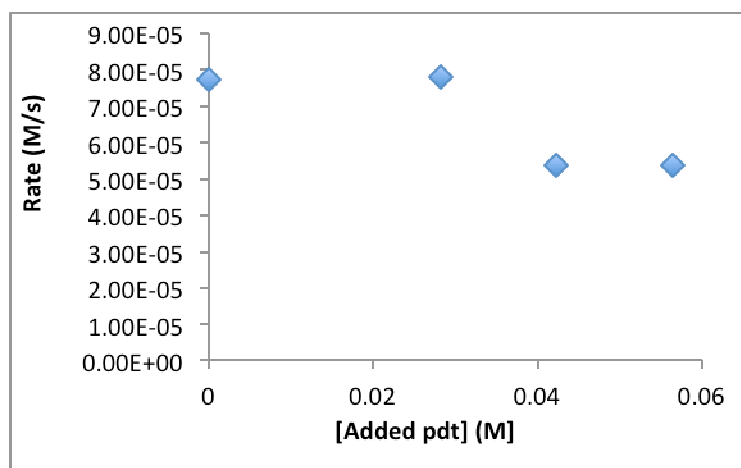


Figure S11. Variation of initial reaction rate with added S-H insertion product. Thiol (0.207 M), MDA (0.072 M), Added methyl 2-(*p*-tolylthio)acetate (0, 0.0282, 0.0423, and 0.0564 M), Ir(TTP)CH₃ (12.3 μM) in CDCl₃ at 297.7±0.25 K.

Plots of S-H insertion product concentration versus time with $[\text{Ir}(\text{TTP})\text{CH}_3] = 0.0462$ mM, $[\text{MDA}] = 0.072$ M, $[\text{Thiol}] = 0.0513 - 2.09$ M in CDCl_3 at $T = 298.0 \pm 0.36$ K.

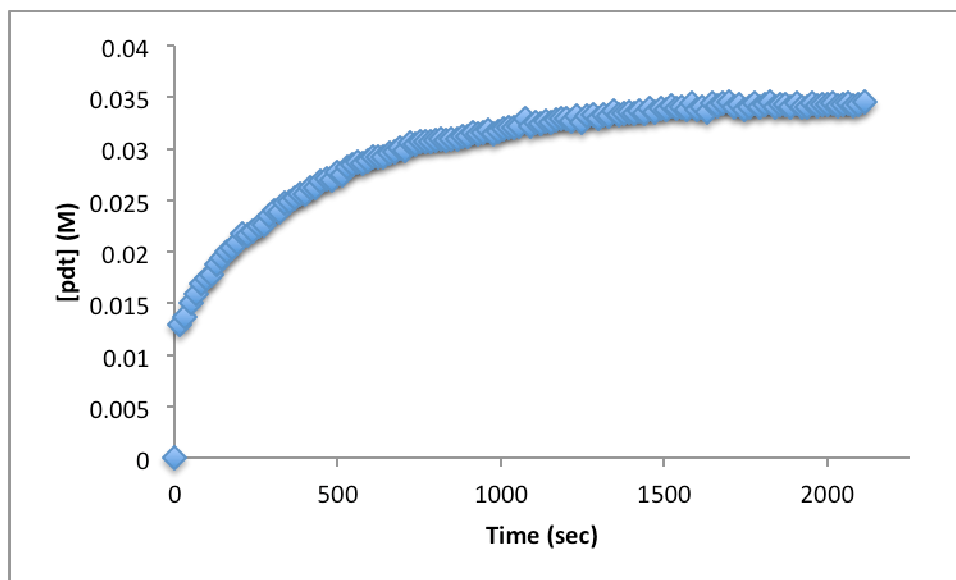


Figure S12. [*p*-Methylbenzenethiol] = 0.0513 M (0.713 equiv relative to MDA)

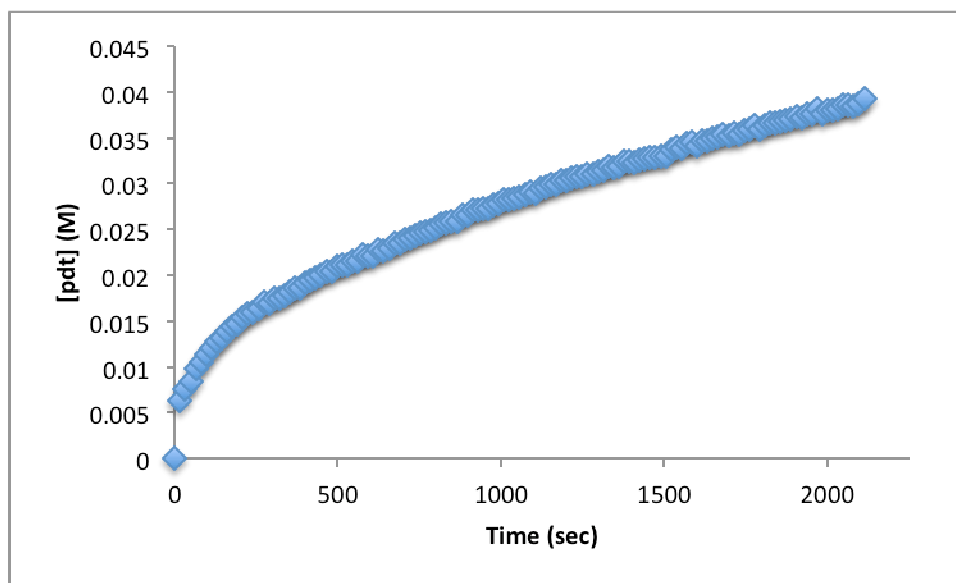


Figure S13. [*p*-Methylbenzenethiol] = 0.104 M (1.44 equiv relative to MDA)

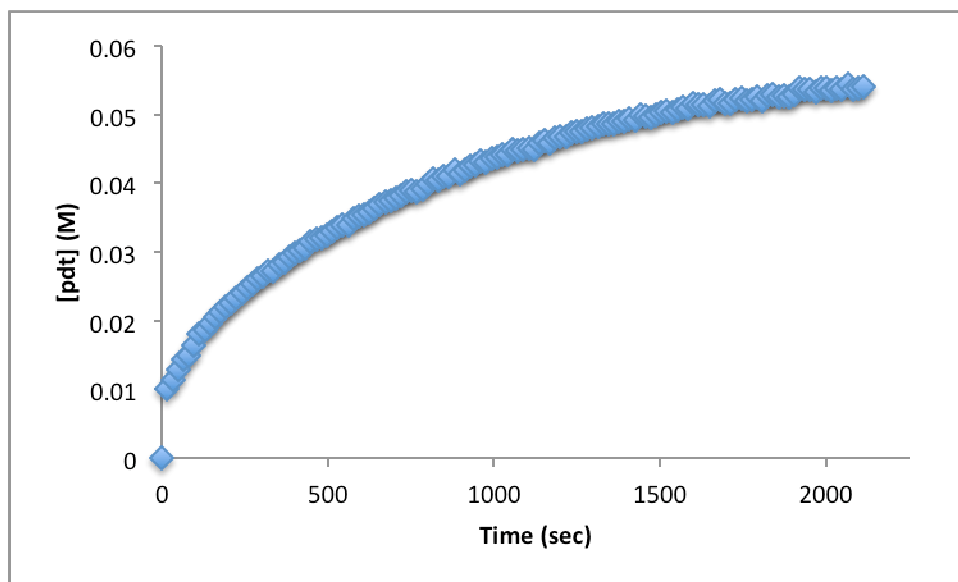


Figure S14. $[p\text{-Methylbenzenethiol}] = 0.207\text{ M}$ (2.88 equiv relative to MDA)

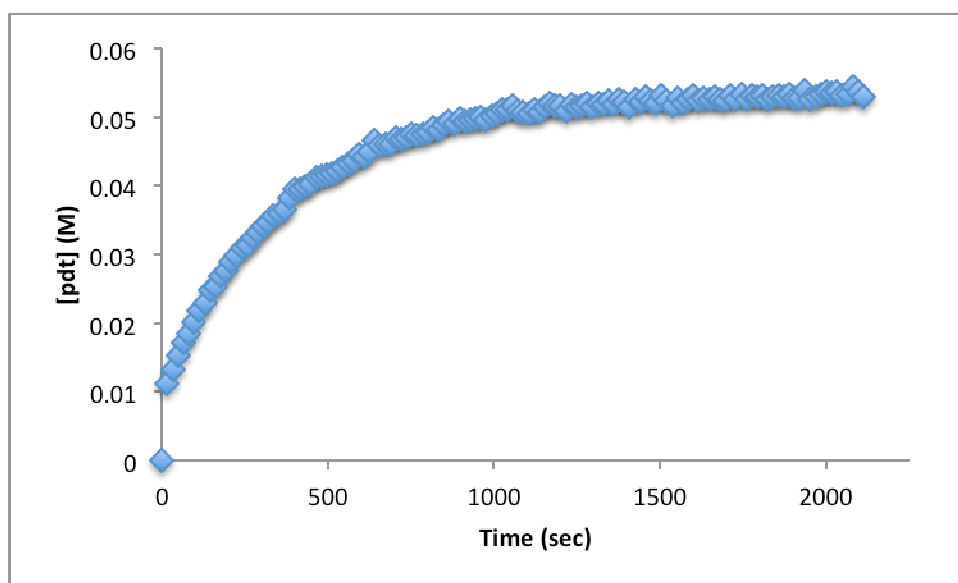


Figure S15. $[p\text{-Methylbenzenethiol}] = 0.414\text{ M}$ (5.75 equiv relative to MDA)

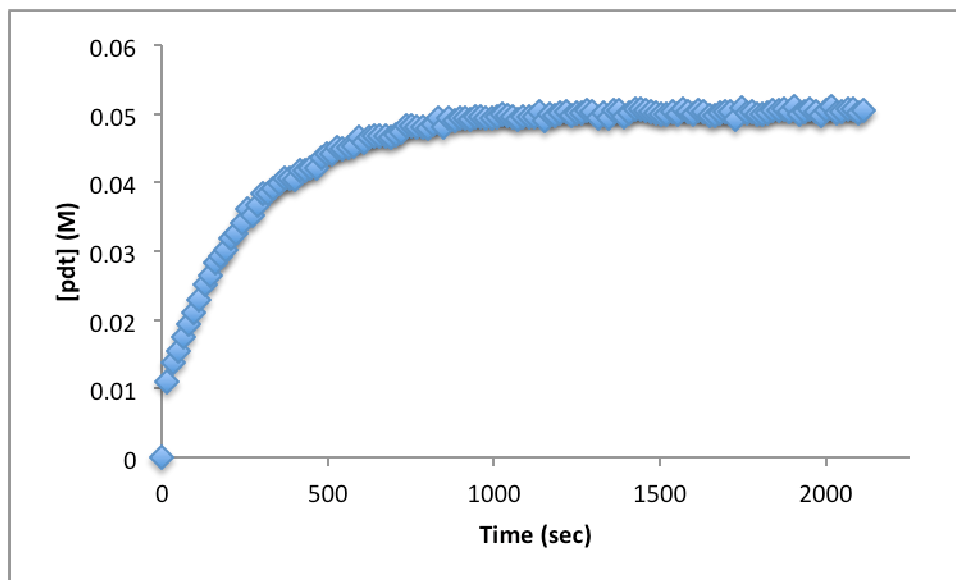


Figure S16. [*p*-Methylbenzenethiol] = 0.570 M (7.92 equiv relative to MDA)

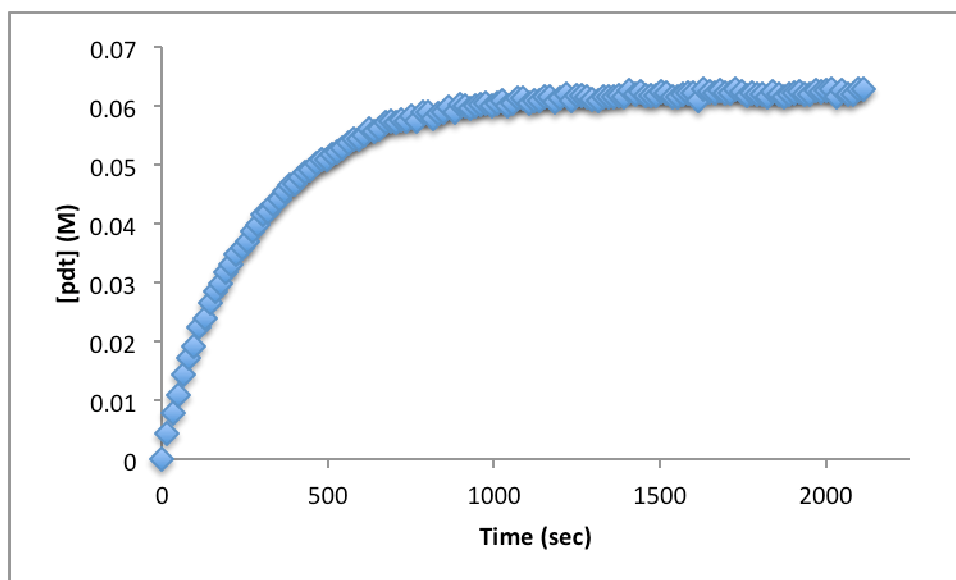


Figure S17. [*p*-Methylbenzenethiol] = 0.827 M (11.5 equiv relative to MDA)

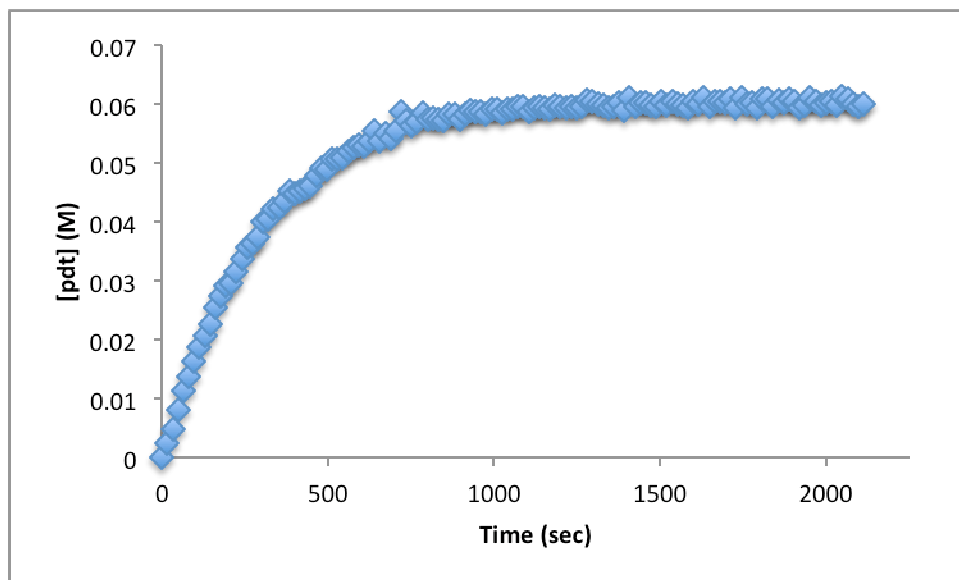


Figure S18. [*p*-Methylbenzenethiol] = 1.22 M (16.9 equiv relative to MDA)

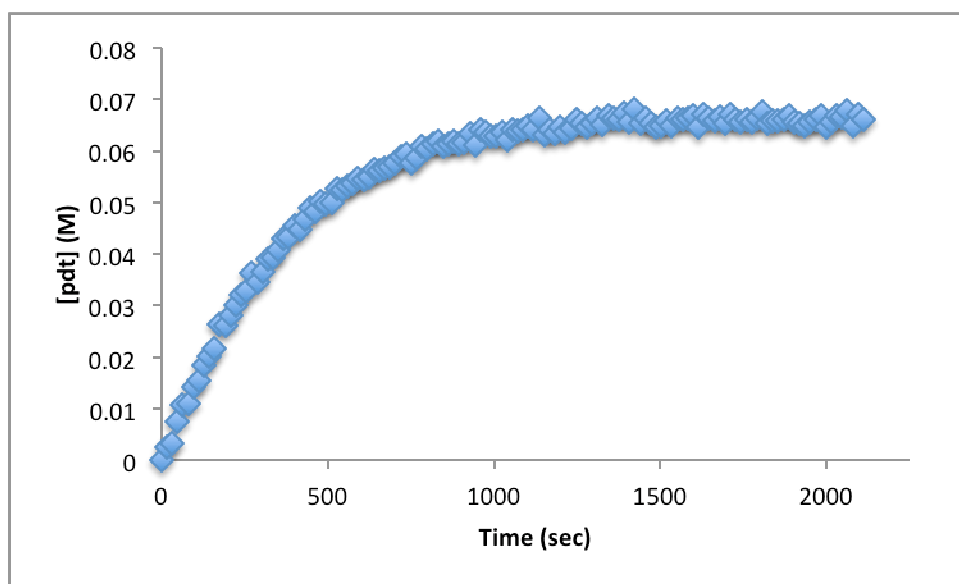


Figure S19. [*p*-Methylbenzenethiol] = 1.65 M (22.9 equiv relative to MDA)

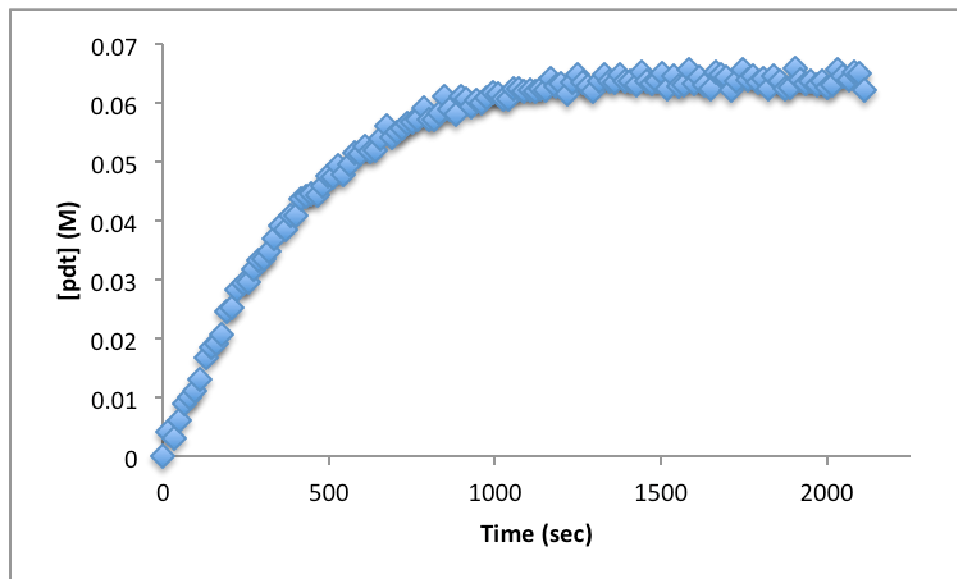


Figure S20. [*p*-Methylbenzenethiol] = 2.09 M (29.0 equiv relative to MDA)

NMR SPECTRA OF NEW THIOETHER COMPOUNDS

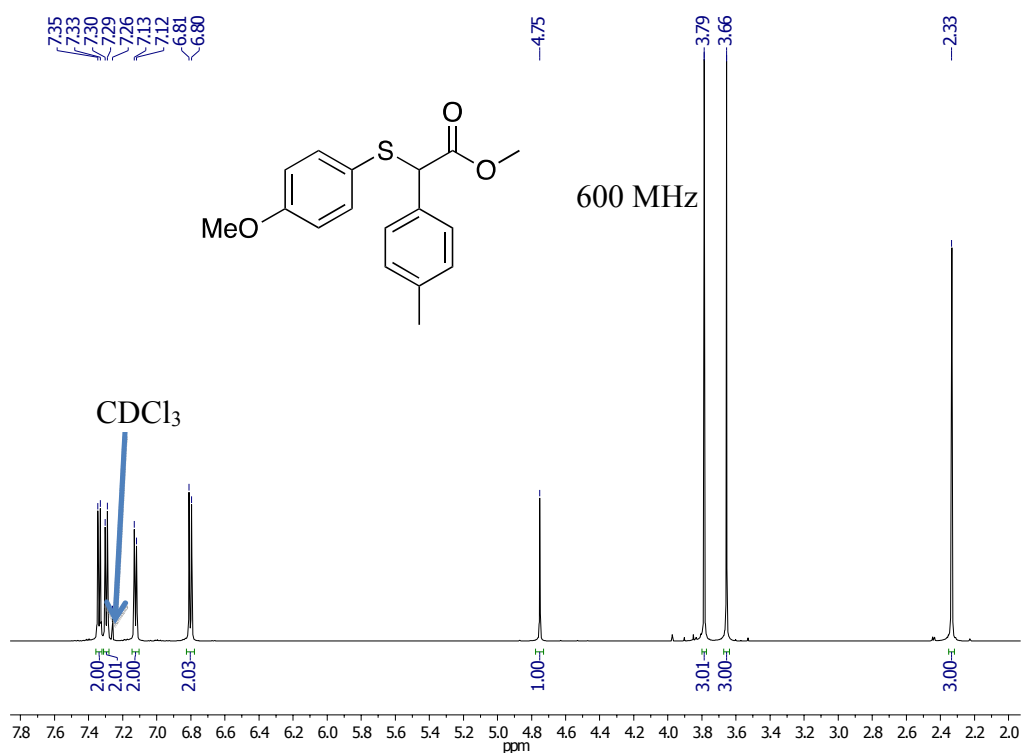


Figure S21. ¹H NMR (600 MHz) spectrum of methyl 2-((4-methoxyphenyl)thio)-2-(*p*-tolyl)acetate

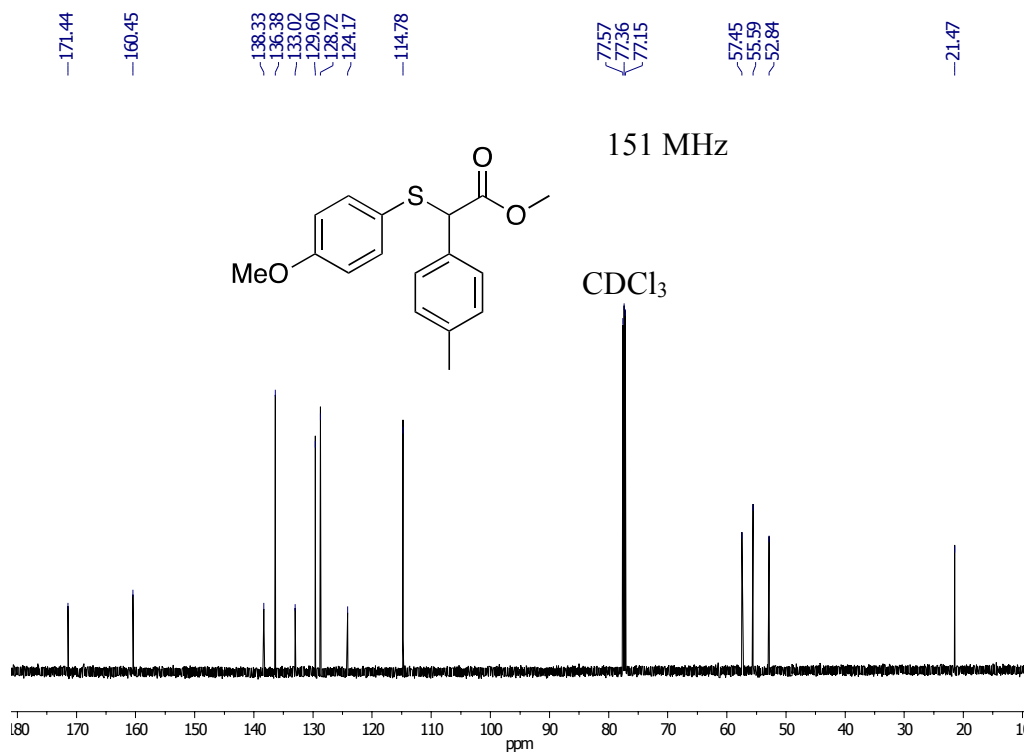


Figure S22. ¹³C NMR (151 MHz) spectrum of methyl 2-((4-methoxyphenyl)thio)-2-(*p*-tolyl)acetate

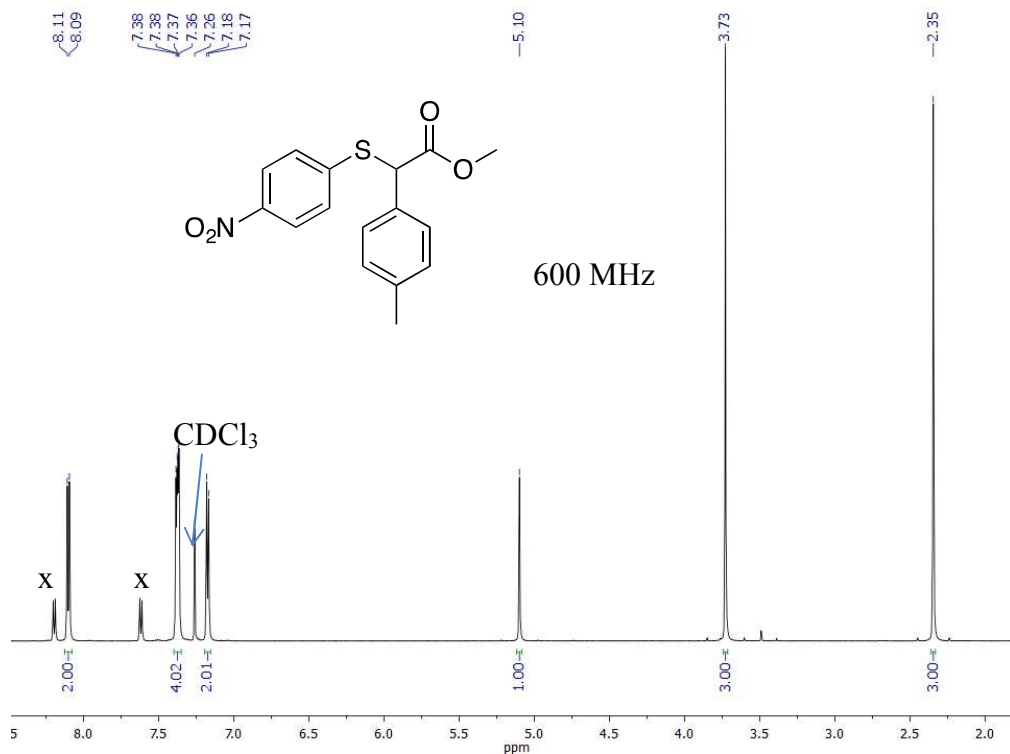


Figure S23. ¹H NMR (600 MHz) spectrum of methyl 2-((4-nitrophenyl)thio)-2-(*p*-tolyl)acetate
 x = *p*-nitrophenyl disulfide impurity from 4-nitrobenzenethiol substrate

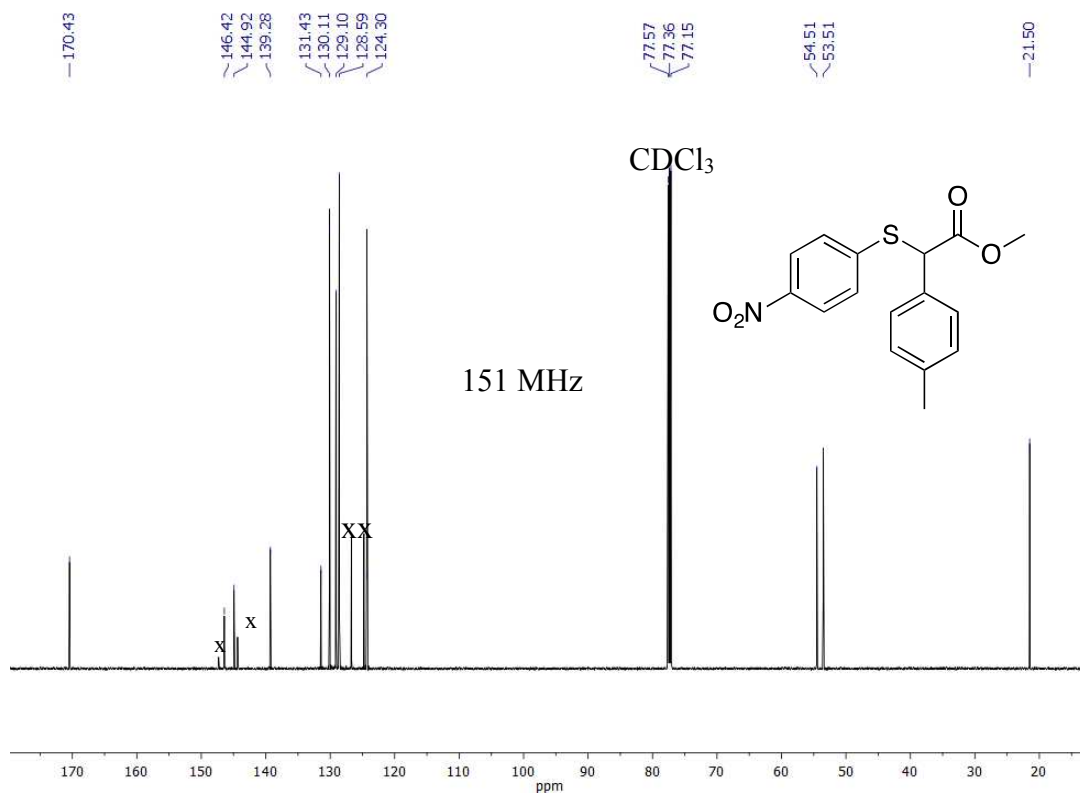


Figure S24. ¹³C NMR (151 MHz) spectrum of methyl 2-((4-nitrophenyl)thio)-2-(*p*-tolyl)acetate

**CHAPTER 4. AEROBIC OXIDATION OF CYCLIC AMINES TO LACTAMS
CATALYZED BY CERIA-SUPPORTED NANOGOLD**

Submitted to *ACS Catal.* for publication

Taiwo O. Dairo, Nicholas C. Nelson, Igor I. Slowing, Robert J. Angelici, and L. Keith Woo

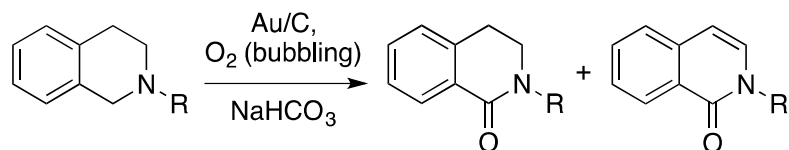
Abstract

The oxidative conversion of cyclic amines to lactams, which are important chemical feedstocks, was efficiently catalyzed by CeO₂-supported gold nanoparticles (Au/CeO₂) and Aerosil 200 in the presence of an atmosphere of O₂. The complete conversion of pyrrolidine was achieved in 6.5 hours at 160 °C, affording a 97% yield of the lactam product 2-pyrrolidone (γ -butyrolactam), while 2-piperidone (δ -valerolactam) was synthesized from piperidine (83% yield) in 2.5 hours. Caprolactam, the precursor to the commercially important nylon-6, was obtained from hexamethyleneimine in 37% yield in 3 hours. During the oxidation of pyrrolidine, two transient species, 5-(pyrrolidin-1-yl)-3,4-dihydro-2H-pyrrole (amidine-5) and 4-amino-1-(pyrrolidin-1-yl)butan-1-one, were observed. Both of these compounds were oxidized to 2-pyrrolidone under catalytic conditions, indicating their role as intermediates in the reaction pathway. In addition to the reactions of cyclic secondary amines, Au/CeO₂ also efficiently catalyzed the oxidation of N-methyl cyclic tertiary amines to the corresponding lactams at 80 °C and 100 °C.

Introduction

Lactams have important uses as feedstocks in many chemical processes, particularly in the plastics and pharmaceutical industries.¹⁻¹³ For example, N-methyl-2-pyrrolidone is widely-used as a solvent,^{4,6} and the lactams 2-pyrrolidone (butyrolactam) and 2-piperidone (valerolactam) can be polymerized into nylon-4 and nylon-5, respectively.^{3,14,15} Furthermore, caprolactam is reported to have biological activity,¹⁶ and is polymerized on a large scale into the widely-used nylon-6.^{2,17-20} Despite their commercial importance, lactams are manufactured by methods that have significant shortcomings, such as multiple reaction steps and substantial waste generation.^{5,6,21} Following earlier reports of the Gif system (Fe, Zn, O₂)-catalyzed oxidation of tertiary amines to the corresponding lactams, albeit in low yields,^{22,23} the development of efficient catalysts for the syntheses of lactams remains an active area of research. An example, recently reported by Milstein and co-workers, employs a ruthenium complex with a pincer ligand that was capable of homogeneously catalyzing the oxidation of cyclic secondary amines to the corresponding lactams, with water as the source of oxygen.²⁴ For that catalyst, reaction times ranged from 48 to 89 hours at 150 °C. Another type of catalyst, supported nanogold, has been shown to catalyze the aerobic oxidation of benzo-fused cyclic amines. For example, Au nanoparticles supported on graphite catalyze the oxidation of benzo-fused cyclic tertiary amines, resulting mostly in the formation of both the corresponding amides and the enamides (Scheme 1).²⁵ Also, Sakurai and co-workers showed that nanogold supported on polyvinylpyrrolidone (PVP) catalyzes the oxidation of 1,2,3,4-tetrahydroisoquinoline and other benzo-fused cyclic secondary amines.²⁶ However, a large amount of NaOH additive (1 – 2 equiv) was required, and the reactions often led to mixtures

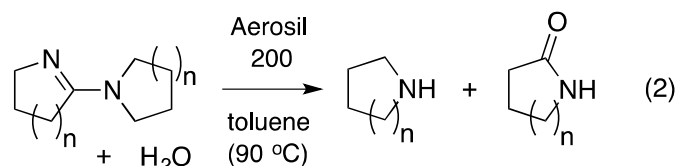
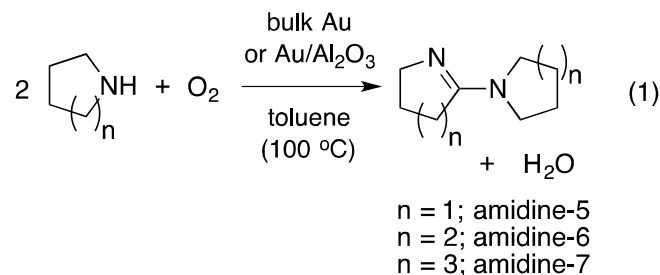
of products. Additionally, the oxidation of a derivative of tetrahydroisoquinoline to the corresponding amide and enamide is catalyzed by polymer-confined Au nanoclusters.²⁷



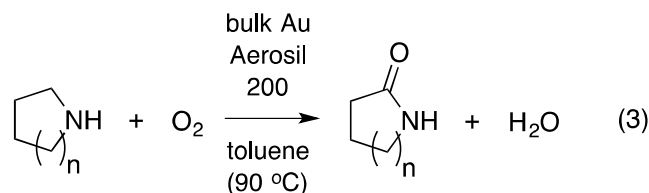
Scheme 1. Aerobic oxidation of cyclic tertiary amines to amides and enamides, catalyzed by graphite-supported gold nanoparticles.²⁵

Following the discovery of the catalytic activity of nanoparticulate CeO₂ and CeO₂-supported nanogold for the oxidation (O₂) of aromatic amines and alcohols,^{28,29} the number of reports has surged on the use of Au supported on CeO₂ as well as mixed CeO₂-metal oxides for amine oxidation reactions. For example, CeO₂-supported nanogold catalyzes the high-pressure (5 bars of O₂) oxidation of benzylamine to N-benzylidenebenzylamine.³⁰ Also, the catalytic activity of *in situ* generated CeO₂-supported nanogold in the oxidation of benzylamine, indoline, dibenzylamine, and N-*t*-butylbenzylamine into the corresponding imines was reported.^{31,32} Furthermore, nanogold supported on CeO₂-Fe₂O₃ catalyzes the oxidation of benzylamine to the imine.³³

We previously reported that bulk Au and alumina-supported Au catalyze the oxidation of cyclic secondary amines to amidines (eq. 1).^{34,35} We also showed that Aerosil 200 (amorphous fumed silicon dioxide) catalyzed the hydrolysis of amidine-5, amidine-6, or amidine-7 into 2-pyrrolidone (42% yield), 2-piperidone (60% yield) or caprolactam (73% yield), respectively, in the presence of H₂O (eq. 2).



Subsequently, we demonstrated that a one-pot combination of bulk Au powder and Aerosil 200 catalyzes the conversion of cyclic secondary amines (eq. 3) directly to lactams.³⁶ Although our one-pot procedure is a novel method for the preparation of lactams, it suffers from the use of a large amount of bulk Au powder (1.00 g per 0.20 mmol of substrate) and gives only low to medium product yields (caprolactam: 11%, 2-pyrrolidone: 35%, and 2-piperidone: 51%).



The ability of CeO₂ to facilitate oxidation reactions^{28,29} and the improved efficiency of Au when supported on high surface area metal oxides,^{34,35} including CeO₂,³⁰ prompted us to explore the activity of Au/CeO₂ in the oxidation of cyclic amines to lactams. We report herein that Au/CeO₂ efficiently catalyzes the oxidation of both cyclic secondary and N-methyl cyclic tertiary amines to the corresponding lactams. The reaction times are much shorter, product yields are higher, and the amount of catalyst loading is much lower than the bulk gold-catalyzed reactions.

Results and Discussion

Catalyst characterization: The Au/CeO₂ catalysts were synthesized as described in the experimental section. Two different loadings of Au (5.4±0.1 and 8.5±0.3 wt%) were prepared by varying the relative amounts of HAuCl₄•3H₂O and CeO₂ used during the syntheses. Nitrogen physisorption studies were used to determine the surface areas of the support and catalysts. The surface areas for the 5.4 and 8.5 wt% Au/CeO₂ catalysts were 146 m² g⁻¹ and 129 m²g⁻¹, respectively (Table S1, Fig. S13). These values were lower than that for the support (180 m² g⁻¹), likely due to the blockage of pores.

Powder X-ray diffraction (PXRD) analysis of Au/CeO₂ showed peaks that were indexed to the cubic fluorite phase of ceria. These peaks were broad, suggesting small ceria crystallites and/or lattice strain. The small crystallite size is consistent with the high surface areas observed. Also present were very low intensity, broad peaks observed around 38°, corresponding to the reflections of fcc-Au. This indicates the presence of small (<5 nm) gold crystallites. Furthermore, scanning transmission electron microscopy (STEM) images (Fig. 1a) showed the presence of spherical Au particles with an average size of 6.5 ± 1.1 nm, consistent with the PXRD data. High-resolution transmission electron microscopy (HR-TEM) of the gold particles showed a 0.23 nm d spacing, which agrees well with the (111) surface termination for Au particles (Fig. 1b).^{39,40} The STEM image (Fig. 1a) also illustrates the porous nature of the catalyst support, consistent with the high surface areas from nitrogen physisorption analysis. The CeO₂ support surface termination is predominantly the (111) plane, as previously reported.³⁸

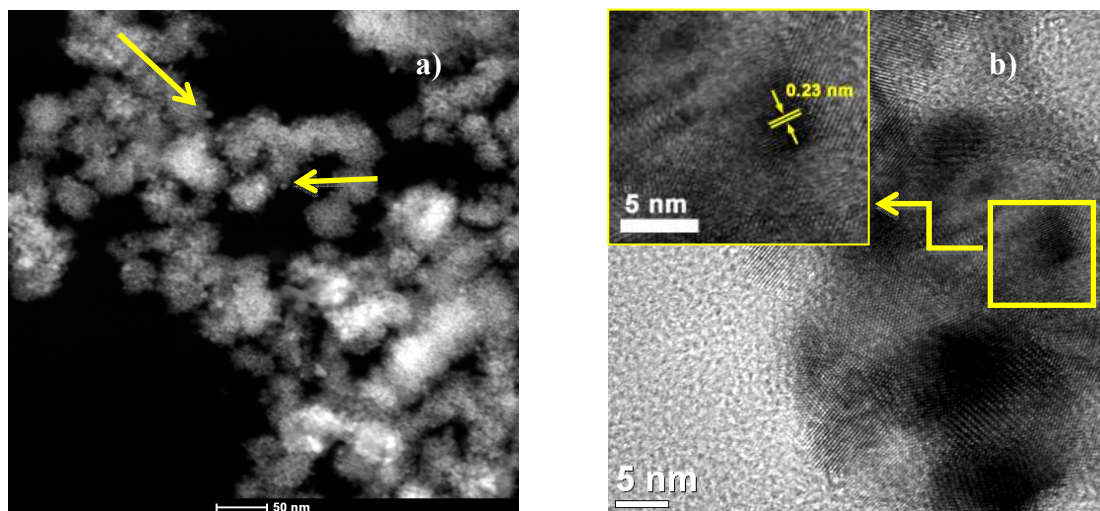
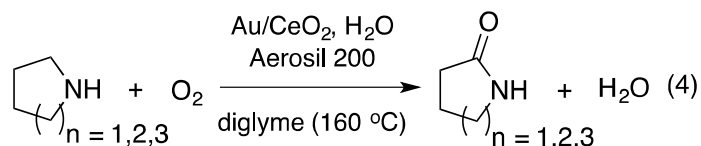


Figure 1. (a) Scanning transmission electron microscopy (STEM) image of the unused 5.4 wt% Au/CeO₂ catalyst. Arrows indicate Au nanoparticles. (b) High-resolution transmission electron microscopy (HR-TEM) image showing the presence of Au particles on the surface of CeO₂ for the unused 5.4 wt% Au/CeO₂ catalyst.

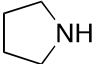
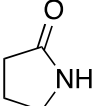
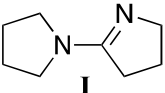
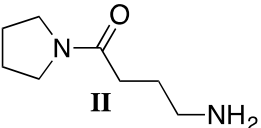
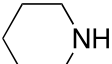
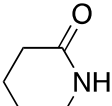
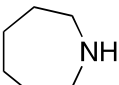
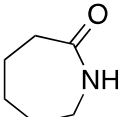
X-ray photoelectron spectroscopic studies were undertaken in order to probe the oxidation state of Au in the supported catalyst. The XPS spectrum (Fig. S18) of a fresh sample of 5.4 wt% Au/CeO₂ showed two peaks in the Au 4f core level region (83 – 93 eV). The spectrum was fitted by splitting into the two spin-orbit 4f_{7/2} and 4f_{5/2} components of Au separated by 3.6 eV.^{41,42} Deconvolution of the spectrum suggests the catalyst consists mainly of metallic Au⁰ (84.0 eV for 4f_{7/2} and 87.6 eV for 4f_{5/2}, 93 %) but also contains a small fraction of oxidized Au⁺¹ (85.8 eV for 4f_{7/2} and 89.4 eV for 4f_{5/2}, 7 %). These results are consistent with the report by Casaletto and co-workers, who obtained a 90:10 atomic ratio of Au⁰ to Au⁺¹ for Au/CeO₂ also prepared by deposition-precipitation. Importantly, they observed high CO oxidation activity for this catalyst compared to other supports and attributed it to the presence of Au⁺¹ and its stabilization as AuO⁻ by the cerium oxide support.⁴²

Au/CeO₂-catalyzed oxidation of cyclic secondary amines to lactams: Gold nanoparticles supported on high surface area (169 – 203 m²/g) CeO₂ (Au/CeO₂), together with Aerosil 200 as a co-catalyst, efficiently catalyze the oxidation of cyclic secondary amines into lactams (eq. 4). Product yields were maximized by varying the temperature and the amounts of water, oxygen, and co-catalyst (Table 1). For pyrrolidine (100 mM), the opti-



-mized reaction conditions involved heating a diglyme solution with 5.4 wt% Au/CeO₂, Aerosil and H₂O (56 equiv relative to pyrrolidine) under one atmosphere of O₂ at 160 °C for 6.5 h. This resulted in complete substrate conversion to give a 97% yield of 2-pyrrolidone (Table 1, entry 1, Fig. 2). When the catalytic oxidation of pyrrolidine to 2-pyrrolidone was carried out under the same conditions, but without the Aerosil co-catalyst, a product yield of 75% (Table 1, entry 3) was achieved. If the reaction was performed under air (1 atm) rather than O₂ (1 atm) keeping all other parameters at optimized reaction conditions, a 93% yield of the lactam product was achieved in a reaction time of 6.5 h (Table 1, entry 6). Under an atmosphere of argon gas, only an 8% yield of 2-pyrrolidone was obtained (Table 1, entry 5). The small amount of observed product was presumably due to the presence of adventitious O₂.⁴³ Varying the amount of added H₂O from 56 equiv, while keeping all other parameters at optimized values, resulted in lower yields of 2-pyrrolidone as follows (Fig. S10): 18% (0 equiv), 34% (10 equiv), 55% (28 equiv), 80% (90 equiv), and 77% (112 equiv). It is also noteworthy that in the presence of CeO₂ alone (without deposited nanogold), lactam formation was not observed, under otherwise optimized reaction conditions.

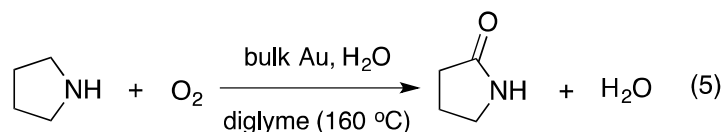
Table 1. Catalytic conversion of cyclic secondary amines, amidine-5 (I), or 4-amino-1-(pyrrolidin-1-yl)butan-1-one (II) to lactams in diglyme solvent, under O₂ (1 atm, unless stated otherwise), at 160 °C^a

Entry	Substrate	Product	Time (h)	Product Yield (%)	TON ^k	TOF ^l (h ⁻¹)
1			6.5	97 ^a	22.4	3.45
2	"	"	6.5	27 ^{a,b}	0.0236	0.00363
3	"	"	6.5	75 ^c	17.4	2.67
4	"	"	6.5	18 ^{b,c}	0.0157	0.00242
5	"	"	6.5	8 ^d	1.85	0.285
6	"	"	6.5	93 ^e	21.5	3.31
7		"	6.5	95 ^f	23.3	3.58
8		"	6.5	96 ^g	21.8	3.36
9			2.5	83 ^a	19.2	7.68
10	"	"	5.5	83 ^h	10.8	1.97
11			3	37 ⁱ	3.43	1.14
12	"	"	3	31 ^j	1.82	0.608
13	"	"	4	19 ^a	4.40	1.10

^a0.444 mmol (100 mM; 1 eq) substrate, 70 mg of 5.4 wt% Au/CeO₂, 111 mg of Aerosil (4.2 eq), 0.45 mL H₂O (56 eq), 4.44 mL diglyme. ^b1.00 g of bulk Au powder used instead of Au/CeO₂. ^cAerosil not added. ^dUnder argon atmosphere. ^eUnder air atmosphere (1 atm). ^f0.235 mmol (100 mM; 1 eq) substrate, 36.6 mg of 5.4 wt% Au/CeO₂, 59 mg of Aerosil (4.2 eq), 0.236 mL of H₂O (56 eq). ^g0.218 mmol (100 mM; 1 eq) substrate, 34 mg of 5.4 wt% Au/CeO₂, 55 mg of Aerosil (4.2 eq), 0.22 mL of H₂O (56 eq). ^h0.444 mmol (100 mM; 1 eq) substrate, 78.8 mg of 8.5 wt% Au/CeO₂, 111 mg of Aerosil (4.2 eq), 0.45 mL H₂O (56 eq), 4.44 mL diglyme. ⁱ0.20 mmol (40 mM; 1 eq) substrate, 78.8 mg of 5.4 wt% Au/CeO₂, 50 mg of Aerosil (4.2 eq), 0.20 mL of H₂O (56 eq). ^j0.20 mmol (40 mM; 1 eq) substrate, 78.8 mg of

8.5 wt% Au/CeO₂, 50 mg of Aerosil (4.2 eq), 0.20 mL of H₂O (56 eq). ^kTON is defined as the number of moles of product per mole of Au. ^lTOF is defined as TON per hour of reaction time.

To demonstrate the superiority of Au/CeO₂ over bulk gold powder in the catalytic oxidation of amines into lactams, 1.00 g of Au powder was used under conditions optimized for 5.4 wt% Au/CeO₂, in the catalytic oxidation of pyrrolidine. This reaction gave a 27% yield of 2-pyrrolidone after 6.5 h (Table 1, entry 2, eq. 5), as compared with a 97% product yield obtained with Au/CeO₂ (Table 1, entry 1), which shows that 3.78 mg of Au in Au/CeO₂ is more effective as a catalyst than 1.00 g of bulk gold powder.



With Aerosil 200, lactam yield = 27% at 6.5 h
 Without Aerosil 200, lactam yield = 18% at 6.5 h

Furthermore, the use of bulk gold without Aerosil under the same conditions produced 18% of 2-pyrrolidone from the oxidation of pyrrolidine (Table 1, entry 4, eq. 5), as compared with a 75% yield in the Au/CeO₂-catalyzed reaction without Aerosil (Table 1, entry 3). Notably, the oxidation of pyrrolidine catalyzed by bulk gold at a lower temperature (100 °C in toluene), without Aerosil, gave 93% yield of amidine-5 (eq. 1, n = 1), and not 2-pyrrolidone.³⁶

The scalability of the reaction was demonstrated by increasing the pyrrolidine concentration 10-fold, from 0.1 M (0.444 mmol) to 1.06 M (4.76 mmol), in diglyme but using the same amount of Au/CeO₂ catalyst and Aerosil. The reaction solution was heated under an O₂ atmosphere at 160 °C with 70 mg of 5.4 wt% Au/CeO₂, 111 mg of Aerosil and

2.38 mL of H₂O (28 equiv. relative to pyrrolidine). After 10 h of heating, GC analysis revealed a 99% amine substrate conversion and an 84% yield of 2-pyrrolidone, representing a

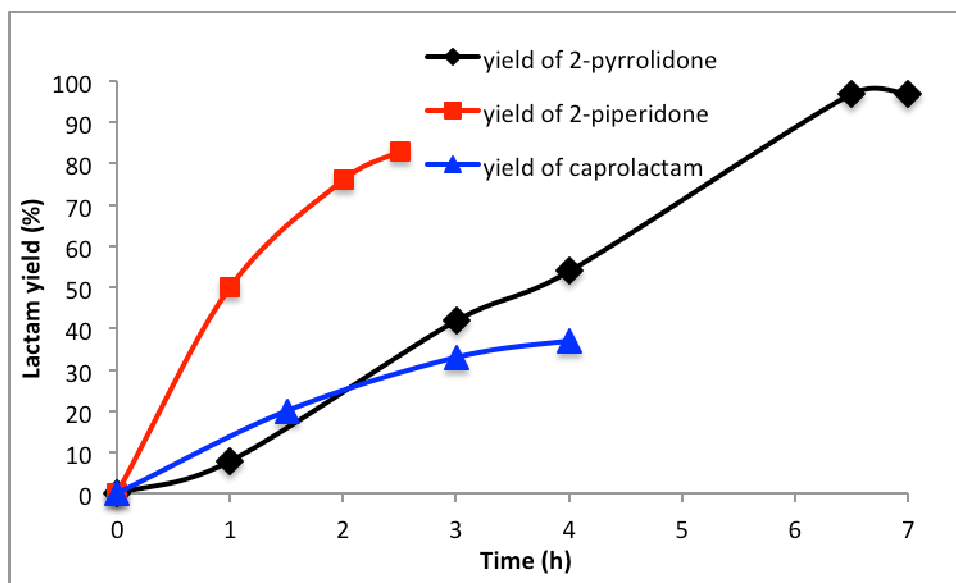


Figure 2. Lactam product yields during the Au/CeO₂-Aerosil-catalyzed oxidation of cyclic amines in diglyme at 160 °C under optimized conditions. (a) pyrrolidine to 2-pyrrolidone: 0.444 mmol (100 mM) pyrrolidine, 70 mg of 5.4 wt% Au/CeO₂, 111 mg of Aerosil (4.2 eq), 0.45 mL H₂O (56 eq), 4.44 mL diglyme; (b) piperidine to 2-piperidone: 0.444 mmol (100 mM) piperidine, 70 mg of 5.4 wt% Au/CeO₂, 111 mg of Aerosil (4.2 eq), 0.45 mL H₂O (56 eq), 4.44 mL diglyme; (c) hexamethyleneimine to caprolactam: 0.20 mmol (40 mM) hexamethyleneimine, 78.8 mg of 5.4 wt% Au/CeO₂, 50 mg of Aerosil (4.2 eq), 0.20 mL of H₂O (56 eq), 5.0 mL diglyme.

TON of 207, based on the moles of Au in the Au/CeO₂ catalyst (TON = mol of product per mole of Au).

A heterogeneity test of the catalyst was performed using a hot filtration technique. First, a reaction was run using a mixture containing 100 mM pyrrolidine in diglyme together with the Au/CeO₂-Aerosil catalyst, H₂O and dodecane (internal standard) at 160 °C under optimized conditions. After 40 min of reaction, a 22% yield of 2-pyrrolidone was obtained. At this point, the hot mixture was filtered and the solution phase was heated again at 160 °C under an O₂ atmosphere. After 5 h, no further conversion of the remaining pyrrolidine occurred,

demonstrating that the catalytically active species is not in the solution phase of the reaction and that the Au/CeO₂-Aerosil solid is the active catalyst.

In assessing the recyclability of the catalyst, the Au/CeO₂-Aerosil solids recovered from an optimized pyrrolidine oxidation reaction that produced a 98% yield of 2-pyrrolidone were washed with diglyme until no lactam was detected by GC in the rinsate (see experimental section). The washed and air-dried catalyst used in a second catalytic cycle produced an 88% yield of 2-pyrrolidone. However, when the recovered catalyst was washed, dried, and used in a third catalytic cycle, only a 14% yield of 2-pyrrolidone was obtained.

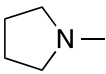
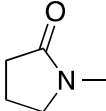
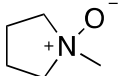
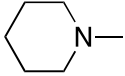
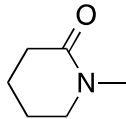
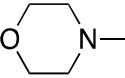
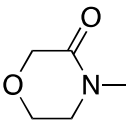
After the Au/CeO₂ catalyst sample had been used in 3 catalytic runs, its XPS spectrum remained unchanged from that of the freshly prepared material (Figs S18a and S18b). However, powder x-ray diffraction (PXRD) analysis of the Au/CeO₂ catalyst recovered from the third catalytic cycle showed that the Au crystallite size had grown from around 5 nm (for the fresh catalyst; Fig. S14a) to 29 nm (for the used catalyst; Fig. S14b). Also, TEM and STEM images (Fig. S15b and S16b, respectively) of the used catalyst also revealed aggregated gold of about 200-nm sizes. Such an increase in gold particle size would lead to a reduction in the number of catalytically active sites on the Au surface, which could be the reason for the decreased activity upon recycling. A sharp drop in catalytic activity was also observed during the Au/TiO₂-catalyzed oxidation of glycerol to lactic acid at 90 °C after 5 catalytic runs; this loss of activity was attributed to an increase in the size of the gold particles.⁴⁰

The scope of the reaction was expanded to additional cyclic secondary amines. Treatment of piperidine (eq. 4, n = 2) under the optimized conditions for the catalytic oxidation of pyrrolidine (100. mM, 0.444 mmol) afforded an 83% yield of 2-piperidone in 2.5 h, with a

100% conversion of the piperidine substrate (Table 1, entry 9). The use of 78.8 mg of 8.5 wt% Au/CeO₂ in place of 70 mg of 5.4 wt% Au/CeO₂ also gave an 83% yield of 2-piperidone, albeit at a longer reaction time of 5.5 h (Table 1, entry 10). Thus, the optimized reaction conditions for the oxidation of both pyrrolidine and piperidine were the same.

The optimized conditions for the oxidation of the 7-membered cyclic amine, hexamethyleneimine, into caprolactam (eq. 4, $n = 3$) involved a 40 mM solution of hexamethyleneimine (0.200 mmol) in diglyme, 78.8 mg of 5.4 wt% Au/CeO₂, 50 mg of Aerosil 200, and 0.20 mL of H₂O (56 equiv relative to substrate), resulting in a 37% yield of the product (100% substrate conversion) in 3 h (Table 1, entry 11). Doubling the amount of H₂O under these conditions gave only a 16% product yield. When 78.8 mg of 8.5 wt% Au/CeO₂ was used in place of the 78.8 mg of 5.4 w% Au/CeO₂ under the optimized conditions, a 31% caprolactam yield was obtained in 3 h, with complete substrate conversion (Table 1, entry 12). However, when the catalytic oxidation of hexamethyleneimine was carried out under the optimized conditions used for the oxidation of pyrrolidine and piperidine, a 19% yield of caprolactam (100% conversion of the substrate) was obtained in 4 h (Table 1, entry 13). Thus, a lower substrate concentration (40 mM) was more effective than a higher concentration (100 mM) for the catalytic oxidation of hexamethyleneimine to caprolactam. The use of 5 mol% of NaOH or K₂CO₃ as additives^{24,44,45} in the reaction, while keeping all other parameters optimized, resulted in a 17% yield of caprolactam in each case, with 100% substrate conversion. It is noteworthy that prolonged heating after complete substrate conversion generally resulted in the appearance of several unidentified peaks in the GC chromatograms.

Table 2. Catalytic conversion of N-methyl cyclic tertiary amines into lactams in 1,4-dioxane solvent, under O₂ atmosphere (1 atm), unless stated otherwise.

Entry	Substrate	Product	Temp (°C)	Time (h)	Product yield (%)	TON ⁿ	TOF ^o (h ⁻¹)
1			80	3.5	97 ^a	24.7	7.04
2	"	"	100	3.5	98 ^b	22.9	6.55
3	"	"	100	3.5	94 ^{b,c}	22.0	6.28
4	"	"	80	10.5	90 ^b	21.1	2.01
5	"	"	80	3.5	8 ^{a,d}	2.03	0.581
6	"	"	80	3.5	4 ^{a,e}	1.02	0.290
7	"	"	80	10	97 ^{a,f}	24.7	2.47
8		"	80	3.5	9 ^a	2.29	0.654
9			100	4	97 ^g	21.4	5.35
10	"	"	100	3	76 ^h	16.8	5.58
11	"	"	100	3	56 ⁱ	12.3	4.12
12	"	"	80	18	79 ⁱ	17.4	0.968
13			100	10	72 ^j	17.0	1.70
14	"	"	100	13.5	60 ^k	14.1	1.05
15	"	"	100	24	34 ^l	8.01	0.334
16	"	"	100	24	1 ^m	0.236	0.00982

^a0.488 mmol (108 mM; 1eq) substrate, 70 mg of 5.4 wt% Au/CeO₂, 0.45 mL H₂O (51 eq), 4.54 mL 1,4-dioxane. ^b0.449 mmol (101 mM; 1eq) substrate, 70 mg of 5.4 wt% Au/CeO₂, 111 mg of Aerosil (4.1 eq), 0.45 mL H₂O (56 eq), 4.48 mL 1,4-dioxane. ^cAerosil not added. ^dH₂O not added. ^eUnder argon atmosphere. ^fUnder air atmosphere. ^g0.423 mmol (95 mM; 1eq) substrate, 70 mg of 5.4 wt% Au/CeO₂, 1.80 mL H₂O (236 eq), 4.45 mL 1,4-dioxane. ^h0.423 mmol (95 mM; 1 eq) substrate, 70 mg of 5.4 wt% Au/CeO₂, 0.90 mL H₂O (118 eq), 4.45 mL 1,4-dioxane. ⁱ0.423 mmol (95 mM; 1eq) substrate, 70 mg of 5.4 wt% Au/CeO₂, 0.45 mL H₂O

(59 eq), 4.45 mL 1,4-dioxane. ^j0.452 mmol (101 mM; 1eq) substrate, 70 mg of 5.4 wt% Au/CeO₂, 0.90 mL H₂O (110 eq), 4.48 mL 1,4-dioxane. ^k0.452 mmol (101 mM; 1eq) substrate, 70 mg of 5.4 wt% Au/CeO₂, 1.80 mL H₂O (220 eq), 4.48 mL 1,4-dioxane. ^l0.452 mmol (101 mM; 1eq) substrate, 70 mg of 5.4 wt% Au/CeO₂, 0.45 mL H₂O (55 eq), 4.48 mL 1,4-dioxane. ^m0.452 mmol (101 mM; 1eq) substrate, 70 mg of 5.4 wt% Au/CeO₂, 4.48 mL 1,4-dioxane. ⁿTON is defined as the number of moles of product per mole of Au. ^oTOF is defined as TON per hour of reaction time.

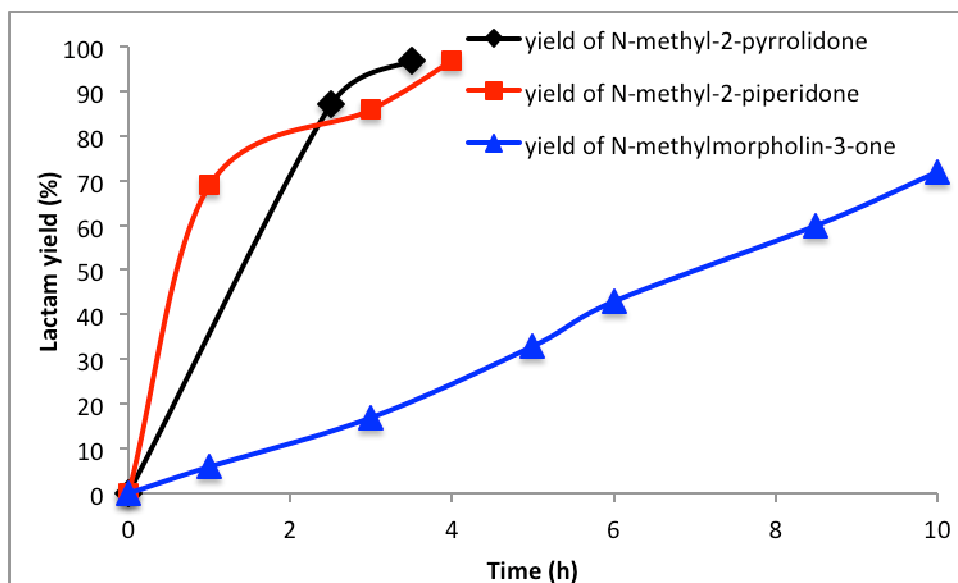


Figure 3. Lactam product yields during the Au/CeO₂-catalyzed oxidation of tertiary cyclic amines under optimized conditions. (a) 0.488 mmol (107.5 mM) N-methylpyrrolidine substrate, 70 mg of 5.4 wt% Au/CeO₂, 0.45 mL H₂O (51 eq), in 4.54 mL of 1,4-dioxane at 80 °C; (b) 0.423 mmol (95 mM) N-methylpiperidine substrate, 70 mg of 5.4 wt% Au/CeO₂, 1.80 mL H₂O (236 eq), in 4.45 mL of 1,4-dioxane at 100 °C; (c) 0.452 mmol (101 mM) N-methylmorpholine substrate, 70 mg of 5.4 wt% Au/CeO₂, 0.90 mL H₂O (110 eq), in 4.48 mL of 1,4-dioxane at 100 °C.

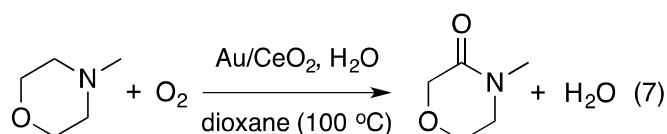
of the amine substrate (Table 2, entry 5). Furthermore, only a 4% yield of N-methyl-2-pyrrolidone was obtained after 3.5 h of heating a dioxane-solution of N-methylpyrrolidine with 5.4 wt% Au/CeO₂ and H₂O at 80 °C under an atmosphere of argon (Table 2, entry 6). In addition, when the catalytic oxidation of N-methylpyrrolidine was carried out in air, rather than an O₂ atmosphere, a 49% yield of N-methyl-2-pyrrolidone was obtained after 3.5 h, as compared with the 97% yield obtained after 3.5 h when the reaction was carried out in an O₂

atmosphere. However, when the air reaction was allowed to proceed for a total of 10 h, a 97%-yield of the lactam product was obtained. (Table 2, entry 7). Noteworthy also, is the finding that under otherwise optimized reaction conditions, no reaction occurred in the presence of CeO₂ alone (without deposited nanogold).

N-methyl-2-piperidone was also synthesized by the catalytic oxidation of N-methylpiperidine with O₂ (eq. 6, n = 2). The optimized conditions for this reaction involve heating a 95 mM dioxane solution of N-methylpiperidine (0.423 mmol) with 70 mg of 5.4 wt% Au/CeO₂ and 1.80 mL H₂O (236 equiv relative to the amine) at 100 °C for 4 h resulting in a 97% yield of N-methyl-2-piperidone and a 100% conversion of the substrate (Table 2, entry 9; Fig. 3). Halving the amount of added H₂O (i.e. 118 equiv relative to the amine), but keeping all other conditions optimized, resulted in a 76% yield of N-methyl-2-piperidone (100% substrate conversion) in 3 h (Table 2, entry 10). A further decrease in the amount of H₂O (59 equiv relative to the amine) led to only a 56% yield of N-methyl-2-piperidone in 3h (100% conversion of substrate, Table 2, entry 11). When this reaction (with 59 equiv of added H₂O) was carried out at 80 °C, a 79% product yield and a 97% substrate conversion were achieved after 18 h (Table 2, entry 12), indicating that the catalytic oxidation of N-methylpiperidine to N-methyl-2-piperidone proceeded much faster (3 h versus 18 h) but with a lower product yield (56% versus 79%) at a higher temperature (100 °C versus 80 °C).

N-methylmorpholine was also oxidized by O₂ in the presence of 5.4 wt% Au/CeO₂ (eq. 7) to give N-methylmorpholin-3-one. The ¹H and ¹³C NMR data (see supporting information) of the isolated product were different from those reported for the lactone 4-methylmorpholin-2-one.^{46,47} Furthermore, 2D NMR analysis confirmed that the lactam, and not the lactone, was formed from the current Au/CeO₂-catalyzed oxidation reactions of N-methylmorpholine. For

example, HMBC revealed a strong 3-bond heteronuclear coupling between the N-methyl protons and the CO carbon (Fig. S9). In the lactone 4-methylmorpholin-2-one, such coupling would be across four (4) bonds, and would be too weak to be observed. Under optimized conditions, a 72% yield of N-methylmorpholin-3-one (100% substrate conversion) was obtained after 10 h, when a 101 mM dioxane solution of the amine substrate (0.452 mmol) was heated at 100 °C with 5.4 wt% Au/CeO₂ in the presence of 0.90 mL (110 equiv relative to substrate) of H₂O (Table 2, entry 13; Figs. 3 and S11).



In addition, doubling the amount of H₂O under optimized conditions (220 equiv instead of 110 equiv) led to a slightly lower (60%) yield of N-methylmorpholin-3-one and 99% substrate conversion after a longer reaction time of 13.5 h (Table 2, entry 14, Fig S11). Under the same conditions, but using only 0.45 mL of H₂O (55 equiv relative to the substrate), only a 34% yield of N-methylmorpholin-3-one was obtained from an 81% conversion of the N-methylmorpholine, after 24 h (Table 2, entry 15, Fig S11). Furthermore, when H₂O was eliminated from the optimized conditions, the yield of N-methylmorpholin-3-one was only 1% (56% conversion of N-methylmorpholine) after a reaction time of 24 h (Table 2, entry 16, Fig. S11).

Reaction pathways for the formation of lactams from cyclic secondary and tertiary amines

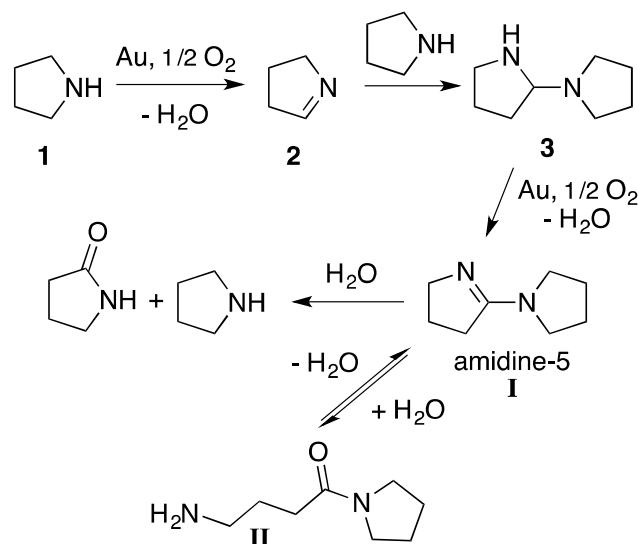
a. Mechanism for the oxidation of cyclic secondary amines to lactams.

In the optimized catalytic Au/CeO₂-Aerosil system, GC monitoring during the oxidation of pyrrolidine to 2-pyrrolidone revealed the appearance of two new GC peaks, at 9.18 and

10.98 min, during the course of the reaction. These two peaks gradually disappeared as the product peak (6.50 min) continued to grow in intensity, suggesting the involvement of reaction intermediates. Analysis of the reaction mixture by GC-MS led to the assignment of these two transient peaks to 5-(pyrrolidin-1-yl)-3,4-dihydro-2*H*-pyrrole (amidine-5, **I**, Scheme 2) and 4-amino-1-(pyrrolidin-1-yl)butan-1-one (**II**). Additional support for the role of amidine-5 (**I**) and compound **II** as intermediates was derived from their independent syntheses and conversion to 2-pyrrolidone, under the optimized conditions for pyrrolidine oxidation. Specifically, under the optimized conditions for the catalytic oxidation of pyrrolidine, 0.235 mmol of amidine-5 (**I**) produced 0.447 mmol of 2-pyrrolidone (95% yield, Table 1, entry 7), which is close to the 2:1 stoichiometry expected for the conversion of **I** to 2-pyrrolidone. Similarly, treatment of compound **II** (0.218 mol) under catalytic conditions produced 0.419 mmol of 2-pyrrolidone (96% yield, Table 1, entry 8).

A likely pathway for the catalytic oxidation of pyrrolidine (**1**) is shown in Scheme 2. Previous evidence from the bulk gold powder-catalyzed reaction suggested that the first step involved the oxidative dehydrogenation of the amine substrate to give the imine (**2**).^{34,35} Reaction of the imine with pyrrolidine³⁴ would give diamine **3**, which subsequently undergoes oxidative dehydrogenation to afford amidine-5 (**I**). The formation of **II** presumably resulted from the reversible hydrolysis of the C=N bond of amidine-5 (**I**) (Scheme 2). Compound **II** is not directly on the pathway from pyrrolidine to 2-pyrrolidone, but it re-enters that pathway by converting to **I**.

In contrast to the reaction of pyrrolidine, in which amidine-5 (**I**) was identified as an intermediate, amidine-6 or amidine-7 were not observed as intermediates during the Au/CeO₂-Aerosil-catalyzed oxidation of piperidine or hexamethyleneimine, respectively.



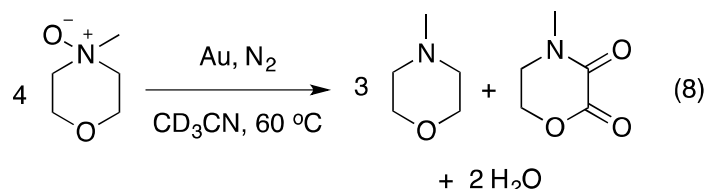
Scheme 2. Possible pathway for the Au/CeO₂-Aerosil-catalyzed oxidation of pyrrolidine to 2-pyrrolidone via amidine-5 (I) and 4-amino-1-(pyrrolidin-1-yl)butan-1-one (II).

The 6- or 7-membered analogs of intermediate **II** were also not observed. However, amidine-6 and amidine-7 were formed when bulk gold catalyzed the oxidation (O_2) of the cyclic amines, as previously reported;^{34,36} this result suggests that the oxidations of the 6- and 7-membered ring amines (eq. 4) also proceed through amidine intermediates. In the previously reported bulk gold/Aerosil-catalyzed oxidation of hexamethyleneimine, the relatively low yield of caprolactam was attributed to the relatively low production of amidine-7.³⁶ Thus, the lower yields of 2-piperidone (83%) and caprolactam (37%) from piperidine and hexamethyleneimine, respectively, are a likely consequence of the relatively small amounts of amidine-6 and 7 formed from the oxidative dehydrogenation step.

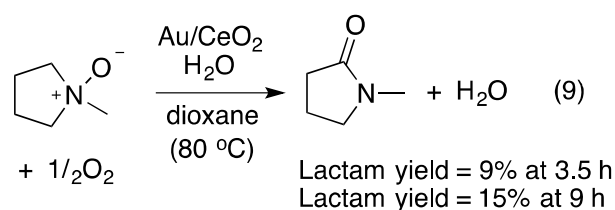
b. Oxidation of N-methyl cyclic tertiary amines to lactams.

Because of the presence of the N-methyl group in the N-methyl cyclic amines, it is not possible for these amines to be oxidized to imines as proposed in the first step (Scheme 2) for

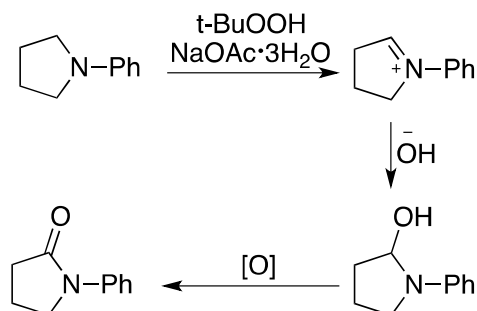
the cyclic secondary amines. No intermediates that might suggest a mechanism for the oxidation of N-methylpyrrolidine to its lactam (eq. 6, $n = 1$) were detected by GC during the reaction. However, a previous report demonstrated that tertiary amines, such as triethylamine and pyridine, are converted to their N-oxides in the presence of a carbon-supported Au catalyst and O_2 (1 - 2 atm) in H_2O at 70 and 90 °C.⁴⁸ In addition, we previously reported that bulk Au catalyzes the conversion of N-methylmorpholine-N-oxide into N-methylmorpholine (74% yield) and N-methyl-morpholine-2,3-dione (14% yield) after 48 h of heating at 60 °C (eq. 8).⁴⁹ Thus, it seemed plausible that an N-methylmorpholine-N-oxide intermediate would convert to the N-methylpyrrolidone product in the presence of a Au catalyst. However, when N-methylpyrrolidine-N-oxide was treated with O_2 under the optimized conditions used for t-



he catalytic oxidation of N-methylpyrrolidine, only a 9% yield of N-methyl-2-pyrrolidone was obtained (Table 2, entry 8) after the optimized reaction time (3.5 h). The yield increased to 15% after a total reaction time of 9 h (eq. 9). The low yield of N-methyl-2-pyrrolidone obtained from N-methylpyrrolidine-N-oxide (as compared to a 97% lactam yield from N-methylpyrrolidine; Table 2, entry 1) under the same optimized conditions suggests that amine N-oxides represent a minor pathway, or are not involved, in the catalytic oxidation of the cyclic tertiary amines studied here.

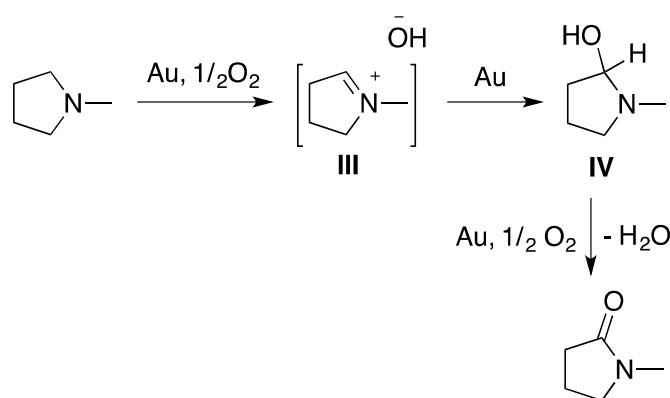


A possible alternate intermediate in the catalytic oxidation of the cyclic tertiary amines is an iminium ion. Such species have been generated from tertiary amines in the presence of molecular oxygen as well as other oxidants.^{25,50-54} For example, during the oxidation (O_2) of N-phenyl tetrahydroisoquinoline, catalyzed by graphite-supported Au nanoparticles, Che and co-workers proposed the generation of a cationic iminium intermediate, which was subsequently trapped by nucleophiles.²⁵ Furthermore, an iminium intermediate was proposed to have been generated during the copper-catalyzed oxidative cross-dehydrogenative-coupling of N-phenyl tetrahydroisoquinoline with nitroalkanes and malonates in the presence of atmospheric pressure of O_2 .⁵⁴ In addition, a cationic iminium species was suggested as an intermediate during the $NaClO_2$ oxidation of tertiary allylamines into 2,3-epoxyamides.⁵² More recently, Rao and Periasamy reported the oxidation of N-phenyl and N-(*p*-tolyl)pyrrolidine to the corresponding amides in the presence of *t*-butyl hydroperoxide as an oxidant and *t*-BuOK as a base. In that report, an N-phenyl pyrrolidinium intermediate was proposed (Scheme 3).⁵⁰



Scheme 3. Proposed generation of N-phenylpyrrolidinium during the oxidation of N-phenylpyrrolidine.⁵⁰

Under the optimized conditions for the current Au/CeO₂-catalyzed oxidation of N-methylpyrrolidine into N-methyl-2-pyrrolidone, it is conceivable that the N-methylpyrrolidinium cation **III** is generated, which then undergoes a rearrangement to the hemiaminal compound **IV** (Scheme 4). The resulting hemiaminal could then undergo oxidation to give the N-methylated lactam product. Although this is a plausible mechanism, none of the proposed intermediates have been detected or identified.



Scheme 4. Proposed pathway for the Au/CeO₂-catalyzed oxidation of N-methylpyrrolidine to N-methyl-2-pyrrolidone via an iminium intermediate.

Conclusions

Nanogold (6.5 ± 1.1 nm) supported on high surface area ($169 - 203$ m²/g) CeO₂ nanoparticles is active in the oxidation (1 atm O₂) of pyrrolidine, piperidine, and hexamethyleneimine to give 2-pyrrolidone (97% yield; eq 4, $n = 1$), 2-piperidone (83% yield; eq. 4, $n = 2$), and caprolactam (37% yield; eq. 4, $n = 3$). Studies suggest that these conversions proceed in two distinguishable steps (Scheme 2). The first involves a gold-catalyzed reaction of the amine with oxygen to give an amidine (eq. 1). This reaction is also catalyzed by bulk gold³⁴ and Au/Al₂O₃^{35,36}. The second step involves hydrolysis of the

amidine to give the lactam and the cyclic amine (eq. 2). This reaction occurs to some extent at 160 °C even without a hydrolysis catalyst, as pyrrolidine gives a 27% yield of 2-pyrrolidone using only a bulk gold catalyst. However, at 100 °C, bulk gold gives only amidine-5, indicating that amidine-5 is not hydrolyzed at the lower temperature.³⁴⁻³⁶ The addition of Aerosil 200 to the bulk gold-catalyzed reaction does give 2-pyrrolidone (35%), even at 90 °C, because Aerosil catalyzes the hydrolysis of the amidine. It appears that the CeO₂ support in the present study also catalyzes the amidine hydrolysis to give a 97% yield (at 6.5 h) of the lactam using Au/CeO₂ under optimized conditions.

The N-methyl cyclic tertiary amines are also oxidized (O₂) to the corresponding lactams at temperatures (80 - 100 °C) that are milder than those (160 °C) used for the cyclic secondary amines. Using the Au/CeO₂ catalyst (eq. 6,7) under optimized reaction conditions, N-methylpyrrolidine, N-methylpiperidine, and N-methylmorpholine are converted to N-methyl-2-pyrrolidone (97% yield; eq. 6, n = 1), N-methyl-2-piperidone (97% yield; eq. 6, n = 2), and N-methylmorpholin-3-one (72% yield; eq. 7). The mechanism of the Au/CeO₂-catalyzed oxidation of N-methylated cyclic tertiary amines to their lactams (eq. 6 and 7) is clearly different from that for the oxidation of cyclic secondary amines (eq. 4), since the N-methyl substituent prevents oxidative dehydrogenation to form the initial imine (Scheme 2).

These oxidations of cyclic amines to lactams using 1 atm O₂ and the heterogeneous Au/CeO₂ catalyst open the door to a new method of preparing lactams.

Experimental Section

All reagents were obtained from commercial sources (Sigma-Aldrich, Fisher Scientific, and Acros Organics) and used without further purification. Toluene, THF, and CH₂Cl₂ were

dried and deoxygenated by passage through columns of alumina and reduced copper. Ultra pure water was obtained from a Milli-Q[®] UV plus water purification system. Aerosil 200 was a gift from the Evonik Degussa Corporation. NMR spectra were obtained using Varian MR 400 MHz and Bruker AVIII 600 MHz spectrometers. NMR peak positions were referenced against residual proton (δ 7.26 ppm) or ¹³C (77.36 ppm) resonances in CDCl₃. HRMS data were collected on an Agilent 6540 QTOF accurate mass MSMS instrument.

GC and GC-MS analyses: GC analyses of reaction mixtures were performed on an HP-6890 instrument equipped with an HP-5 capillary column (30 m length, 0.25 mm internal diameter, 0.25 μ m film thickness, 5% phenyl, 95% methyl silicone polymer). Reaction products were identified by comparing their GC retention times with those of authentic samples and yields were determined by GC integrations relative to dodecane as an internal standard. GC-MS analyses were carried out using an Agilent 7890A-5975C instrument, equipped with an HP-5MS column.

Electron Microscopy: Transmission electron microscopy (TEM) was carried out on a FEI Tecnai G2 F20 field emission microscope and a scanning transmission electron microscope (STEM) operating at 200kV (point-to-point resolution <0.25 nm and a line-to-line resolution of <0.10 nm). TEM samples were prepared by placing 2-3 drops of dilute ethanol suspensions onto lacey-carbon-coated copper grids. The compositions of the Au/CeO₂ structures were characterized by elemental mapping and energy dispersive X-ray spectroscopy (EDS) in the STEM mode.

Surface Area and Porosimetry: Textural properties of the CeO₂ support and Au/CeO₂ catalysts were measured by nitrogen sorption isotherms at -196 °C in a Micromeritics Tristar analyzer. Surface areas were calculated using the Brunauer-Emmett-Teller method, and the pore size distribution was calculated by the Barrett-Joyner-Halenda (BJH) method. Prior to surface area measurements, samples were pretreated under flowing N₂ gas for 6 h at 100 °C.

ICP-OES analyses: The Au loadings on the CeO₂ support were determined using a PerkinElmer Optima 2100 DV inductively coupled plasma-optical emission spectroscope (ICP-OES). Catalyst samples (5 mg) were digested for 24 h in an aqueous solution containing a mixture of HF and HCl (0.18 and 5.0 v/v %, respectively). A 1-mL aliquot was then diluted to 10 mL with a 10 v/v % aqueous aqua regia solution.

X-ray Photoelectron Spectroscopy (XPS): The XPS analysis was carried out using a PHI 5500 multitechnique system with a standard Al X-ray source. Charge correction was done by setting the Ce 3d binding energy peak to 882.66 eV.³⁷

Procedure for the preparation of ceria-supported gold (Au/CeO₂) catalysts: The synthesis and characterization of the CeO₂ support (169 – 203 m²/g) was published earlier.³⁸ The supported catalysts were prepared according to a procedure reported by Pérez et al.³⁰ HAuCl₄•3H₂O (213 mg, 0.541 mmol) was dissolved in ultra pure water (390 mL). The solution was then added to a CeO₂ suspension (1.00 g in 13 mL water). Following pH adjustment to 10, using 0.2 M aqueous NaOH, the resulting suspension was stirred for 18 h at room temperature. After filtration, the supported catalyst was washed with water (400 mL in

40-mL aliquots) until the wash was free of chloride ions, as indicated by the absence of a AgCl precipitate when the tenth 40 mL wash was treated with 0.001 M aqueous AgNO₃. After being washed, the solid was dried under reduced pressure at room temperature. Thereafter, the supported catalyst was treated with sec-phenethyl alcohol at 160 °C for 20 min. After filtration, the resulting powder was washed with water and acetone, then dried overnight under reduced pressure at room temperature. The gold loading was found to be 5.4 ± 0.1 wt% (by ICP-OES). To obtain a gold loading of 8.5 ± 0.3 wt%, the same procedure described above was employed, using 213 mg (0.541 mmol) of H₂AuCl₄•3H₂O and 500 mg of CeO₂.

Procedure for the Au/CeO₂-catalyzed conversion of cyclic secondary amines to lactams, in the presence of O₂, as illustrated by the reaction of pyrrolidine: A 100-mL Schlenk flask, equipped with a high-vacuum Teflon stopcock, was charged with a stir bar and 70 mg of 5.4 wt% Au/CeO₂ catalyst (3.78 mg, 0.0192 mmol of Au). This was followed by the addition of 111 mg of Aerosil 200 (amorphous fumed silicon dioxide), 0.45 mL of ultra-pure water, 1.11 mL of a 400. mM stock solution of pyrrolidine (0.444 mmol) in diglyme solvent, and 3.33 mL of a 23.8-mM dodecane stock solution (0.0793 mmol internal standard) in diglyme. The reaction flask was purged through the side arm with oxygen for 1 min and sealed with the stopcock. (A pure oxygen atmosphere, achieved by a more rigorous exclusion of air, led to lower lactam yields and the formation of a variety of unidentified products, in addition to the lactam. None of the by-products were identified). The contents of the sealed flask were stirred at 160 °C in an oil bath. The mole ratio of gold atoms to substrate was 1:23. To monitor the course of the reaction, the mixture was cooled periodically to ambient

temperature and an aliquot was withdrawn for GC analysis. Then the reaction flask was purged again with O₂, re-sealed, and re-heated to 160 °C. After 6.5 h of reaction time, 100% substrate conversion was achieved, with a 97% yield of 2-pyrrolidone. The catalytic conversions of the intermediates amidine-5 (**I**) and [4-amino-1-(pyrrolidin-1-yl)butan-1-one] (**II**) into 2-pyrrolidone followed the same procedure. When the reaction of pyrrolidine was carried out under a pure air atmosphere, the same procedure was followed as above, but without the oxygen gas purge.

Procedure for the treatment of pyrrolidine with Au/CeO₂ under an argon atmosphere: After a 100-mL Schlenk flask was charged with a stir bar, 70 mg of 5.4 wt% Au/CeO₂ catalyst, 111 mg of Aerosil 200, 0.45 mL of ultra-pure water, pyrrolidine in diglyme, and dodecane (internal standard) as described above, the reaction vessel was degassed with three freeze-pump-thaw cycles, back-filled with argon, and sealed. Stirring and heating the reaction mixture at 160 °C produced an 8% GC yield of 2-pyrrolidone after 6.5 h.

Catalyst reusability: An initial catalytic run was set up as described in Section 2.7 with 70 mg of 5.4 wt% Au/CeO₂ catalyst, 111 mg of Aerosil 200, 0.45 mL of ultra-pure water, 0.444 mmol of pyrrolidine, and 0.0793 mmol of dodecane (internal standard) in diglyme. After periodic GC analysis of the reaction solution during the first catalytic run (6.5 h of heating at 160 °C), the Au/CeO₂-Aerosil catalyst was recovered by filtration of the reaction mixture. The recovered catalyst was rinsed repeatedly with 5-mL aliquots of diglyme, until the catalyst was free of the lactam, as determined by GC analysis of the rinse. The catalysts

were further rinsed with two 5-mL aliquots of acetone. The rinsed and air-dried catalyst was then used in subsequent catalytic runs, as described above.

Procedure for the Au/CeO₂-catalyzed conversion of N-methyl cyclic tertiary amines into lactams, in the presence of O₂, as illustrated by the reaction of N-methylpyrrolidine: A 100-mL Schlenk flask, equipped with a high-vacuum Teflon stopcock was charged with a stir bar and 70 mg of 5.4 wt% Au/CeO₂ catalyst (3.78 mg, 0.0192 mmol Au). This was followed by the addition of 0.45 mL of ultra-pure water, 2.66 mL of 1,4-dioxane, 1.21 mL of a 404-mM stock solution of N-methylpyrrolidine (0.488 mmol) in 1,4-dioxane, and 0.67 mL of a dodecane (internal standard) stock solution (120. mM) in 1,4-dioxane. The reaction flask was purged through the side arm with oxygen for 1 min and sealed with the stopcock. The contents of the flask were stirred at 80 °C in an oil bath. The mole ratio of gold atoms to substrate was 1:25. GC analysis was performed as described above, for the reactions of cyclic secondary amines. At 3.5 h of reaction time, a 100% substrate conversion was achieved with a 97% yield of N-methyl-2-pyrrolidone. When the reaction of N-methylpyrrolidine was carried out under an air atmosphere, the same procedure was followed as above, but without the purge with oxygen gas. Periodic GC analysis of the reaction solution revealed a 97% yield of N-methyl-2-pyrrolidone after 10 hours of heating at 80 °C. When the reaction was carried out under an argon atmosphere, using the procedure outlined above for pyrrolidine substrate, GC analysis of the reaction solution after 3.5 hours of heating at 80 °C revealed a 4% yield of N-methyl-2-pyrrolidone.

Preparation and characterization of amidine-5 (I): Amidine-5 was synthesized by treating 221 mg (3.09 mmol) of pyrrolidine in 75 mL of toluene with O₂ in the presence of 1.135 g of bulk gold catalyst, according to a published procedure.³⁴ The oily product was isolated by filtration of the reaction mixture and removal of the toluene solvent under reduced pressure (190 mg, 1.37 mmol, 89% yield). ¹H NMR (400 MHz, CDCl₃): δ 1.86 (m, 4H, CH₂), 1.93 (m, 2H, CH₂), 2.47 (t, 2H, *J* = 8.0 Hz, CH₂), 3.35 (t, 4H, *J* = 8.0 Hz, CH₂), 3.64 (t, 2H, *J* = 8.0 Hz, CH₂). ¹³C NMR (101 MHz, CDCl₃): δ 24.15, 25.82, 32.86, 47.78, 56.95, 166.85. HRMS (+ESI): calcd for [MH]⁺ (C₈H₁₅N₂)⁺ *m/z* 139.1235; found *m/z* 139.1230.

Preparation and characterization of [4-amino-1-(pyrrolidin-1-yl)butan-1-one] (II):

Intermediate **II** was synthesized, starting from γ -aminobutyric acid.

Syntheses of compounds A, B, C, and II

Synthesis of 4-((*tert*-butoxycarbonyl)amino)butanoic acid (A): This compound was prepared according to published procedures used for the syntheses of related compounds.^{55,56} In air, a 100-mL round-bottomed flask was charged with γ -aminobutyric acid (1.06 g, 10.2 mmol), NaOH (2.70 g; 67.5 mmol, 6.62 eq), and di-*tert*-butyl dicarbonate (Boc₂O) (2.80 g; 12.7 mmol, 1.25 eq); then 10 mL each of THF and Millipore H₂O were added. The mixture was allowed to stir in air for 18 hours, after which, 1M aqueous HCl was used to reduce the pH from 13.0 to 4.0. After extraction with 3 x 20 mL ethyl acetate, the combined organic layer was dried over anhydrous Na₂SO₄, then evaporated under reduced pressure, to afford compound **A** as a colorless gel. Yield: 58% (1.20 g, 5.90 mmol). ¹H NMR (400 MHz,

CDCl₃): δ 1.44 (s, 9H, CH₃), 1.82 (m, 2H, CH₂), 2.40 (t, 2H, $J = 7.2$ Hz, CH₂), 3.19 (m, 2H, CH₂), 4.67 (br, 1H), 5.71 (br, 1H).

Synthesis of *Tert*-butyl (4-oxo-4-(pyrrolidin-1-yl)butyl)carbamate (B): Compound **B** was prepared by methods used previously for the syntheses of related compounds.^{57,58} In air, a 500-mL round-bottomed flask was charged with **A** (1.20 g, 5.90 mmol), *N*-(3-dimethylaminopropyl)-*N'*-ethylcarbodiimide hydrochloride (EDC.HCl) (1.57 g, 8.11 mmol, 1.37 eq), *N*-hydroxysuccinimide (HOSU) (0.966g, 8.23 mmol, 1.39 eq), and dry CH₂Cl₂ (163 mL). The flask was quickly capped with a rubber septum, and the mixture was stirred under N₂ atmosphere (a syringe needle, attached to an N₂-filled balloon was inserted into the septum) for 4.5 hours, after which *N,N*-diisopropylethylamine (DIPEA) (8.0 mL, 45.5 mmol, 7.71 eq) and pyrrolidine (1.4 mL, 16.7 mmol, 2.83 eq) were introduced into the flask via syringe. After stirring for an additional 17 hours, the CH₂Cl₂-solution was concentrated under reduced pressure, and the pH was brought down to 1.50, using 1 M aqueous HCl. After separating the aqueous layer, the organic layer was extracted 4 times with 50 mL of Millipore H₂O. The organic layer was dried over anhydrous Na₂SO₄ and then evaporated under reduced pressure to afford compound **B** as a white solid. Yield: 65% (0.983 g, 3.83 mmol). ¹H NMR (400 MHz, CDCl₃): δ 1.42 (s, 9H, CH₃), 1.84 (m, 4H, CH₂), 1.94 (m, 2H, CH₂), 2.30 (t, 2H, $J = 7.2$ Hz, CH₂), 3.17 (m, 2H, CH₂), 3.42 (m, 4H, CH₂), 4.89 (br, 1H).

Synthesis of 4-oxo-4-(pyrrolidin-1-yl)butan-1-aminium 2,2,2-trifluoroacetate (C): Compound **C** was synthesized according to the procedure reported for a related compound.⁵⁹ In air, a 20-mL scintillation vial was charged with **B** (0.970 g, 3.78 mmol) and trifluoroacetic

acid (TFA) (5.4 mL, 70.2 mmol, 18.6 eq), and the mixture was allowed to stir at 25 °C for 1 hour. Excess TFA was removed under reduced pressure, and the viscous oil that remained was recrystallized from CH₂Cl₂-diethyl ether. The resulting white solid product was washed with 5 x 17 mL-aliquots of diethyl ether, and then further dried under reduced pressure. Yield: 77% (0.785 g, 2.90 mmol). Anal. Calcd for C₁₀H₁₇F₃N₂O₃: C, 44.44; H, 6.34; N, 10.37. Found: C, 44.45; H, 6.27; N, 10.45. ¹H NMR (400 MHz, CDCl₃): δ 1.86 (m, 2H, CH₂), 1.98 (m, 4H, CH₂), 2.48 (t, 2H, *J* = 8.0 Hz, CH₂), 3.06 (t, 2H, *J* = 8.0 Hz, CH₂), 3.40 (m, 4H, CH₂), 8.45 (br, 3H, NH₃)(see Fig. S3). ¹³C NMR (101 MHz, CDCl₃): δ 22.53, 24.59, 26.25, 32.51, 39.95, 46.27, 47.04, 116.99 (q, *J* = 293. Hz, CF₃), 162.13 (q, *J* = 35.20 Hz, COO), 171.29 (NCO)(see Fig. S4). HRMS (+ESI): calcd for [M – CF₃COO]⁺ ([C₈H₁₇N₂O]⁺) *m/z* 157.1341; found *m/z* 157.1335.

Synthesis of 4-amino-1-(pyrrolidin-1-yl)butan-1-one] (II): In a glovebox, a 20-mL scintillation vial was charged with **C** (0.737 g, 2.73 mmol), sodium hydride (NaH) (0.329 g, 13.7 mmol, 5.02 eq), and 12.5 mL of CH₂Cl₂. The mixture was vigorously stirred for 11 hours at room temperature, and then filtered. Evaporation of the filtrate under reduced pressure afforded compound **II** as a light yellow oil. Yield: 53% (0.225 g, 1.44 mmol). ¹H NMR (400 MHz, CDCl₃): δ 1.40 (br, 2H, NH₂), 1.81 (m, 4H, CH₂), 1.90 (m, 2H, CH₂), 2.29 (t, 2H, *J* = 8.0 Hz, CH₂), 2.72 (t, 2H, *J* = 8.0 Hz, CH₂), 3.40 (m, 4H, CH₂) (see Fig. S5). ¹³C NMR (101 MHz, CDCl₃): δ 24.68, 26.39, 29.00, 32.35, 42.19, 45.91, 46.88, 171.61 (NCO)(see Fig. S6). HRMS (+ESI): calcd for [MH]⁺ ([C₈H₁₇N₂O]⁺) *m/z* 157.1341; found *m/z* 157.1334.

Synthesis of N-methylpyrrolidine-N-oxide: N-methylpyrrolidine-N-oxide was prepared using a published procedure.⁶⁰ In air, a 20-mL scintillation vial was charged with N-methylpyrrolidine (0.865 g, 9.85 mmol) and a stir bar, and then cooled in an ice bath (0 °C). Aqueous 30% H₂O₂ (1.75 g, 15.4 mmol, 1.56 eq), also at 0 °C, was added dropwise into the vial over the course of 11 min, and the mixture was stirred at this temperature for 4 h, then at 23 °C, for an additional 20 h. The mixture was then treated with a catalytic amount of MnO₂ (0.004 g, 0.046 mmol, 0.00467 eq), in order to decompose the excess H₂O₂,⁶¹ then stirred under ambient conditions for 1h 20 min, after which time, evolution of heat and O₂ gas had ceased. After the initial removal of volatiles under reduced pressure, further drying was effected by dissolving the oily crude product in CH₂Cl₂. The resulting solution (in a 50-mL round-bottomed flask) was then treated with powdered CaH₂ (2.06 g, 48.9 mmol, 4.96 eq), first at 23 °C (in air) for 15 min, then under reflux at 40 °C for 1 h (under N₂ atmosphere from a syringe needle, attached to an N₂-filled balloon inserted into the septum covering the condenser attached to the reaction flask).⁶² After filtration to remove the solids, the liquid was evaporated under reduced pressure, and the residue was recrystallized from CH₂Cl₂-hexanes, N-methylpyrrolidine-N-oxide was obtained as an off-white solid. Yield: 61% (0.604 g, 5.97 mmol). ¹H NMR (600 MHz, CDCl₃): δ 1.99 (m, 2H, CH₂), 2.47 (m, 2H, CH₂), 3.31 (s, 3H, CH₃), 3.44 (m, 4H, CH₂). ¹³C NMR (101 MHz, CDCl₃): δ 22.46, 57.01, 70.25 (The ¹H NMR data reported here match those reported in the literature).⁶²

Synthesis and isolation of N-methylmorpholin-3-one: This compound was prepared using the experimental procedure outlined for the oxidation of cyclic tertiary amines into the corresponding lactams (see above). After treating 45.8 mg (0.453 mmol) of N-

methylmorpholine in 4.48 mL of dioxane with O₂ in the presence of 70 mg of 5.4 wt% Au/CeO₂ and 0.9 mL of H₂O (110 equiv. relative to the amine substrate) for 10 h at 100 °C, the reaction mixture was cooled to ambient temperature, then filtered over medium frit. Removal of volatiles from the filtrate under reduced pressure afforded the lactam product as brown oil. Yield: 65% (33.9 mg, 0.294 mmol). ¹H NMR (400 MHz, CDCl₃): δ 2.99 (s, 3H, CH₃), 3.37 (m, 2H, CH₂), 3.88 (m, 2H, CH₂), 4.16 (s, 2H, CH₂). ¹³C NMR (101 MHz, CDCl₃): δ 34.21, 48.63, 63.97, 68.38, 167.30 (CO). HRMS (+ESI): calcd for [MH]⁺ ([C₅H₁₀NO₂]⁺) *m/z* 116.0712; found *m/z* 116.0707.

References

- (1) Harreus, A.; Backes, R.; Eichler, J.-O.; Feuerhake, R.; Jakel, C.; Mahn, U.; Vogelsang, R. In *Ullmann's Encyclopedia of Industrial Chemistry* 2011, p 1-7.
- (2) Dahlhoff, G.; Niederer, J. P. M.; Hoelderich, W. F. *Catal. Rev.* **2001**, *43*, 381-441.
- (3) Estes, L.; Schweizer, M. In *Ullmann's Encyclopedia of Industrial Chemistry* 2011, p 1-17.
- (4) Ledoux, A.; Kuigwa, L. S.; Framery, E.; Andrioletti, B. *Green Chem.* **2015**, *17*, 3251-3254.
- (5) Tanielyan, S. K.; More, S. R.; Augustine, R. L.; Tosukhowong, T.; Ozmeral, C.; Roffi, K.; Shmorhun, M.; Glas, J. *Top. Catal.* **2014**, *57*, 1582-1587.
- (6) White, J. F.; Holladay, J. E.; Zacher, A. A.; Frye, J. G.; Werpy, T. A. *Top. Catal.* **2014**, *57*, 1325-1334.
- (7) Hashimoto, K. *Prog. Polym. Sci.* **2000**, *25*, 1411-1462.
- (8) Haaf, F.; Sanner, A.; Straub, F. *Polym. J.* **1985**, *17*, 143-152.
- (9) Ye, L. W.; Shu, C.; Gagosz, F. *Org. Biomol. Chem.* **2014**, *12*, 1833-1845.
- (10) Trost, B. M. *Angew. Chem. Int. Ed. Engl.* **1989**, *28*, 1173-1192.

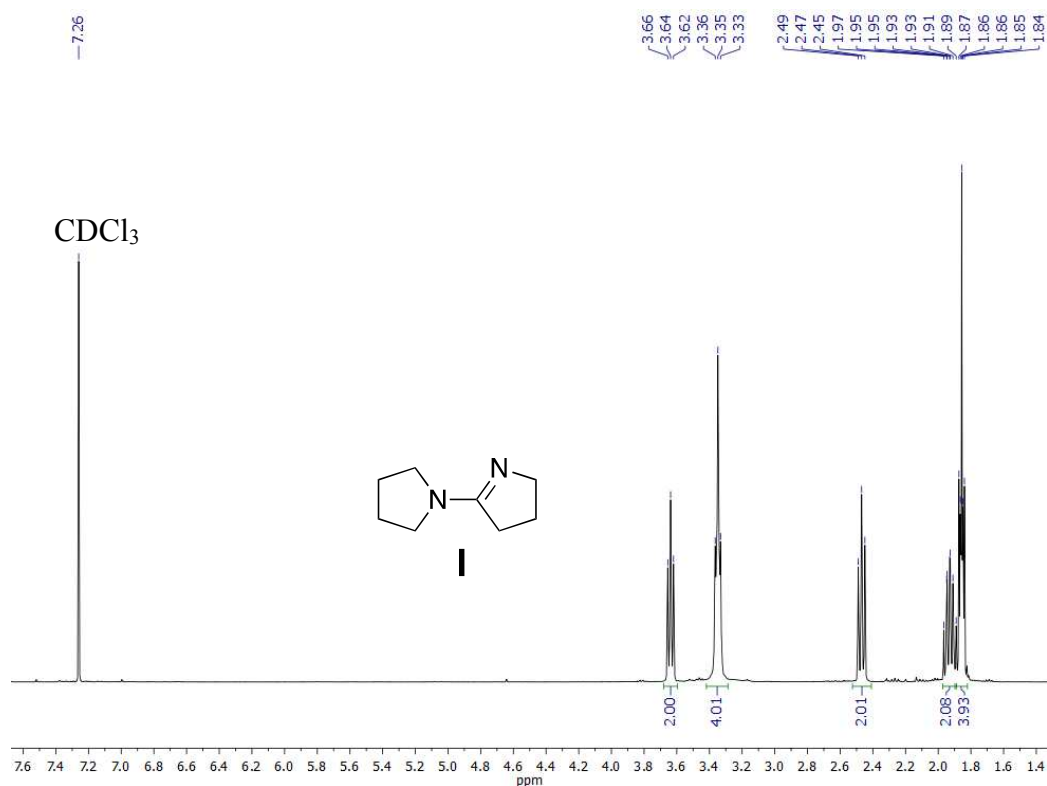
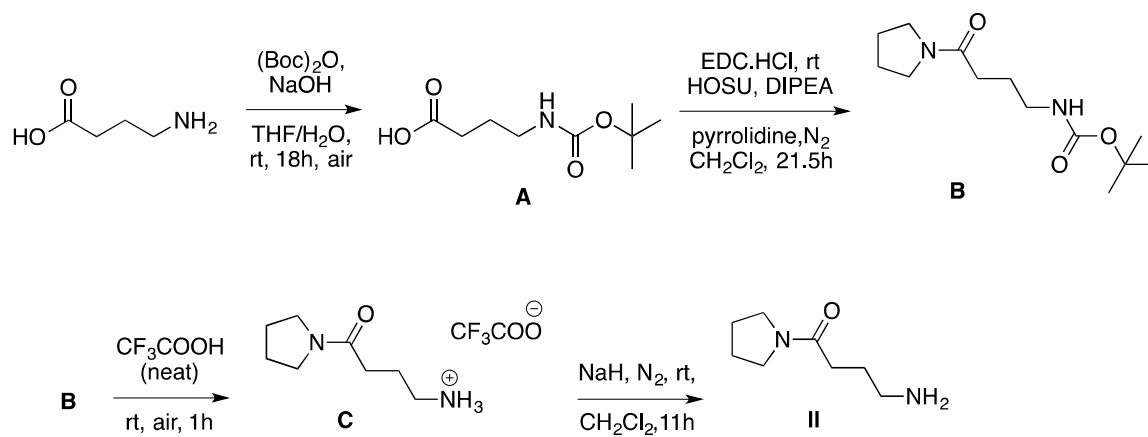
- (11) Janecki, T. In *Natural Lactones and Lactams: Synthesis, Occurrence and Biological Activity*; Wiley-VCH: Weinheim, Germany, 2013, p 101-106.
- (12) Udipi, K.; Dave, R. S.; Kruse, R. L.; Stebbins, L. R. *Polymer* **1997**, *38*, 927-938.
- (13) Usuki, A.; Kojima, Y.; Kawasumi, M.; Okada, A.; Fukushima, Y.; Kurauchi, T.; Kamigaito, O. *J. Mater. Res.* **1993**, *8*, 1179-1184.
- (14) Alger, M. *Polymer Science Dictionary* 2nd ed.; Chapman and Hall: London, U.K., 1997.
- (15) Ravve, A. *Principles of Polymer Chemistry*; 2nd ed.; Kluwer Academic/Plenum Publishers: New York, 2000.
- (16) Kammerer, C.; Prestat, G.; Madec, D.; Poli, G. *Acc. Chem. Res.* **2014**, *47*, 3439-3447.
- (17) Ritz, J.; Fuchs, H.; Kieczka, H.; Moran, W. C. In *Ullmann's Encyclopedia of Industrial Chemistry* 2011, p 2.
- (18) Sekiguchi, H. In *Ring-opening polymerization*; Ivin, K. J., Saegusa, T., Eds.; Elsevier: London, 1984; Vol. 2, p 809.
- (19) Sebenda, J. *J. Macromol. Sci. Chem.* **1972**, *A 6*, 1145-1199.
- (20) Puffr, R.; Stehlicek, J. In *Encyclopedia of polymeric materials*; Salamone, J. C., Ed.; CRC Press: Boca Raton, FL, 1996; Vol. 7.
- (21) Thomas, J. M.; Raja, R. *Proc. Natl. Acad. Sci. USA* **2005**, *102*, 13732-13736.
- (22) Barton, D. H. R.; Boivin, J.; Gaudin, D.; Jankowski, K. *Tetrahedron Lett.* **1989**, *30*, 1381-1382.
- (23) Murata, S.; Miura, M.; Nomura, M. *J. Chem. Soc., Perkin Trans. 1* **1987**, 1259-1262.
- (24) Khusnutdinova, J. R.; Ben-David, Y.; Milstein, D. *J. Am. Chem. Soc.* **2014**, *136*, 2998-3001.
- (25) So, M. H.; Liu, Y. G.; Ho, C. M.; Che, C. M. *Chem. Asian J.* **2009**, *4*, 1551-1561.
- (26) Preedasuriyachai, P.; Chavasiri, W.; Sakurai, H. *Synlett* **2011**, 1121-1124.
- (27) Miyamura, H.; Morita, M.; Inasaki, T.; Kobayashi, S. *Bull. Chem. Soc. Jpn.* **2011**, *84*, 588-599.
- (28) Abad, A.; Concepcion, P.; Corma, A.; Garcia, H. *Angew. Chem. Int. Ed.* **2005**, *44*, 4066-4069.

- (29) Griirane, A.; Corma, A.; Garcia, H. *Science* **2008**, 322, 1661-1664.
- (30) Perez, Y.; Aprile, C.; Corma, A.; Garcia, H. *Catal. Lett.* **2010**, 134, 204-209.
- (31) Aschwanden, L.; Mallat, T.; Krumeich, F.; Baiker, A. *J. Mol. Catal. A: Chem.* **2009**, 309, 57-62.
- (32) Aschwanden, L.; Mallat, T.; Maciejewski, M.; Krumeich, F.; Baiker, A. *Chemcatchem* **2010**, 2, 666-673.
- (33) Sudarsanam, P.; Selvakannan, P. R.; Soni, S. K.; Bhargava, S. K.; Reddy, B. M. *RSC Adv.* **2014**, 4, 43460-43469.
- (34) Zhu, B. L.; Angelici, R. J. *Chem. Commun.* **2007**, 2157-2159.
- (35) Zhu, B. L.; Lazar, M.; Trewyn, B. G.; Angelici, R. J. *J. Catal.* **2008**, 260, 1-6.
- (36) Klobukowski, E. R.; Mueller, M. L.; Angelici, R. J.; Woo, L. K. *ACS Catal.* **2011**, 1, 703-708.
- (37) Romeo, M.; Bak, K.; Elfallah, J.; Lenormand, F.; Hilaire, L. *Surf. Interface Anal.* **1993**, 20, 508-512.
- (38) Nelson, N. C.; Manzano, J. S.; Sadow, A. D.; Overbury, S. H.; Slowing, I. I. *ACS Catal.* **2015**, 5, 2051-2061.
- (39) Purushothaman, R. K. P.; van Haveren, J.; van Es, D. S.; Melian-Cabrera, I.; Meeldijk, J. D.; Heeres, H. J. *Appl. Catal., B* **2014**, 147, 92-100.
- (40) Shen, Y. H.; Zhang, S. H.; Li, H. J.; Ren, Y.; Liu, H. C. *Chem. Eur. J.* **2010**, 16, 7368-7371.
- (41) Naumkin, A. V.; Kraut-Vass, A.; Gaarenstroom, S. W.; Powell, C. J. *NIST X-ray Photoelectron Spectroscopy Database*.
- (42) Casaletto, M. P.; Longo, A.; Martorana, A.; Prestianni, A.; Venezia, A. M. *Surf. Interface Anal.* **2006**, 38, 215-218.
- (43) Lazar, M.; Zhu, B. L.; Angelici, R. J. *J. Phys. Chem. C* **2007**, 111, 4074-4076.
- (44) Zope, B. N.; Hibbitts, D. D.; Neurock, M.; Davis, R. J. *Science* **2010**, 330, 74-78.
- (45) Biella, S.; Castiglioni, G. L.; Fumagalli, C.; Prati, L.; Rossi, M. *Catal. Today* **2002**, 72, 43-49.
- (46) Murahashi, S. I.; Naota, T.; Ito, K.; Maeda, Y.; Taki, H. *J. Org. Chem.* **1987**, 52, 4319-4327.

- (47) Endo, Y.; Backvall, J. E. *Chem. Eur. J.* **2011**, *17*, 12596-12601.
- (48) Della Pina, C.; Falletta, E.; Rossi, M. *Top. Catal.* **2007**, *44*, 325-329.
- (49) Klobukowski, E. R.; Angelici, R. J.; Woo, L. K. *Catal. Lett.* **2012**, *142*, 161-167.
- (50) Rao, G. A.; Periasamy, M. *Synlett* **2015**, *26*, 2231-2236.
- (51) Li, Z. P.; Bohle, D. S.; Li, C. J. *Proc. Natl. Acad. Sci. USA* **2006**, *103*, 8928-8933.
- (52) Fuentes, L.; Osorio, U.; Quintero, L.; Hopfl, H.; Vazquez-Cabrera, N.; Sartillo-Piscil, F. *J. Org. Chem.* **2012**, *77*, 5515-5524.
- (53) Boess, E.; Schmitz, C.; Klusmann, M. *J. Am. Chem. Soc.* **2012**, *134*, 5317-5325.
- (54) Basle, O.; Li, C. J. *Green Chem.* **2007**, *9*, 1047-1050.
- (55) Ma, S. T.; Jiao, B.; Ju, Y. J.; Zheng, M. J.; Ma, R. X.; Liu, L.; Zhang, L.; Shen, X. C.; Ma, C. C.; Meng, Y.; Wang, H.; Qi, Y. K.; Ma, X. D.; Cui, W. P., *Eur. J. Med. Chem.* **2011**, *46*, 556-566.
- (56) Xiao, J. C.; Xu, J. L.; Cui, S.; Liu, H. B.; Wang, S.; Li, Y. L., *Org. Lett.* **2008**, *10*, 645-648.
- (57) Montalbetti, C. A. G. N.; Falque, V., *Tetrahedron* **2005**, *61*, 10827-10852.
- (58) Valeur, E.; Bradley, M., *Chem. Soc. Rev.* **2009**, *38*, 606-631.
- (59) Hartwig, S.; Nguyen, M. M.; Hecht, S., *Polym. Chem.* **2010**, *1*, 69-71.
- (60) Searles, S. 1-methylpyrrolidine-1-oxide. U.S. Patent 3,239,535, March 8, 1966.
- (61) Coperet, C.; Adolfsson, H.; Khuong, T. A. V.; Yudin, A. K.; Sharpless, K. B., *J. Org. Chem.* **1998**, *63*, 1740-1741.
- (62) Volz, H.; Gartner, H., *Eur. J. Org. Chem.* **2007**, 2791-2801.

Supporting Information

Synthesis of 4-amino-1-(pyrrolidin-1-yl)butan-1-one] (II)

Fig. S1. ^1H NMR (400 MHz) spectrum of amidine-5 (**I**) in CDCl_3

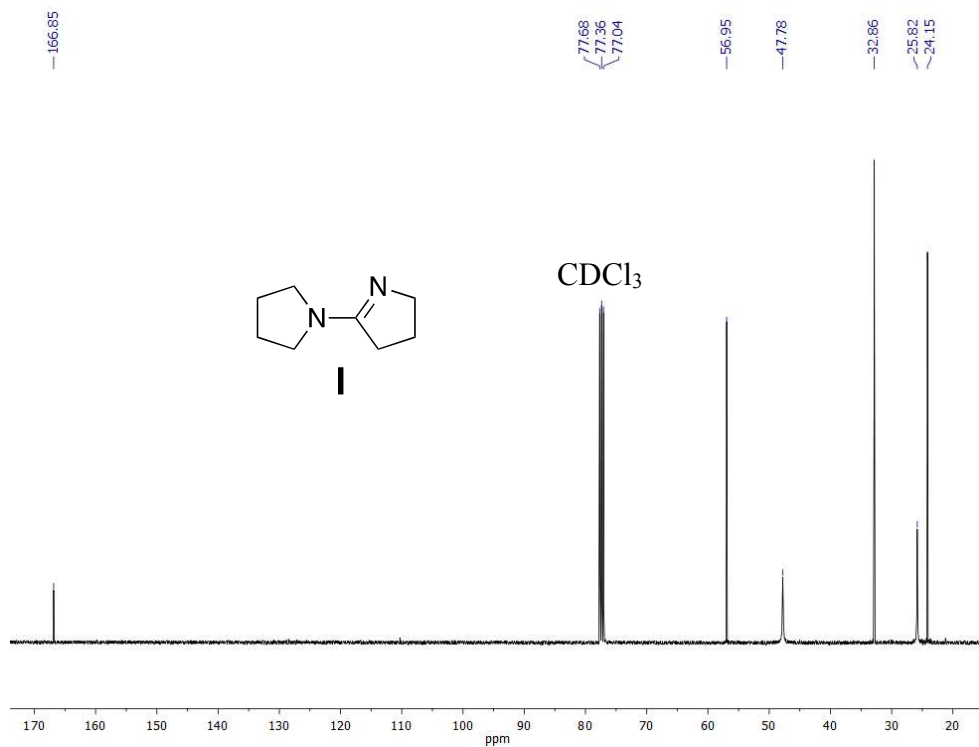


Fig. S2. ^{13}C NMR (101 MHz) spectrum of amidine-5 (I) in CDCl_3

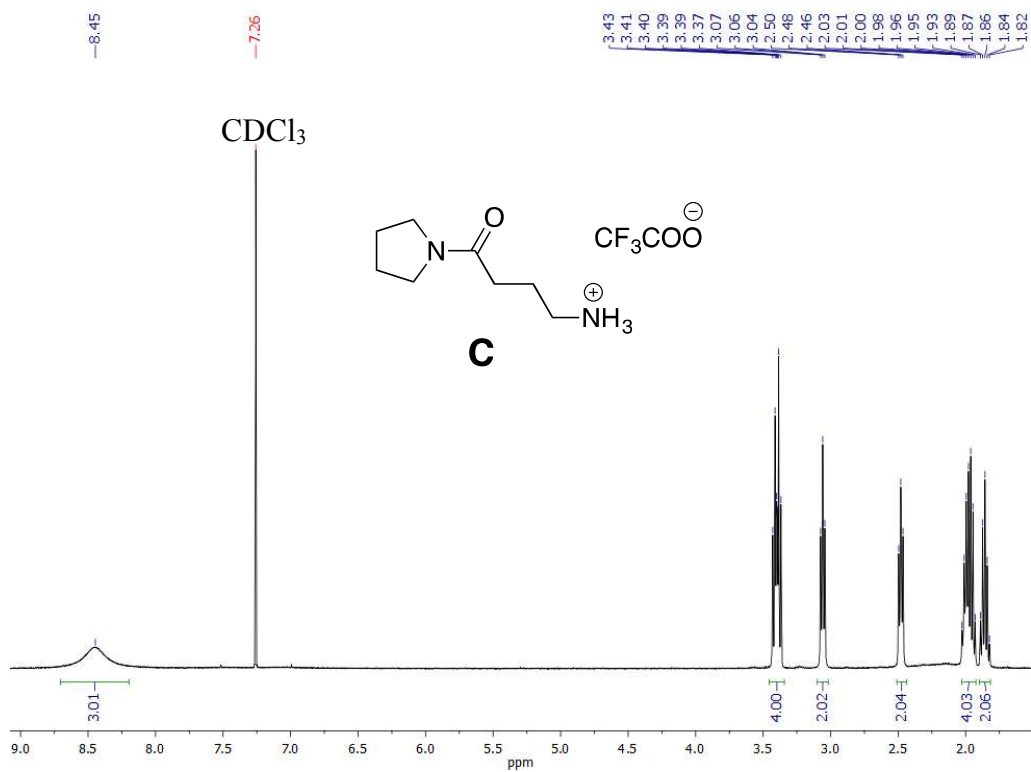


Fig. S3. ^1H NMR (400 MHz) spectrum of 4-oxo-4-(pyrrolidin-1-yl)butan-1-aminium 2,2,2-trifluoroacetate (C) in CDCl_3

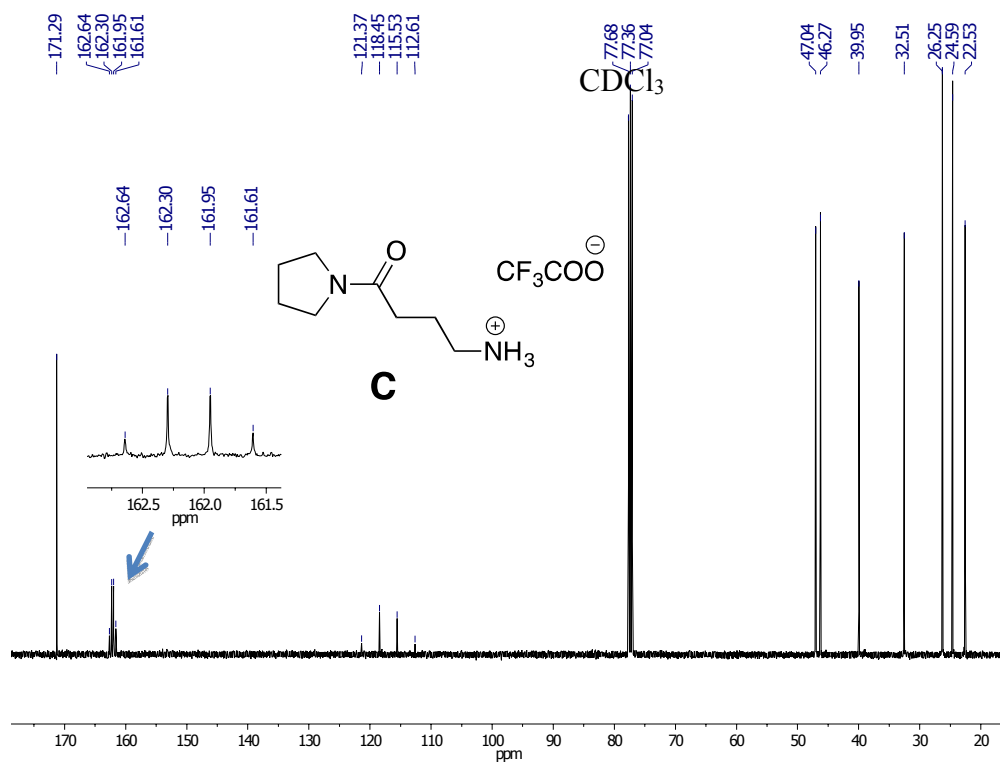


Fig. S4. ¹³C NMR (101 MHz) spectrum of 4-oxo-4-(pyrrolidin-1-yl)butan-1-aminium 2,2,2-trifluoroacetate (**C**) in CDCl₃

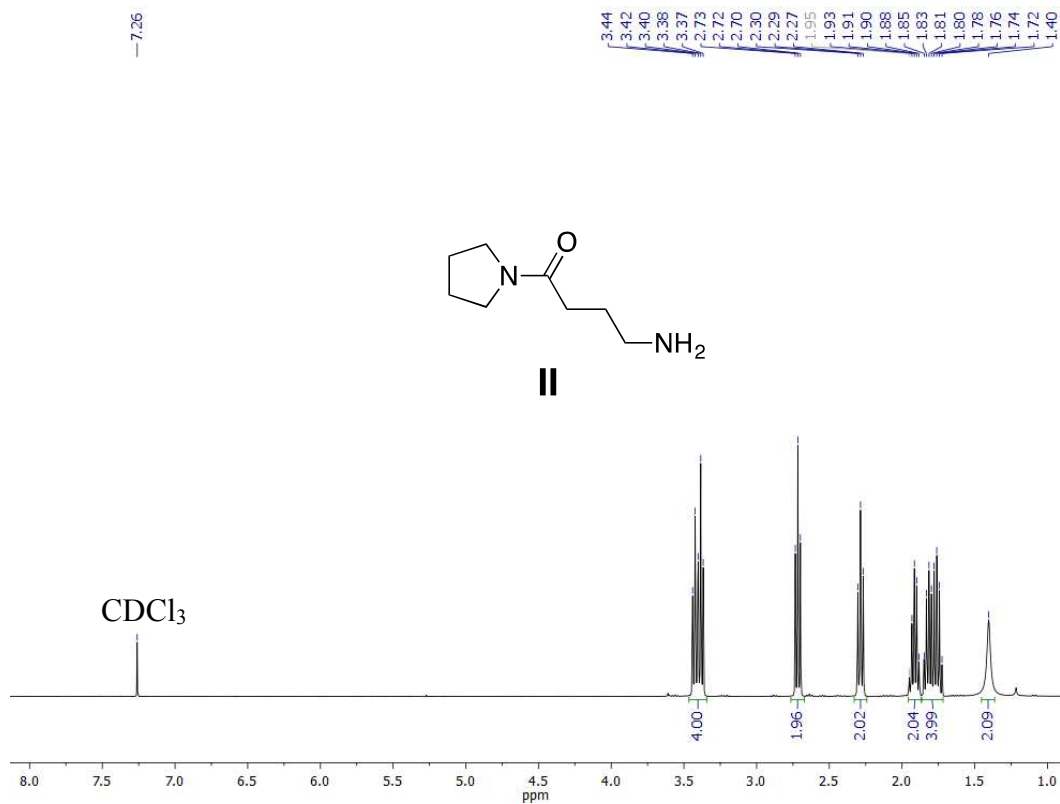


Fig. S5. ¹H NMR (400 MHz) spectrum of 4-amino-1-(pyrrolidin-1-yl)butan-1-one (**II**) in CDCl₃

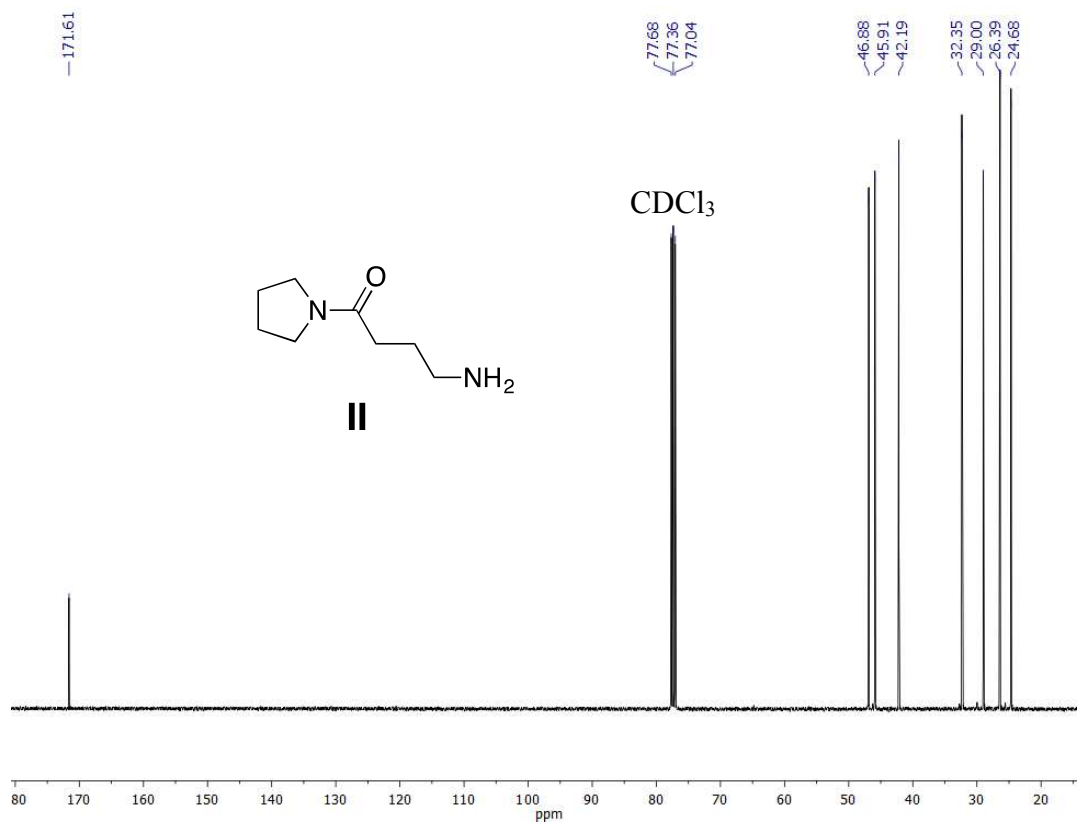


Fig. S6. ^{13}C NMR (101 MHz) spectrum of 4-amino-1-(pyrrolidin-1-yl)butan-1-one (II) in CDCl_3

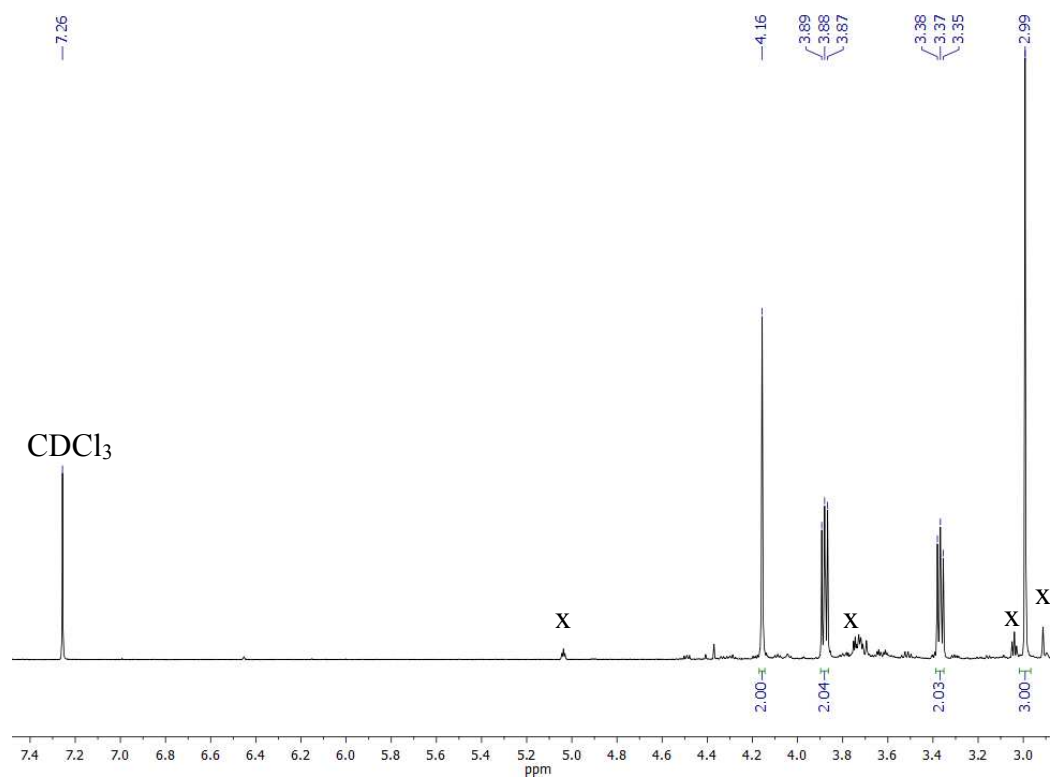


Fig. S7. ^1H NMR (400 MHz) spectrum of N-methylmorpholin-3-one in CDCl_3

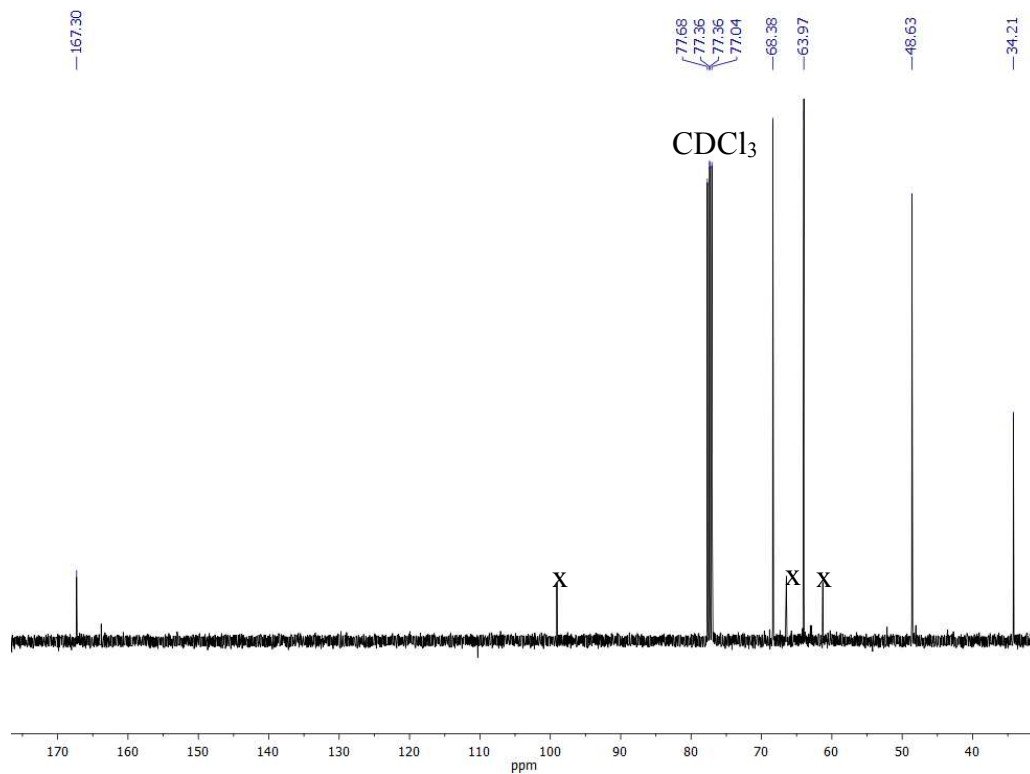


Fig. S8. ^{13}C NMR (101 MHz) spectrum of N-methylmorpholin-3-one in CDCl_3

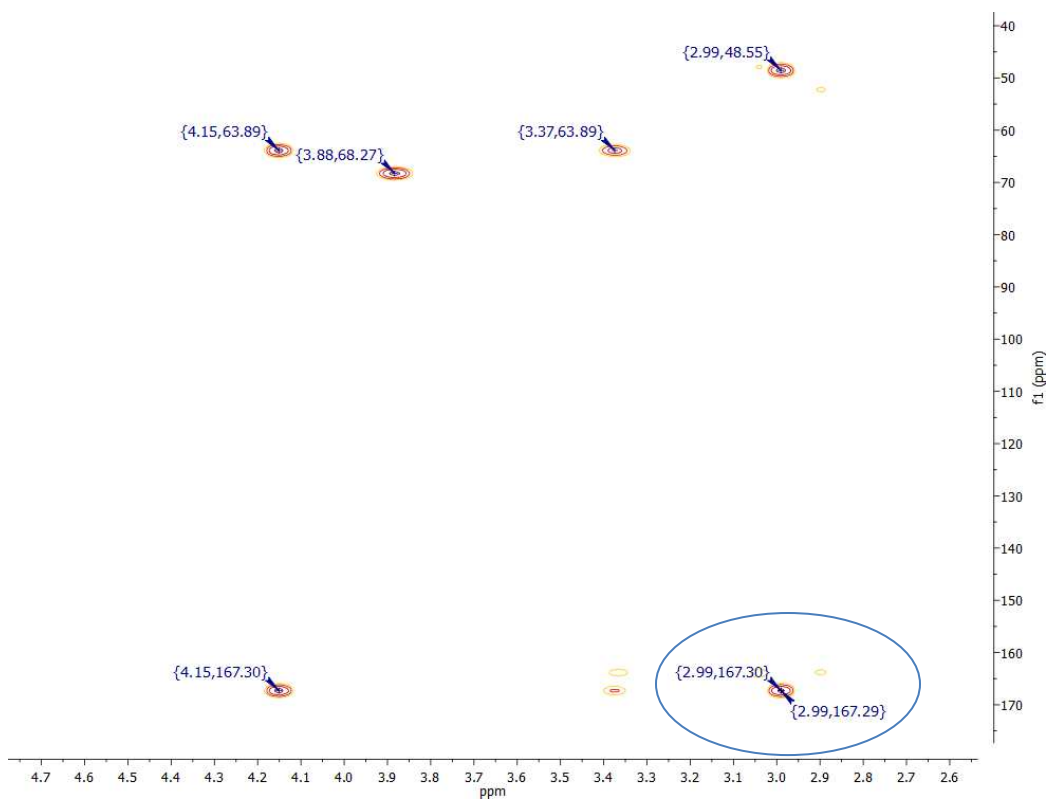


Fig. S9. HMBC spectrum (400 MHz) of N-methylmorpholin-3-one in CDCl_3 . The circled cross peak shows a 3-bond heteronuclear coupling between the N-methyl protons (2.99 ppm) and the CO carbon (167.30 ppm).

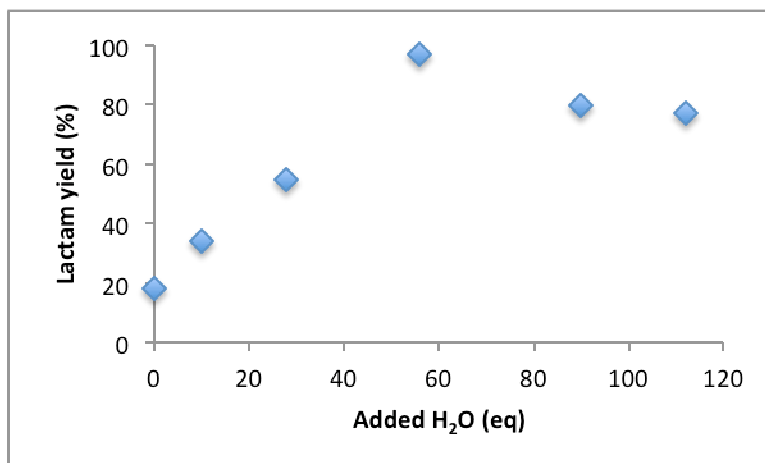


Fig. S10. Plot of 2-pyrrolidone yields versus different equivalents of added H₂O. Conditions: 0.444 mmol (100 mM; 1 eq) pyrrolidine, 70 mg of 5.4 wt% Au/CeO₂, 111 mg of Aerosil (4.2 eq), 4.44 mL of diglyme, 160 °C. Added H₂O are 0, 10, 28, 56, 90, and 112 eq. Yields shown were determined at 6.5 h of reaction for all eq of added H₂O

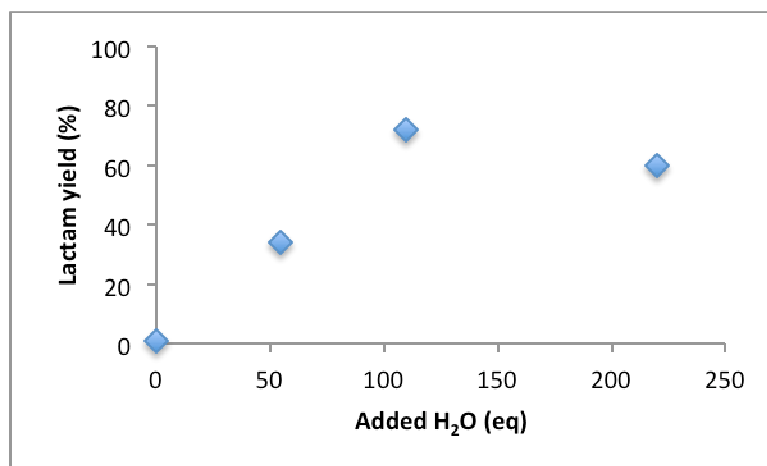


Fig. S11. Plot of N-methylmorpholin-3-one yields versus different equivalents of added H₂O. Conditions: 0.452 mmol (101 mM) N-methylmorpholine, 70 mg of 5.4 wt% Au/CeO₂, 4.48 mL of 1,4-dioxane, 100 °C. Added H₂O are 0, 55, 110, 220 eq. Yields shown were determined: i.) At 24 h of reaction for 0 eq of added H₂O ii.) At 24 h of reaction for 55 eq of added H₂O iii.) At 10 h of reaction for 110 eq of added H₂O iv.) At 13.5 h of reaction for 220 eq of added H₂O.

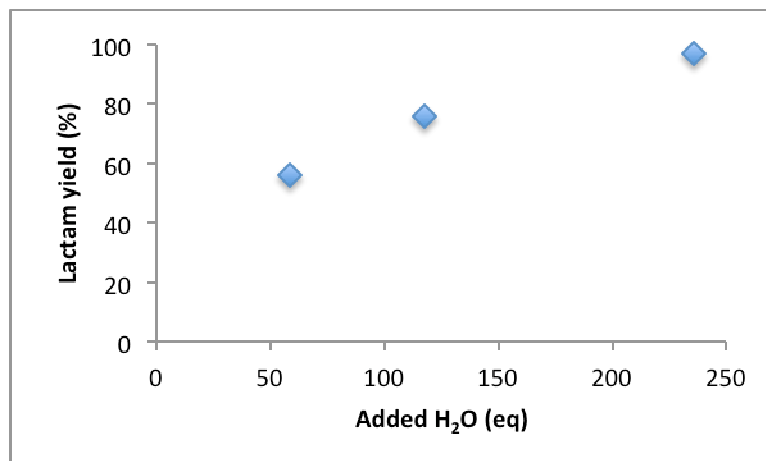


Fig. S12. Plot of N-methyl-2-piperidone yields versus different equivalents of added H₂O. Conditions: 0.423 mmol (95 mM) N-methylpiperidine, 70 mg of 5.4 wt% Au/CeO₂, 4.45 mL of 1,4-dioxane, 100 °C. Added H₂O are 59, 118, 236 eq. Yields shown were determined: i.) At 3 h of reaction for 59 eq of added H₂O (100% substrate conversion) ii.) At 3 h of reaction for 118 eq of added H₂O (100% substrate conversion) iii.) At 4 h of reaction for 236 eq of added H₂O (100% substrate conversion).

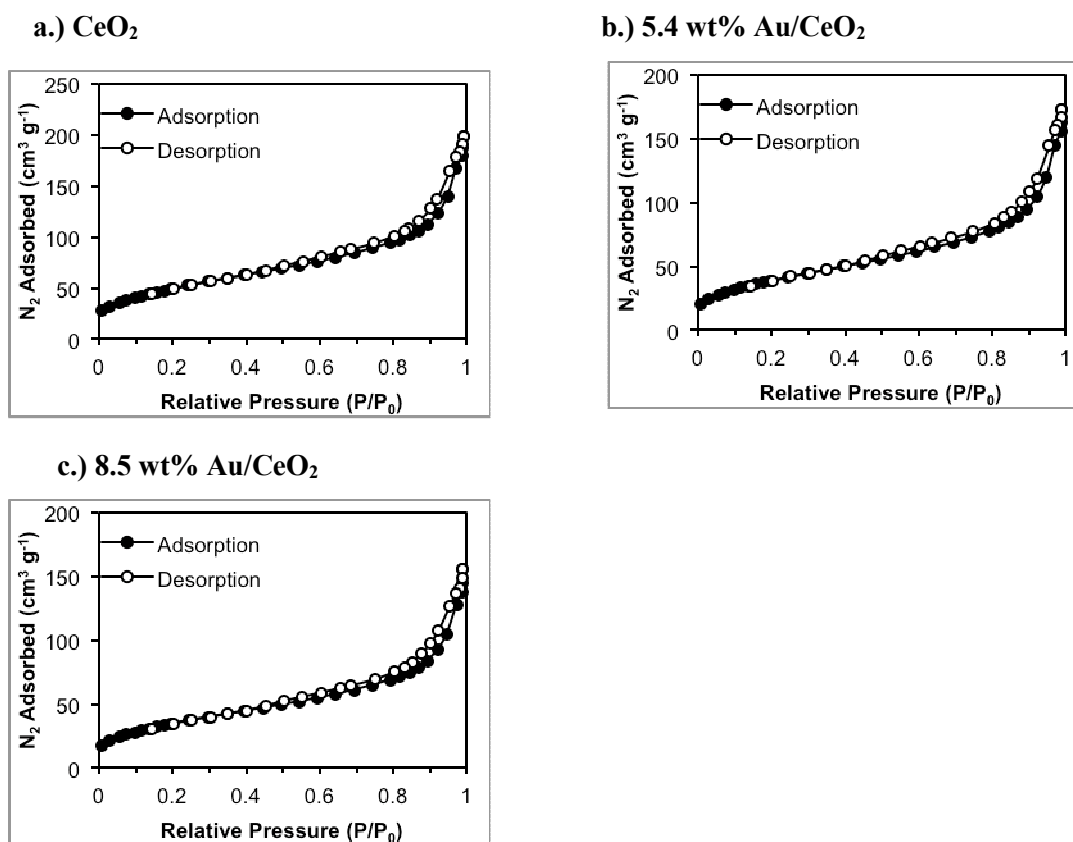
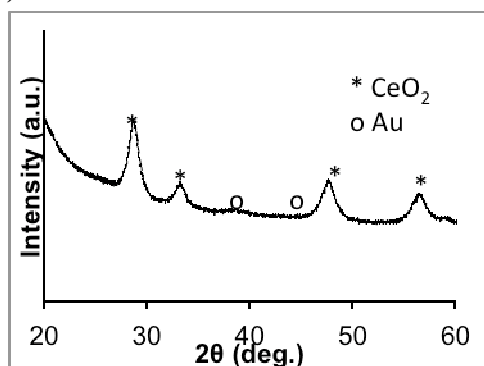
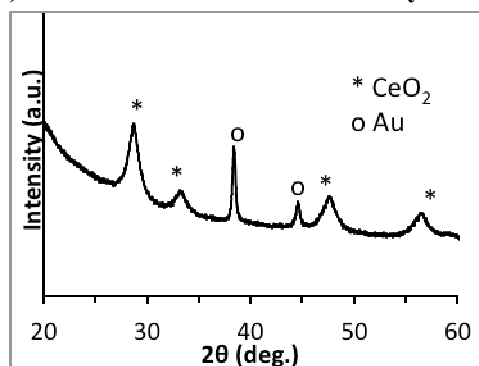
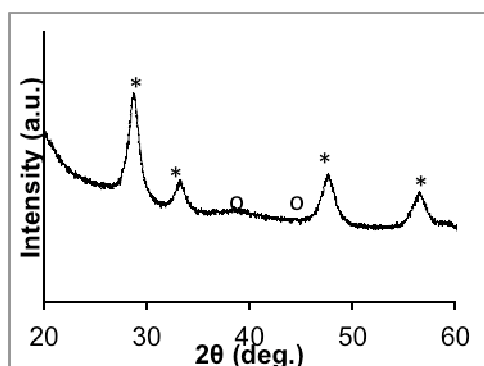
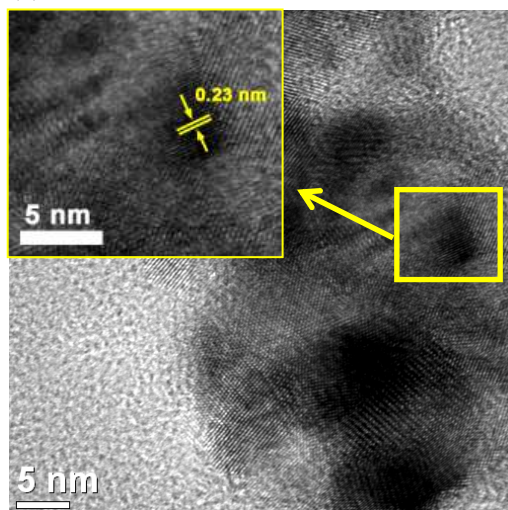


Fig. S13. Nitrogen physisorption isotherms for a.) CeO₂, b.) 5.4 wt% Au/CeO₂, c.) 8.5 wt% Au/CeO₂

a.) Fresh 5.4 wt% Au/CeO₂b.) 5.4 wt% Au/CeO₂ after 3 catalytic runsc.) Fresh 8.5 wt% Au/CeO₂Fig. S14. Wide-angle PXRD patterns of Au/CeO₂ with reference to CeO₂ peaks (*) and Au peaks (o)

(a)



(b)

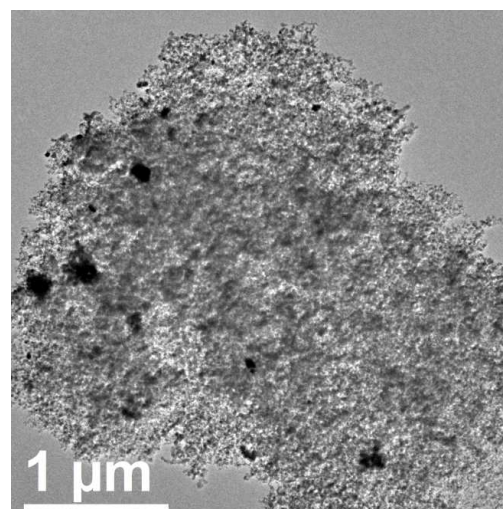


Figure S15. a.) High-resolution transmission electron microscopy (HR-TEM) image of the fresh (unused) 5.4 wt% Au/CeO₂ catalyst. b.) HR-TEM image of the 5.4 wt% Au/CeO₂ catalyst after three catalytic runs. The dark spots indicate agglomerated Au.

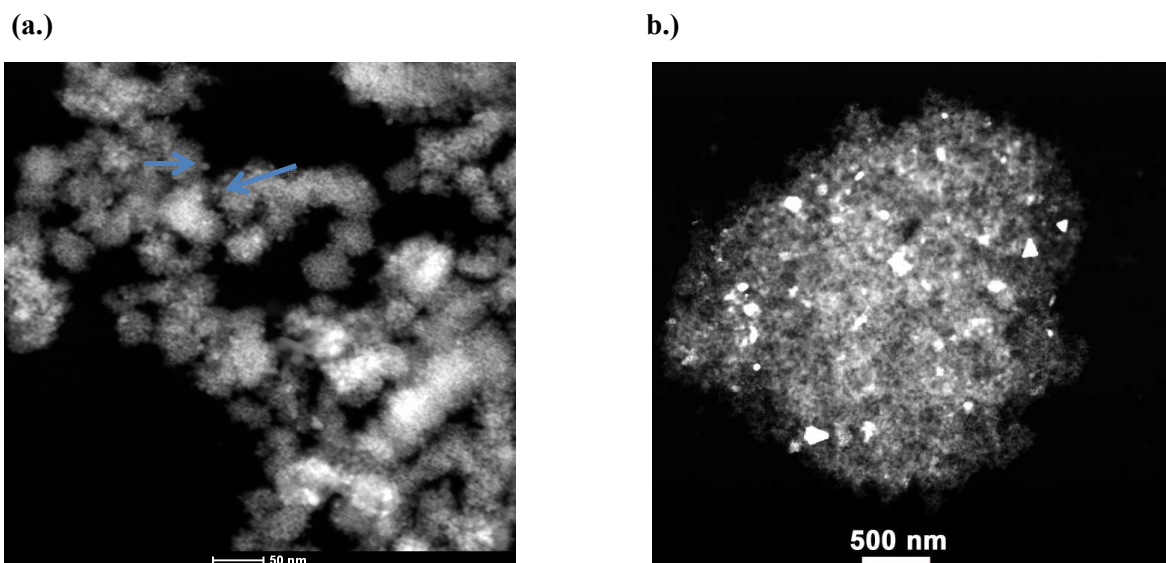


Figure S16. (a) Scanning transmission electron microscopy (STEM) image of the fresh (unused) 5.4 wt% Au/CeO₂ catalyst. Arrows point to the Au nanoparticles. (b) STEM image of the 5.4 wt% Au/CeO₂ catalyst after three catalytic runs. The bright spots indicate the presence of agglomerated Au.

a.)

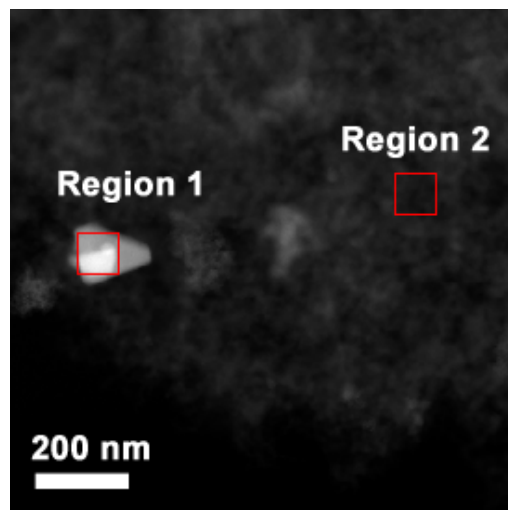


Fig. S17. a.) STEM image of 5.4 wt% Au/CeO₂ after three catalytic runs, showing region 1 with agglomerated Au, and region 2 having relatively small amount of Au.

b.)

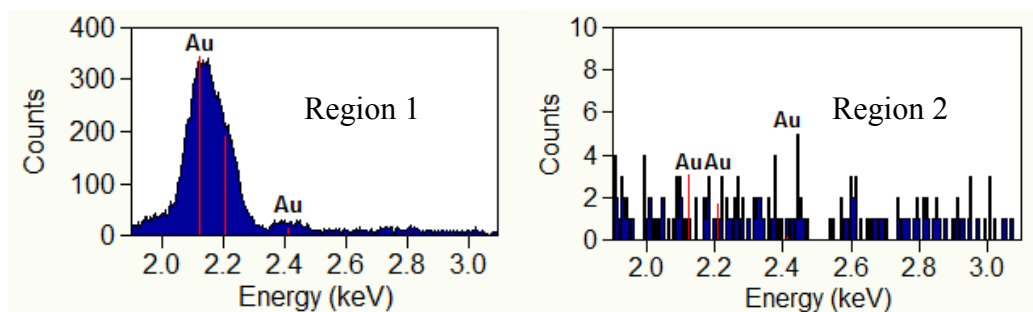
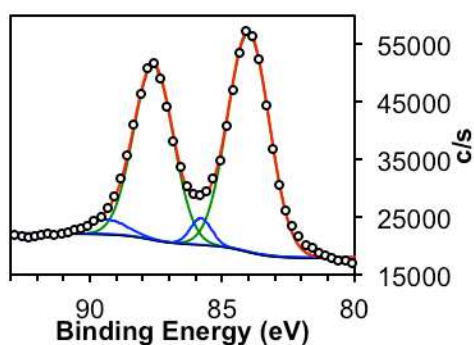


Fig. S17. b.) EDX maps of regions 1 and 2.

a.)



b.)

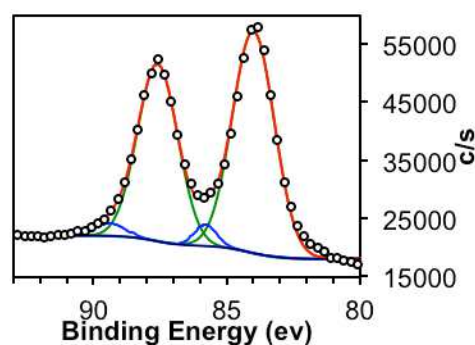


Fig. S18. XPS spectra of the Au 4f core level of 5.4 wt% Au/CeO₂ a.) freshly prepared, and b.) after three catalytic runs. Circles are experimental datapoints, red line is the cumulative fit, green lines are deconvoluted spin-orbit 4f_{7/2} and 4f_{5/2} components of Au⁰ (84.0 and 87.6 eV respectively), and blue lines are deconvoluted spin-orbit 4f_{7/2} and 4f_{5/2} components of Au⁺¹ (85.8 and 89.4 eV respectively)

Table S1. Physical properties of CeO₂ and Au/CeO₂ catalysts

Entry	Sample	Au loading (wt. %) ^a	Surface Area (m ² g ⁻¹)	Pore Volume (cm ³ g ⁻¹)
1	CeO ₂	-	182	0.26
2	Au/CeO ₂	5.4	146	0.22
3	Au/CeO ₂	8.5	129	0.20

^aDetermined by ICP-OES analysis.

CHAPTER 5. PELIMINARY RESULTS OF THE NANOGOLD-CATALYZED SYNTHESIS OF N,N'-DISUBSTITUTED UREAS FROM THE REACTIONS OF AMINES WITH CARBON MONOXIDE AND OXYGEN

Abstract

N,N'-substituted ureas are known for the biological and pharmaceutical applications. We have found that ceria-supported nanogold (Au/CeO₂) catalyzes the synthesis of these urea derivatives from the room temperature reactions of amines with CO and O₂. N,N'-di-n-butylurea was isolated in 75% yield, while the isolated yields of N,N'-dicyclohexylurea and N,N'-diisopropylurea were 40% yield and 37% yield, respectively.

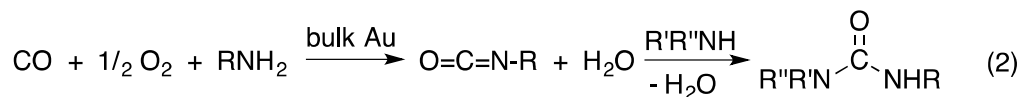
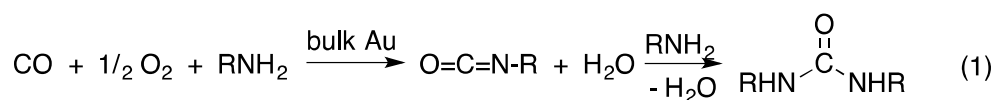
Introduction

Substituted ureas are popularly known for their industrial and pharmaceutical applications.^{1,2} They have found specific use as antiviral drugs in the treatment of HIV/AIDS,³⁻⁵ anticonvulsants,⁶ antidepressants and antiemetics.^{7,8} Nitrosoureas, which are made from the nitrosation of substituted ureas,⁹ are used in cancer treatment,¹⁰ while N,N'-dicyclohexylurea has also been shown to lower blood pressure.¹¹ Over the years, the large scale manufacture of substituted ureas has involved the use of phosgene (COCl₂),¹ a toxic gas.^{12,13} Consequently, a great deal of research has gone into finding alternative ways of synthesizing them.

Gabriele and co-workers⁴ have reported the catalytic activity of palladium(II) iodide (PdI₂) during the conversion of aliphatic and aromatic amines into substituted ureas in the presence of CO, air, and CO₂. While the product yields were generally very good, 100

equivalents of KI (relative to the amine substrate) were added to the reaction mixtures, and reaction temperatures were typically 100 °C, with gas pressures up to 60 atmospheres. That report was later followed by another one, which utilized potassium tetraiodopalladate (K_2PdI_4) as catalyst, and gas mixtures comprising 10 atmospheres and 15 atmospheres of CO and air, respectively.¹⁴ Yields of substituted ureas obtained from aliphatic amines ranged from 42 – 99%, while the product yields from the reactions of aromatic amines were between 32 and 96%. Reaction temperatures were up to 110 °C. A selenium heterocyclic compound has also been reported to catalyze the conversion of aromatic amines into substituted ureas in the presence of ionic liquids, air, and CO, at 60 – 90 °C.¹⁵ Furthermore, N,N'-disubstituted ureas have been synthesized from palladium-catalyzed reductive alkylation reactions in the presence of hydrogen gas as a reducing agent. In that work, disubstituted ureas were obtained from the reactions of monosubstituted ureas, as well as silylated ureas. In each case, the alkylating agents were aldehydes.¹⁶ The synthesis of monosubstituted and N,N'-disubstituted ureas have been reported from the reactions of benzotriazole-1-carboxamide with primary and secondary amines,¹⁷ while a series of mono-, di-, and trisubstituted ureas have also been synthesized from the zirconium(IV)-catalyzed reactions of amines with carbonates and carbamates.¹⁸ Furthermore, Li and co-workers have reported the conversion of primary benzyl alcohols into N,N'-disubstituted ureas in the presence of hypervalent iodine compounds and sodium azide. In most cases, benzamides were obtained as co-products in appreciable yields.¹⁹ Disubstituted ureas have been synthesized from iodosylbenzene-mediated reactions between amides and amines,²⁰ while urea derivatives have also been synthesized from microwave-²¹ and electrochemistry-assisted²² reactions.

Angelici and co-workers have demonstrated the catalytic activity of bulk gold powder in a number of amine oxidation reactions, which have resulted in the formation of several organic moieties such as carbodiimides,²³ trisubstituted ureas,^{24,25} imines,²⁶⁻²⁸ enamines,²⁹ and lactams.³⁰ Furthermore, bulk gold powder has been shown to catalyze the oxidative amination of carbon monoxide at 45 °C to give disubstituted (eq. 1) and trisubstituted ureas (eq. 2).³¹ Isocyanate intermediacy was inferred from the observation that the reaction of di-*n*-propylamine [(*n*Pr)₂NH; a secondary amine] did not result in urea formation. However, react-



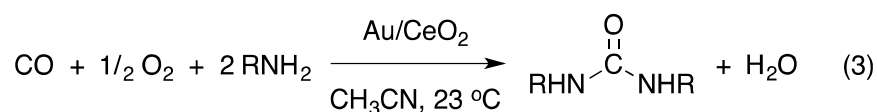
-ion of an equimolar mixture of aniline (PhNH₂) and di-*n*-propylamine with CO and O₂ resulted in the formation of the trisubstituted urea (*n*Pr)₂NH(CO)NHPh. Unfortunately, stoichiometric amounts of bulk gold catalyst (1.00 g per 0.5 mmol of amine substrate) were utilized for the transformations in that study.

Supported nanogold-based catalysts have been shown to be very active catalysts for oxidation reactions of amine substrates.³²⁻⁴⁰ Notably, our group has found that ceria-supported nanogold is very active for the oxidation of secondary and tertiary amines into the corresponding lactams.⁴¹ We report herein, that ceria-supported nanogold also catalyzes the oxidative (1 atmosphere of O₂) amination of CO into N,N'-substituted ureas at 23 °C.

Results and Discussion

Au/CeO₂-catalyzed aerobic oxidation of primary amines into N,N'-disubstituted ureas in the presence of CO: Ceria-supported gold nanoparticles (Au/CeO₂), efficiently

catalyze the oxidative carbonylation of primary amines into N,N'-disubstituted ureas at ambient temperature (eq. 3).



When 0.220 mmol of n-butylamine (ⁿBuNH₂) was stirred at room temperature with 40 mg of 5.4 wt% Au/CeO₂ for 48 hours, N,N'-di-n-butylurea was isolated in 75% yield, in addition to

Table 1. Catalytic conversion of n-butylamine to N,N'-dibutylurea in acetonitrile solvent, in the presence of CO and O₂ (CO + O₂ ~ 1 atm), at 23 °C^a

Entry	Substrate	Time	Urea (%) ^d	Isocyanate (%) ^d
1	ⁿ BuNH ₂	48 h	75 ^a	6 ^a
2	ⁿ BuNH ₂	48 h	53 ^b	5 ^b
3	ⁿ BuNH ₂	48 h	57 ^c	4 ^c

^a0.220 mmol (100. mM) substrate, 40 mg of 5.4 wt% Au/CeO₂ (5 mol% Au), 2.20 mL acetonitrile. ^b80 mg of 5.4 wt% Au/CeO₂ (10 mol% Au) used. ^c40 mg of 8.5 wt% Au/CeO₂ (8.6 mol% Au) used. ^dIsolated yield.

butyl isocyanate as the only side product (Table 1, entry 1). These were the optimized reaction conditions for n-butylamine substrate, because the use of increased loadings of the gold catalyst led to reduced product yields (Table 1, entries 2 and 3). Under the optimized reaction conditions for the synthesis of N,N'-di-n-butylurea, N,N'-diisopropylurea was isolated in 16% yield from the reaction of isopropylamine (Table 2, entry 1). There was no improvement in the yield, when the reaction was repeated at 45 °C, while other parameters were maintained (Table 2, entry 2). However, doubling the length of reaction time of isopropylamine, led to a doubling of the yield of N,N'-diisopropylurea to 37% (Table 2, entry 3). When the reaction of cyclohexylamine was carried out under the optimized conditions for the reaction of n-butylamine, only 4% yield of N,N'-dicyclohexylurea was obtained (Table 2, entry 4), while a doubling of the length of reaction time led to a three fold

Table 2. Catalytic conversion of primary amines and aniline to N,N'-disubstituted ureas in acetonitrile solvent, in the presence of CO and O₂ (CO + O₂ ~ 1 atm), at 23 °C^a

Entry	Substrate	Time	Urea (%) ^e	Isocyanate (%) ^e
1	<i>i</i> PrNH ₂	48 h	16 ^a	N.D. ^a
2	<i>i</i> PrNH ₂	48 h	11 ^b	N.D. ^b
3	<i>i</i> PrNH ₂	96 h	37 ^a	N.D. ^a
4	Cyclohexylamine	48 h	4 ^a	N.D. ^a
5	Cyclohexylamine	96 h	13 ^a	N.D. ^a
6	Cyclohexylamine	96 h	40 ^c	N.D. ^c
7	Cyclohexylamine	96 h	39 ^d	N.D. ^d
8	BnNH ₂	48 h	Trace ^a	Trace ^a
9	BnNH ₂	48 h	5 ^b	1 ^b
10	PhNH ₂	48 h	Trace ^a	Trace ^a
11	PhNH ₂	48 h	N.D. ^b	N.D. ^b
12	PhNH ₂	96 h	Trace ^a	Trace ^a

^a0.220 mmol (100. mM) substrate, 40 mg of 5.4 wt% Au/CeO₂ (5 mol% Au), 2.20 mL acetonitrile. ^bReaction carried out at 45 °C. ^c10 mol% Et₃N added. ^d50 mol% Et₃N added. ^eIsolated yield.

increase in the product yield to 13% (Table 2, entry 5). However, under the optimized conditions for the reaction of n-butylamine (i.e. 0.220 mmol of substrate, 5 mol% of Au catalyst, at 23 °C for 48 h), but with the use of 10 mol% of triethylamine (Et₃N) as an additive,²¹ a ten-fold increase in product yield (40%) was achieved (Table 2, entry 6). Increasing the amount of additive to 50 mol% did not result in a change in product yield (Table 2, entry 7). When the optimized conditions for the n-butylamine reaction were applied to the reaction of benzylamine (BnNH₂), trace amounts of N,N'-dibenzylurea and benzyl isocyanate were obtained (Table 2, entry 8). A repeat of the reaction, but at a different temperature of 45 °C, led to a 5% urea yield and 1% isocyanate yield (Table 2, entry 9). However, a trace amount of N,N'-diphenylurea was obtained under the optimized conditions

for the synthesis of N,N'-di-n-butylurea (Table 2, entry 10). No product was detected and only trace amounts of product were obtained, when either the reaction temperature was increased to 45 °C (Table 2, entry 11), or when the length of reaction time was doubled (Table 2, entry 12).

Conclusions

N,N'-di-n-butylurea was isolated in 75% yield from the Au/CeO₂-catalyzed oxidative carbonylation of n-butylamine at room temperature. N,N'-diisopropylurea was also obtained in 37% yield from the reaction of isopropylamine, while N,N'-dicyclohexylurea was obtained in 40% yield from cyclohexylamine, albeit in the presence of triethylamine as an additive. However, the reaction of benzylamine gave a relatively low urea yield, while trace amounts of N,N'-diphenylurea were obtained from the reaction of aniline. Isocyanate formation from some of the reactions studied suggests that the reactions proceed via an initial formation of one molecule of isocyanate from each molecule of the primary amine substrate. The isocyanate would then be expected to react with another molecule of amine (eq. 1), as proposed previously for the bulk gold-catalyzed reactions.³¹ It is possible that the reactivity of benzylamine, aniline, and other aromatic amines would be improved in the presence of inorganic bases such as NaOH and K₂CO₃, as it has been found in other amine oxidation systems.⁴⁴⁻⁴⁶ Further work will involve the syntheses of N,N'-disubstituted ureas from one-pot mixtures containing aliphatic and aromatic amines, as well as one-pot substrate mixtures of primary and secondary amines.

Experimental Section

All reagents were obtained from commercial sources (Sigma-Aldrich, Fisher Scientific, Alfa Aesar, and Acros Organics) and used without further purification. Toluene, THF, and CH_2Cl_2 were dried and deoxygenated by passage through columns of alumina and reduced copper. Ultra pure water was obtained from a Milli-Q[®] UV plus water purification system. NMR spectra were obtained using a Varian MR 400 MHz spectrometer. NMR peak positions were referenced against residual proton resonances in CDCl_3 and DMSO-d_6 (δ 7.26 ppm and 2.50 ppm, respectively).

Procedure for the preparation of ceria-supported gold (Au/CeO_2) catalysts: The synthesis and characterization of the CeO_2 support (169 – 203 m^2/g) was published earlier.⁴² The supported catalysts were prepared according to a procedure reported by Pérez et al,³⁸ and were characterized earlier.⁴¹

Procedure for the Au/CeO_2 -catalyzed conversion of primary amines to $\text{N,N}'$ -disubstituted ureas, in the presence of CO and O_2 , as illustrated by the reaction of *n*-butylamine: A 50-mL round-bottomed flask was charged with a stir bar, 40 mg of 5.4 wt% Au/CeO_2 catalyst (2.16 mg, 0.0110 mmol of Au), and 2.2 mL of a 100. mM stock solution of *n*-butylamine (16.1 mg, 0.220 mmol) in acetonitrile solvent. The mole ratio of gold atoms to substrate was 1: 20 (5 mol% of Au). The reaction flask was covered with a rubber septum, and two syringe needles attached to two different balloons were inserted into the septum. One of the balloons contained CO , while the other one contained O_2 (size of CO balloon was approximately twice that of O_2 balloon). After stirring at ambient temperature (23 °C) for 48

hours, the mixture was then filtered through fine frit. The fritted funnel was packed with neutral alumina (bottom layer) and celite (upper layer), and the packing was rinsed with aliquots of ethanol. Volatiles were removed from the clear filtrate under reduced pressure, to afford N,N'-di-n-butylurea as a white solid (14.2 mg, 0.0824 mmol, 75% yield). For the isolation of N,N'-diisopropylurea, the packing was also rinsed with ethanol, while the rinsing solvent mixture was a 1:1 ratio of ethanol: ethyl acetate in the case of N,N'-dicyclohexylurea. The urea products were identified by comparing their ^1H NMR spectra with those of authentic samples and/or those found in the literature.^{14,15,21,43}

N,N'-di-n-butylurea¹⁴: ^1H NMR (300 MHz, CDCl_3): δ 0.91 (t, $J = 7.3$ Hz, 6 H), 1.51–1.26 (m, 8 H), 3.18–3.09 (m, 4 H), 5.78 (t, br, $J = 5.1$ Hz, 2 H).

N,N'-diisopropylurea¹⁵: ^1H NMR (400 MHz, DMSO-d_6): δ 1.02 (d, 12 H), 3.86 (m, 2 H), 5.36 (d, 2 H).

N,N'-dicyclohexylurea⁴³: ^1H NMR (300 MHz, DMSO-d_6): δ 0.98 – 1.26 (m, 10H), 1.48 – 1.73 (m, 10H), 3.28 – 3.42 (m, 2H), 5.57 (d, $J = 8.10$ Hz, 2H).

N,N'-dibenzylurea¹⁴: ^1H NMR (300 MHz, DMSO-d_6): δ 4.24 (d, $J = 5.9$, 4 H), 6.48 (t, $J = 5.9$, 2 H), 7.21 – 7.35 (m, 10 H).

References

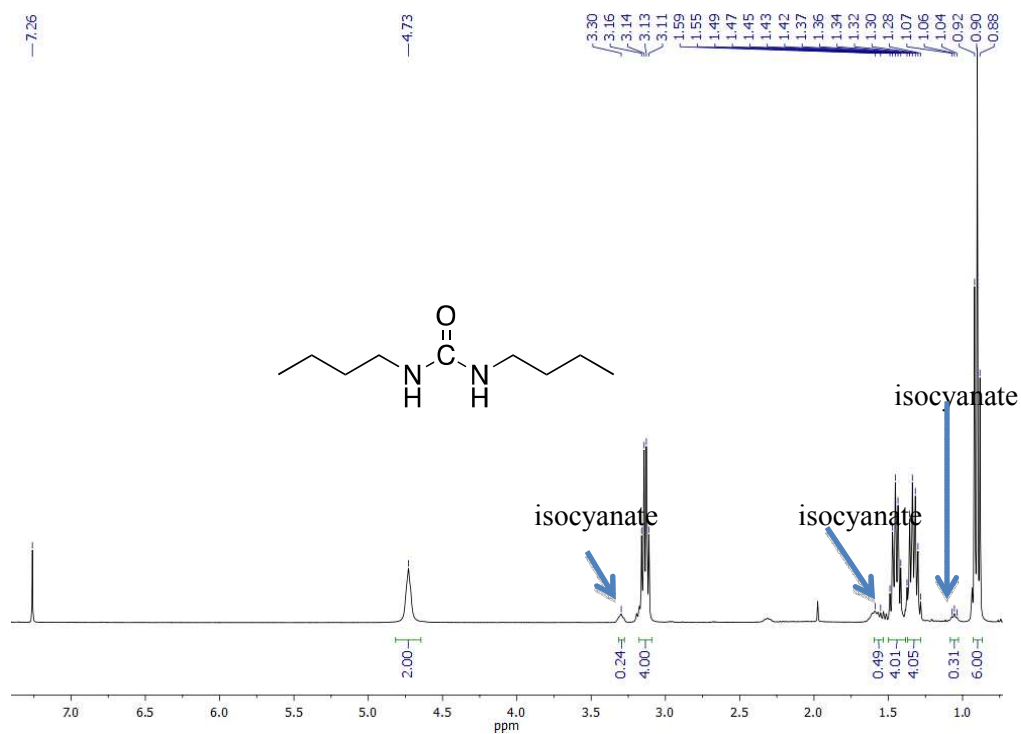
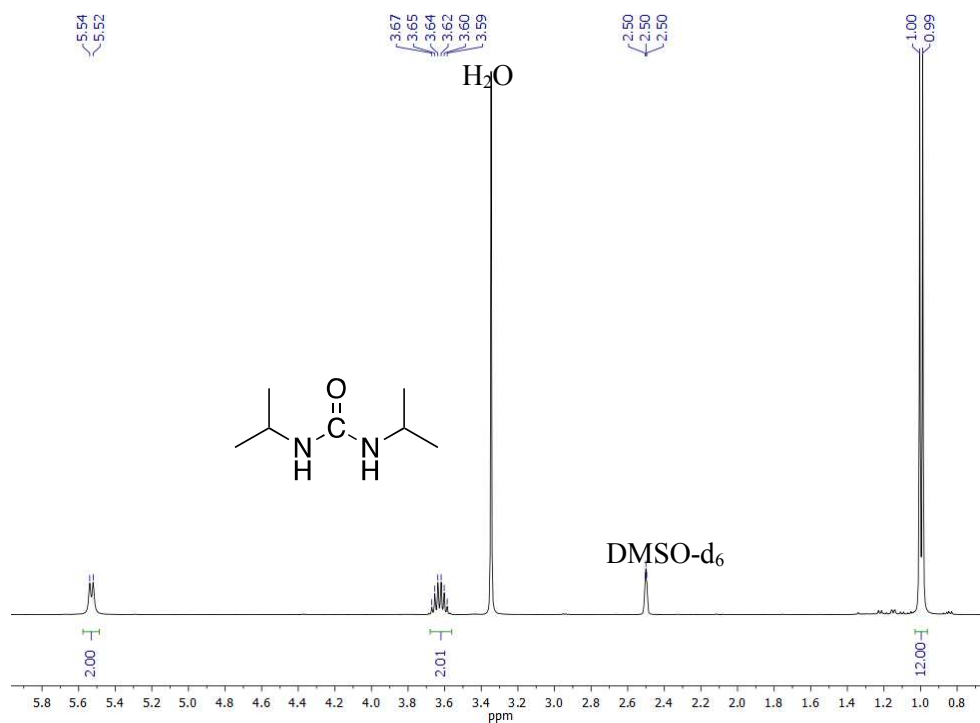
- (1) Bigi, F.; Maggi, R.; Sartori, G. *Green Chem.* **2000**, *2*, 140-148.
- (2) Zhu, Y.; Xia, S.; Zhu, M.; Yi, W.; Cheng, J.; Song, G.; Li, Z.; Lu, P. *Eur. J. Med. Chem.*, **2010**, *45*, 4953
- (3) Batra, S.; Tusi, Z.; Madapa, S. *Curr. Med. Chem.* **2006**, *5*, 135
- (4) Gabriele, B.; Salerno, G.; Mancuso, R.; Costa, M. *J. Org. Chem.* **2004**, *69*, 4741.

- (5) Han, Q.; Chang, C.-H.; Li, R.; Ru, Y.; Jadhav, P.K.; Lam, P.Y.S. *J. Med. Chem.*, **1998**, *41*, 2019–2028
- (6) Nicholas, A.C.; Yielding, K.L. *Mol. Chem. Neuropathol.* **1998**, *35*, 1.
- (7) Boden, P.; Eden, J.M.; Hodgson, J.; Horwell, D.C.; Howson, W.; Hughes, J.; McKnight, A.T.; Meecham, K.; Pritchard, M.C.; Raphy, J.; Ratcliffe, G.S.; Suman-Chauhan, N.; Woodruff, G.N. *Bioorg. Med. Chem. Lett.* **1994**, *4*, 1679
- (8) Guercio, G.; Bacchi, S.; Perboni, A.; Leroi, C.; Tinazzi, F.; Bientinesi, I.; Hourdin, M.; Goodyear, M.; Curti, S.; Provera, S.; Cimarosti, Z. *Org. Process Res. Dev.* **2009**, *13*, 1100
- (9) Iranpoor, N.; Firouzabadi, H.; Pourali, A.-R. *Synthesis* **2003**, 1591-1597
- (10) Tsujihara, K.; Ozeki, M.; Morikawa, T.; Kawamori, M.; Akaike, Y.; Arai, Y. *J. Med. Chem.* **1982**, *25*, 441
- (11) Ghosh, S.; Chiang, P.-C.; Wahlstrom, J.L.; Fujiwara, H.; Selbo, J.G.; Roberds, S.L. *Basic Clin. Pharmacol. Toxicol.* **2008**, *102*, 453.
- (12) Schneider, W.; Diller, W. Phosgene. In *Ullmann's Encyclopedia of Industrial Chemistry* 2000.
- (13) Borak, J.; Diller, W.F. *J. Occup. Env. Med.* **2001**, *43*, 110-119.
- (14) Ca', N.D.; Bottarelli, P.; Dibenedetto, A.; Aresta, M.; Gabriele, B.; Salerno, G.; Costa, M. *J. Catal.* **2011**, *282*, 120-127.
- (15) Tian, F.; Chen, Y.; Wang, X.; Li, P.; Lu, S. *J. Chem.* **2015**, 1-6.
- (16) El Dine, T.M.; Chapron, S.; Duclos, M.-C.; Duguet, N.; Popowycz, F.; Lemaire, M. *Eur. J. Org. Chem.* **2013**, 5445–5454
- (17) Katritzky, A.R.; Kirichenko, N.; Rogovoy, B.V. *ARKIVOC* **2003**, 8-14
- (18) Han, C.; Porco Jr., J.A. *Org. Lett.* **2007**, *9*, 1517-1520
- (19) Li, X.-Q.; Wang, W.-K.; Han, Y.-X.; Zhang, C. *Adv. Synth. Catal.* **2010**, *352*, 2588-2598
- (20) Liu, P.; Wang, Z.; Hu, X. *Eur. J. Org. Chem.*, **2012**, 1994-2000.
- (21) Enquist, P.-A.; Nilsson, P.; Edin, J.; Larhed, M. *Tetrahedron Lett.* **2005**, *46*, 3335–3339
- (22) Chiarotto, I.; Feroci, M. *J. Org. Chem.* **2003**, *68*, 7137-7139.

- (23) Lazar, M.; Angelici, R. J. *J. Am. Chem. Soc.* **2006**, *128*, 10613–10620.
- (24) Lazar, M.; Zhu, B.; Angelici, R.J. *J. Phys. Chem. C* **2007**, *111*, 4074-4076.
- (25) Klobukowski, E.R.; Angelici, R.J.; Woo, L.K. *Organometallics* **2012**, *31*, 2785-2792.
- (26) Zhu, B.; Angelici, R.J. *Chem. Commun.* **2007**, 2157-2159
- (27) Zhu, B.; Lazar, M.; Trewyn, B.G.; Angelici, R.J. *J. Catal.* **2008**, *260*, 1-6
- (28) Klobukowski, E.R.; Angelici, R.J.; Woo, L.K. *Catal. Lett.* **2012**, *142*, 161-167.
- (29) Zhou, Y.; Angelici, R.J.; Woo, L.K. *Catal. Lett.* **2010**, *137*, 8-15.
- (30) Klobukowski, E.R.; Mueller, M.L.; Angelici, R.J.; Woo, L.K. *ACS Catal.* **2011**, *1*, 703-708.
- (31) Zhu, B.; Angelici, R.J. *J. Am. Chem. Soc.* **2006**, *128*, 14460-14461
- (32) Grirrane, A.; Corma, A.; Garcia, H. *Science* **2008**, *322*, 1661-1664.
- (33) Della Pina, C.; Falletta, E.; Rossi, M. *Top. Catal.* **2007**, *44*, 325-329.
- (34) Klitgaard, S.K.; Egeblad, K.; Mentzel, U.V.; Popov, A.G.; Jensen, T.; Taarning, E.; Nielsen, I.S.; Christensen, C.H. *Green Chem.* **2008**, *10*, 419-423
- (35) Aschwanden, L.; Mallat, T.; Grunwaldt, J.-D.; Krumeich, F.; Baiker, A. *J. Mol. Catal. A: Chem.* **2009**, *300*, 111-115.
- (36) So, M. H.; Liu, Y. G.; Ho, C. M.; Che, C. M. *Chem. Asian J.* **2009**, *4*, 1551-1561.
- (37) Aschwanden, L.; Mallat, T.; Krumeich, F.; Baiker, A. *J. Mol. Catal. A: Chem.* **2009**, *309*, 57-62.
- (38) Perez, Y.; Aprile, C.; Corma, A.; Garcia, H. *Catal. Lett.* **2010**, *134*, 204-209.
- (39) Preedasuriyachai, P.; Chavasiri, W.; Sakurai, H. *Synlett* **2011**, 1121-1124.
- (40) Soulé, J.-F.; Miyamura, H.; Kobayashi, S. *Chem. Commun.* **2013**, *49*, 355-357.
- (41) Dairo, T.O.; Nelson, N.C.; Slowing, I.I.; Angelici, R.J.; Woo, L.K. *ACS Catal.* submitted for publication.
- (42) Nelson, N. C.; Manzano, J. S.; Sadow, A. D.; Overbury, S. H.; Slowing, I. I. *ACS Catal.* **2015**, *5*, 2051-2061.

- (43) Gadge, S.T.; Kusumawati, E.N.; Harada, K.; Sasaki, T.; Nishio-Hamane, D.; Bhanage, B.M. *J. Mol. Catal. A: Chem.* **2015**, *400*, 170-178.
- (44) Khusnutdinova, J. R.; Ben-David, Y.; Milstein, D. *J. Am. Chem. Soc.* **2014**, *136*, 2998-3001.
- (45) Zope, B. N.; Hibbitts, D. D.; Neurock, M.; Davis, R. J. *Science* **2010**, *330*, 74-78.
- (46) Biella, S.; Castiglioni, G. L.; Fumagalli, C.; Prati, L.; Rossi, M. *Catal. Today* **2002**, *72*, 43-49.

Supporting Information

Fig. S1. ¹H NMR spectrum of N,N'-di-n-butylurea in CDCl₃Fig. S2. ¹H NMR (400 MHz) spectrum of N,N'-diisopropylurea in DMSO-d₆

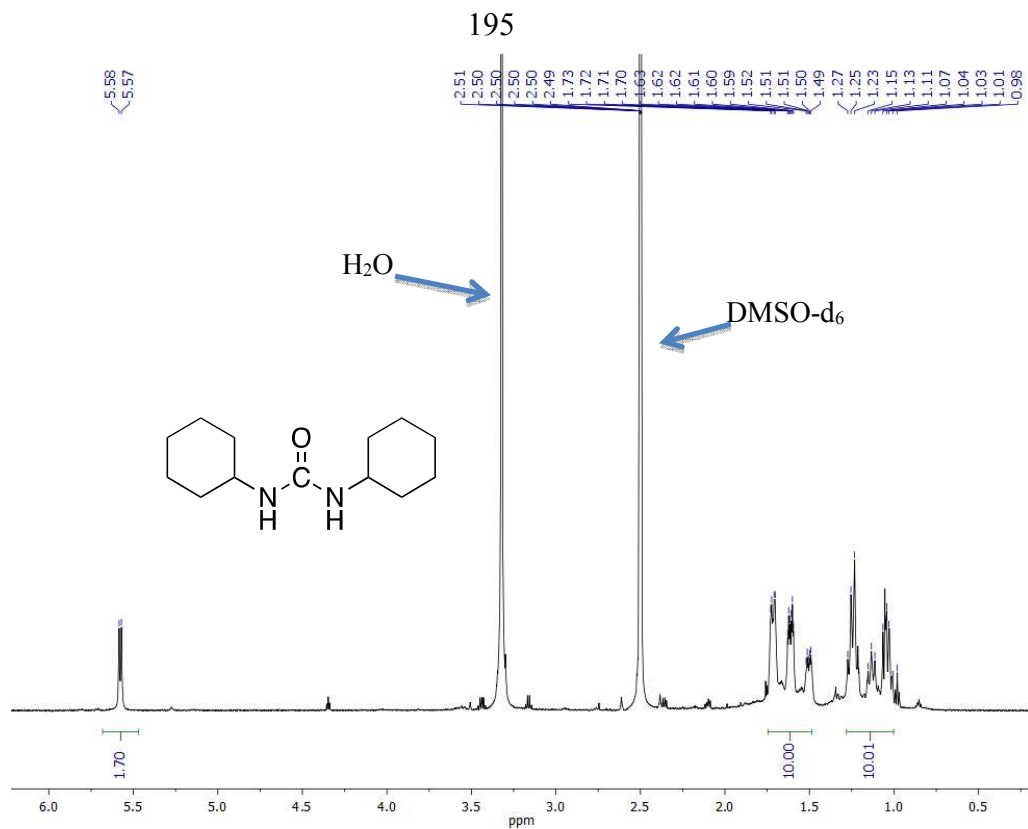


Fig. S3. ^1H NMR (600 MHz) spectrum of N,N'-dicyclohexylurea in DMSO- d_6

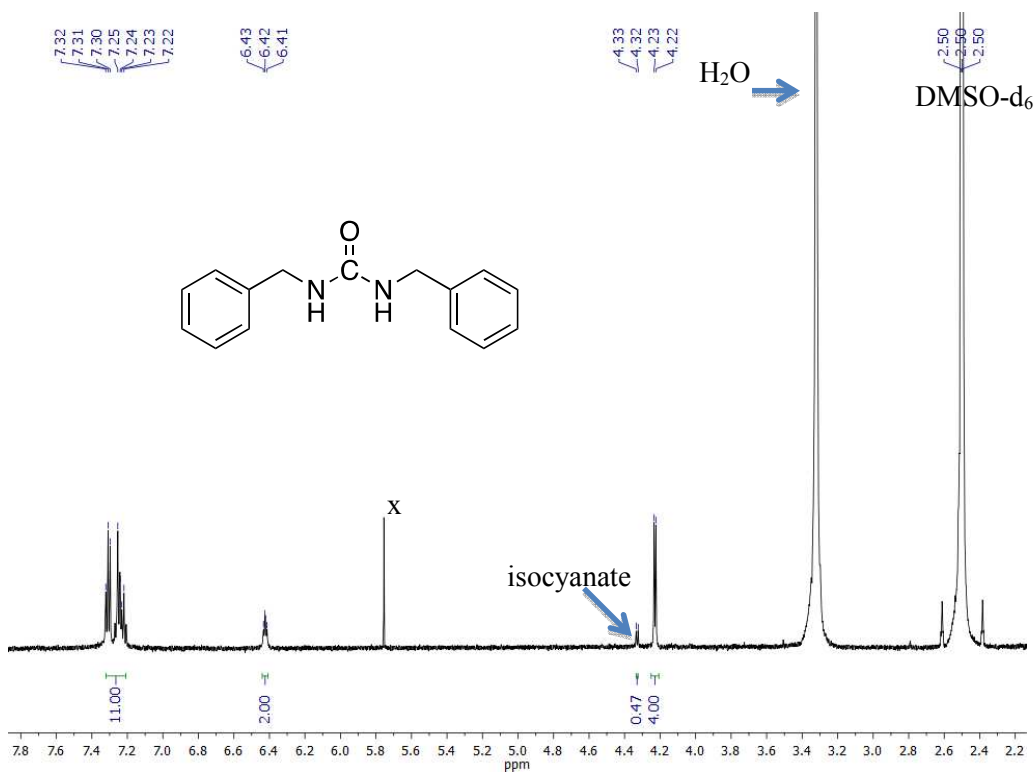


Fig. S4. ^1H NMR (600 MHz) spectrum of N,N'-dibenzylurea in DMSO- d_6

CHAPTER 6. CONCLUSION

Iridium porphyrins and metal oxide-supported nanogold have shown promise as highly efficient catalysts in several chemical transformations. To this end, the research projects presented in this thesis have focused on an exploration of the stoichiometric and catalytic reactivities of iridium(III) porphyrin complexes, as well as the efficient synthesis of industrially important organic molecules via ceria (CeO₂)-supported nanogold-catalyzed amine oxidation reactions.

In this work, we have shown that amine-coordinated iridium porphyrin carbamoyl complexes are readily generated from the interactions of primary amines with the carbonyl ligand of a hexacoordinate iridium porphyrin complex. This led to the isolation of the carbamoyl complexes in high yields. The lability of the amine ligands, at room temperature, was established by variable-temperature NMR studies. Consequently, these ligands were substituted with other stronger binding ligands, such as quinuclidine, 1-methylimidazole, triethyl phosphite, and dimethylphenyl phosphine. This led to the isolation of novel hexacoordinate iridium porphyrin complexes. Equilibrium binding studies revealed the following order for the binding affinities of the ligands: Dimethylphenyl phosphine > triethyl phosphite > 1-methyl imidazole > quinuclidine > primary amines >> triethylamine, tricyclohexylphosphine. Furthermore, depending on the nature of the ligand *trans* to the carbamoyl ligand, each carbamoyl complex reacted with HBF₄ to give either a hexacoordinate iridium carbonyl complex, or a complex, which contains neither a carbamoyl nor a carbonyl ligand. The former product is formed when the *trans* ligand is a nitrogen donor ligand, while the latter product is typically formed from hexacoordinate carbamoyl complexes, which contain *trans* phosphorus donor ligands such as triethyl phosphite or

dimethylphenyl phosphine. On the other hand, hexacoordinate iodo complexes were the products of the reactions of all of the hexacoordinate carbamoyl complexes with methyl iodide, regardless of the nature of the ligand *trans* to the carbamoyl group.

We have also shown that the pentacoordinated $\text{Ir}(\text{TTP})\text{CH}_3$ (TTP is tetratolylporphyrinato) efficiently catalyzes the insertion of the carbene moieties from four different diazoesters into the S-H bond of different aromatic and aliphatic thiols. While the resulting thioether yields were obtained in high yields, equilibrium binding studies revealed that the thiol substrates reversibly bind to iridium, to generate a hexacoordinated complex, $(\text{thiol})\text{Ir}(\text{TTP})\text{CH}_3$. In addition, a Hammett correlation plot showed that electron-rich aromatic thiols bind more strongly to iridium than their electron-deficient counterparts. Competition and trapping experiments also provide evidence for an ylide intermediate, which would be formed from a nucleophilic attack of the thiol substrate on a putative iridium-carbene complex. Furthermore, results of kinetic studies revealed the dual roles played by the thiol substrate during the catalysis: (i.) Thiol binding to the metal center of the catalyst generates the catalytically inactive hexacoordinate iridium complex, $(\text{thiol})\text{Ir}(\text{TTP})\text{CH}_3$ (ii.) The nucleophilic attack of the thiol on the metal carbene generates the thioether product. In the relatively higher thiol concentration regime, thiol binding to iridium is dominant, causing a reduction in the rate of S-H insertion, as most of the iridium catalyst is in the inactive form. At the relatively lower thiol concentration regime, however, nucleophilic attack at the carbene carbon is dominant, leading to the observed faster reaction rates, as the thiol concentration is increased.

Also reported in this thesis, is the efficient one-pot synthesis of secondary and tertiary lactams, which are important chemical feedstocks, from the aerobic oxidation of cyclic

secondary and tertiary amines. The reactions are catalyzed by CeO₂-supported gold nanoparticles (Au/CeO₂) in the presence of 1 atmosphere of O₂, and the secondary and tertiary lactam products were obtained in yields up to 97%. Control experiments also showed that good yields of the secondary lactams are achievable in the absence of Aerosil co-catalyst, while the syntheses of tertiary lactams do not require the co-catalyst at all. The intermediacy of 5-(pyrrolidin-1-yl)-3,4-dihydro-2*H*-pyrrole (amidine-5) and 4-amino-1-(pyrrolidin-1-yl)butan-1-one) in the oxidation of pyrrolidine was established by their independent syntheses and catalytic conversions into 2-pyrrolidone. This provided evidence for an oxidative dehydrogenation first step during the catalytic conversion of the secondary amine substrates into the corresponding lactams.

Finally, promising results were obtained from the room temperature CeO₂-supported gold nanoparticles (Au/CeO₂)-catalyzed synthesis of N,N'-disubstituted ureas from the reactions of primary amines with 1 atmosphere each of CO and O₂. The isolated yield of N,N'-di-*n*-butylurea was 75%, while N,N'-dicyclohexylurea and N,N'-diisopropylurea were isolated in 40% yield and 37% yield, respectively. The detection of small quantities of isocyanate products suggests an initial formation of one isocyanate molecule from each molecule of the primary amine substrate. In analogy to the previously-proposed pathway for the bulk-gold catalyzed reactions, the isocyanate then reacts with another molecule of amine, to generate the N,N'-disubstituted urea product.

In conclusion, this work has further demonstrated the rich stoichiometric and catalytic reactivities of iridium(III) porphyrin complexes, as well as the catalytic applicability of metal oxide-supported nanogold in the synthesis of industrially relevant organic compounds. The discovery that the Au/CeO₂-catalyzed lactam syntheses proceed at a reasonably fast rate in

air, as shown in this work, coupled with the catalytic efficiency (low catalyst loadings and short reaction times) under optimized conditions, implies that our one-pot procedure could be an economically viable alternative method for the industrial manufacture of lactams in the future. Furthermore, it would be interesting to explore the catalytic activities of alloyed nanogold supported on CeO_2 , as well as nanogold supported on mixed metal oxides in the conversion of cyclic amines into lactams. Since bulk gold has been shown to catalyze carbene transfer reactions involving diazo compounds, it would also be worthwhile to probe the catalytic activity of supported nanogold in this class of chemical transformations.